2023

ROLE OF CYSTEINE REDOX STATE IN ALTERING THE EPITHELIAL-MESENCHYMAL TRANSITION IN LUNG CANCER

Md Anisur Rahman
University of the Pacific

ROLE OF CYSTEINE REDOX STATE IN ALTERING THE EPITHELIAL-MESENCHYMAL TRANSITION IN LUNG CANCER

By

Md Anisur Rahman

A Dissertation Submitted

In Partial Fulfillment of the

Requirements for the Degree of

DOCTOR OF PHILOSOPHY

Thomas J. Long School of Pharmacy
Pharmaceutical & Chemical Sciences

University of the Pacific
Stockton, California

2023

ROLE OF CYSTEINE REDOX STATE IN ALTERING THE EPITHELIAL-MESENCHYMAL TRANSITION IN LUNG CANCER

By

Md Anisur Rahman

APPROVED BY:

Dissertation Advisor: John C. Livesey, Ph.D.

Committee Member: Roshanak Rahimian, Ph.D.

Committee Member: David W. Thomas, Ph.D.

Committee Member: Wade A. Russu, Ph.D.

Committee Member: Lisa Wrischnik, Ph.D.

Department Chair: Roshanak Rahimian, Ph.D.

ROLE OF CYSTEINE REDOX STATE IN ALTERING THE EPITHELIAL-MESENCHYMAL TRANSITION IN LUNG CANCER

By

Md Anisur Rahman

Dedication

This dissertation is dedicated to my family and my advisor, who supported me to successfully complete this dissertation.

Acknowledgements

My gratitude first goes to Dr. Livesey for his immense support, guidance, and continuous encouragement since I joined his laboratory. He has guided me to develop gradually as an independent scientist with critical thinking, scientific and technical writing skills. I also appreciate his generosity for personally contributing to funds for my research. I would like to thank Dr. Rahimian, Dr. Thomas, Dr. Russu, and Dr. Wrischnik for serving on my dissertation committee, and for providing valuable suggestions. I express my gratitude to Dr. Jasti for allowing me additional time to complete this dissertation. I would like to especially thank Dr. Chan for allowing me to use his lab equipment on a regular basis. Also, I appreciate Dr. Thomas and Dr. Carlos along with their lab members for allowing me to use some of their equipment. I also acknowledge help from Dr. Razan (from Dr. Rahimian's Lab) for training me on Western Blot. Dr. Hamed (from Dr. Halliwell's Lab) helped me to learn 'Time Lapse video recording' for live fluorescence imaging. The cell culture support from Ms. Marcia Fox is very much appreciated. I would like to thank my fellow graduate student friends including Dr. Uddin, Dr. Akhter, Dr. Nguyen, Dr. Pal, Dr. Tuhin, Dr. Amin, Rfiat, Sky, Hala, Rasha, Ankita, AbdulMalek, Nasim, Moses, Moshiur. I appreciate Ms. Bonnie, Ms. Sonya, Mr. Wolak (IPS) and Ms. Carmen (IPS) for their administrative support. I am grateful to the University of the Pacific for funding my research. Finally, I must acknowledge the support from my family. My parents always encouraged and motivated me for research. My two daughters Rida and Tooba are the joy of my life. I would like to especially acknowledge my wife, Sania. She supported me always by staying with me, took care of me and my children, and made sure I can focus on my research.

ROLE OF CYSTEINE REDOX STATE IN ALTERING THE EPITHELIAL-MESENCHYMAL TRANSITION IN LUNG CANCER

Abstract

By Md Anisur Rahman

University of the Pacific
2023

Epithelial - mesenchymal transition is a process by which cancer cells increase their capability for metastasis. EMT involves conversion of epithelial cells into a mesenchymal phenotype which makes cancer cells more invasive and motile. Lung cancer has the highest mortality rate among different types of cancers globally. Lung cancer exists in various types, the most prevalent of which is non-small cell lung cancer (NSCLC). Several factors, including oxidative stress, can induce EMT in cancer cells. However, the mechanism of how reactive oxygen species (ROS)-induced changes in cysteine redox state affect EMT remains elusive. Our studies aim to understand this mechanism by inducing cysteine redox state alteration with intracellular ROS generation, particularly inside A549 lung adenocarcinoma cells (a type of NSCLC). We also seek to determine how subcellular generation of peroxide influences EMT progression.

We successfully generated hydrogen peroxide (H_2O_2) intracellularly using several methods including plasmid-based chemo-genetic approaches, by increasing H_2O_2 persistence with peroxidase enzyme inhibition, and by quinone metabolism. First, we used commercially available plasmids containing a peroxide generator. These plasmids deliver the gene coding for the enzyme D-amino acid oxidase (DAAO) which metabolizes D-amino acids and produces hydrogen peroxide which can be detected by the 'HyPer' fluorescent sensor, also a part of the fusion protein coded by the plasmid. By altering D-alanine concentrations, we were also able to regulate hydrogen peroxide production. We

generated hydrogen peroxide at different subcellular locations (cytoplasm, nucleus, mitochondria). EMT progression was evaluated in each manner of H_2O_2 increase (whether by generation or persistence) by morphology observation, EMT-related marker protein expression change, as well as measurements of cell motility rate.

Our studies found that H_2O_2 generation in the cytoplasm induces EMT in A549 cells, particularly when the peroxidase enzyme catalase is inhibited. This treatment resulted in production of the mesenchymal phenotype (elongated, loosely connected cells), downregulated the epithelial marker E-cadherin and upregulated the mesenchymal marker N-cadherin. The motility assay also showed a trend toward faster movement. Similar results were also obtained when catalase or catalase plus thioredoxin reductase was inhibited to increase H_2O_2 persistence. Quinone metabolism to generate H_2O_2 did not show EMT-related marker expression changes but showed an enhanced rate of motility.

Investigation of the molecular targets of oxidation that promote EMT in the cytosol is in process. Beta-catenin, SMAD2/3, SNAI1/2, and pan-AKT have been selected as the initial cytoplasmic targets. In initial results using a fluorescence-based microplate technique, peroxide persistence by catalase inhibition with 3-aminotriazole showed significantly higher oxidation of SNAI1/2 and pan-AKT, but the reproducibility of this observation must be verified.

In summary, this research has shown that the cytoplasm is the probable subcellular location inside A549 cells where the molecular target of cysteine oxidation leading to EMT is present. Peroxide persistence by catalase inhibition also induces EMT and the probable molecular targets may be SNAI1/2 and pan-AKT.

Table of Contents

List of Tables

Table

List of Figures

Figure

List of Abbreviations

2-OG	2-Oxoglutarate
3-AT	3-amino-1,2,4-triazole
ADC	Adenocarcinoma
AKT	Ak strain transforming
AP-1	Activator protein 1
Axl	A receptor tyrosine kinase gene
BCA	Bicinchoninic acid
Bcl-2	B-cell lymphoma 2
Bcl-xL	B-cell lymphoma-extra large
BMI1	B lymphoma Mo-MLV insertion region 1 homolog
BSO	Buthionine sulfoximine
BTG2	B-cell translocation gene 2
CAT	Catalase
CCL2	C-C Motif Chemokine Ligand 2
Cdc25	Cell division cycle 25
CDKs	Cyclin-dependent kinases
CFP	Cyan Fluorescent Protein
Chk	Csk homology kinase (Chk)
CIAP1/2	cellular inhibitor of apoptosis protein ½
c-jun	Cellular homolog of oncoprotein v-jun
c-Myc	Cellular Myc
CREB	cAMP-response element binding protein

Csk	C-terminal Src kinase
CSN2	COP9 signalosome 2
Cys	Cysteine
DAAO	D-amino acid oxidase
DDR	DNA Damage Response
DHMEQ	Dehydroxymethylepoxyquinomicin
DMNQ	2,3-dimethoxy-1,4-naphthalenedione
D-PBS	Dulbecco's Phosphate Buffered Saline
DTT	1-4-dithiothreitol
ECAD	E-Cadherin
ECM	Extracellular matrix
EDTA	Ethylenediaminetetraacetic Acid
EGF	Epidermal Growth Factor
EGFR	Epidermal Growth Factor Receptor
Egr-1	Early Growth Response Protein-1
ELISA	Enzyme-linked immunosorbent assay
EMP	Epithelial-Mesenchymal Plasticity
EMT	Epithelial to Mesenchymal Transition
EMT-TFs	EMT-related Transcription Factors
ERK	Extracellular signal-regulated Kinase
FAK	Focal adhesion kinase
FBS	Fetal Bovine Serum
FGF	Fibroblast Growth Factor
FGMA2	High mobility group A2

FHC	Ferritin heavy chain
F-MAL1	Fluorescent maleimide-1
FMAL-2	Fluorescent maleimide-2 (AlexaFluor 647-C2-maleimide)
FN1	Fibronectin-1
FOX	Forkhead box
FPN	Ferroportin
GAPDH	Glyceraldehyde-3-phosphate dehydrogenase
GF	Growth Factors
GFP	Green Fluorescent Protein
GPS	Glutamine-Penicillin-Streptomycin
GPX	Glutathione peroxidase
Grx1	Glutaredoxin
GSH	Glutathione
GSK3β	Glycogen Synthase Kinase-3β
GST	Glutathione transferases
HBSS	Hank's Balanced Salt Solution
HEPES	4-(2-hydroxyethyl)-1-piperazineethanesulfonic acid
HGF	hepatocyte growth factor
HIF-1α	Hypoxia-Inducible Factor-1α
HRE	Hypoxia-response element
IBB	Intercept Blocking Buffer
ICW	In-Cell Western assay
IFN-γ	Interferon-γ
JAK	Janus kinase

JNK	JUN N-terminal kinase
KLF4	Kruppel-like factor 4
LATS2	Large tumor suppressor 2
LB	Lysogeny broth
LCC	Large cell carcinoma
LCN2	Lipocalin-2
LIP	Labile iron pool
L-OH	Lipid alcohol
L-OOH	Lipid peroxide
LOX	Lipoxygenase
MAPK	Mitogen-activated protein kinase
MCF	Macrophage chemotactic factor
MDM2	Mouse double minute 2
MEK	Mitogen-activated protein kinase kinase
MET	Mesenchymal to Epithelial Transition
miRNA	microRNAs
MMP	Matrix metalloproteinases
MnTBAP	Manganese tetrakis-benzoic acid porphyrin
MT1-MMP	Membrane type 1 matrix metalloproteinase
NAC	N-acetyl cysteine
NADPH	Nicotinamide Adenine Dinucleotide Phosphate
NCAD	N-Cadherin
NES	Nuclear Exclusion Sequence
NFκB	Nuclear Factor-kappa B

NICD	Notch intracellular domain
NO	Nitric Oxide
NOX	NADPH oxidase
NSCLC	Non-Small Cell Lung Cancer
O_2-$^{\bullet}$	Superoxide anion radical
$^1O_2$	Singlet oxygen
O_3	Ozone
OBB	Odyssey Blocking Buffer
OCT	Octamer-binding transcription factor
$^{\bullet}$OH	Hydroxyl radical
-OONO	Peroxynitrite
$p16^{INK4A}$	Cyclin-dependent kinase inhibitor 2A
PAK1	p21 activated kinase 1
PAR	Partitioning defective proteins
PARP3	Poly (ADP-ribose) polymerase 3
PBST	PBS with Tween-20
PDGF	Platelet-derived growth factor
PD-L1	Programmed cell death ligand 1
PEP	PEST domain-enriched tyrosine phosphatase
PHD	Prolyl hydroxylase domain
PI3K	Phosphatidylinositol-3 kinase
PKC	Protein kinase C
PKD1	Protein Kinase D1
PRC2	Polycomb repressive complex 2

PRRX1	Prospero homeobox protein 1
Prx	Peroxiredoxins
PTEN	Phosphatase and tensin homolog
PTP	Phosphotyrosine-phosphatase
PUFA-PE	Polyunsaturated fatty acid - phosphatidyl ethanolamine
Rac1	Ras-related C3 botulinum toxin substrate 1
RAF	Rapidly accelerated fibrosarcoma
RAS	Rat Sarcoma
Rho-GTPase	Ras homologous-GTPase
ROCK	Rho Kinase
ROS	Reactive Oxygen Species
RPMI 1640	Roswell Park Memorial Institute 1640
RSH/RS−	Reactive sulfhydryl state
RS_{OX}	Oxidized thiols
RTK	Receptor tyrosine kinase
S.O.C. medium	Super Optimal broth with Catabolite repression
SCC	Squamous Cell Carcinoma
SCLC	Small Cell Lung Cancer
SDS	Sodium dodecyl-sulfate
SDS-PAGE	Sodium dodecyl-sulfate polyacrylamide gel electrophoresis
SHP	SH2-containing protein tyrosine phosphatase
SMAD	Suppressor of Mothers against Decapentaplegic
SNAI1	Zinc Finger Protein SNAI1 (SNAIL)
SNAI2	Zinc Finger Protein SNAI2 (SLUG)

$:SO_2$	Sulphonyl radical
SOD	Superoxide dismutase
Sox	Sry-related HMG box
Src	Steroid Receptor Coactivator
STAT	Signal transducers and activators of transcription
TCEP	Tris-carboxyethylphosphine
TFR1	transferrin receptor 1
TG2	Transglutaminase 2
TGFβ	Transforming Growth Factor-β
TGX	Tris-Glycine eXtended shelf life
TNF	Tumor necrosis factor
Trx	Thioredoxin
TrxR	Thioredoxin reductase
TSP1	Thrombospondin-1
TWIST	Transcription Factor TWIST
Tyr	Tyrosine
VEGF	Vascular endothelial growth factor
Wnt	Wingless/Integrated
ZEB	Zinc finger E-box-binding homeobox
α-SMA	α-Smooth Muscle Actin

CHAPTER 1: INTRODUCTION

Epithelial-mesenchymal transition (EMT) is a process by which epithelial cells are converted to mesenchymal cells. Such conversion makes the cells more invasive with enhanced motility (1). Although EMT is a normal physiological process during early embryonic development and tissue repair, it may lead to organ fibrosis and metastasis in cancer. It is estimated that about 90% of cancer-related deaths are due to metastasis (2). Among different types of cancers, lung cancer is the deadliest one with the second highest prevalence rate. Non-Small Cell Lung Cancer (NSCLC) is the most common form of lung cancer (about 80%-85%) (3) and remains undiagnosed in most patients before it undergoes metastasis. Several factors, including reactive oxygen species (ROS), can modulate EMT(4, 5). However, the molecular mechanism by which ROS induces EMT is not yet known.

This project was designed to investigate the role of thiol redox state in modulating EMT in NSCLC cells. The A549 cell line (adenocarcinoma type) was used, and thiol redox state changes were induced in various ways. The approaches to alter thiol redox states involved the application of extracellular hydrogen peroxide (H_2O_2), the intracellular generation of H_2O_2 within different subcellular compartments of the cells (cytoplasm, nucleus, and mitochondria), peroxidase inhibition to allow the accumulation of naturally generated H_2O_2, and drug metabolism to generate H_2O_2 in the cytoplasmic compartment. The process of EMT was also measured in various ways, including morphology observation, scratch wound healing assay, western blot and in-cell Western assays. In order to investigate the molecular targets altered by H_2O_2, a microplate reader technique 'Redoxifluor' was used (6).

EMT was found to be induced in the presence of the generation of H_2O_2 in the cytoplasmic compartment or the accumulation of H_2O_2 produced by cellular metabolism. In the observation of cellular morphology, scratch wound healing assays, and in western blot analyses of specific marker

proteins, epithelial-mesenchymal plasticity was observed. The search for specific protein targets of that both react with H_2O_2 and are instrumental in triggering EMT was inconclusive.

Our specific aims were:

1. To generate H_2O_2 in different locations inside A549 cells using various chemical and biological methods.
2. To evaluate the relationship between H_2O_2 generation at various intracellular locations and the progression of EMT.
3. To find out the molecular target(s) whose function is/are changed by these cysteine-redox alterations.

CHAPTER 2: LITERATURE REVIEW

Natural aging, unwanted accidents, and disasters can cause death, but by leading to the death about 10 million people in 2020, cancer ranks as a leading cause of death worldwide (7). Cancer cells can develop in nearly any organ and a typical feature of cancer cells is their ability to proliferate uncontrollably (8, 9). However, cancers have been broadly classified as benign or malignant based on their ability to spread and invade other organs. The ability to spread and invade other organs is the deadly feature of cancer cells, known as metastasis.

Cancer cells are named according to the organ or tissue from which they develop (9). For example, cancer developed from liver cells is called hepatic or liver cancer. However, among different types of cancer, lung cancer is a leading cause of cancer-related death although breast cancer is the most prevalent one (7) (Figure 2.1).

2.1 Lung Cancer

When the cells in the lung develop cancer, it is called lung cancer (10). The most dangerous fact about lung cancer is it may metastasize to lymph nodes or brain. One of the major causes of lung cancer is tobacco smoking (11). However, non-smokers may also develop lung cancer through exposure to tobacco smoke in their environment, termed “passive” or second-hand smoke (12). Also, genetically someone can be susceptible to developing cancer. Lung cancer can be broadly divided into two major categories: Non-Small Cell Lung Cancer (NSCLC) and Small Cell Lung Cancer (SCLC) (13).

Figure 2.1

Prevalence and Mortality of Three Major Cancer Types Worldwide, 2022

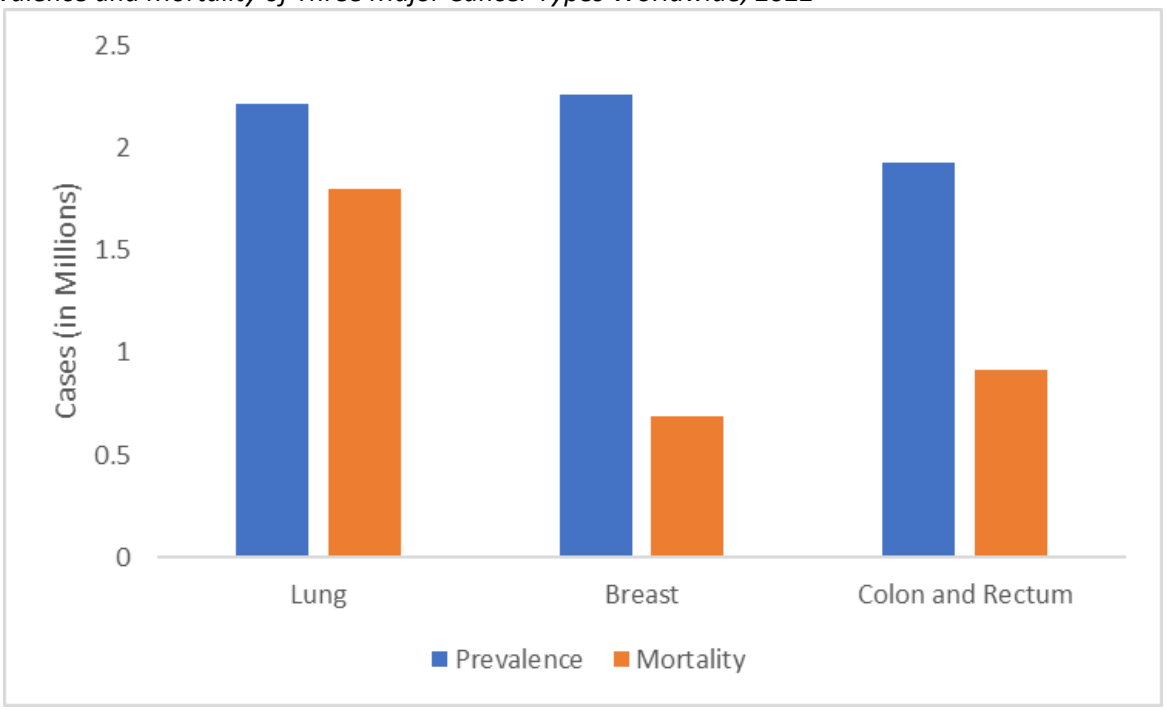

[Adapted from (7)]

2.1.1 Non-Small Cell Lung Cancer (NSCLC)

This is the most common type with about 80-85% of lung cancer cases and is usually diagnosed at the advanced stage (stage 3 or 4) (14-16). NSCLC can be further divided into adenocarcinoma (ADC), squamous cell carcinoma (SCC) and large cell carcinoma (LCC) types. Adenocarcinoma develops in glandular cells which are usually present at the outer side of the lungs. Squamous cell carcinomas typically develop in the cells which line the inner part of the lung airways, particularly in the bronchi. Large cell carcinoma is the fastest growing NSCLC and can start from anywhere in the lung.

2.1.2 Small Cell Carcinoma (SCLC)

Although small cell carcinomas (SCLC) are not very common, only about 10%-15%, this type of lung cancer is more aggressive. It is in most cases detected when metastases have already developed (14). SCLC is also known as 'oat cell cancer'.

2.1.3 Pathophysiology of Lung Cancer

The Lung is a very complex organ with different cell types involved in the exchange of gases (oxygen and carbon dioxide) between blood and inhaled air (13). The inhaled air may contain infectious agents as well as toxic or carcinogenic materials. Infectious agents can be destroyed by the immune system whereas large particulates are removed from the larger airways by ciliary action. However, chronic exposure to infectious agents or toxic elements may induce a group of lung cells to become transformed. These cells proliferate uncontrollably by escaping regulatory mechanisms of the cell cycle and immune recognition of transformed cells (17).

At the molecular level, the damage is mostly associated with alteration of genes (*i.e.* mutations), including rearrangement or copy number alterations of various oncogenes or tumor suppressor genes (18).

2.2 Metastasis

Metastasis is one of the major hallmarks of cancer. Most cancer related deaths are due to metastasis. According to a recent publication in the Journal of the National Cancer Institute (19), Over 600,000 metastatic cancer cases (breast, prostate, lung, colorectal, bladder or melanoma) in United States were estimated to occur in 2018. This number is projected to go up to 700,000 cases by 2025.

Metastasis is the process by which cancer cells spread to various other parts of the body (20-23). The metastatic cascade involves five sequential events shown in Figure 2.2 (20). The first step is known as 'Invasion', where cancer cells leave the primary tumor and invade the epithelial lining of the organ. Next, 'Intravasation' occurs where cancer cells invade the blood or lymphatic vessel endothelium and is followed by 'Circulation' in the blood. Then, through 'extravasation' cancer cells invade the vascular endothelium again to enter another organ site where they finally establish a nascent metastatic site. This final step is also known as colonization.

Cancer cell metastasis (24) and chromosomal defects (25) can trigger the metastasis cascade. Many of these steps are facilitated by a process known as 'Epithelial-Mesenchymal Transition' or EMT (24, 26).

2.3 Epithelial-Mesenchymal Transition (EMT)

Epithelial cells are tightly attached to each other on a basement membrane (27). Therefore, they exhibit apical and basal polarity and are not able to move. Many tumors arise from epithelial cells (adenocarcinomas). To enter the metastasis, cascade some cancer cells must be detached from the tumor in order to acquire motile and invasive abilities (24, 26). Mesenchymal cells are long, elongated, spindle shaped, separated, or loosely connected to each other with the ability to move in any direction. Moreover, their shape allows them to invade easily.

Figure 2.2

5 major steps of metastasis

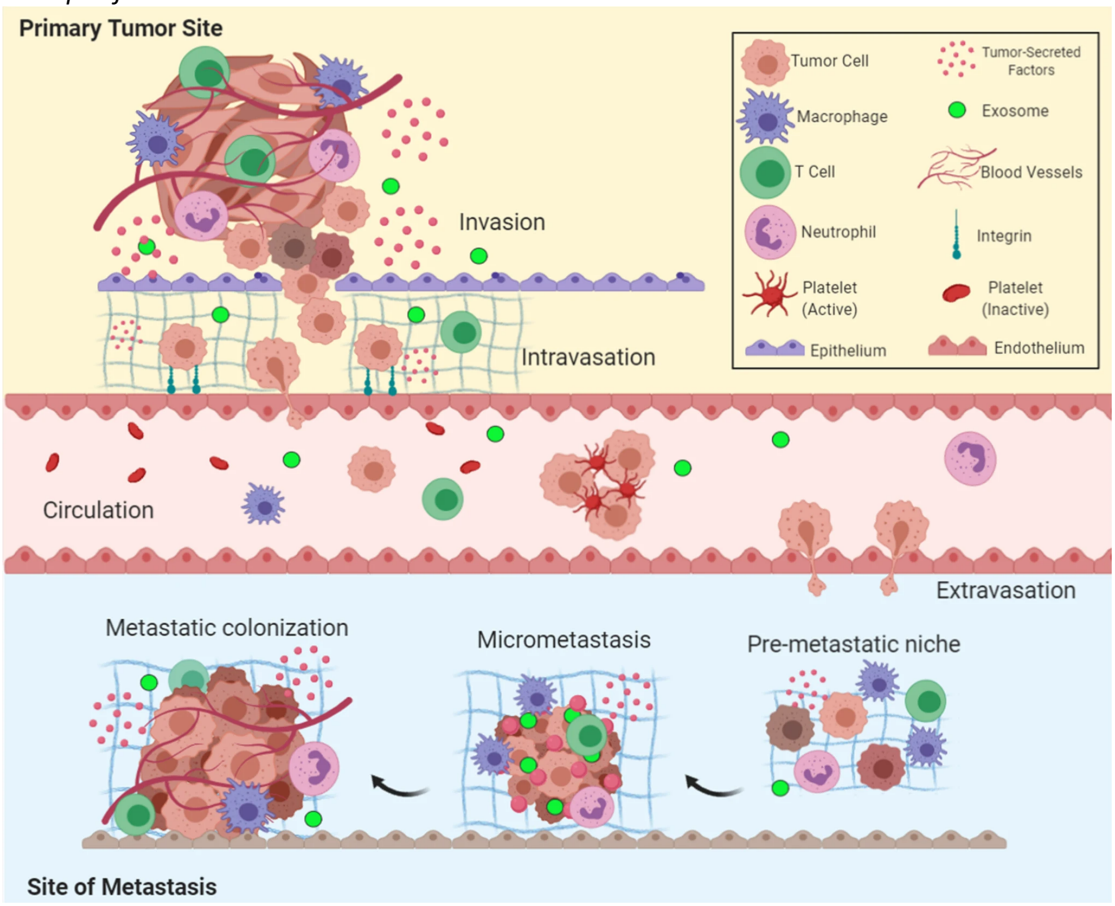

Cancer cells leaving the primary tumor and invading the epithelial lining of the primary organ (Invasion); Then invading the blood vessel endothelium (Intravasation); Circulating in the blood (Circulation); Invading blood vessels again to enter the extracellular matrix of a second organ (Extravasation) and finally localization of cancer cells at the secondary organ (Colonization).

Image [Adapted from (20)]

Many factors, including Transforming Growth Factor-β (TGFβ) and Epidermal Growth Factor (EGF) may induce these epithelial cells to become mesenchymal (28, 29), increasing their capability to enter the metastasis cascade (Figure 2.3B) (30-35). This plasticity of epithelial cells to gain mesenchymal characteristics is known as epithelial-mesenchymal transition (EMT). However, the opposite (*i.e.* mesenchymal-epithelial transition or MET) (36) also occurs at the colonization step of the metastasis cascade to form secondary tumors (Figure 2.3A). EMT as well as MET also take place during embryonic development, tissue repair, and fibrosis (28, 36-39).

EMT has recently come to be known as Epithelial-Mesenchymal Plasticity (EMP) (27), because cells undergoing EMP can co-exist at various states in between true epithelial and mesenchymal phenotypes. Also, the 'Plasticity' of EMP means these cells have the ability to move quickly between these various states.

2.3.1 Mechanism of EMT

EMT starts with the dismantling of different types of junctions that allow epithelial cells to establish and maintain their attachment to one another (Figure 2.3.1) (40). With the loss of these junctions, they also lose apical/basal polarity when Crumbs, Partitioning defective (PAR) and Scribble complexes are disrupted (41, 42). At this point, epithelial gene expression is reduced and mesenchymal gene expression is enhanced.

Figure 2.3A

EMT and MET

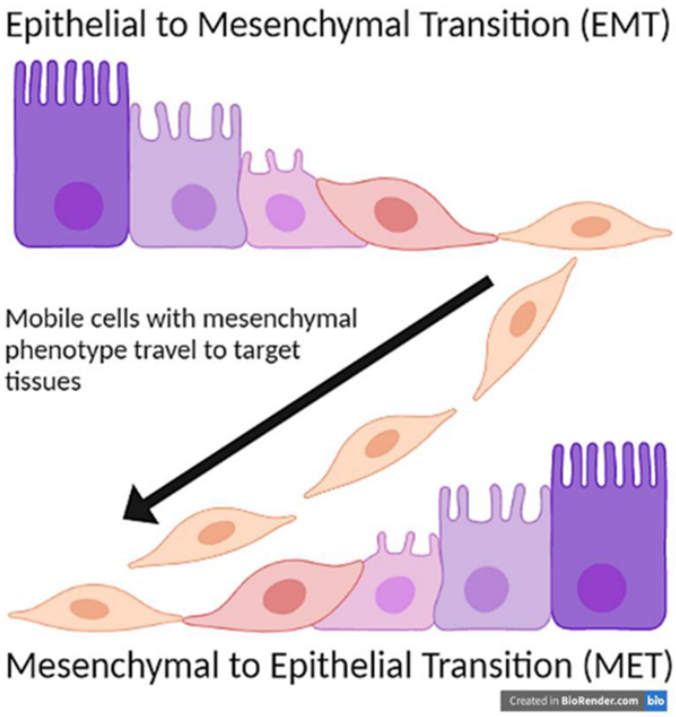

[Image adapted from (43)]

Figure 2.3B

EMT Contributing to Cancer Metastasis

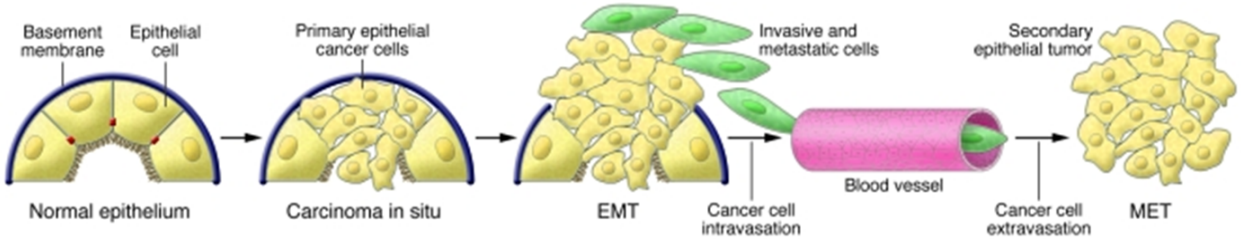

[Image Adapted from (28)]

Figure 2.3.1

EMT Mechanism

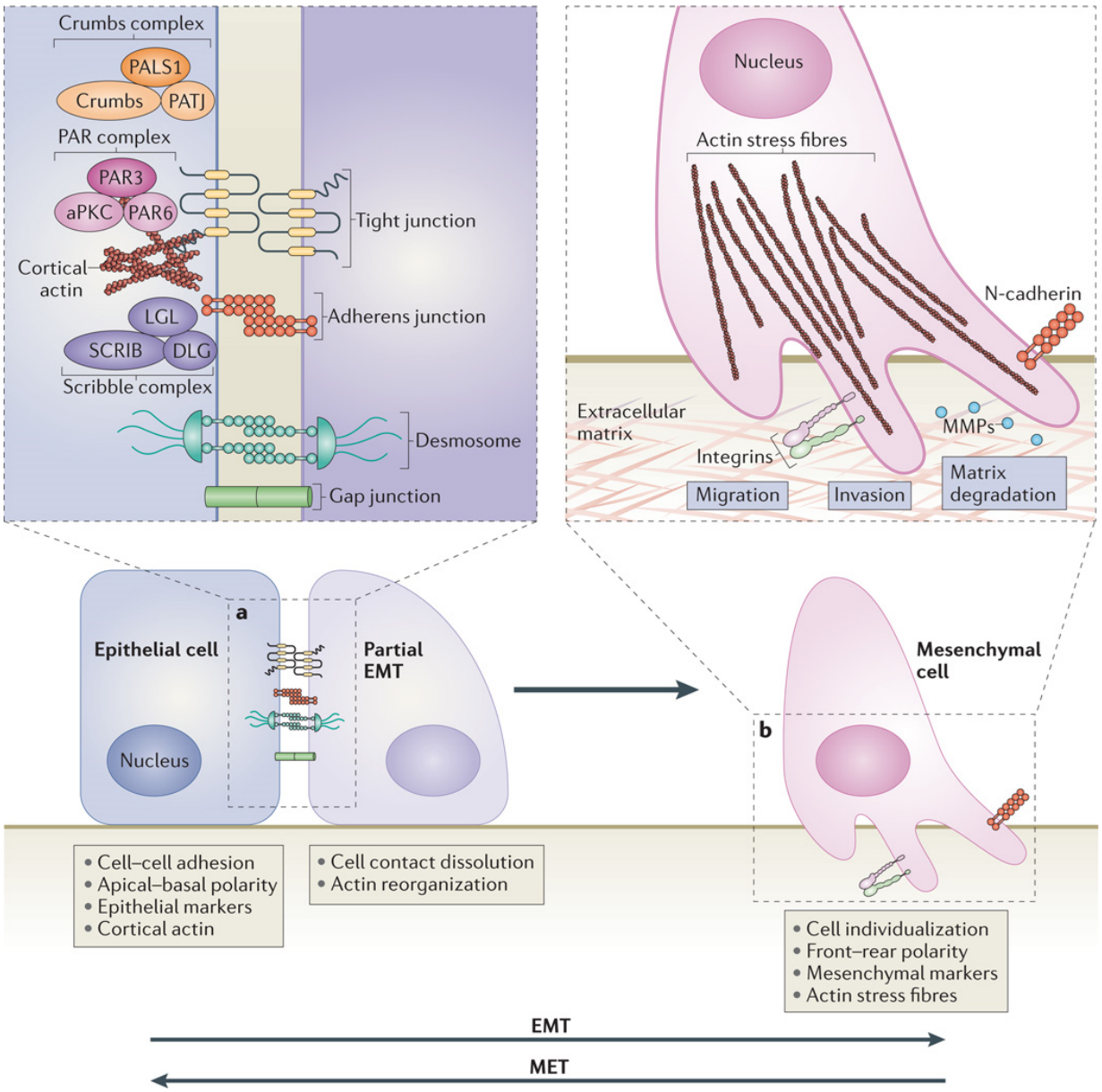

[Image Adapted from (40)]

As these epithelial and mesenchymal gene expressions are altered, the actin architecture is reorganized. Cells start to gain higher motility and invasiveness by upregulating expression of MMPs (Matrix metalloproteinases) which degrade the surrounding extracellular matrix (ECM) proteins. At the same time, developing lamellipodia, filopodia, and invadopodia also contribute to high motility and invasiveness.

2.3.2 EMT Regulatory Network

EMT is regulated by a complex network where EMT-related Transcription Factors (EMT-TFs) are induced or repressed (Figure 2.3.2) (4). The three main EMT-TF families are the L (a zinc-finger-binding transcription factor) (44, 45), TWIST (a basic helix-loop-helix (bHLH) factor) (46, 47) and ZEB (a zinc-finger E-box binding homeobox factor) (48, 49) protein families. Several cell signaling pathways such as TGFβ/Smad, Wnt/β-Catenin, GF/MAPK/NFκB, Notch/NICD, Hypoxia/HIF1α may stimulate the EMT-TFs. At the post transcriptional and translational level, the EMT-TFs can be further regulated. The stimulated EMT-TFs can ultimately lead to EMT (50). With the induction of EMT, several epithelial markers, including E-Cadherin, Occludins, Claudins, Cytokeratin, Epithelial adhesion, and polarity genes which confer adhesive properties, are downregulated. At the same time, several mesenchymal markers responsible for invasion and motility (*e.g.*, N-Cadherin, Vimentin, MMPs, Fibronectin, β1 and β3 integrins), regulation of immunity (e.g. TGFβ, PD-L1, TSP1, CCL2, LCN2) and stemness (Bmi1, Sox2, KLF4) are upregulated (Figure 2.3.2). Cancer cell stemness is a property of malignant tumors, where a group of cells has the capability to differentiate into various cell types within the tumor. Although there is evidence of EMT associated with enhanced stemness of cancer cells, there are some conflicting findings as well (4).

Figure 2.3.2

EMT Regulatory Network

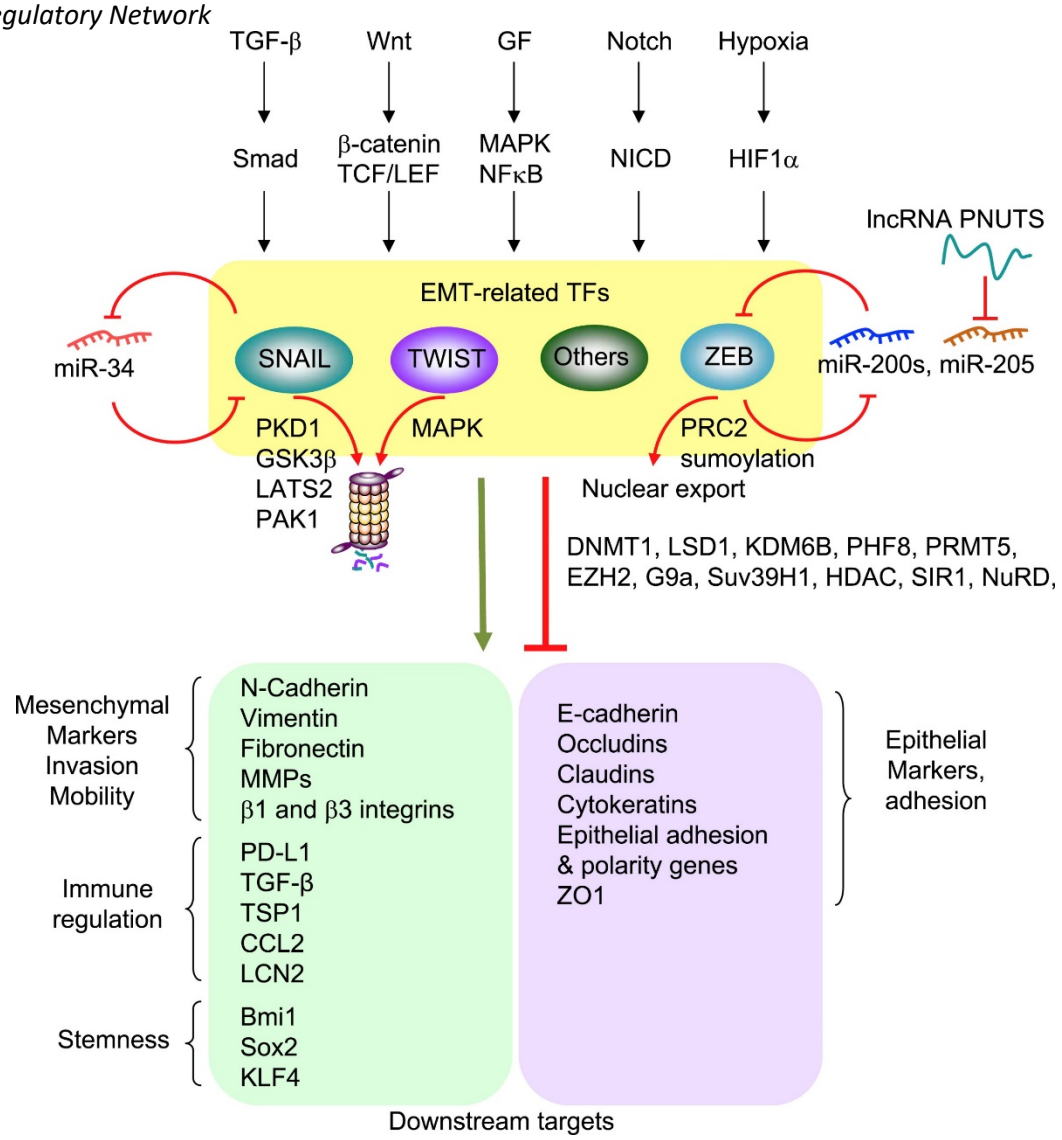

EMT is induced by activating the EMT-related TFs via several signaling pathways including Hypoxia.

[Image Adapted from (4)]

2.3.3 Role and Regulation of EMT-TFs

2.3.3.1 SNAI

The zinc finger binding transcription factor SNAI is one of the major transcription factors that represses E-Cadherin to control EMT (51). It has subfamilies of which SNAI1 and SNAI2 (or SLUG) induce EMT by repressing epithelial markers and by activating mesenchymal markers (52). Several studies have shown the significant roles played by 1 and 2 during embryonic development as well as cancer progression (53-56). Also, it has been established that SNAI1 can induce EMT by suppressing genes responsible for tight junctions and apical-basal polarity (57, 58). Additional studies showed SNAI1 can directly stimulate some mesenchymal genes, including FN1 (a fibronectin gene) and VIM (Vimentin) (59-61). Both SNAI1 and SNAI2 have been reported to act in concert with other EMT-related transcription factors, such as TWIST (40, 62).

SNAI1 can be phosphorylated by GSK3β (Glycogen synthase kinase-3β) in two steps: First, inside the nucleus, phosphorylation causes expulsion of SNAI1 from the nucleus; at the second step GSK3β phosphorylation will facilitate degradation of SNAI1 by ubiquitination (40). PKD1 (protein kinase D1) can also phosphorylate SNAI1 and eject it from the nucleus. However, PAK1 (p21 activated kinase 1) and LATS2 (large tumor suppressor 2) mediated phosphorylation can keep the phosphorylated SNAI1 inside the nucleus, enhancing its EMT induction potential. On the other hand, SNAI2 also activates EMT. SNAI2 is regulated when p53 recruits it to the MDM2 (mouse double minute 2) complex and expels 2 to the cytoplasm for ubiquitination. Major signaling pathways inducing SNAI expression are TGFβ, WNT, Notch pathways, and growth factors (GF) acting through RTK pathways (62).

2.3.3.2 TWIST

TWIST1 and TWIST2 belong to the bHLH family of transcription factors which also induce EMT by suppressing epithelial genes and by stimulating mesenchymal genes (40). However, repression of E-Cadherin by TWIST is not direct, it requires SNAI2 to be activated (63). Like the SNAIs, TWIST1 is also

important for EMT in embryonic development and cancer progression (4). Yang et al. showed that Hypoxia Inducible Factor-1α can stimulate TWIST to induce EMT (64). Overexpression of TWIST has been reported to enhance invasiveness and thereby facilitate metastasis (65, 66). MAPK p38 (mitogen-activated protein kinase) , JNK (JUN N-terminal kinase) and ERK (Extracellular signal-regulated Kinase) phosphorylate TWIST and insert it into the nucleus to induce EMT (40). Under hypoxia, HIF1α is the major signaling pathway inducing TWIST expression, resulting in EMT (64).

2.3.3.3 ZEB

ZEB1 and ZEB2 are the two members of the ZEB family (4). Their binding to the E-box elements is responsible for the suppression of E-cadherin (67, 68). However, they can also repress the expression of other tight junction genes as well as apical-basal polarity complex components, thereby contributing to EMT (69-71). They facilitate EMT progression by inducing the mesenchymal marker proteins vimentin and N-Cadherin as well (71, 72). ZEB proteins are also essential during embryonic development (73, 74). A study published in 2017 showed that expression of ZEB1 in a murine pancreatic cancer model was crucial to initiate metastasis and invasiveness efficiently (75). However, two studies in 2013 and 2014 showed ZEB1 and ZEB2 functioning opposite to each other in malignant melanoma where ZEB1 acted as a tumor inducer while ZEB2 was a tumor suppressor (76, 77).

Regulation of ZEB involves sumoylation of ZEB2 by PRC2 (Polycomb repressive complex 2), which expels it from the nucleus, thereby controlling ZEB activity (40). Also, SNAI1 and TWIST1 have been found to induce ZEB1 expression (78). At the post-transcriptional level, ZEB expression is suppressed by microRNAs (miRNA), especially members of the miR-200 family (79). The major signaling pathways activating ZEB expressions include TGFβ, WNT, and RAS-MAPK signaling activated by growth factors (40, 62).

Apart from the above three major EMT-TFs, there are several other TFs that also take part in regulating EMT. For example, Fox and Sox transcription factors, PRRX1, HGMA2 act as EMT regulators

(30, 40). Also, genetic modifications, alternative splicing, miRNA and other non-coding RNA modulation, and translational and post-translational modifications are also involved in EMT-TFs regulation (4).

2.4 Reactive Oxygen Species (ROS)

Reactive oxygen species (ROS) are continuously generated under aerobic conditions in different cellular compartments including at the plasma membrane, the cytoplasm, peroxisomes, membranes of mitochondria and endoplasmic reticulum, microsomal cytochrome P450 enzymes, and flavoprotein oxidases (80-82). ROS are known to participate in several intracellular signaling programs such as apoptosis, cell cycle progression, and aging. Also, as indicated in Figure 2.3.2, HIF1α can induce EMT via stimulating EMT-TFs (4), particularly the expression of TWIST under hypoxic conditions. Hypoxia enhances oxidative stress at least partly by generating various reactive oxygen species (ROS) which include superoxide (O_2^-), H_2O_2, and hydroxyl radicals ($^{\cdot}OH$) and their reaction products (83). ROS are highly reactive unstable molecules containing oxygen, a high concentration of which may cause cell death via DNA, RNA, and protein damage inside cells (84). Several studies have shown that ROS generation can induce EMT (80, 85-88).

ROS can exist in two major forms: (i) Free Oxygen form [*e.g.* superoxide (O_2-$^{\bullet}$), nitric oxide (NO), hydroxyl radical ($^{\bullet}OH$), sulphonyl radical ($:SO_2$) and (ii) Non-radical form [*e.g.* hydrogen peroxide (H_2O_2), ozone (O_3), singlet oxygen ($^1O_2$), among others (89, 90).

2.4.1 ROS Generation and Its Role in Physiology

The most significant sources of ROS in cells include the oxidation of NADPH by NADPH oxidase (NOXs) (91) or the leakage of electrons from Complexes I or III in the electron transport chain in mitochondria (92). Both processes produce superoxide (O_2-•). One or more forms of superoxide dismutase (SOD) then assist native (uncatalyzed) dismutation and convert the superoxide into H_2O_2 (87). The dismutation reactions as follows (93):

$$2O_2^{\cdot -} + 2H^+ = H_2O_2 + O_2$$

Compared to other ROS, particularly the free radical types, H_2O_2 is more stable and produced substantially inside the cells (94). It is the major ROS known to be involved in the redox-dependent regulation of cellular processes (95-97). H_2O_2 can oxidize cysteine residues of proteins; it is at this point that redox signaling (§2.4.2) is thought to occur (98-100). H_2O_2 can also be converted to hydroxyl free radical when it reacts with transition metal ions (the Fenton reaction) resulting in oxidative stress through macromolecular damage (101). However, cells also produce antioxidants such as peroxiredoxins (Prdx), glutathione (GSH), glutathione peroxidase (GPX), catalase (CAT), which convert H_2O_2 into water (102). The overview of this ROS generation and biological fate has been illustrated in Figure 2.4.1.

Figure 2.4.1

ROS Generation and Roles

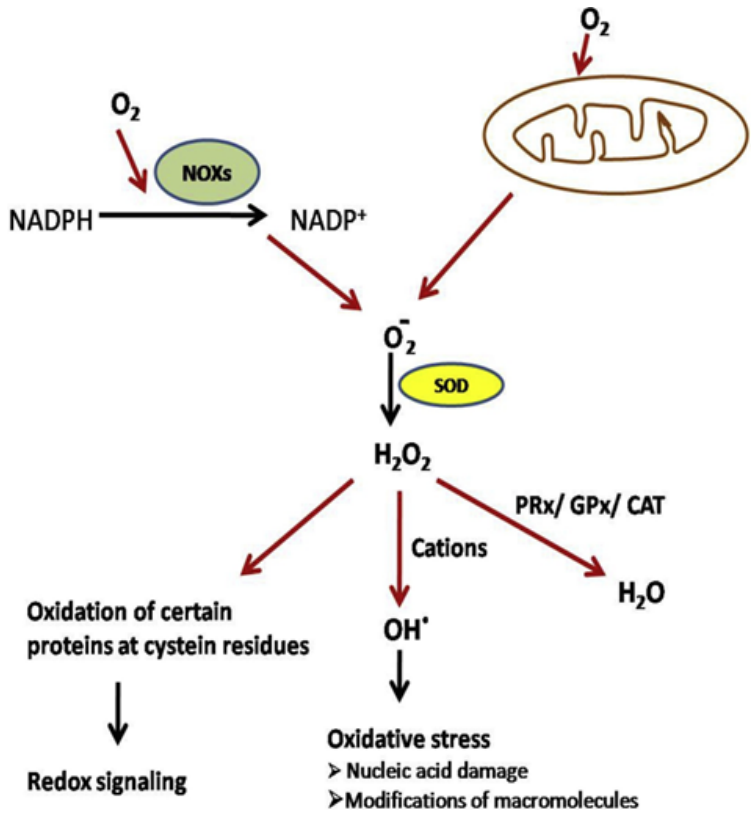

[Images Adapted from (87)]

An important physiological role of ROS is that they are produced in phagocytic cells when destroying engulfed pathogens (103). Therefore, over-production of antioxidants may lead to a pathological state by neutralizing and interfering with this physiological 'waste disposal' function of ROS (104).

2.4.2 Redox Signaling

Redox signaling, which begins after oxidation of cysteine residues of target proteins, is a physiological cell signaling process required for cells to survive and function properly (102, 105). Redox signaling occurs when ROS act as stimuli to modulate the activity of signaling proteins. Redox signaling with an elevated ROS level can also result in a pathological condition (oxidative stress) by the excessive generation of ROS. As a result, levels of different cellular antioxidants including SODs, GSH, GPx, Peroxiredoxin (Prx) are elevated to protect the cells (102). The concentration of H_2O_2 can raise up to approximately 100 nM (106). At a lower concentration of intracellular H_2O_2 enables normal cellular function such as proliferation, differentiation, migration, and angiogenesis (Figure 2.4.2). As the concentration rises a bit more, stress responses and adaptation occur by the cells. However, when the concentration rise even higher, pathological conditions arises including inflammation, fibrogenesis, metastasis, cell death (Figure 2.4.2).

Figure 2.4.2

Estimated H_2O_2 concentrations with related Cellular Responses

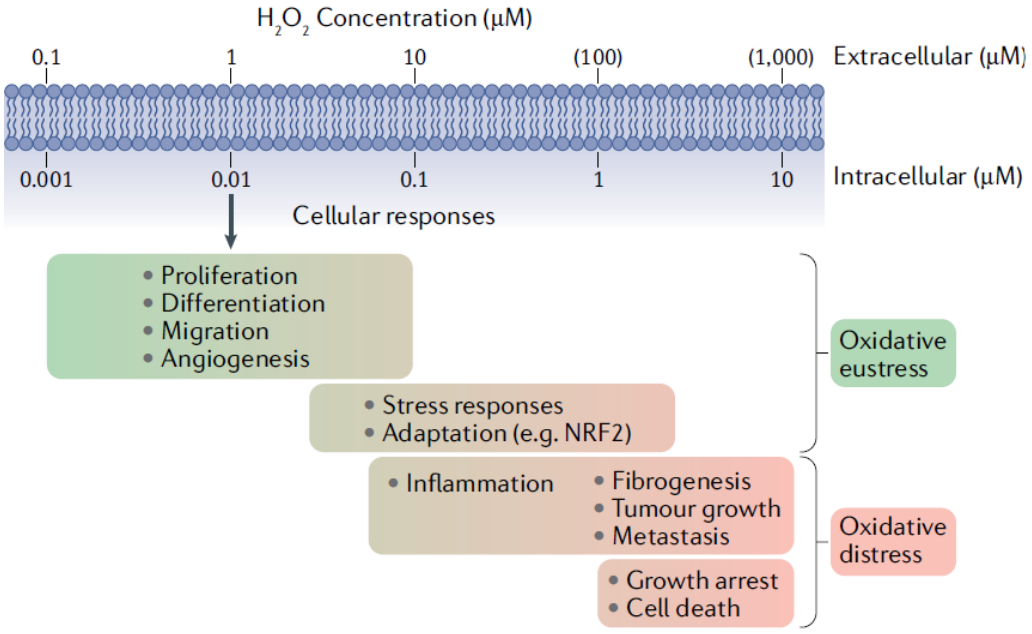

[Adapted from (106)]

ROS signaling has been reported to be involved in tissue homeostasis and adaptation (80). The pathways known to be activated by ROS include Akt/protein kinase B, p42/p44 MAPK, p38 MAPK, Rho-GTPase, the Smads cascades, Ras-Raf-MEK-ERK (extracellular signal regulated kinase), signal transducers and activators of transcription (STAT), and protein kinase C (PKC), NF-κB and p21 kinase. Also, a wide variety of gene families, including MMPs, integrins, growth factors (EGF, EGFR, VEGF, and others), TGF-β, HIF-1, HGF, NADPH oxidases (Nox), p53, Bcl-2, caspase are also reported to be modulated by ROS (107-113). Moreover, some transcription factors including NF-κB, C-Jun and HIF-1 are also reported to be redox sensitive and involved in several cell-survival pathways (109).

2.5 Antioxidants

Antioxidants are substances with the ability to react with and eliminate ROS, thereby reducing their oxidation of cellular components (114, 115). These can be either naturally produced inside the cells (*e.g.,* catalase, thioredoxin reductase, glutathione, and others) (116-120) or can be provided exogenously (*e.g.*, ascorbic acid through citrus, vitamin E through diet, etc.) (121-124).

2.5.1 Catalase

Catalase is a cellular antioxidant enzyme with the capability of neutralizing H_2O_2 by converting it to oxygen and water (125). Additionally, catalase can decompose peroxynitrite (126, 127), oxidize nitric oxide to nitrogen dioxide (128). It also exhibits low oxidase activity (129, 130). The usual subcellular locations of catalase are peroxisomes, cytoplasm and mitochondria (125, 131-133). It is also found in the cytoplasmic membrane of cancer cells (134). It is very hard to measure the exact amount of catalase present in the cells as it is lost during tissue management or processing (135). However, a study showed catalase level along with H_2O_2 removal rate among various cell lines including lung A549 cells (136) (Figure 2.5.1). The study found a strong correlation between the rate constant at which these cell lines remove extracellular H_2O_2 and the effective number of fully active catalase molecules per cell (R^2 =0.88).

Catalase has been reported to be downregulated in many studies leading increased H_2O_2 level (137-141). Such elevated H_2O_2 level can activate pathways leading to cancer cell proliferation, migration and invasion (142-144). Catalase can be inhibited by 3-amino-1,2,4-triazole (3AT) (145-147). A major application 3AT is as a herbicide (148), but it is also teratogenic and carcinogenic (149).

Figure 2.5.1

Catalase Level and Activity among Various Cancer Cell lines

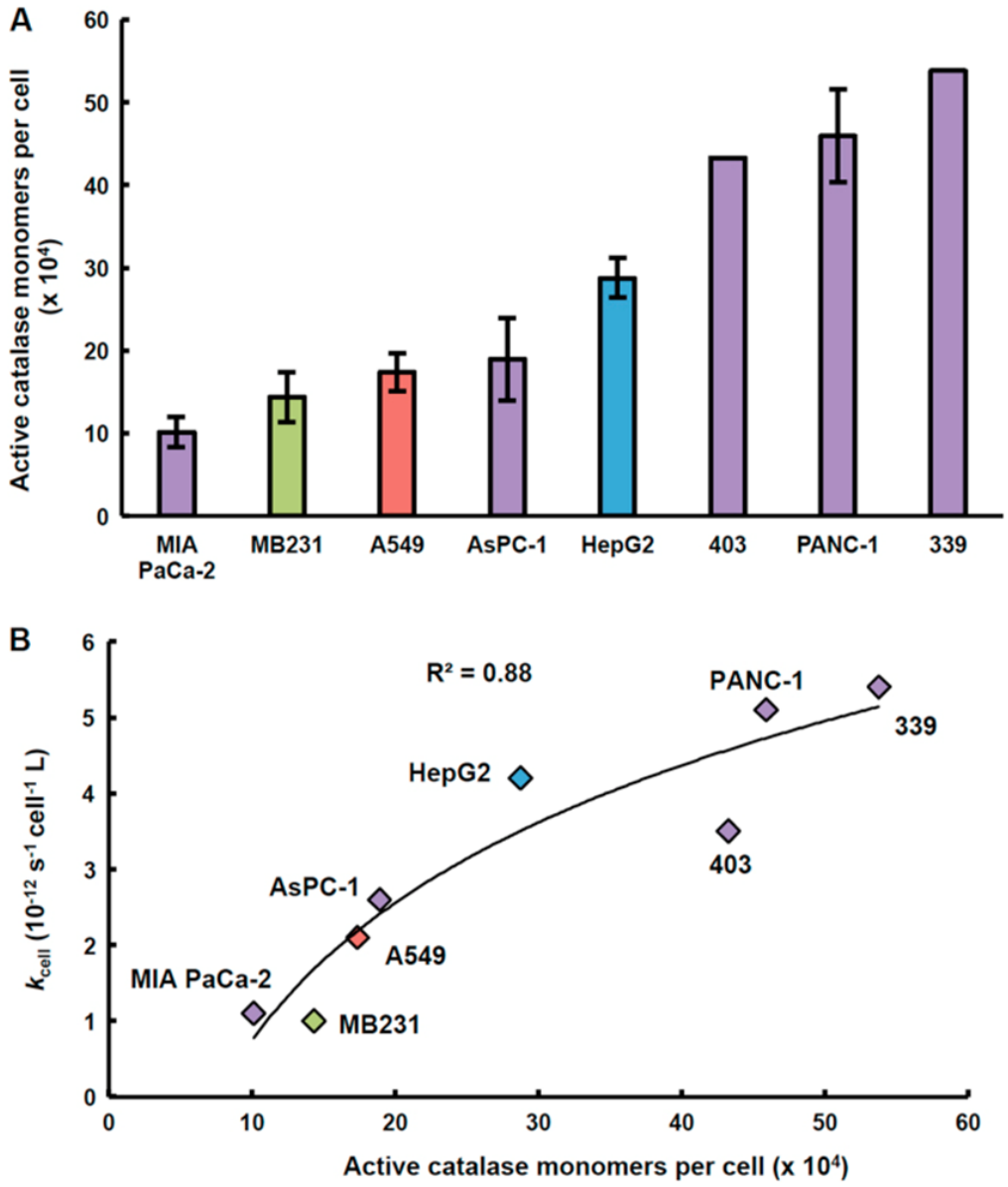

[Adapted from (136)]

2.5.6 Thioredoxin reductase (TrxR)

The thioredoxin system is composed of the small protein thioredoxin along with its cognate reductase enzyme and NADPH (150). These proteins are chemically a part of the flavoprotein family of pyridine nucleotide-disulfide oxidoreductases, which also includes lipoamide dehydrogenase, glutathione reductase, and mercuric ion reductase (151). Inside cells, thioredoxin-I (Trx) and glutaredoxin 1 (Grx1) are present in the cytosol and thioredoxin-2 (Trx2) is in the mitochondria (152, 153). Through the disulfide reductase activity of thioredoxin, this antioxidant system controls protein dithiol/disulfide balance to protect against oxidative stress (154). Additionally, the Trx system has been reported to repair DNA and proteins via reducing ribonucleotide reductase and methionine sulfoxide reductases (150). A study showed Trx expression in some lung cancer lines (155) (Figure 2.5.6). The A549 cell line was found to express a high level of Trx. Auranofin, a gold-containing small molecule, can be used to inhibit TrxR (156) to enhance H_2O_2 concentrations.

Figure 2.5.6

Western Blot Results Showing High Expression Level of Trx among four different Lung Cancer Cell Lines

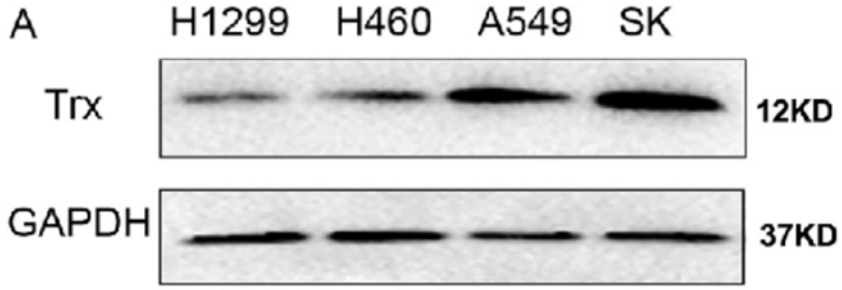

[Adapted from (155)]

ROS can act to either suppress or promote cancer progression. Therefore, the role of antioxidants as cancer treatments is also unclear. For instance, several studies have shown that many forms of glutathione transferases (GST) prevent the progression of skin, liver, and colon cancer in mice (157-160). Glutathione peroxidases (161-163) and TRX system (164) have also been found to suppress tumor growth in several studies. However, these antioxidant systems have also been reported to promote cancer progression. For example, several studies with various glutathione (GSH)-related enzymes such as GPX and GST, and the Trx system have been shown to promote tumor growth (165-172).

However, externally supplied antioxidants may also create oxidative stress. Vitamin C has been reported to generate ROS when it is oxidized to dihydroxyascorbate (173, 174). Alpha-tocopherol (Vitamin E) which is well known to have anti-tumor potential (175) has also been found to promote cancer in a multi-center clinical trial (176-178). N-acetyl cysteine (NAC) and vitamin E have also been found to induce lung cancer and melanoma progression (179, 180).

2.6 Role of ROS in Cancer

The role of ROS in cancer is very dose-dependent, either suppressing or promoting tumor growth (181). The role of ROS in cancer is illustrated below (Figure 2.6.1). Tumor suppression occurs by activation of the Ras-Raf-MEK-ERK pathway which induces the p38 MAPK cascade (182). p38 activation suppresses tumor growth by inducing apoptosis, cell cycle arrest, senescence by oncogenes or inflammation, DNA damage response (DDR).

Figure 2.6.1

Dual Role of ROS on Tumor Suppression and Progression [Adapted from (87)]

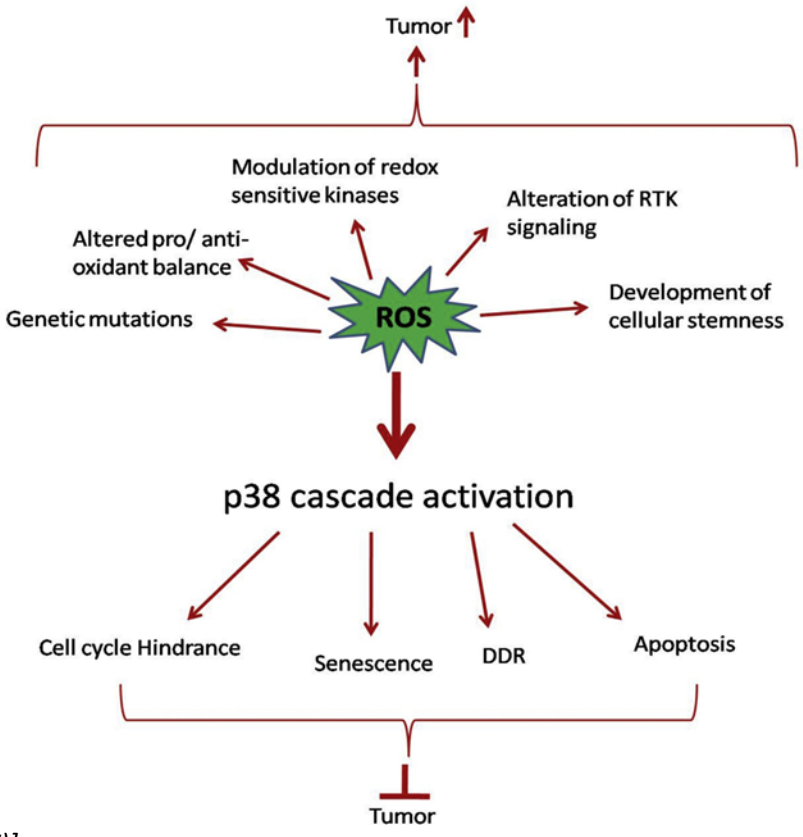

[Adapted from (87)]

Phosphorylation of p38 is reported to activate the tumor-suppressing activities of downstream p53 and $p21^{WAF1}$(182) (Figure 2.6.2). Also, cell cycle inhibitors such as p16INK4A, p14/p19 can also be upregulated to suppress tumor. Regulating kinases associated with DNA damage can also activate p38 when ROS damages DNA (183) (Figure 2.6.2). A co-activator of p53, $p18^{Hamlet}$, can also be stimulated to induce apoptosis (184, 185). DDR activated p38 can also inhibit two important mitotic phosphatases, cdc25B and cdc25C, resulting in cell-cycle arrest (186, 187).

Figure 2.6.2

ROS regulating Ras-Raf-MEK-ERK signaling and p38 Pathway

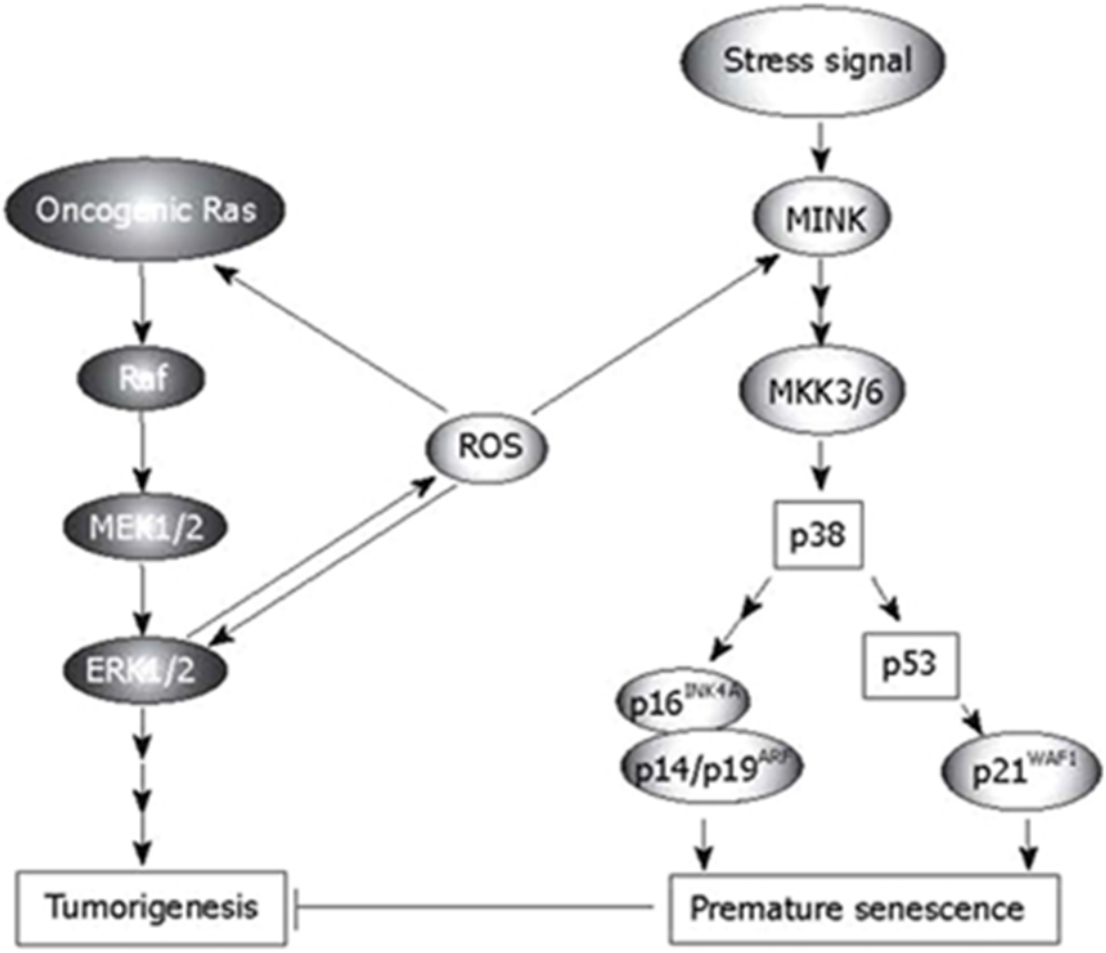

[Adapted from (181)]

One of the major reasons for the stimulation of tumor growth by ROS is that cells continue to grow with damaged or faultily repaired DNA leading to mutations (188, 189). These mutations are base pair deletions in most cases.(190-192). Mutations of oncogenes or tumor suppressor genes are reported to induce tumor progression (189). For example, in p53 tumor suppressor gene, transversions of the DNA bases G to T is very common in cancer (193-195). ROS can modulate the redox sensitive kinases such as Src, JAK, PI3K, Akt, MAPK, thereby activating oncogenes leading to cancer progression (189).

Receptor tyrosine kinases (RTKs) are also known to generate an increased amount of ROS which can be activated by EGF, PDGF, FGF, TNF, IFN-γ, and interleukins (196). Such increased ROS level can activate oncogenic Ras which in turn conveys downstream signaling through Raf, MEK1/2 and ERK1/2 (181) to induce tumor progression (Figure 2.8.1). Several oncogenes, such as c-myc, c-jun, and CREB, can be activated by ERK leading to cell proliferation after inhibiting apoptosis (197). Ras can also be stimulated by ROS generated by NOX-1 enzyme activity, which in turn facilitates angiogenesis via increased VEGF expression (198). This angiogenesis helps provide more nutrients to tumor cells, thereby stimulating their growth and proliferation (199-202). However, oxidative stress from increased ROS can translocate the cytoplasmic transcription factor thioredoxin into the nucleus where it can induce nuclear signaling factors (e.g. redox factor-1) and transcription factors such as AP-1, NFκB, and Egr-1 (203). These transcription factors support tumor growth in various ways. AP-1 activation induces cyclin-D and CDKs leading to proliferation (189, 203). NFκB helps cell survival by- regulating cIAP1/2, Bcl-2 and Bcl-xL (204); by upregulating VEGF and MMP-9 expression, angiogenesis and metastasis are facilitated (205).

2.7 Role of ROS in Ferroptosis

Ferroptosis is an iron-dependent programmed cell death process (206-209). It can occur in many diseases including cancer, neurodegenerative disorders, and ischemia-reperfusion injury, among

others. The process starts with increased intracellular iron concentration leading to increased highly reactive ROS generation particularly by the Fenton reaction. A large amount of ROS utilizes excessive amounts of glutathione (GSH) leaving the membrane lipid peroxidation unchecked. Excessive lipid peroxidation damages the membranes of organelles and/or cell membranes resulting in loss of membrane integrity and ultimately cell death (Figure 2.7).

Figure 2.7

Ferroptosis Regulatory Pathway

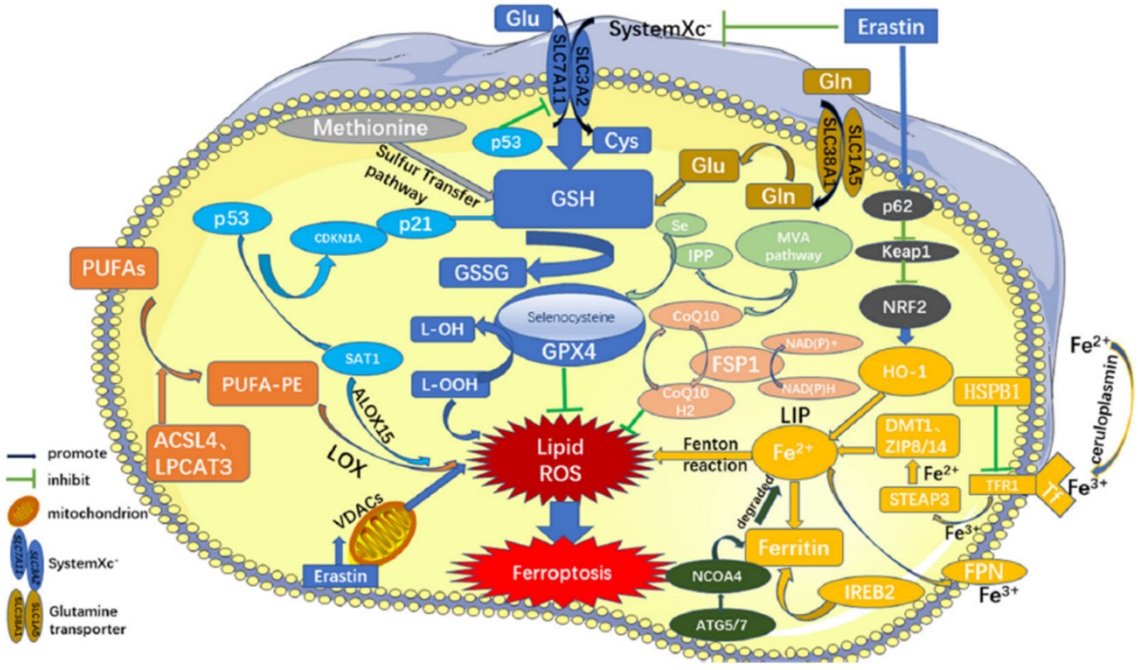

[Adapted from (206)]

The intracellular iron concentration can go increase in several ways (206) (Figure 2.7). Iron is normally transported by transmembrane receptor-1 as Fe^{3+} into the cell, which is converted to Fe^{2+} by Six-Transmembrane Epithelial antigens of the phosphate-3. These Fe^{2+} ions are known as labile iron pool (LIP) which are not membrane bound and are used for normal cellular function. Some are stored complexed with ferritin in the lysosome. Excessive Fe^{2+} can be excreted out of the cells by a membrane transporter FPN (Ferroportin). Overexpression or defective TFR1 and FPN can increase the intracellular LIP. Fe^{2+} from LIP can generate large amounts of highly reactive ROS through the Fenton reaction (Fe^{2+}+ H_2O_2 = Fe^{3+}+ OH^-+ $OH^{\cdot}$). The increased ROS level can oxidize more PUFA-PE (polyunsaturated fatty acid - phosphatidyl ethanolamine) to generate lipid peroxides (L-OOH). GSH is one of the major enzymes neutralizing the ROS and excessive ROS generation due to high LIP leads to overconsumption of GSH. The GSH is also required to activate GPX4 (Glutathione peroxidase) which converts L-OOH into lipid L-OH. As increased ROS overwhelms the GSH dependent antioxidation, GPX4 remains inactive and excess L-OOH are not neutralized. L-OOH cause membrane oxidization leading to loss of membrane integrity. As a result, the cell death takes place.

2.8 Role of ROS in EMT

The role of ROS in EMT has been reported in many studies and reviews (5, 80, 86, 210). TGFβ has been reported to increase ROS level followed by EMT induction primarily through MAPK pathway activation, and then subsequently ERK/Smad pathway (211). Various mechanisms can be involved in these processes. Release of iron (in the form of the labile iron pool [LIP]) from ferritin heavy chain (FHC) was reported for such ROS elevation in the process of promoting TGFβ induced EMT (212). Also, TGFβ can also elevate ROS by inhibiting the mitochondrial complex IV and by the upregulation of NOX4 (213). The antioxidant system can also be disturbed by TGFβ leading to increased ROS level and EMT (210). For example, deletion of GSH is promoted by TGFβ, which leads to imbalanced intracellular redox homeostasis. Several recent studies showed that oxidative stress promotes EMT via TGFβ/Smad,

Wnt/β-catenin, and JNK1/ β-catenin pathways in lens epithelial cells (214, 215). Another study showed that the Wnt/ β-catenin pathway is involved in inducing EMT in liver cancer (216). Also, stimulation of Poly (ADP-ribose) polymerase 3 (PARP3) by TGFβ induced ROS has been reported to promote EMT in breast cancer (217). Such EMT induction by ROS involved TG2-l-E-Cadherin axis modulation to increase SOX2 and OCT4 expression.

TNF-α, an inflammatory cytokine, is also reported to elevate ROS level (80). The increased ROS level can potentially activate NF-κB. Activation of NF-κB has been reported to induce EMT via cell-cell dissociation caused by upregulation of TWIST1, 1, 2 (SLUG) and ZEB1/2 (218). Also, activated NF-κB helps to maintain the mesenchymal phenotype and increases metastatic potential through inducing transcription of vimentin and matrix metalloproteinases as well as CSN2 (COP9 signalosome 2) (219). Dong et al. reported EMT induction in MCF-7 breast cancer cells by TNF-α which was facilitated by NF-κB through upregulation of L (220). Dong et al. reported EMT induction in MCF-7 breast cancer cells by TNF-α which was facilitated by NF-κB through upregulation of or DHMEQ (an NF-κB inhibitor) to reverse such EMT (83, 221, 222). Also, another antioxidant, catalase reversed the NF-κB mediated EMT indicating that H_2O_2 to be a potential inducer of NF-κB mediated EMT (223).

ROS has been reported to induce EMT during hypoxia (87). HIF-1 (Hypoxia Inducing Factor-1) is another important factor known to induce EMT through activating EMT related TFs including TWIST, 1 and ZEB1 (210, 224, 225). ROS has been found to induce EMT via HIF-1/LOX/E-Cadherin pathway (226). Also, β-catenin phosphorylation has been reported to induce EMT through ROS stimulated HIF-1α activation (227). HIF-1 has two subunits, α and β, which form a heterodimer under hypoxic conditions. This heterodimer then binds to the hypoxia-response element (HRE) after translocating to the nucleus (228). The activation of the HIF-1 pathway involves several steps. In the normal cellular oxygen environment, HIF-1 is hydroxylated at several proline residues via O_2, or 2-oxoglutarate (2-OG), and ferrous iron (Fe^{2+}) activation of prolyl hydroxylase domain (PHD) enzymes. In hypoxia, ROS

accumulation causes oxidation of Fe^{2+} to Fe^{3+} (229, 230), at the same time hydroxylation of PHD is blocked. As a result, HIF-1 pathway gets activated. However, a receptor tyrosine kinase member, Axl has been found to be a direct target of HIF mediated EMT (231). Axl can activate Rac1 followed by ROS accumulation. Also, treatment with H_2O_2 causes excessive phosphorylation of Axl, which activates PI3K/Akt cascade resulting in increased cell migration (232).

PI3K/Akt pathway can also activate NF-κB followed by EMT (233) (Figure 2.8.1). PI3K/Akt activation is closely related to GSK-3β inhibition leading to β-catenin stabilization which in turn activates SLUG and upregulates mesenchymal vimentin (234). Apart from Axl phosphorylation, ROS can also suppress phosphatase and tensin homolog (PTEN) activity, thereby inducing EMT (235). PTEN is known for PI3K/Akt regulation and ROS inactivates PTEN by forming a disulfide bond between two cysteine residues (Cys124 and Cys71) (236, 237). The role of PI3K/Akt pathway inducing ROS mediated EMT was confirmed by using wortmannin (a PI3K inhibitor), which hampered ROS production through restricting the translocation of NOX4 (238).

In addition to PI3K/Akt, focal adhesion kinase (FAK) and the tyrosine kinase Src also play vital roles in promoting EMT through regulating actin rearrangements leading to enhanced cell motility (210) (Figure 2.8.1). FAK is a non-receptor type tyrosine kinase known to be expressed ubiquitously. It is involved in signal transduction and facilitates spreading and migration of cells via kinase-dependent or independent mechanisms (239, 240). Lawson et al. reported that FAK recruits talin to nascent adhesions, thereby regulating cell motility (241). An activated FAK-Src complex is formed when clustering of integrin receptors occurs during cell association with extracellular matrix proteins and induces auto-phosphorylation of FAK (242). Activation of FAK then activates RhoA/ROCK pathway which in turn results in focal adhesion (FA) and actin stress fiber formation. Also, another FAK complex known as FAK-p130Cas complex may result in ECM degradation by incorporating MT1-MMP into focal adhesions (243). FAK can also interact with Mdm2 which cause proteasomal degradation of p53 (244).

ROS have been reported to modulate FAK activation, but redox alteration of specific cysteine residues in FAK is not well studied (210). When ROS is generated by NOX enzymes, phosphotyrosine-phosphatase (PTP) is inhibited which increases phosphorylation of FAK^{Y397}. As a result, focal adhesions are stabilized along with actin polymerization (Figure 2.8.1) (245).

Figure 2.8.1

Roles of ROS in Regulating EMT

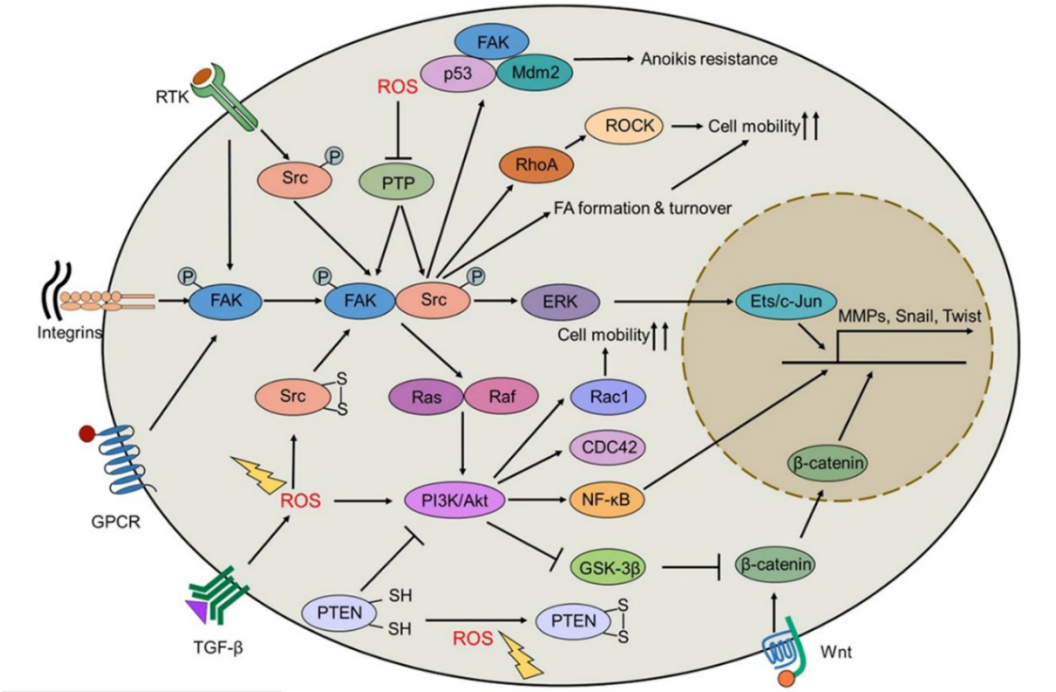

[Adapted from (210)]

Dysregulation of various GF signaling pathways such as EGFR, VEGFR and FGFR, may lead to overexpression of Src in cancer cells. Activation of Src can increase cell motility through focal adhesion turnover, promote cell detachment from tumor via MMP upregulation and E-Cadherin downregulation, and phosphorylation of adhesion components of cadherin e.g. p120-catenin (210, 246-248). Src has also been reported to help maintain the mesenchymal phenotype by disrupting cell adhesion. This disruption occurs when Src cooperates with MAPK and ROCK leading to peripheral accumulation of phospho-myosin(249).

The activity of Src is controlled by phosphorylation of two tyrosine residues Tyr416 (activates Src) and Tyr527 (inactivates Src) (250). Tyr527 phosphorylation is controlled by C-terminal Src kinase (Csk) and Csk homology kinase (Chk). On the other hand, Tyr527 dephosphorylation is induced by PTPs, such as SH2-containing protein tyrosine phosphatase 1/2 (SHP-1 and SHP-2), PEST domain-enriched tyrosine phosphatase (PEP) and low-molecular-weight protein tyrosine phosphatase (LMW-PTP). ROS has been reported to affect the phosphorylation and dephosphorylation of Src. Out of 5 cysteine residues in the Src sequence, two (Cys245 and Cys487) are sensitive to oxidative activation by ROS (251). The importance of ROS to Src activation was proven in several studies. For instance, Src-FAK signaling was inhibited when mitochondrially-derived ROS decreased by the action of tumor suppressor B-cell translocation gene 2 (BTG2) in prostate cancer (252). Also decreased level of NOX-derived ROX inactivated Src (253). Several studies reported reversible oxidation can control the function of PTPs, including SHP-1, SHP-2 and LMW-PTP (254-257). Also, enhanced Src phosphorylation was reported in a number of studies when the cysteine residues in the catalytic PTP domain are altered by oxidation (258-260).

In our project, we investigated the role of metabolically-generated peroxide at different subcellular locations (cytoplasm, nucleus and mitochondria) on EMT progression in lung adenocarcinoma A549 cell lines. However, this project started with investigating the ability of

extracellular H_2O_2 application to trigger EMT, as a study by Gorowiec et al. reported in 2009. In that study, 12 days were required to detect an effect of H_2O_2 on EMT in A549 cell lines (261). Until recently, there was no study on subcellular ROS generation related to EMT. We hypothesized that identifying a subcellular location would suggest where the trigger or target is for EMT induction. As noted previously, EMT is triggered by alterations in the activity of Wnt/beta-catenin, TGFb/Smad, PI3K/Akt pathways. Therefore, in this project, the search for an oxidizable molecular redox alteration target focused initially on beta-catenin, smad2/3 and Akt. A fluorescence technique, redoxifluor, was used to examine both global and protein-specific cysteine-redox ratios. A large change was observed in the global cys-redox after peroxide generation, but so far, nothing was significant for the specific proteins noted above.

The identity of the protein whose oxidation induces EMT is unknown. A multiplicity of protein targets has been proposed (Figure 2.3.2 and 2.8.1), (214, 215, 227, 233), but no definitive identification has been made. Thus we undertook to test the hypothesis that protein-thiol oxidation is responsible for inducing EMT. To test this hypothesis, we investigated three specific aims:

1. To generate H_2O_2 in different locations inside A549 cells using various chemical and biological methods.
    a. Chemogenetic, quinone metabolism and peroxide persistence by peroxidase inhibition were used to increase the concentration of H_2O_2.
2. To evaluate the relationship between H_2O_2 generation at various intracellular locations and the progression of EMT.
    a. Morphology observation, EMT-related marker protein expressions and motility assays were performed to evaluate EMT induction after H_2O_2 generation.
3. To find out the molecular target(s) whose function is/are changed by these cysteine-redox alterations.

a. A fluorescence based microplate technique (Redoxifluor) was used to identify the cysteine-thiol redox state alteration of the potential molecular targets.

CHAPTER 3: MATERIALS AND METHODS

3.1 Cell Culture

3.1.1 Cell Line

Lung adenocarcinoma cell line (A549) was used. Source: ATCC (American Type Culture Collection).

3.1.2 Culture Media, Buffers, Reagents and Routine Procedure

RPMI 1640 medium with HEPES modification (25mM HEPES) from Sigma-Aldrich (Cat# R5886) supplemented with 10% Fetal Bovine Serum (FBS) and Glutamine-Penicillin-Streptomycin (GPS). D-PBS (Dulbecco's Phosphate Buffered Saline; Sigma-Aldrich # D8537), Modified, without calcium chloride and magnesium chloride, was used as wash buffer for cell culture procedures. 1X Trypsin-EDTA (Sigma-Aldrich # T3924) was used for cell recovery procedures. Routine cell cultures were passaged when cells reached 70 – 80% confluence and diluted from 1:5 to 1:20.

3.1.3 Method for Cryo-Preservation of Cells

Cryo-Preservation of cells in multiple vials was necessary for long term storage. After sedimentation, media from above the cell pellet was completely removed. Cells were resuspended in ATCC serum-free freezing media. Samples of 1 mL were added to each Cryo-vial. The vials were placed in an isopropanol bath and slowly frozen overnight at '-80°C'. Then the vials were transferred to liquid nitrogen for long term storage.

3.1.4 Method for Recovering Cryo-Preserved Cells

A vial of cells was removed from liquid nitrogen with appropriate safety precautions. The vial was thawed immediately by holding it under running tap water. Once thawed, the cell suspension was quickly added to 9 mL of RPMI complete media and centrifuged at 200*g* for 5 minutes and resuspended for growth.

3.2 Preparation of Bacterial Growth Media

3.2.1 Preparation of Agar Plates (Ampicillin)

Ampicillin agar plates were prepared whenever required for bacterial transformation. Ampicillin agar plates were prepared as all the plasmids used in this project had the ampicillin resistance site. The formula used for these plates are shown in the table below:

Table 3.2.1A

Formula for a 250 mL LB Agar Solution (Ampicillin Antibiotic final concentration: 100 µg/mL)

Ingredient	Amount
LB Agar Powder (Product#)	10 g
Deionized Water	250 mL
Ampicillin (Product#) 100mg/mL	250 µL

Stock Ampicillin was prepared as a concentration of 100 mg/mL in deionized water, which was then filter sterilized, aliquoted and were stored at -20°C.

According to the formula above (Table 3.2.1A), ingredients were weighed, mixed, and then dissolved the agar with vigorous shaking in an appropriate Pyrex bottle. The bottle was then taken for autoclaving according to the following set-up Condition:

Table 3.2.1B

Autoclave Condition for Sterilizing LB Agar Solution

Exhaust Selector	Slow (Liquids)
Temperature	110°C (230°F)
Timer	30 minutes

After 30 minutes of autoclave, The bottle was then allowed to cool down to 55°C in a pre-set water bath. When the temperature came down to 55°C, 250 µL of stock Ampicillin (thawed on ice) was added carefully to it in a sterile zone and mixed with gentle shaking. Agar solution was then added to each cell culture dish very quickly without forming any bubble (Otherwise the agar solution would solidify inside the bottle). After solidification of agar, the plates were covered, put inside a disinfected storage box, and stored at 4°C.

NOTE: All the steps after autoclaving were performed within the sterile zone created by Bunsen burner flame.

3.2.2 Preparation of LB Broth (Ampicillin):

For bacterial transformation, LB broth was also prepared whenever required. For each 1000 mL LB broth solution 25 g of LB broth powder (Miller) was required. We used to prepare either 400 mL for long term storage (6 months) and 100 mL for immediate uses. The Ampicillin antibiotic concentration was as same as for LB agar plate explained above. The general procedure is explained below:

The required amount of LB broth powder was weighed and mixed with vigorous shaking in a Pyrex bottle. Then it was autoclaved similarly as explained for agar plates. The solution was allowed to cool and when room temperature is achieved, the Ampicillin stock solution was added, then mixed gently in a sterile condition. After mixing the LP broth bottle was stored at 4°C. This solution was suitable to use for 6 months.

3.3 Plasmids Used for Intracellular and Subcellular H_2O_2 Generation

In this project, a total of four different plasmid DNA sequences were used. All of the plasmids had a localization sequence specific to express D-amino acid oxidase (DAAO) which can catalyze the oxidation of a D-amino acid (e.g. D-Alanine) to generate H_2O_2. There was also a fluorescent tag 'HyPer' within the plasmid sequence. HyPer can react with H_2O_2 and increase fluorescence. With increased generation of H_2O_2, the fluorescence intensity of HyPer increases (262, 263). Two different forms

("generations") of 'HyPer' were used; the third generation and the 7th generation named as such by the inventor of the HyPer fluorescent protein (264). The excitation and emission spectra of third generation HyPer are shown in Figure 3.3.A a. Also, it was interesting that with increased concentrations of H_2O_2, the fluorescence intensity goes down in the 420 nm region and increases at about 500 nm (Figure 3.3.Ab) (263). This allows ratiometric analysis of the 'HyPer' oxidation state.

The excitation and emission spectra of the 7th generation of HyPer is shown in Figure 3.3.B below (264).

3.3.1 pAAV-HyPer-DAAO-NES

This plasmid incorporates the 3rd generation of HyPer, the sequence of DAAO (from *R. gracilis*) and expresses HyPer in the cytoplasm, by virtue of the nuclear exclusion sequence (Figure 3.3.1) (262, 265).

3.3.2 HyPer7.2-DAAO-NES

This plasmid was also used to deliver DAAO (Synthetic) with 7th generation 'HyPer' in the cytoplasm (Figure 3.3.2)(266).

3.3.3 HyPer7.2-DAAO-NLS

This is also a plasmid with 7th generation HyPer, but the DAAO (synthetic) and HyPer are expressed in the nucleus with this plasmid (Figure 3.3.3) (266).

Figure 3.3 A

'HyPer' Excitation and Emission Spectra and Fluorescence Intensity Changes with Different Concentrations of H_2O_2

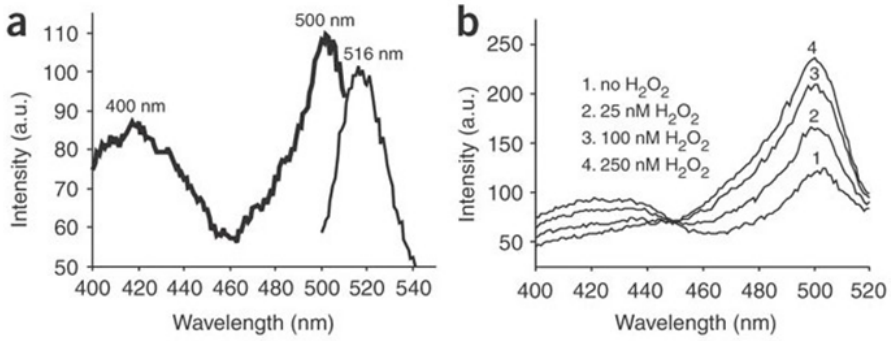

[Belousov et al., 2006 (263)]

Figure 3.3.B

The Excitation and Emission Spectra of 7th Generation of HyPer

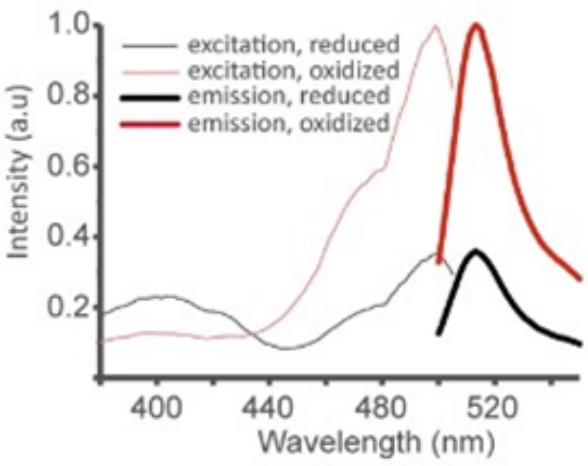

[Pak *et al.*, 2020, (264)]

Figure 3.3.1

pAAV-HyPer-DAAO-NES Plasmid Map

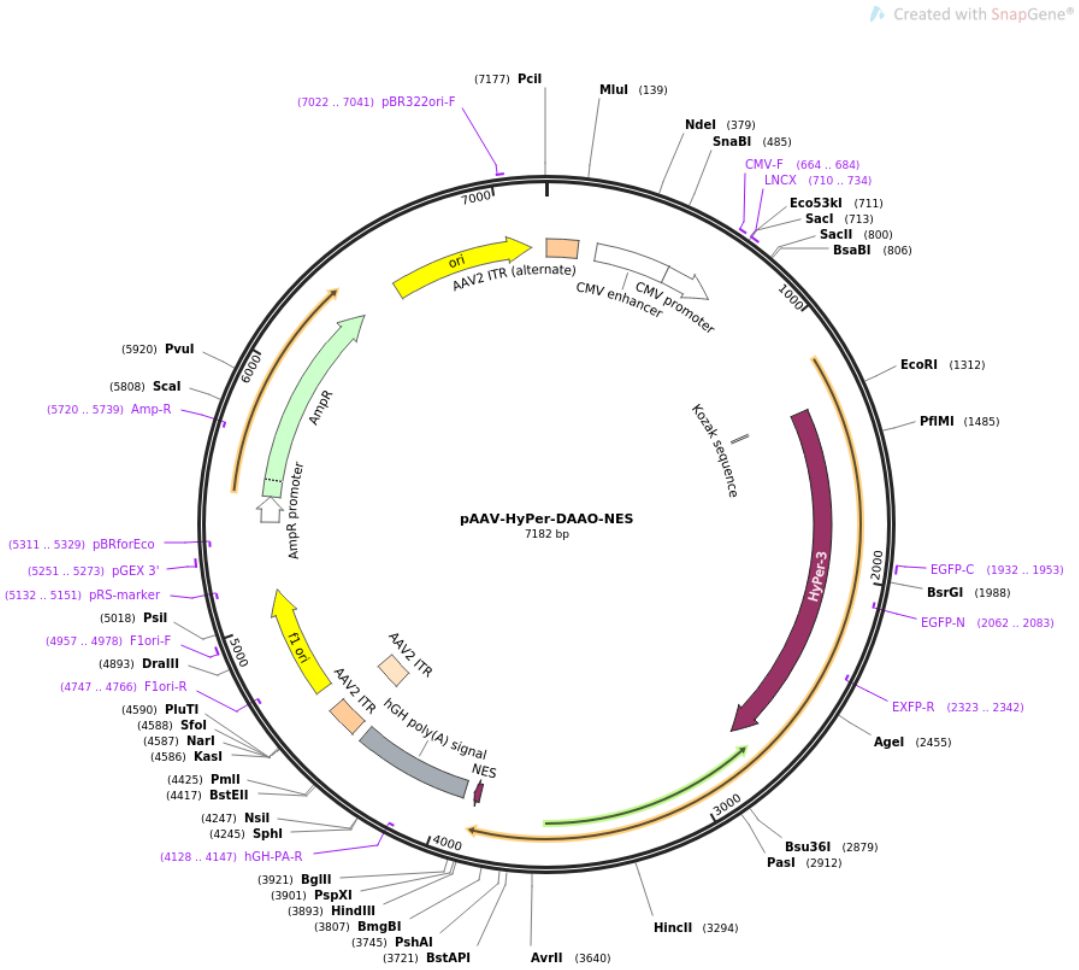

[Adapted from (262, 265)]

Figure 3.3.2

HyPer7.2-DAAO-NES Plasmid Map

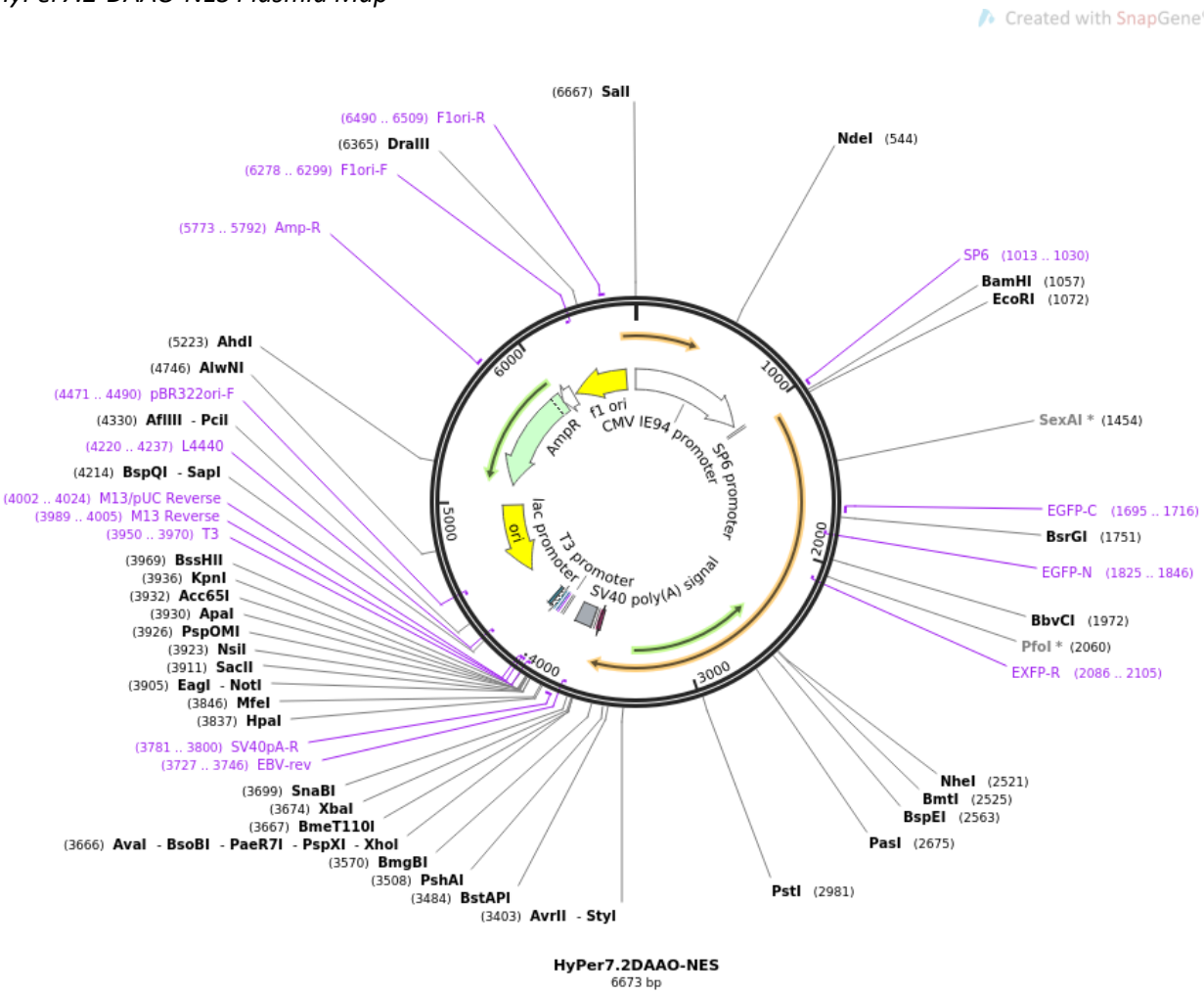

[Adapted from (266)]

Figure 3.3.3

HyPer7.2-DAAO-NLS Map

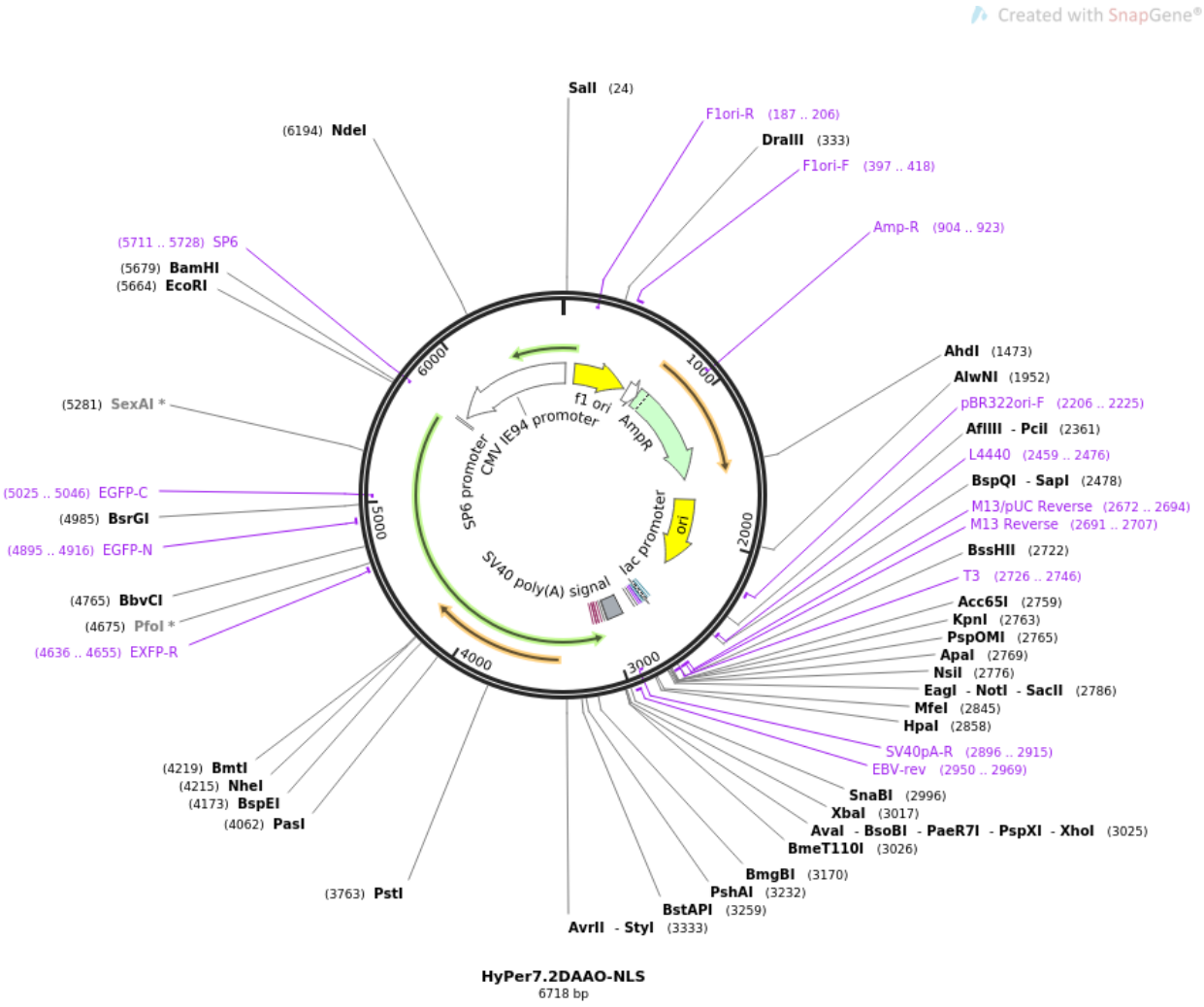

[Adapted from (266)]

3.3.4 HyPer7.2-DAAO-mito

This plasmid was used to deliver DAAO (synthetic) and 7th generation HyPer to the mitochondria (Figure 3.3.4)(266)

3.4 Plasmid Processing Methods

3.4.1 Plasmid Processing Method from Commercial Agar Stab

All plasmids used in this project were received as transformed bacteria in agar stab culture format from addgene (Watertown, MA). Once received they were stored at 4°C before processing (usually stable for about 2 weeks) (267). All plasmids were ampicillin resistant in this project, so only ampicillin agar plates and ampicillin LB broths were used. The plasmids were processed from these agar stabs further by following the general protocol from addgene (267). The procedure involved streaking the bacterial sample on an agar plate and incubating at 37°C for about 24 hours. Next, clear and round single bacterial colonies were selected, transferred to LB broth for overnight (about 12-16 hours) inoculation at 37 °C from where plasmids were purified using 'Monarch Plasmid Miniprep kit' of New England biomedicine (NEB, Cat# T1010S) and following their protocol (268). After purification, the concentrations of plasmids were measured using a NanoDrop spectrometer (ThermoFisherScientific). These purified plasmids were then stored at -20°C freezer.

3.4.2 Bacterial Transformation and Maxi-Prep Purification Method

Bacterial Transformation was performed using high efficiency competent *E.coli*, purchased from New England Biolabs (NEB, Product # C2987H). Important materials required were S.O.C. growth medium (Thermofisher# 15544034), incushaker, Heat block, ampicillin agar plate, inoculating glass spreader, Bunsen burner, 70% ethanol, beaker, ice, and bacterial incubator, Centrifuge Machine Eppendorf 5810R.

Figure 3.3.4

HyPer7.2-DAAO-mito Map

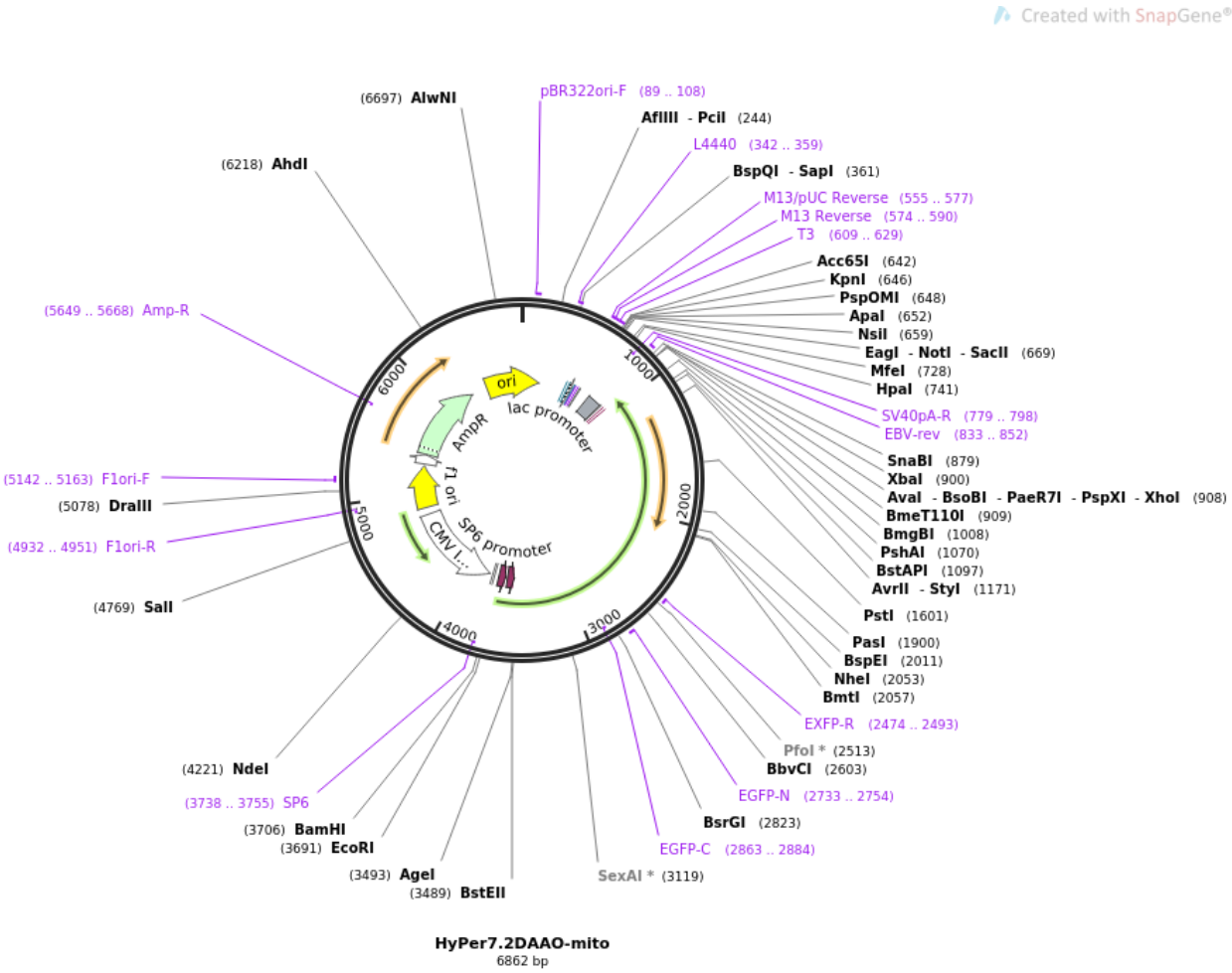

[Adapted from (266)]

The bacterial transformation method was performed according to the guideline from addgene protocol (269). After transformation, further steps of overnight LB broth inoculation and purification were followed according to the protocol of PureLink HiPure Plasmid Filter DNA Purification Kit, (Thermofisher Cat# K210017) (270). The concentration plasmid from each tube was then measured and stored at -20°C. After Plasmid purification, the concentrations of plasmids were measured using using ThermoFisher NanoDrop Lite Spectrophotometer (ThermoFisher).

3.4.3 Restriction Digest Analysis

Using the online NEB cutter tool several restriction enzymes (Single cutter) were found which could be used for the restriction digest analysis. For each plasmid used in this project, we purchased the required enzymes from NEB and the protocols came with each enzyme. We selected the blunt end cutter so that no re-annealing could take place. Both one-enzyme and two-enzyme restriction digest analyses were performed for each plasmid. For pAAV-HyPer-DAAO-NES plasmid (7182 bp), BsaB1 (271) (cuts at 806 bp) and Psil-v2 (272) (cuts at 5018 bp) enzymes were used. For HyPer-7 plasmids, Hpal (273) and PshAl (274) restriction enzymes were used. The cutting positions of these plasmids on HyPer-7 plasmids are illustrated (Figure 3.4.3).

Figure 3.4.3

Cutting Sites on HyPer7.2 Plasmids by HpaI and PshAI restriction enzymes

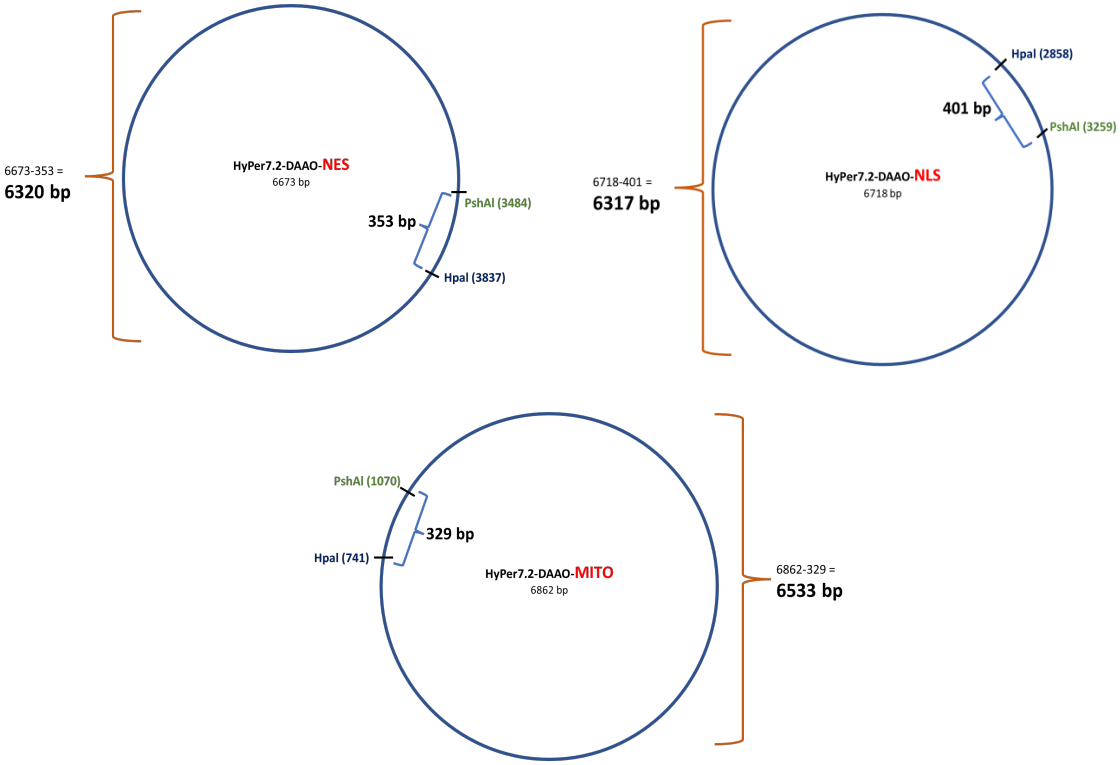

The materials and equipment required for restriction digest analysis included Nuclease free water, Cutsmart or rCutsmart buffers, required enzymes, agarose powder, 1X TAE, gel loading dye (SYBR-Safe DNA Gel Stain, ThermoFisher Scientific, Invitrogen Cat# S33102), DNA loading Buffer (Gel Loading Dye, Purple (6X), NEB #B7025), DNA Ladder (1 Kb DNA Ladder, NEB# N3232S); Heat block, Microwave, Electronic balance. For each restriction digest, maximum 1 ug plasmids DNA was adequate according to manufacturer's guidline. A 50 µL reaction mixture was set up for each plasmid with one enzyme or two enzymes. Here, Formula for restriction digest analysis of HyPer7.2 plasmids using one-enzyme (Table 3.4.3A) and Two enzyme (Table 3.4.3B) methods is shown as an example.

The reaction mixture tubes were incubated at 37C in the heat-block for 15 minutes. Next, 7 µL DNA loading Buffer (Purple) + 7 µL of plasmid DNA from each tube for each sample load were mixed, and transferred into pre-assigned gel pockets (Left side: one enzyme digest; Right side: two enzymes digest). DNA ladder (1kb) was then loaded. The electrophoresis was then carried out for 30 minutes at 100 mV. Then gel was transferred on to a Blue light transilluminator where images of the DNA bands were captured and saved for analysis.

3.4.4 Long Term Storage Procedure of Plasmids

After confirming the purity of the plasmids, it was necessary to make glycerol stocks for the long term storage (275). Addgene protocol was followed here (267). The 50% glycerol solution was prepared by adding 1 part 100% Glycerol to 1-part Sterile Deionized Water. For each plasmid, 500 µL of the overnight LB broth culture was added to 500 µL of 50% Glycerol in each 1.5 mL sterile microcentrifuge tube. In this project, two glycerol stocks were prepared for each plasmid. These glycerol stocks were then stored at -80°C where they should be stable for many years.

Table 3.4.3 A

Formula for One-Enzyme Restriction digest by HpaI:

Component	Amount (µL)
Plasmid DNA Suspension	0.5
rCutSmart buffer	5
HpaI	1
Nuclease-free water	Q.s to make 50 µL (Here, 43.5 µL)

Table 3.4.3 B

Formula for Two Enzyme Restriction digest by PshAl and Hpal:

Component	Amount (µL)
Plasmid DNA Suspension	0.5
rCutSmart buffer	5
PshAl	1
Hpal	1
Nuclease-free water	Q.s to make 50 µL (Here, 42.5 µL)

3.5 Transfection Methods

A549 cells were transfected with various plasmids containing H_2O_2 generator DAAO with localization sequences for cytoplasm, nucleus, and mitochondria. For transfecting the cells both chemical and electroporation methods were used. For chemical methods, Lipofectamine 3000 Transfection Reagent (ThermoFisher # L3000015) and PolyJet *in Vitro* DNA Transfection Reagent (Signagen # SL100688) were used. Methods with both chemical reagents are described as follows:

3.5.1 Transfecting A549 Cells with Lipofectamine 3000 Transfection Reagent

This reagent was used at the initial stage of this project. pAAV-HyPer-DAO-NES plasmid which contained the third generation of HyPer was mostly transfected with this reagent (Thermofisher Cat# L3000015). The typical method involved seeding the cells a day before in such concentration so that they reach about 70-80% confluency at the time of transfection. Then transfections were carried out in antibiotic-free RPMI Media following the manufacturer's protocol (276), returned to the CO_2 incubator at 37°C. After 2 days, the cells were observed with EVOS Auto microscope for transfection efficiency and quality.

3.5.2 Transfecting A549 Cells with PolyJet In Vito DNA Transfection Reagent

Due to very high toxicity, use of the Lipofectamine 3000 reagent was discontinued. PolyJet *In Vitro* DNA Transfection agent (Signagen, Frederick, MD) (Cat# SL100688) was used as the alternative which showed much better transfection efficiency with almost no cytotoxicity. After performing a few trials of DNA to PolyJet ratio, 1:2 ratio was found to be optimum for transfection in A549 cells. Cells were seeded a day before transfection at such number so that they reach at least 70-80% confluency at the time of transfection. The transfection was then carried out according to the manufacturer's general protocol (277). Transfection efficiency and quality were observed under the EVOS auto microscope 1 – 2 days after transfection.

Electroporation method of transfection was also attempted using the Beckman xxx instrument. With several modifications of the protocol, optimization was attempted. However, electroporation did not show better results compared to the chemical methods. As this method was not used to observe any end results, the method is not described here.

3.5.3 Method of Observing Transfection Efficiency

To observe transfection efficiency, the GFP (Green Fluorescent Protein) channel in the EVOS auto microscope was used. HBSS (Hank's Balanced Salt Solution, Sigma# H8264) was used instead of regular media to avoid background of phenol red. Both 10x and 20x lenses were used. With 10x objective lens, the efficiency of transfection was evaluated whereas with the 20x objective lens the subcellular localization was confirmed.

3.5.4 Methods to Evaluate 'HyPer' Function in Transfected Cells

It was necessary to confirm if 'HyPer' is responsive to increased H_2O_2 production inside the cells. To do so two approaches were taken: first with GFP and CFP channels of EVOS Auto microscope and second with chemiluminescence method using 'AquaSpark Peroxide Probe 510' (BioSynth # A-8170_P00). The first method worked conveniently with the early generation of HyPer plasmid (pAAV-HyPer-DAAO-NES) as their excitation and emission wavelengths were very close to GFP and CFP.

3.5.5 Fluorescence Microscopy Based Evaluation:

24 well plates were used for these experiments. Cells were transfected with pAAV-HyPer-DAAO-NES plasmids. After 48 hours of transfection, media was replaced with HBSS and the transfection was confirmed with EVOS Auto microscope in the GFP channel. The 'Time Lapse' recording function was set up to take images of specific cells from each well at fixed intervals (both GFP and CFP channels). After the first set of images were acquired, D-Alanine solution (at various concentrations depending on the experiment) was quickly added to the assigned wells. The time lapse was run for about 2 hours in most experiments. At the end of time lapse imaging, the images were collected and analyzed using the

Fiji (Image J) software and the statistical analysis was performed using GraphPad Prism. This method was not compatible with the latest generation of HyPer7.2 plasmids as their excitation and emission spectrum were too remote from the GFP and CFP channels and our EVOS Auto microscope did not have the appropriate channels to detect the fluorescence changes of HyPer7.2 (Figure 3.2). So, the second method, the chemiluminescence method was used to determine HyPer7.2 functionality.

3.5.6 Chemiluminescence Assay Based Evaluation:

Luminescence assays involve quantifying an analyte by chemical generation of a light-emitting unstable structure. The usual range of luminescence is from 300 to 800 nm in the visible to near visible range (278). In this project, AquaSpark™ 510 Peroxide Probe (Biosynth-carbosynth, Tel-Aviv University) (279) was used to determine the amount of H_2O_2 generated by various metabolic reactions, including DAAO and the metabolism of dimethoxy-naphthoquinone and menadione It is a dioxetane based molecule which can react with H_2O_2 and result in luminescence (280).

In this method, a 96-well plate was used where cells were transfected with HyPer7.2 plasmids. After 48 hours of transfection, the transfection efficiency as well as subcellular localization were confirmed by EVOS Auto Microscope in the GFP channel. AquaSpark-510 solution was prepared by diluting the 10mM stock solution 1000 times. Media from all wells were removed and washed with 1X D-PBS. Diluted AquaSpark solution was added to each well (100µL/well). Treatments of D-Alanine and other controls were added to wells in at least quadruplicate. The plate was then placed in the plate reader (Spectramax ID3) and the light production of each well was measured every two minutes for 3 hours at the following setup (Table 3.5.6):

At the end of reading/scanning, data were transferred to Microsoft Excel. The Data were first organized in Excel to integrate 20 to 60 minutes of data after an initial dark-adaptation period and then statistical analysis was performed using GraphPad Prism.

Table 3.5.6

Plate Reader Scan Parameters for Chemiluminescence Assay

Kinetic	Luminescence	Plate Type	More Settings	PMT & Optics
Time: 3:00:00 Interval 00:02:00 Reads 91 Reading from B2:G11	LM1=All	96 Well Coastar Blk/Clrbtm Up Height 14.3mm (no lid)	Read Order Column Temperature = 37°C	Integration 1000msec Read Height 1.00mm

3.6 Methods to Induce Redox State Alteration

Several methods were applied to induce redox state change in A549 cells.

3.6.1 By Applying Extracellular H_2O_2

Media from the plates/wells were removed, washed with D-PBS, then cells were treated for 1 hour with 400 µM H_2O_2 in serum-free RPMI stock media supplemented with antibiotics. After 1 hour, treatment media was replaced with RPMI complete media and returned to the CO_2 incubator at 37°C where cells were allowed to grow further.

3.6.2 By Generating Intracellular H_2O_2 with Chemo-Genetic Approach

Cells were seeded in 100mm cell culture dishes and transfected with specific plasmids for expressing the H_2O_2 generator D-amino acid oxidase at different subcellular locations. After 48 hours of transfection, specific subcellular transfection was confirmed with EVOS Auto microscope on GFP channel. Then cells were detached by trypsinization, resuspended in 2 mL RPMI complete media, counted using the Specter 3 Automatic cell counter. A specific number of transfected cells were then seeded into 6-well plates or new cell culture dishes. Cells were then allowed to attach and grow for at least 12 hours. Next, cells were serum starved for at least 24 hours (in some experiments, serum starvation was not applied). After 24 hours of serum starvation (or 36 hours after re-seeding), a specific concentration of D-Alanine (according to the specific experiment plan) was added to the cells. Controls in this method were untreated cells, D-Alanine with Peroxidase inhibitors (3-Aminotriazole, Auranofin). Treatment was applied for various durations, but in most experiments, it was for about 24 hours.

3.6.3 By Generating Cytoplasmic H_2O_2 Chemically with DMNQ (2,3-dimethoxy-1,4-naphthalenedione)

Cells were seeded and on the next day when they reached at about 70% confluent, serum starvation started. After 24 hours of serum starvation, DMNQ solution in RPMI complete media (in most cases 10 µM) was added, incubated inside the CO_2 incubator at 37°C for 1 hour. After 1 hour, treatment media was replaced with fresh RPMI complete media, and returned to the CO_2 incubator at 37°C.

3.6.4 By Inhibiting Peroxidase Inhibition

This method also did not require any transfection but was performed on both transfected and non-transfected cells. The initial steps are the same as discussed for both transfected and non-transfected cells. After 24 hours of serum starvation, media was removed and peroxidase inhibitor solutions made in RPMI complete media (25mM 3-amino-1,2,4-triazole (3AT) or 2 μM Auranofin either alone or together) and then returned to the CO_2 incubator at 37°C. After 6 hours, treatments were removed, fed with fresh RPMI complete media, and returned to the CO_2 incubator at 37°C.

3.7 Evaluating EMT

EMT progression of A549 cells was measured in several ways after altering the redox state. Transforming Growth Factor β1 (TGFβ1 5 ng/mL or 10 ng/mL) was used as a positive control and untreated cells were used as a negative control. TGFβ1 was usually applied to cells 48 hours prior to the last day of growth. The progression of EMT was evaluated by the following methods:

3.7.1 By Morphology Observation

After removal of the redox state alteration treatments, cells were allowed to grow for up to 8 days. There was a 50% media change every other day during this period. With a phase contrast microscope, cells were observed for any phenotypic changes from Day 03, 05, and 07 after removal of thiol redox treatments. The mesenchymal cells would show elongated spindle like shape, loosely connected with surrounding cells.

3.7.2 By Scratch-Wound Healing Assay

These experiments were performed in 6-well plates following a well-established protocol and optimizing the conditions for our laboratory (281). After removing the redox state altering treatment, cells were allowed to grow for 5 to 7 days with 50% media replacement every other day. Two days before the cell lysate collection (either day 03 or day 05, dependent on experiment plan), cells were scratched horizontally and/or vertically with a 200 μL sterile pipette tip. Images of scratch areas at

specific points were captured using the 'Time Lapse' function of the EVOS Auto microscope at 10x lens Phase contrast mode. Images from the same location were captured at different intervals (usually at 12 hours, 24 hours, 36 hours and 48 hours). After collecting all the images, data were saved electronically. Images were then analyzed using (Fiji InageJ) software with the Montpellier Resources Imagerie Wound Healing Tool plugin (Montpellier, France). The wound healing was measured as percent (%) of open area from time zero '0'. These data were then statistically analyzed by GraphPad Prism software.

3.7.3 By In-Cell Western (ICW) Method

These experiments were performed using black-sided, clear-bottom 96-well plates and optimizing the well-established protocol of LI-COR or our laboratory conditions (282). After removing the redox state altering treatments, cells were allowed to grow up to 5-7 days with 50% media replacement every 48 hours. On the final day, media from all the wells were discarded, washed with D-PBS and fixed with Four percent formaldehyde solution (made in D-PBS). After fixation, formaldehyde solution was discarded, cells were permeabilized with 0.1% Triton-X washes (prepared in D-PBS), and then blocked with either (i) Odyssey Blocking Buffer (OBB) or (ii) Intercept Blocking Buffer (IBB) for about 2 hours at room temperature. Primary antibody solutions (prepared by diluting them in OBB or IBB) were added at the end of blocking to appropriate wells according to a pre-set plate map. The plate was then wrapped with foil, incubated overnight at 4°C on a rocking table. Next day, Primary antibody solutions were discarded, cells were washed with 0.1% Tween 20 in PBS, secondary antibody solution with Cell tag 700 Stain (LICOR # 926-41090) in OBB or IBB was added to each well, incubated at room temperature on the orbital shaker (100 RPM) for 2 hours. Next, antibody solutions were then discarded, washed with 0.1% Tween 20 in PBS. At the end of the final wash, the wash buffer was discarded and taken for scanning with an Odyssey CLx Imaging System. The scanning was performed in plate mode using both the 800 and 700 channels, data were saved and stored electronically. LICOR ImageStudio

software was used to analyze the data, transferred to an excel sheet where data were organized. Statistical analysis was performed using GraphPad Prism.

3.7.4 By Western Blot (WB)

The Western blot experiments were performed by optimizing the general protocol for Western Blotting (283) from BIO-RAD according to our laboratory conditions. The cells were grown and treated in either 100 mm cell culture dishes or 6-well plates for these experiments. After removing the redox state altering treatments, cells were allowed to grow from 5-7 days with 50% media replacements every other day. Pre-diluted 1X RIPA Buffer solution was supplemented with 5 µL/mL of Protease Inhibitor Cocktail (Sigma) and 5 µL/mL of 200 mM phenyl methyl sulfonyl fluoride solution (in ethanol), added immediately before cell lysate collection.

3.7.4.1 Cell Lysate Preparation

Media from the well or petri-dish was removed, washed with ice cold D-PBS. 1X RIPA Buffer was then added to the well/petri-dish (250 µL /well of 6-well or 1 mL/100 mm petri-dish). Cells were scraped, cell lysate from specific well/petri-dish was collected in the respective ice-cold microcentrifuge tube. Next, these tubes were centrifuged at 14,000 RPM for 20 minutes at 4°C. After centrifugation, the supernatant solutions were collected in other ice-cold microcentrifuge tubes. 10 µL from each sample tube was taken and added to 90 uL of Deionized water (10 fold dilution) to perform protein quantification by BCA Assay (will be discussed later). At this point, the lysates were divided into aliquots and stored at -80°C.

3.7.4.2 Buffer Preparation

1X Tris/Glycine/SDS Electrophoresis Buffer (BioRad # 1610772 diluted in deionized water) was used as Running Buffer, 1X Tris-Glycine Buffer (BioRad# 1610771 diluted in deionized water and ethanol) was as Wet-Transfer Buffer, and 0.1% Tween 20 in PBS+deionized water was used as Wash Buffer.

Blocking Buffer was purchased from LICOR (Intercept Blocking Buffer, IBB, LICOR# 927-70001). Buffers were stored at 4°C before proceeding for SDS gel Run step.

3.7.4.3 SDS-Gel Run

Materials and equipment needed: Laemmli Buffers (either 2X (BIO-RAD# 1610737) or 4X (BIO-RAD # 1610747) supplemented with 2-Mercaptoehanol, Criterion Cell SDS Gel Electrophoresis system (BIO-RAD# 1656001), Criterion pre-cast TGX gels (types varied depending on the experiment need) from BIO-RAD, BIO-Rad PowerPac basic (BioRad # 1645050).

After thawing the cell lysate aliquots, gel loading samples were prepared by diluting each sample with deionized water and Laemmli Buffers according to pre-calculation. In each diluted sample, the total protein amount was 20 μg, final Laemmli buffer concentration became 1X. These loading samples were then boiled at 95°C for 5 minutes, then allowed to cool down to room temperature. While cooling, the Criterion Cell SDS Gel Electrophoresis system was prepared by placing two Criterion pre-cast TGX gels (types varied depending on the experiment need) immersed in running buffer. After cooling to room temperature, samples and protein ladders were loaded on gels according to a pre-set gel map. The gel was then run with the Bio-Rad PowerPac basic for 60 minutes (80V for 5 minutes, 150V for next 5 minutes and finished at 200V for about 50 minutes).

3.7.4.4 Blotting

Nitrocellulose membranes (Bio-Rad # 1620112) were prepared to match the gel size used, soaked in transfer buffer at 4°C. When electrophoresis was finished, each gel was attached to a nitrocellulose membrane at the center of the blot cassette, sandwiched by filter paper and sponges on both sides. The blot cassettes were then placed in the transfer tank immersed in Transfer Buffer. A gel pack and magnetic stirrer were added to the tank. The tank was closed and was run at 4°C, at 100 V for 60 minutes.

3.7.4.5 Blocking and Primary Antibody Incubation

After the blot transfer, the nitrocellulose membranes were carefully separated from gels, cut into two pieces with the help of ladder guide in such a way that the top part contained the target protein, and the bottom part contained the loading control protein GAPDH. Each part of the membrane was transferred, completely immersed in IBB inside an opaque black incubation box, blocked by incubation for about 1 hour on an orbital shaker at 100 RPM at room temperature. Next, Blocking buffers (IBB) were removed, the primary antibody solutions were added to their assigned boxes and incubated overnight on a rocker at 4°C.

3.7.4.6 Secondary Antibody Application

On the next day, the primary antibodies were removed, washed at least 3 times with wash buffer (on orbital shakerat 100 RPM for 5 minutes). Secondary antibody solutions (IRDye 800; LICOR in IBB) were added and incubated at room temperature on the orbital shaker at 100 RPM for 1-2 hours. The membranes were washed at least 3 times with the wash buffer followed by one wash with 1X PBS and scanned with an Odyssey CLx system. After the scan, data were saved and stored electronically, protein expression was quantified with ImageStudio software, data were organized in excel sheet and then statistically analyzed with GraphPad Prism software.

3.8 BCA Assay for Protein Quantification

The bicinchoninic acid (BCA) assay was performed to determine protein concentration in the cell lysates collected for western blots. Pierce BCA Protein Assay Kit (Thermoscientific Cat# 23225 and 23227) was used for these assays. The cell lysate samples were diluted 10 times and the microplate protocol was performed following the manufacturer's procedure (284).

3.9 RedoxiFluor Methods

RedoxiFluor is a recently-developed fluorescence method for measuring protein thiol redox changes across global cellular proteins as well as measuring thiol redox changes in individual proteins (6)

(Figure 3.9). The method involves sequential derivatizations with thiol-reactive fluorescent tags, before and after mild chemical reduction of thiol oxidation products.

Figure 3.9

Redoxifluor Technique

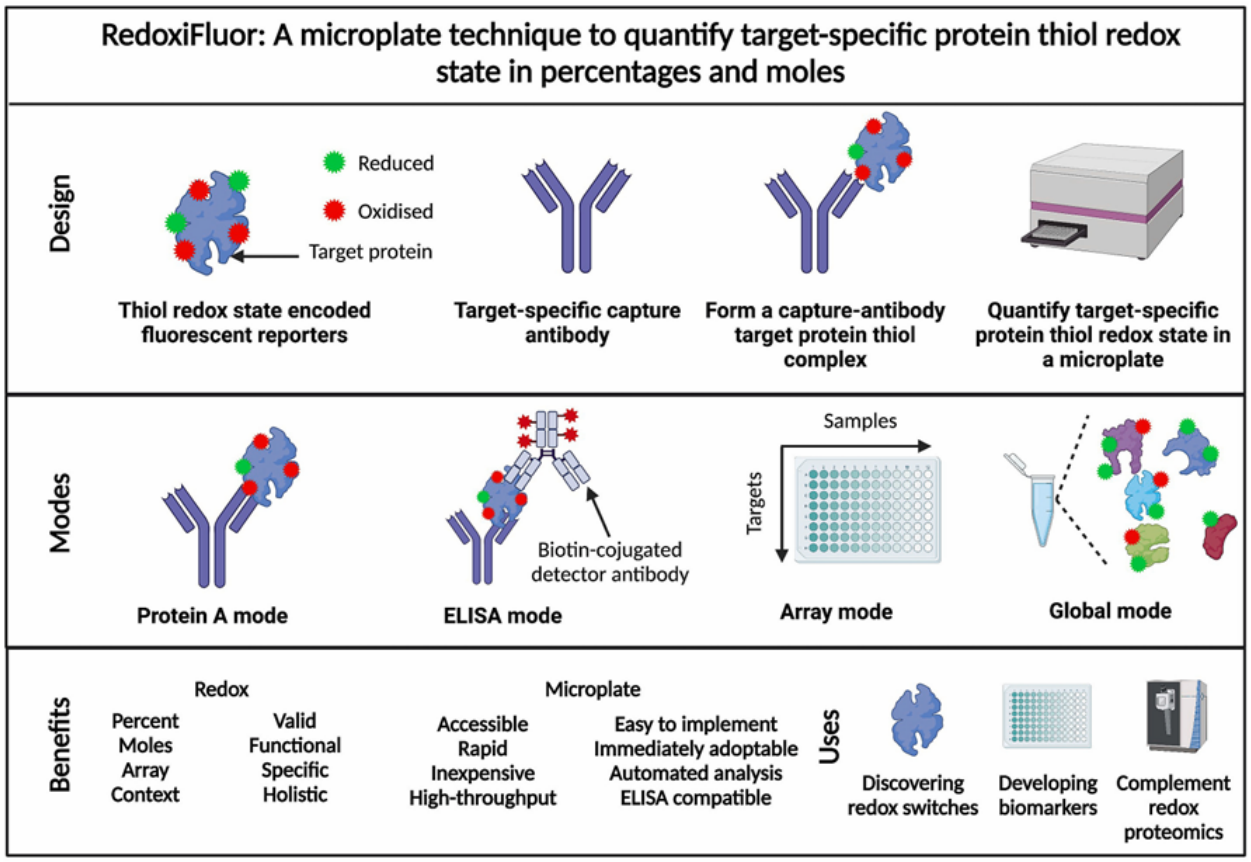

[Adapted from *(6)]*

Reduced thiols are labelled as ‘Green’ and oxidized thiols as ‘Red’ with thiol reactive maleimide fluorescent reporters (Figure 3.8). Depending on the target protein, a specific capture antibody is immobilized in a microplate. The target protein from the samples is captured by this antibody which can then be measured using a microplate reader. This method can be used in different modes such as Protein-A mode, ELISA mode, array mode and the global mode. Protein A mode is used to quantify relative thiol redox state change in percentage, ELISA mode can be used for quantifying the changes in percentage and in moles.

In Redoxifluor method, the fluorescent maleimide (F-MAL1) is used to bind to the reduced thiols by thioether bond utilizing the Michael addition reaction (6). Then, by using 1-4-dithiothreitol (DTT) or tris-carboxyethylphosphine (TCEP), the reversibly oxidized thiols (RS_{OX}) are reduced to maleimide reactive sulfhydryl state (RSH/RS−) via sulphur exchange reactions. After that the second fluorescent maleimide reporter (F-MAL2), which is spectrally different, is used to label the sulfhydryl state (RSH/RS−). Using a plate reader, the signals from F-MAL1 and F-MAL2 can be measured and then be used to calculate thiol-redox state change in percentage.

Protein-A mode of Redoxifluor method was used to find out the probable molecular targets where redox state change might happen. First, cell lysates were collected in a similar manner to western blot lysates. The difference here was that in the RIPA Lysis Buffer, Fluorescein-5-Maleimide (FMAL1) was added at 2.5 mM concentration. After centrifugation at 4°C for 20 minutes, the supernatant was collected. Lysate supernatant was passed through a size-exclusion spin columns to remove excess FMAL-1. Then 5 mM neutral-Tris-CarboxyEthyl Phosphine was added to the flow through for 30 minutes on ice to reduce disulfides, sulfenic acids and persulfide oxidation products. Excess TCEP was removed using a second size-exclusion spin columns, added 1mM AlexaFluor 647-C2-maleimide (FMAL2) and incubated on ice for 60 minutes. Excess FMAL2 was removed with a third size-exclusion spin column. Samples were then stored at -80°C.

For the analysis of specific protein oxidation, the “Protein-A” redoxiFluor method was followed (6). Pre-labeled Protein-A coated well strips (Biomat, Italy) were assembled in the plate rack. The wells were washed (hydrated) three times at room temperature (2 min/wash) with 200 µL PBS with 0.1% Tween-20 (PBST) with orbital shaking at 450 RPM. 100 µL/well of binding buffer (50% SuperBlock in PBST) was added followed by 0.1 µg/well capture antibody. The plate was sealed with acetate film and incubated at room temperature for 30 to 90 minutes on a plate shaker at 450 RPM. Wells were washed three times at room temperature with PBST using orbital shaker at 450 RPM. Fluorescence-derivatized samples were diluted at 1:4 ratio with PBS and 100 µL of each sample was loaded into triplicate wells. The plate was sealed with acetate plate film. The plate was then incubated for 4 hours in the dark at room temperature at 400 RPM. Then wells were again washed 3 times with PBST followed by one wash with PBS only to remove Tween 20.

After removal of the final wash, 100 µL of elution buffer (4% w/v sodium dodecyl sulfate) was added to each well, the plate was sealed and incubated in the dark at room temperature for 1 hour at 600 RPM. F-MAL signals were then measured on a fluorescence plate reader (SpectraMax ID3) for 100 ms at the appropriate wavelengths (FMAL1 480nm excitation; 540nm emission; FMAL2 635nm excitation; 685nm emission). Data were saved and stored electronically, organized in excel and statistically analyzed with GraphPad Prism.

3.10 Statistical Analysis

GraphPad Prism (Version 9.5.1) was used to do statistical analyses. To compare means between two groups, unpaired two-tailed t-tests were performed. One-way ANOVA was performed to compare means when there were three or more groups and only one factor was considered. 95% Confidence interval was established for all analyses. The multiple comparison correction method of Dunnett was used when comparing treatments to a control group.

CHAPTER 4: RESULTS

4.1 A549 Cells are stimulated to undergo EMT by TGFβ1

Transforming Growth Factor β1 is a well-established inducer of EMT (285) and was used at a concentration of 5 ng/mL (286) as the positive control in this project. Initially, 5ng/mL TGFβ1 was applied for 48 hours in serum free medium supplemented with antibiotics. Later in the project, the 5ng/mL TGFβ1 treatment was applied for 48 hours in complete medium (supplemented with 10% serum and antibiotics) immediately after serum starvation for 24 hours, as this pretreatment was more effective in inducing EMT in A549 cells. During the treatment process, EMT progression was evaluated by morphology change observation (§3.7.1) and motility change observation (3.7.2) every 12 hours. At the end of 48 hours, EMT-related markers were measured by immunoassays such as western blot (3.7.4) or in-cell western (§3.7.3) assays.

4.1.1 TGFβ1 Treatment induces changes in Morphology and Motility

Morphological changes (elongated and loosely connected cells) were not clearly detectable with TGFβ1 treatment as cells were confluent after 48 hours of treatment, regardless of treatment condition. Motility changes were observed in most of the scratch wound healing assays. Compared to untreated cells, there was a trend toward faster wound healing by TGFβ1 treated cells at 12, 24, 36, and 48 hours after scratching (Figure 4.1.1), however, the results did not reach at significant level due to variability.

Figure 4.1.1

Motility Change by TGFβ1 Treatment

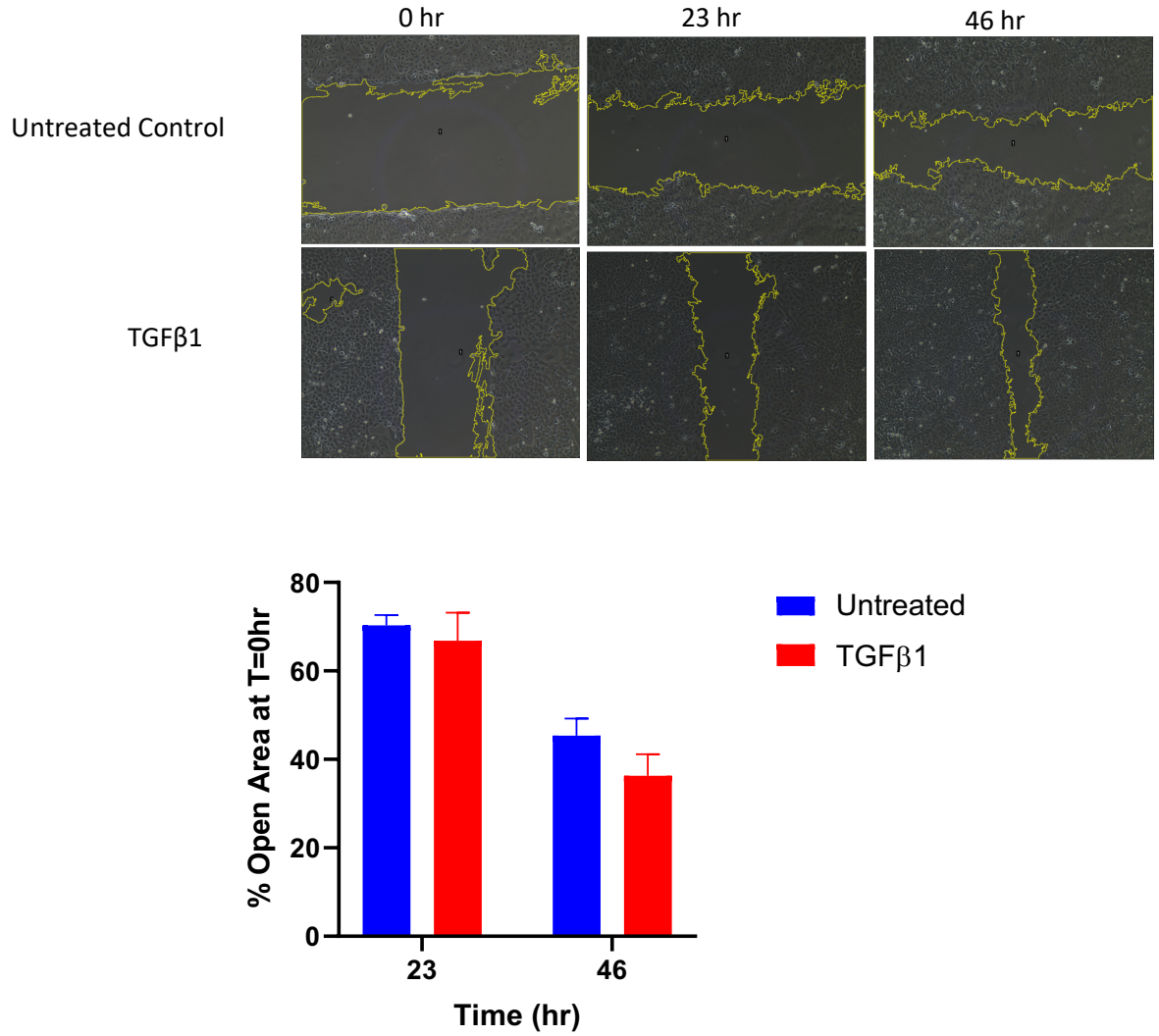

Motility change by TGFTβ1 treatment; Top: Wound healing progress images at different time points; Bottom: Statistical Analysis of % open area as an indicator of wound healing rate. Paired t-test (Two Tailed), 95% CI, n=3.

4.1.2 TGFβ1 Treatment induced Changes in EMT Marker Protein Expression

Both in-cell western and western blot assays showed EMT progression through changes of EMT related markers (decrease of epithelial marker E-Cadherin and increase of mesenchymal marker N-Cadherin) after 48 hours of TGFβ1 treatment (Figure 4.1.2). However, the 24-hour serum starvation prior to the treatment in complete medium showed more extensive changes in EMT marker proteins compared to the initial induction methods used in this project. In those initial methods, there was no prior serum starvation and treatment was in serum-free medium for 48 hours.

4.2 In-Cell Western (ICW) Assays Measuring Extracellular H_2O_2 Effect on EMT

4.2.1 Extracellular H_2O_2 induces EMT-related marker changes on day 10 and 12

According to Gorowiec et al.(261), it takes about 10 days to develop a detectable mesenchymal phenotype after H_2O_2 treatment in lung epithelium. The In Cell Western method was used to determine if that is true for A549 cells. Two 96-well plates were used for two different time points (10 days and 12 days) where cells were exposed to 400 µM H_2O_2 applied extracellularly for 1 hour in RPMI serum-free medium. After the treatment, cells were allowed to grow and then were fixed on day 10 and day 12. The cells in TGFβ1+H_2O_2 group had 1 hour treatment of 400 µM H_2O_2 at 'Day 0' and 5ng/mL TGFβ1 in serum free medium was added at 48 hours before cell fixation.

The epithelial marker E-Cadherin expression decreased significantly for both time points, although another epithelial marker Zona Occludins-1 was minimally suppressed on day 10 (Figure 4.2.1B) compared to untreated control cells. However, the mesenchymal markers (N-Cadherin, α-SMA and Fibronectin) showed mixed results. On day 10, but not on day 12, only TGFβ1+H_2O_2 group showed significant upregulation of α-SMA. However, the positive control TGFβ1 also did not result in significant mesenchymal marker expression on day 10 and 12 (excluding fibronectin on day 12) compared to untreated cells (Figure 4.2.1).

Figure 4.1.2

TGFβ1 Treatment Changed Expression of EMT-related Marker Significantly

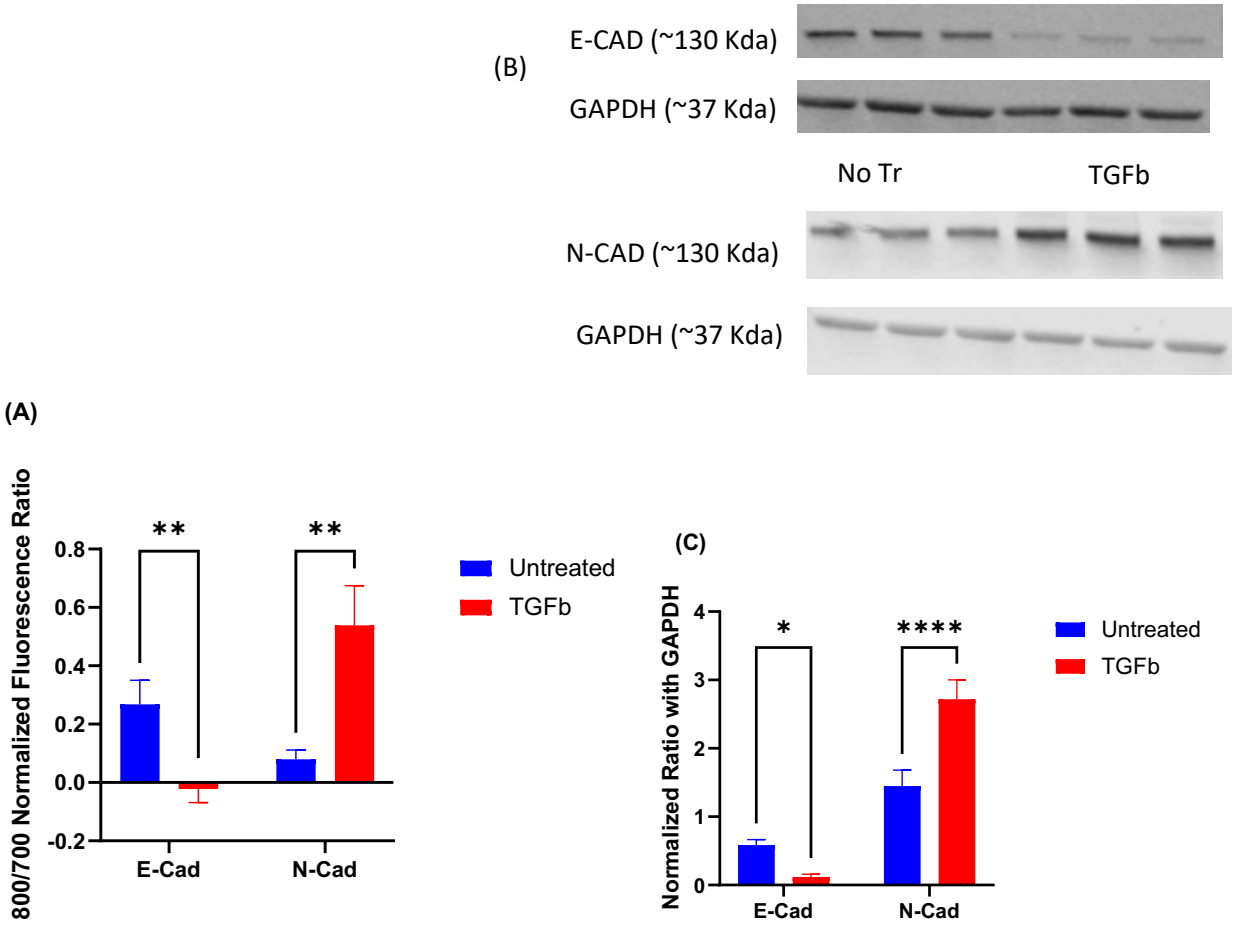

Change of EMT related marker expression after 48 hours of 5ng/mL TGFβ1 treatment, (A) ICW assay showed significant downregulation of epithelial marker E-Cadherin (E-Cad) and upregulation of mesenchymal marker N-Cadherin (N-Cad) by 48-hours treatment of TGFβ1 in serum-free medium; (B) Western blot showing similar EMT related marker expression changes by 48 hour TGFβ1 treatment in complete media after 1 day serum starvation, (C) statistical analysis of Western blot showing such changes were significant. Unpaired t test (Two Tailed), 95% CI, (for A, n=4, for C n=3) P: <0.0001(****), 0.0021(**), 0.0332(*).

Figure 4.2.1

Expression of Epithelial and Mesenchymal Markers on Day 10 and Day 12 After 400 µM H_2O_2 Treatment

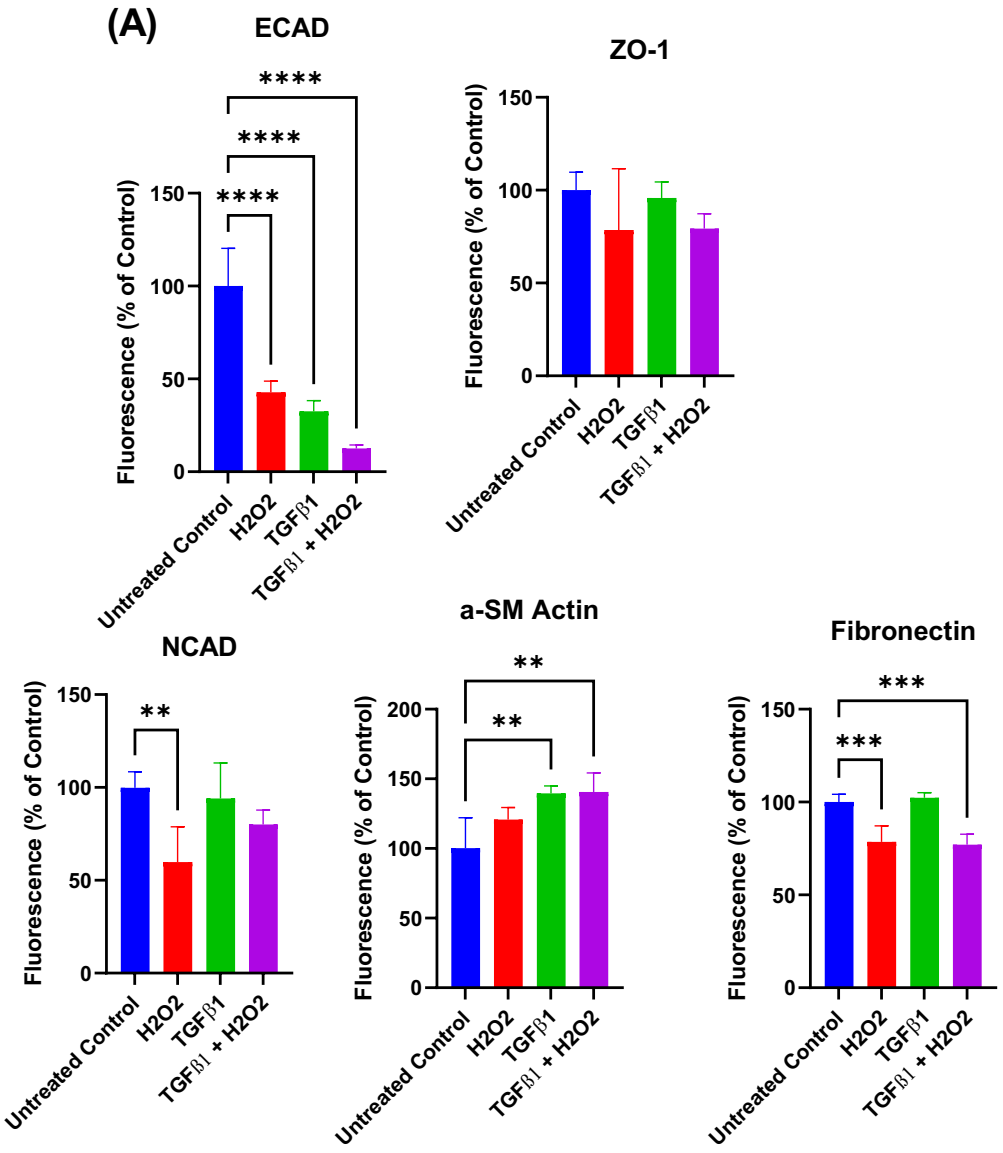

Expression of Epithelial and Mesenchymal Markers after 400 µM H2O2 Treatment on (A) Day 10 and (B) Day 12 in ICW Study. ONE WAY ANOVA, 95% CI, n=4, P: <0.0001(****), 0.0002(***), 0.0021(**), 0.0332(*).

Figure 4.2.1 Continued:

Expression of Epithelial and Mesenchymal Markers on Day 10 and Day 12 After 400 µM H_2O_2 Treatment

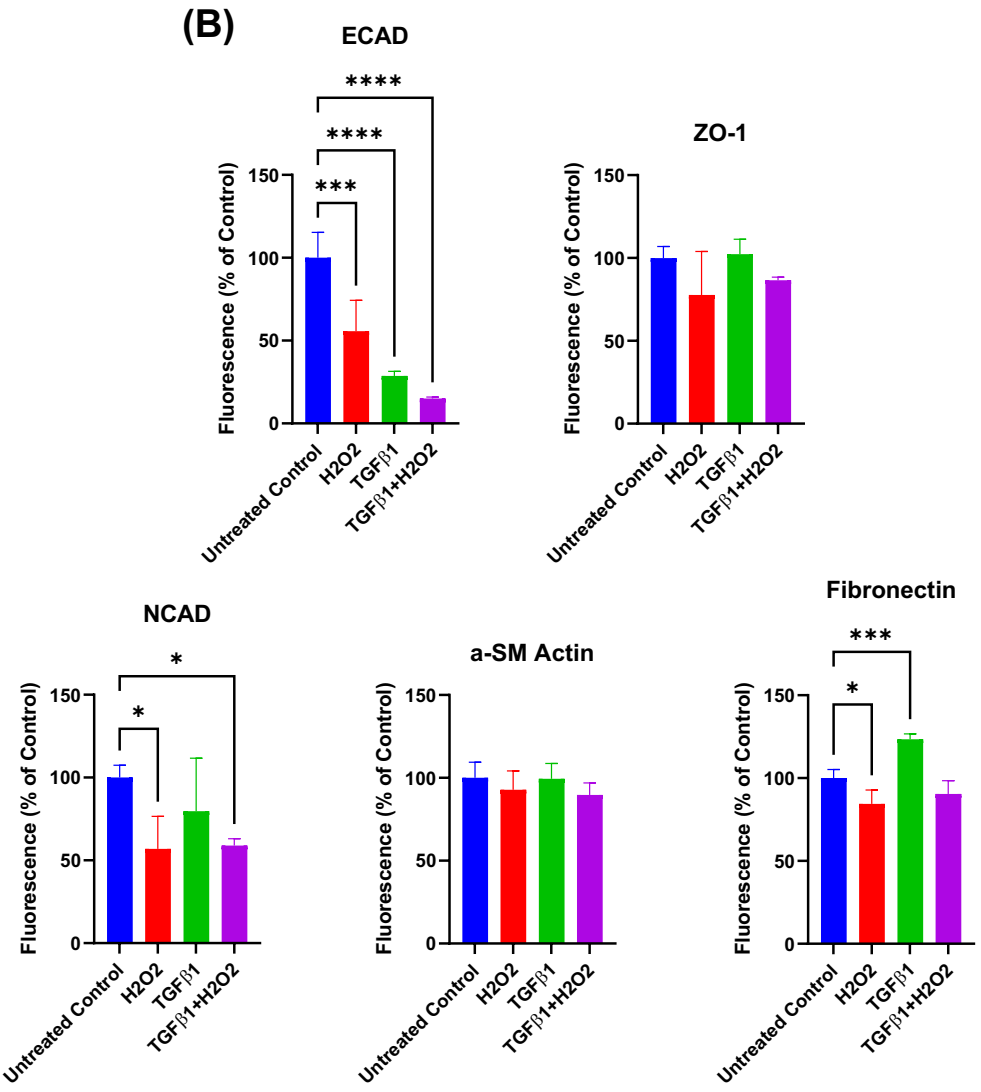

(Continued) Expression of Epithelial and Mesenchymal Markers after 400 µM H2O2 Treatment on (A) Day 10 and (B) Day 12 in ICW Study. ONE WAY ANOVA, 95% CI, n=4, P: <0.0001(****), 0.0002(***), 0.0021(**), 0.0332(*).

4.2.2 Time course ICW Experiments further confirmed H_2O_2 induced EMT Progression with significant downregulation of epithelial marker E-Cadherin

In time-course ICW experiments, A549 cells were treated with 400 µM H_2O_2 for 1 hour in RPMI serum-free medium. Cells were fixed and processed for ICW on days 02, 04, 06, 08, 10, 12, and 14. For each time point, the positive control TGFβ1 (5ng/mL) in serum-free medium was added 48 hours before fixing the cells. E-Cadherin expression decreased compared to untreated cells from day 04 and became significant on day 08. The expression of the mesenchymal marker fibronectin was not increased compared to untreated control cells (Figure 4.2.2). However, the positive control (5ng/mL TGFβ1) also did not induce EMT in this experiment.

4.3 Extracellular H_2O_2 Induces EMT as measured by western blot of marker proteins

To investigate the extracellular H_2O_2 effect on EMT, standard western blot methods were used. The cells were exposed to similar experimental conditions as described in §4.2, however for this set, cells were grown in 100 mm cell-culture dishes. After the 1-hour treatment with 400 µM H_2O_2 in serum free media, cells were allowed to grow in complete media for up to 8 days. TGFβ1 (5ng/mL in serum-free media) was added about 48 hours prior to cell lysate collection for appropriate cell culture dishes. Morphology of the cells was observed every day (Figure 4.3.1) and cell lysates were collected at pre-selected time points (Day 6, Day 07 and Day 08). Western blot assays were then performed to determine epithelial E-cadherin and mesenchymal fibronectin expression changes. The Western blot results showed downregulation of E-Cadherin and upregulation of Fibronectin (on day 06 and 07) as shown in Figure 4.3.2A and Figure 4.3.2B.

Figure 4.2.2

Time Course ICW Experiment Shows Significant E-Cadherin Downregulation at about Day 08

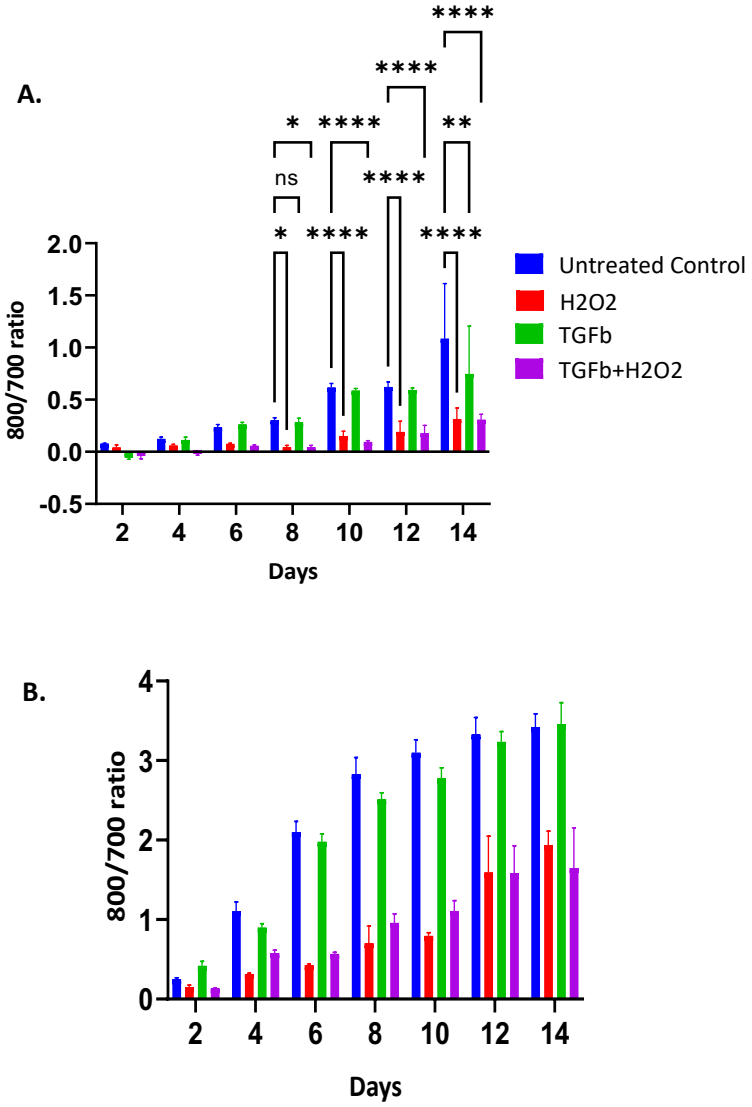

ICW time course experiment showed (A) Downregulation of epithelial E-Cadherin from day 4 compared to untreated control, significant from day 08; (B) Fibronectin expression was lower compared to untreated cells, TWO WAY ANOVA, 95% CI, n=4,P: <0.0001(****), 0.0002(***), 0.0021(**), 0.0332(*).

4.3.1 Morphology Changes Started from Day 04 after Extracellular H_2O_2 Application

A549 cells started to show phenotypic changes from day 04 and on day 05 the morphological change was very clearly detected with spindle like elongated and loosely connected cells (Figure 4.3.1).

4.3.2 Western Blot Results showed EMT Progression through EMT related Marker Expression Changes on Day 06, 07 and 08.

Western blot analysis showed decreased expression of epithelial E-cadherin on day 06, 07, and 08 compared to untreated control cells (Figure 4.3.2A), and such downregulation was most significant on day 07. Similarly, the mesenchymal marker fibronectin results also showed significant upregulation on day 07 compared to untreated controls (Figure 4.3.2B).

Figure 4.3.1

EMT Progression by 400 µM H_2O_2 Detected by Phenotypic Change on Days 01-05

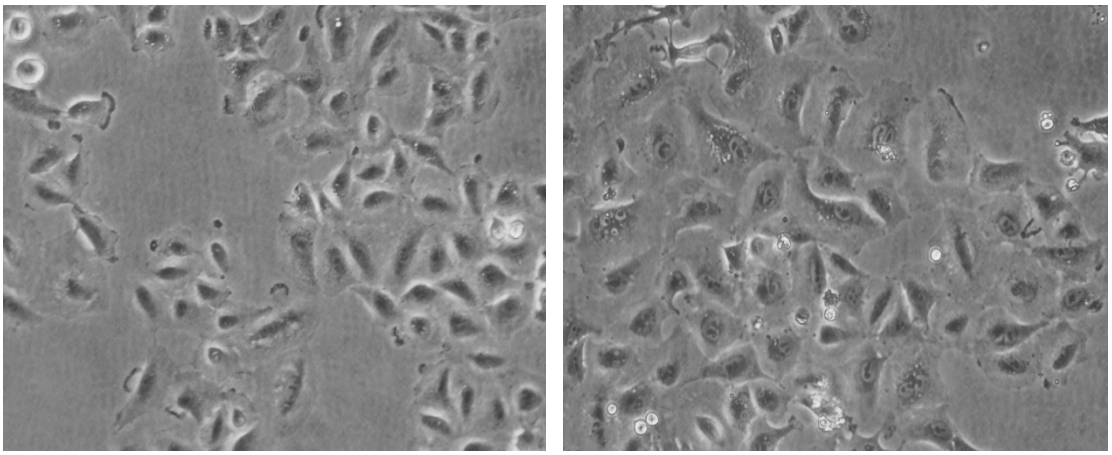

Day 01

Day 02

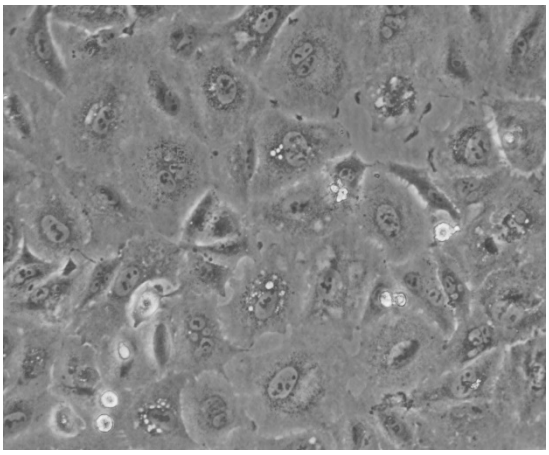

Day 04

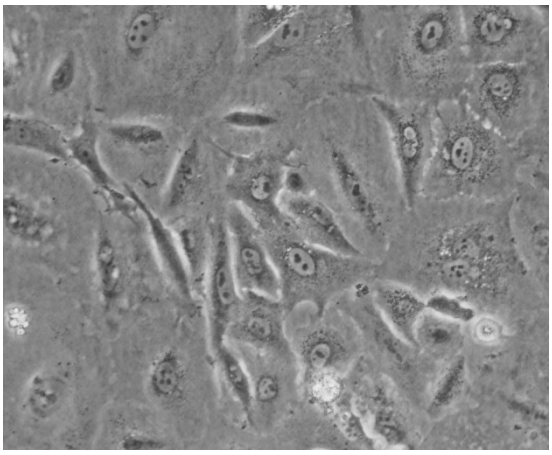

Day 05

EMT Study with 400 µM H_2O_2 for 1 hour in serum-free media resulted in EMT progression detected by phenotypic changes starting from Day 04 and Day 05

Figure 4.3.2A

Western Blot Results of E-Cadherin Expression Changes on Day 06, 07 and 08

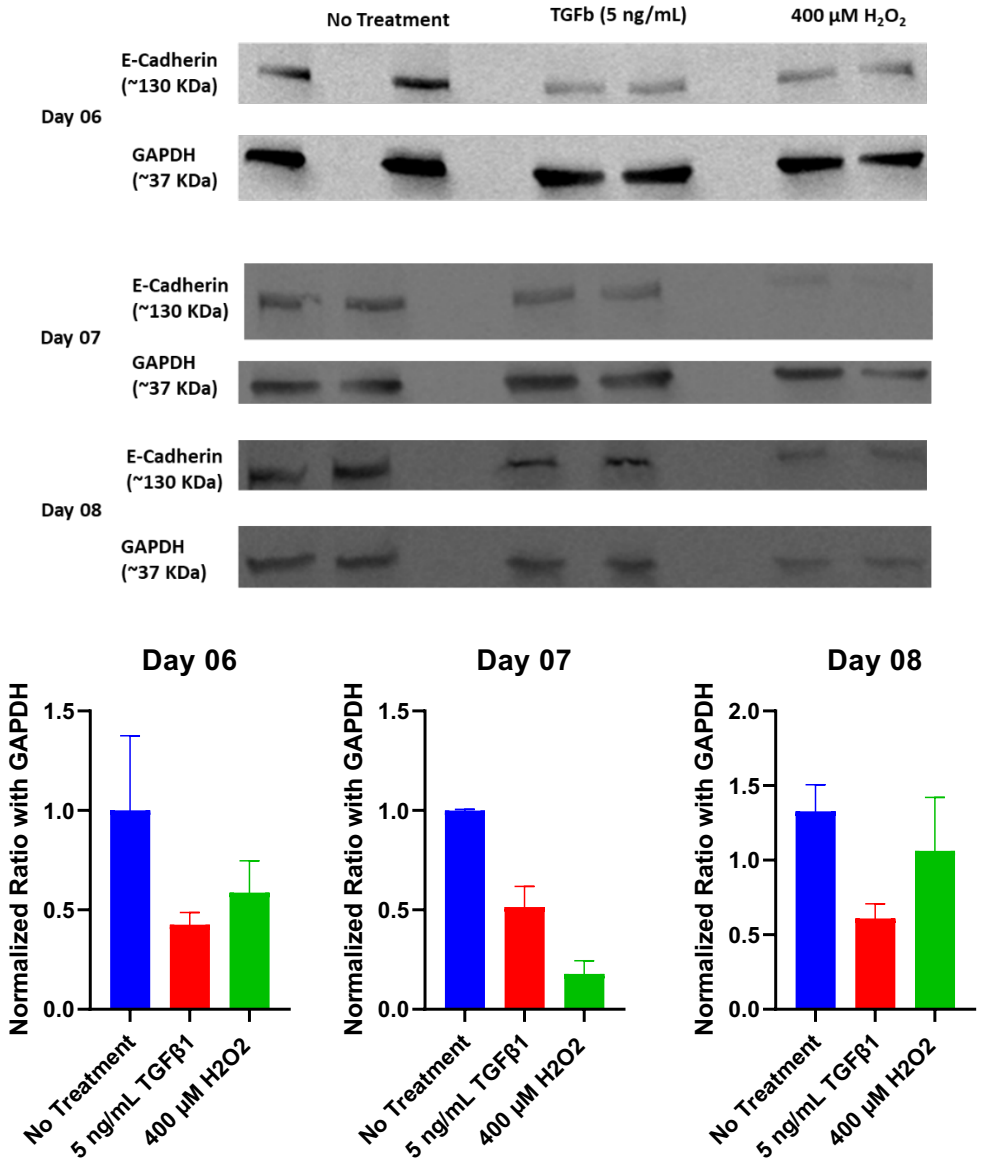

Western blot for epithelial marker E-Cadherin expression changes on different time points after 400 µM H_2O_2 treatment for 1 hour in serum-free media compared to untreated cells. Top: Decreased expression of E-Cadherin on Day 06, 07 and 08. Analysis showing E-Cadherin expression was downregulated.

Figure 4.3.2B

Western Blot Results of Fibronectin Expression Changes on Day 06, 07 and 08

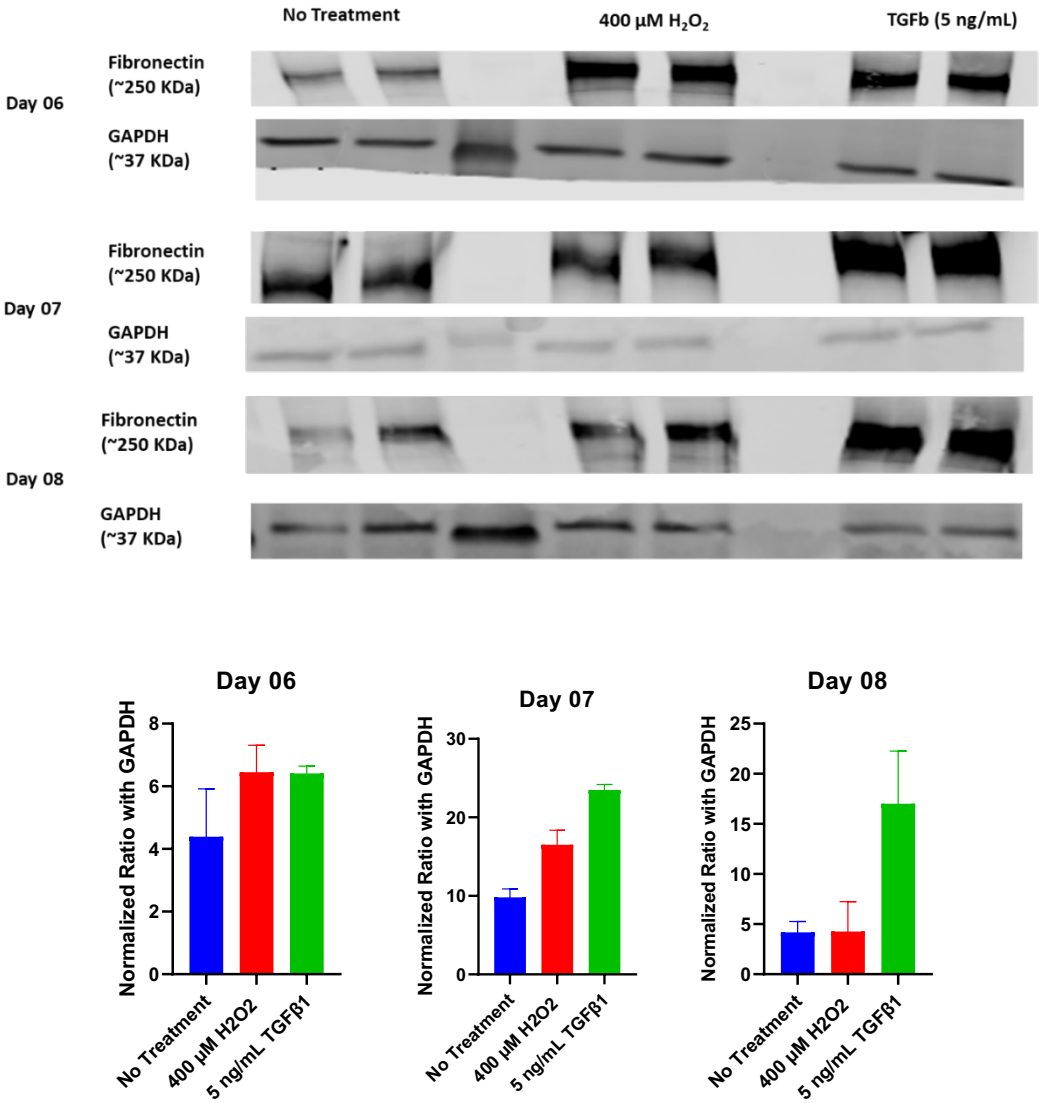

Western blot for mesenchymal marker Fibronectin expression changes on different time points after 400 µM H_2O_2 treatment for 1 hour in serum-free media compared to untreated cells. Top: Increased expression of fibronectin on Day 06, 07 and 08. Bottom: Analysis showing Fibronectin expression was upregulated on day 06 and 07.

4.4 Intracellular H_2O_2 Generation

To generate H_2O_2 intracellularly, several approaches were utilized. These approaches included chemo-genetic methods with various plasmids (containing the peroxide generator D-Amino Acid Oxidase), peroxidase inhibition to increase the persistence of naturally produced intracellular H_2O_2, and chemical methods with quinone metabolism.

4.4.1 Plasmids Expansion and Purification for Chemo-genetic Peroxide Production

All the plasmids were expanded by bacterial transformation and then purified (§3.4.1). The first attempt was made with pAAV-HyPer-DAAO-NES, a gift from the Thomas Michel lab, addgene Plasmid#119164 (description in Chapter 3, §3.3.1). After purifying this plasmid with the mini-prep kit (§3.4.1), restriction digest analysis (§3.4.3) with BsaBI and Psil-V2 was performed, which cut this plasmid at positions 806 bp and at 5018 bp, respectively. The digest with BsaBI only showed one single clear band at the position corresponding to the 7000 bp region (plasmid size is 7182 bp) (Figure 4.4.1.1A). Next, the digest with both enzymes showed two clear bands at about 4000 bp and 3000 bp levels (Figure 4.4.1.1B). As this analysis showed purity, pAAV-HyPer-DAAO-NES was then expanded by bacterial transformation, purified using a Maxiprep kit (§3.4.2), and then verified by restriction digest analysis with the same two enzymes as explained above (Figure 4.4.1.1B).

More advanced generations of plasmids with HyPer7-DAAO were obtained as gifts of Thomas Michel Lab (addgene plasmids#168301, #168302 and #168304) for subcellular delivery of DAAO to generate hydrogen peroxide in the cytoplasm, nucleus, and mitochondria of transfected cells respectively. These plasmids were also processed in a similar way, but their restriction digest analysis was performed with two other enzymes HpaI and PshAI. HpaI cuts HyPer7.2-DAAO-NES at 3837 bp, HyPer7.2-DAAO-NLS at 2858 bp and HyPer7.2-DAAO-Mito at 741 bp. PshAI cuts HyPer7.2-DAAO-NES at 3484 bp, HyPer7.2-DAAO-NLS at 3259 bp and HyPer7.2-DAAO-Mito at 1070 bp. Both miniprep and maxiprep purifications resulted in pure plasmids. After the miniprep purification, the digests with HpaI

alone showed a single clear band at between 7000 and 8000 bp region for all three plasmids (Figure 4.4.1.2). Also, the HpaI+PshAI showed two bands, one strong and clear band at little above 6000 bp and a very faint band at about 300-400 bp (Figure 4.4.1.2) confirming that the plasmids were pure. The same restriction digest results (Figure 4.4.1.3 to Figure 4.4.1.5) were observed when each plasmid was expanded by bacterial transformation followed by Maxi-prep purification. All these results confirmed the purity of the plasmids used in this project.

Figure 4.4.1.1A

Restriction Digest Analysis of MiniPrep Purified pAAV-HyPer-DAAO-NES Plasmid

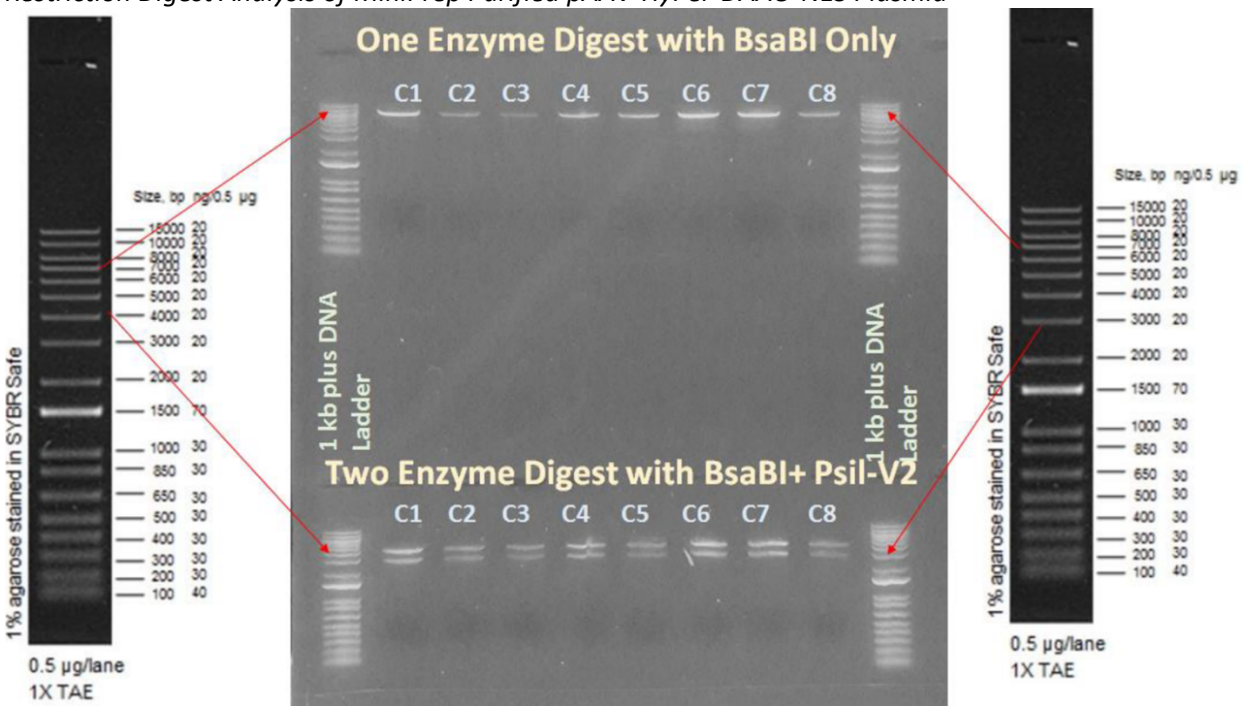

Restriction Digest Analysis confirmed purity of pAAV-HyPer-DAAO-NES plasmids purified with miniprep, 'C' represents bacterial colonies from where samples were taken.

Figure 4.4.1.1B

Restriction Digest Analysis of MaxiPrep Purified pAAV-HyPer-DAAO-NES Plasmid

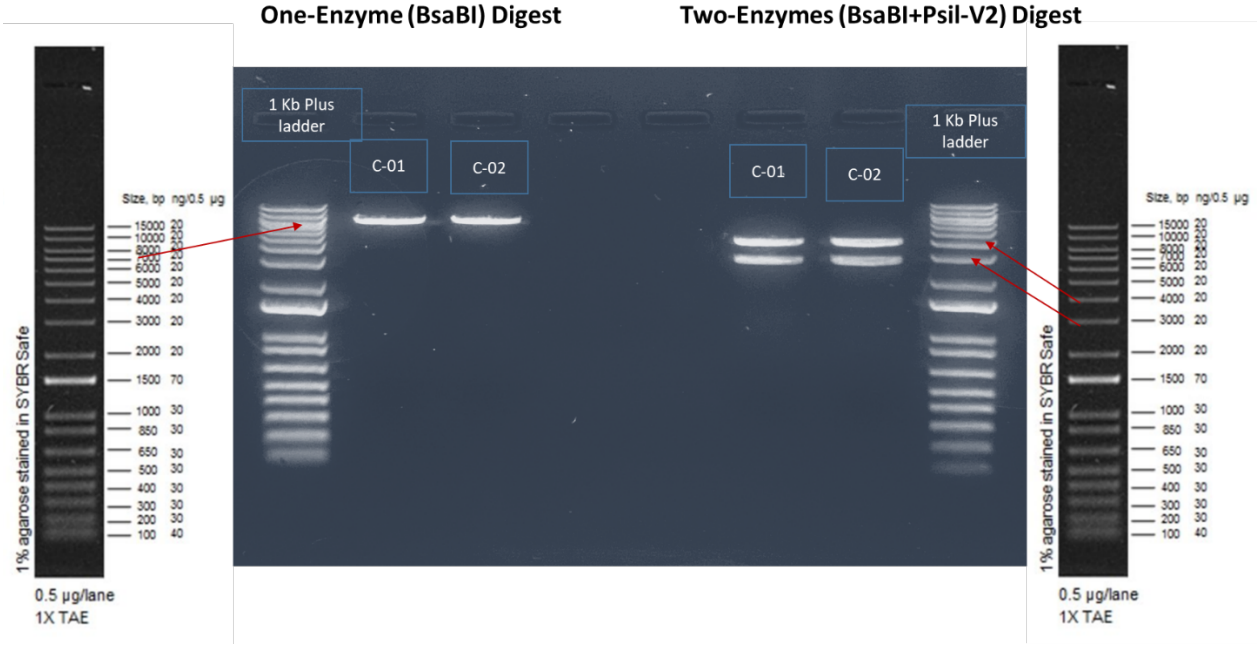

Restriction Digest Analysis confirmed purity of pAAV-HyPer-DAAO-NES plasmids purified with MaxiPrep Kit, 'C' represents bacterial colonies from where samples were taken.

Figure 4.4.1.2

Restriction Digest Analysis Confirmed Purity of HyPer7.2-DAAO Plasmids

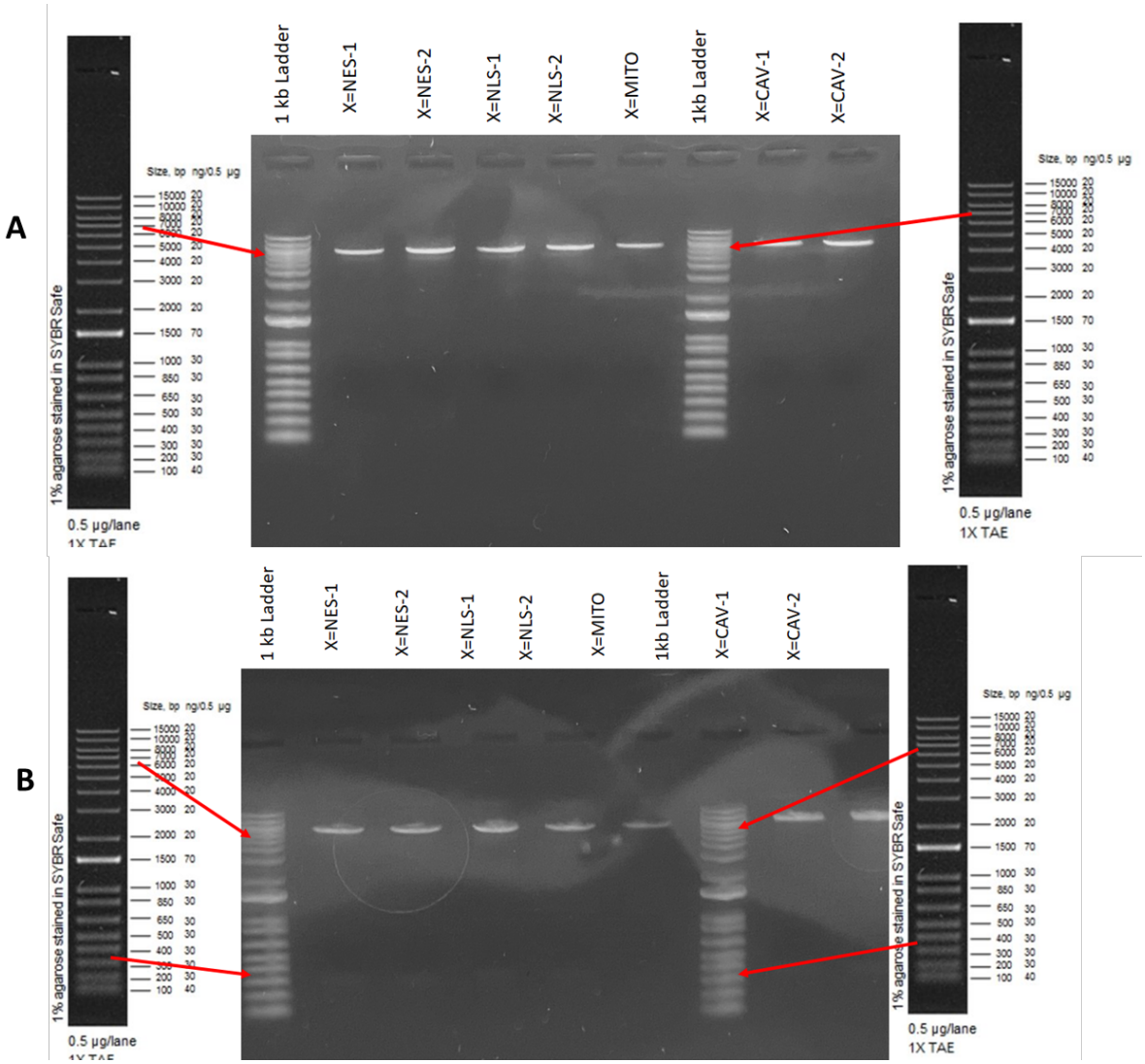

Restriction Digest Analysis Confirming Purity of HyPer7.2-DAAO-'X' plasmids (A) Only with HpaI enzyme (Bands were close to 7000 bp) (B) with HpaI+PshAI enzymes (Bands appeared at about 6500 bp and at 350 bp (very fade). NOTE: Here, 'X'=CAV was also purified, but was not used in the project.

Figure 4.4.1.3

Restriction Digest Analysis Confirming Purity of HyPer-DAAO-NES Plasmids (Maxi-Prep Purified)

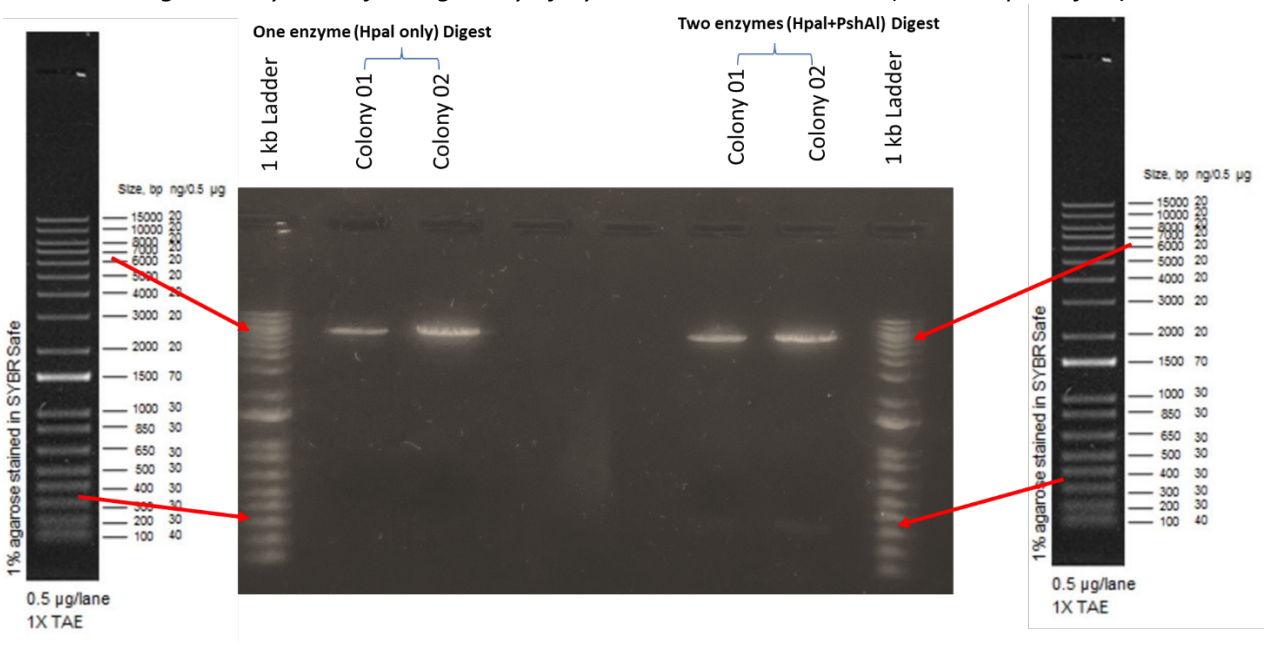

Restriction Digest Analysis, HyPer7.2-DAA-**NES** Plasmids (bands appeared at about 6500 bp and at 350 bp (very fade)

Figure 4.4.1.4

Restriction Digest Analysis Confirming Purity of HyPer-DAAO-NLS Plasmids (Maxi-Prep Purified)

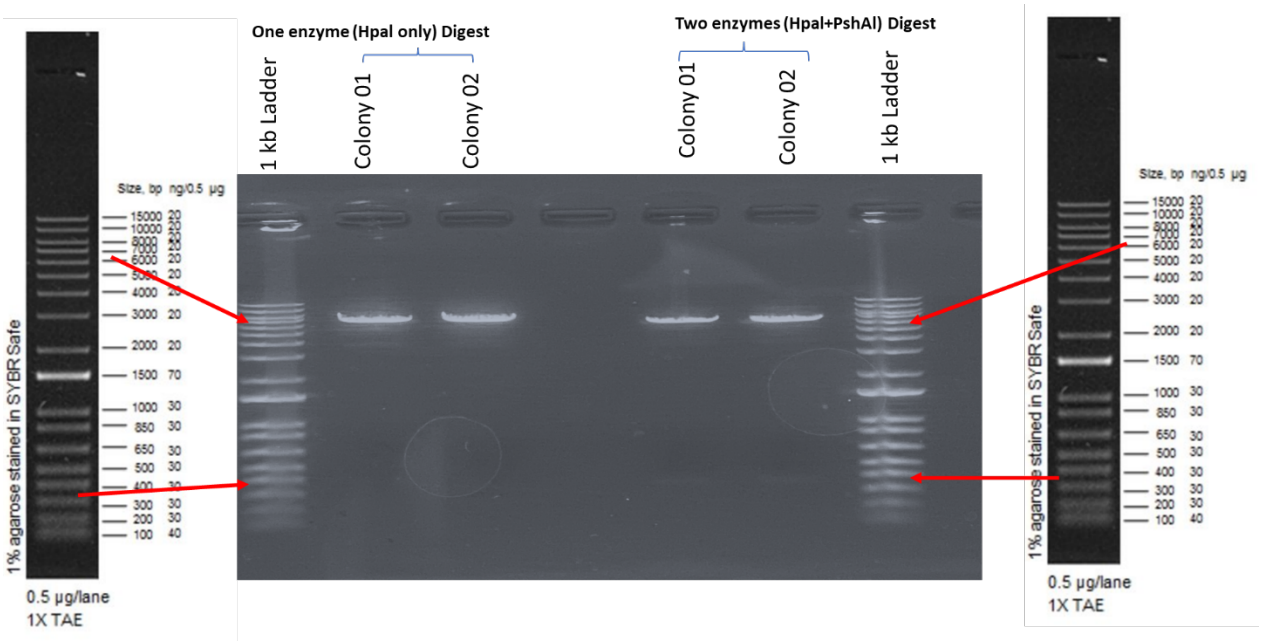

Restriction Digest Analysis, HyPer7.2-DAA-**NLS** Plasmids (bands appeared at about 6500 bp and at 350 bp (very fade)

Figure 4. 4.1.5

Restriction Digest Analysis Confirming Purity of HyPer-DAAO-Mito Plasmids (Maxi-Prep Purified)

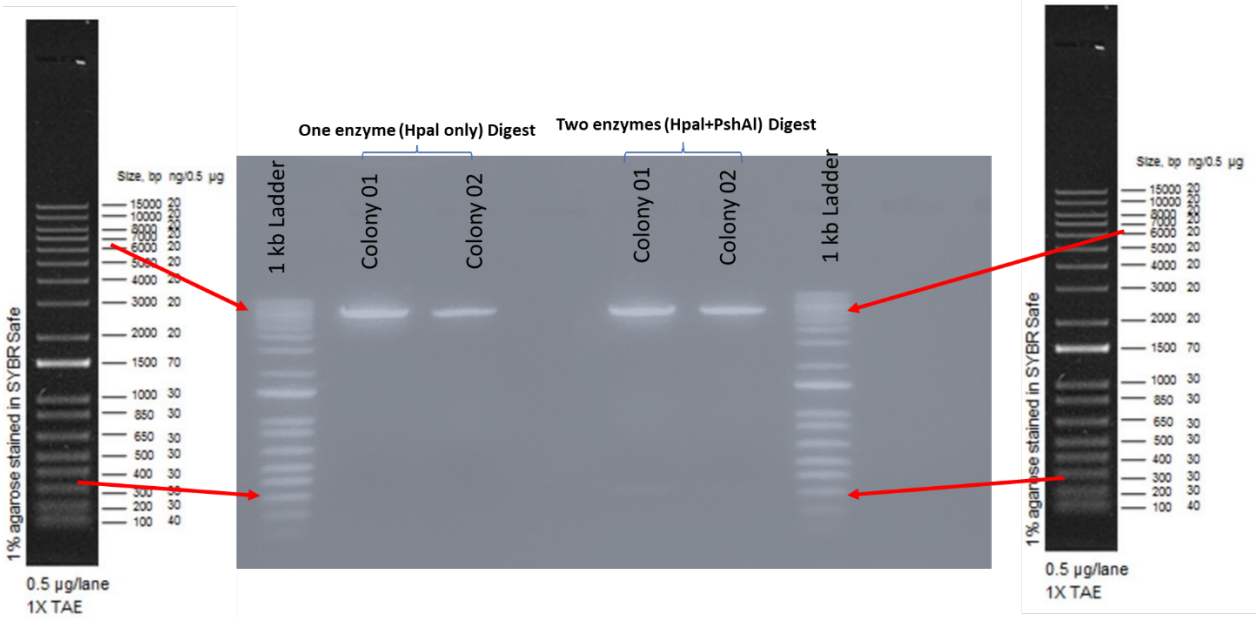

Restriction Digest Analysis, HyPer7.2-DAAO-**Mito** Plasmids (bands appeared at about 6500 bp and at 350 bp (very fade)

4.4.2 Transfection of pAAV-HyPer-DAAO-NES Plasmids into A549 Cells Resulted in Cytoplasmic Localization of DAAO and Peroxide Generation by D-Alanine

Transfection with pAAV-HyPer-DAAO-NES, resulted in cytoplasmic localization of 'DAAO' and 3rd generation 'HyPer' (Figure 4.4.2.1 and 4.4.2.2). Treatment of transfected cells with D-Alanine resulted in increased H_2O_2 production detected by the fluorescence increase of 'HyPer' (§3.3) with GFP and CFP channels (Figure 4.4.2.1). However, there was no change of fluorescence when transfected cells were treated with L-Alanine (Figure 4.4.2.2).

4.4.3 D-Alanine increased HyPer fluorescence in a Concentration-dependent Manner in DAAO-Transfected Cells.

By changing D-Alanine concentrations, a dose-response effect was found in cells transfected with DAAO, when delivered by the pAAV-HyPer-DAAO-NES plasmid. In an initial experiment, the D-Alanine concentrations used were 2mM, 5 mM, 10 mM and 15 mM with a 15 mM L-Alanine control group (Figure 4.4.3A). As these concentrations produced a saturated fluorescence image, a subsequent experiment showed a dose-response effect at concentrations of 250 µM, 500 µM, 750 µM, 1mM, 2 mM D-Alanine with a 2 mM L-Alanine control. In this experiment, the dose-response effect reached the plateau at 750 µM D-Alanine (Figure 4.4.3B). The concentrations were adjusted further in following experiments and 600 µM D-Alanine was found to be the concentration with the highest 'HyPer' fluorescence response (Figure 4.4.3C). However, there was no detection of fluorescence change by HyPer below 200 µM D-Alanine and the effect started to appear from 400 µM D-Alanine.

Figure 4.4.2.1

Cytoplasmic Localization of DAAO & HyPer by pAAV-HyPer-DAAO-NES Transfection and H_2O_2 Generation by D-Alanine

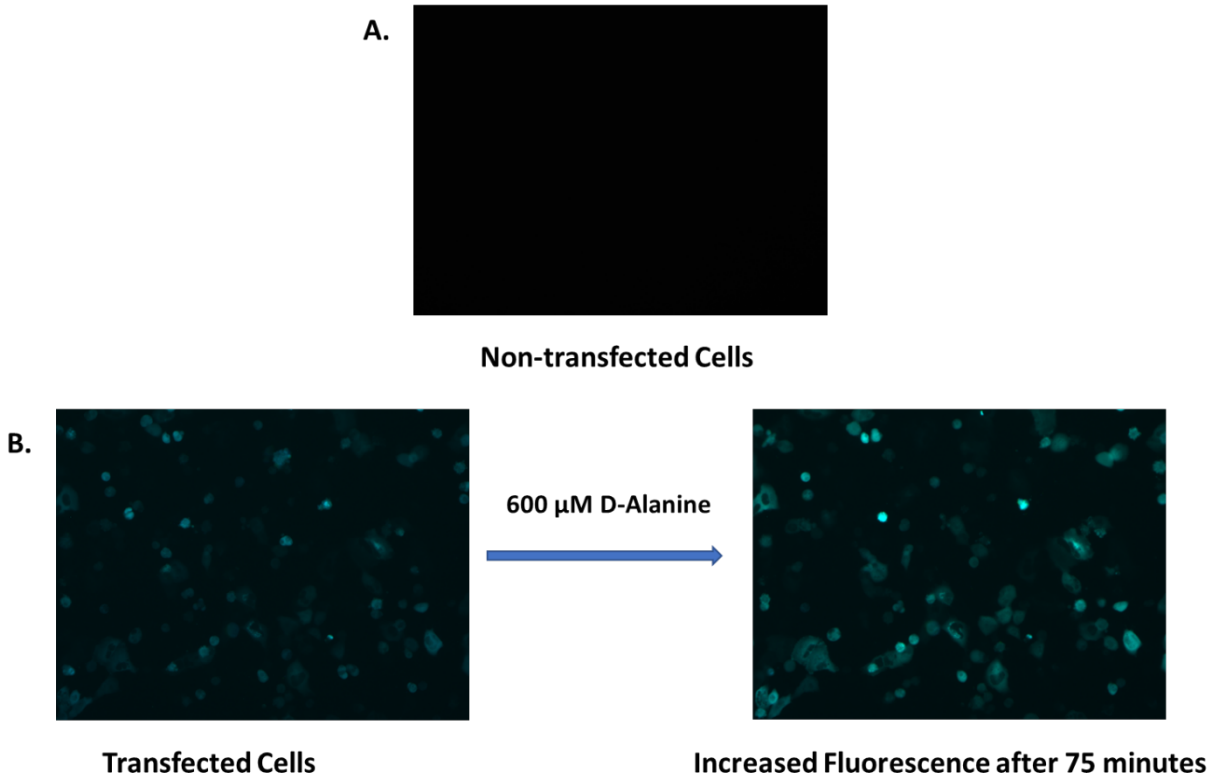

Cytoplasmic localization of DAAO and HyPer detected with GFP and CFP Channels, (A) No fluorescence detected in non-transfected cells; (B) Transfected cells were detected with dark nucleus at the center. Addition of 600 µM D-Alanine resulted in increased fluorescence of HyPer indicating cytoplasmic H_2O_2 production

Figure 4.4.2.2

Cytoplasmic Localization of DAAO & HyPer and No H_2O_2 Generation by L-Alanine

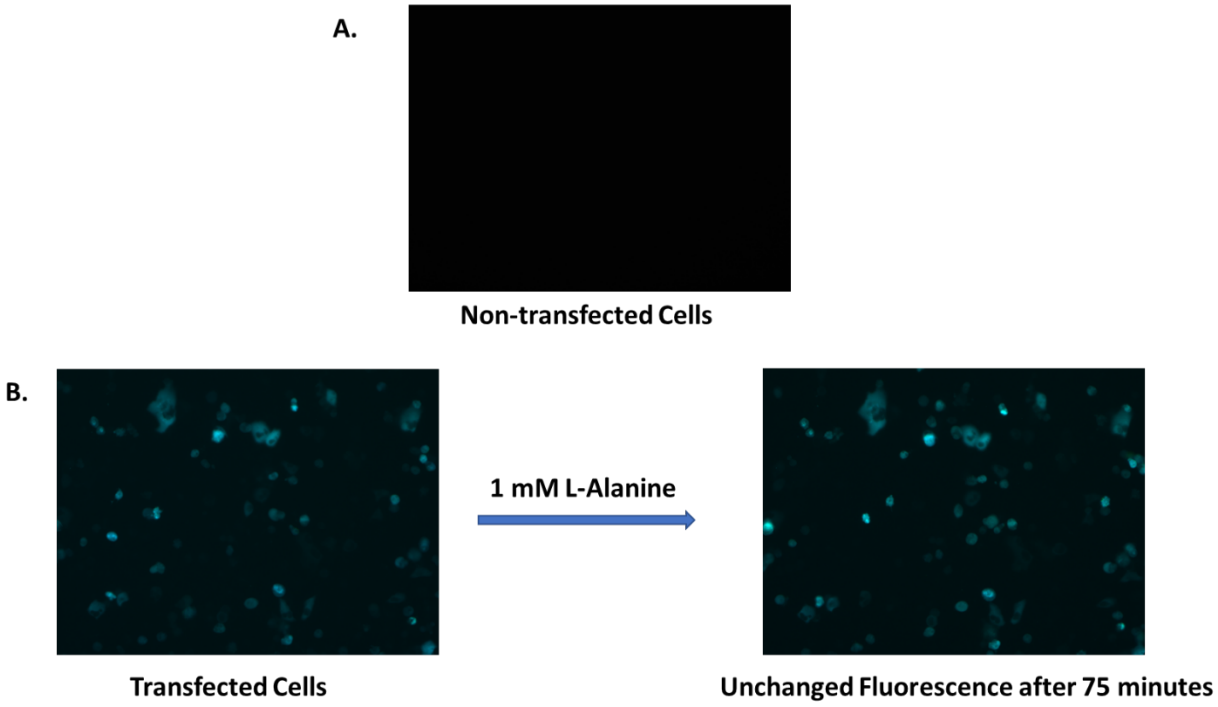

Cytoplasmic localization of DAAO and HyPer detected with GFP and CFP Channels, (A) No fluorescence detected in non-transfected cells; (B) Transfected cells were detected with dark nucleus at the center. Addition of 1 mM L-Alanine did not change fluorescence of HyPer confirming D-Alanine specific functionality of DAAO.

Figure 4.4.3

Dose-Response Relationship between D-Alanine and DAAO Activity

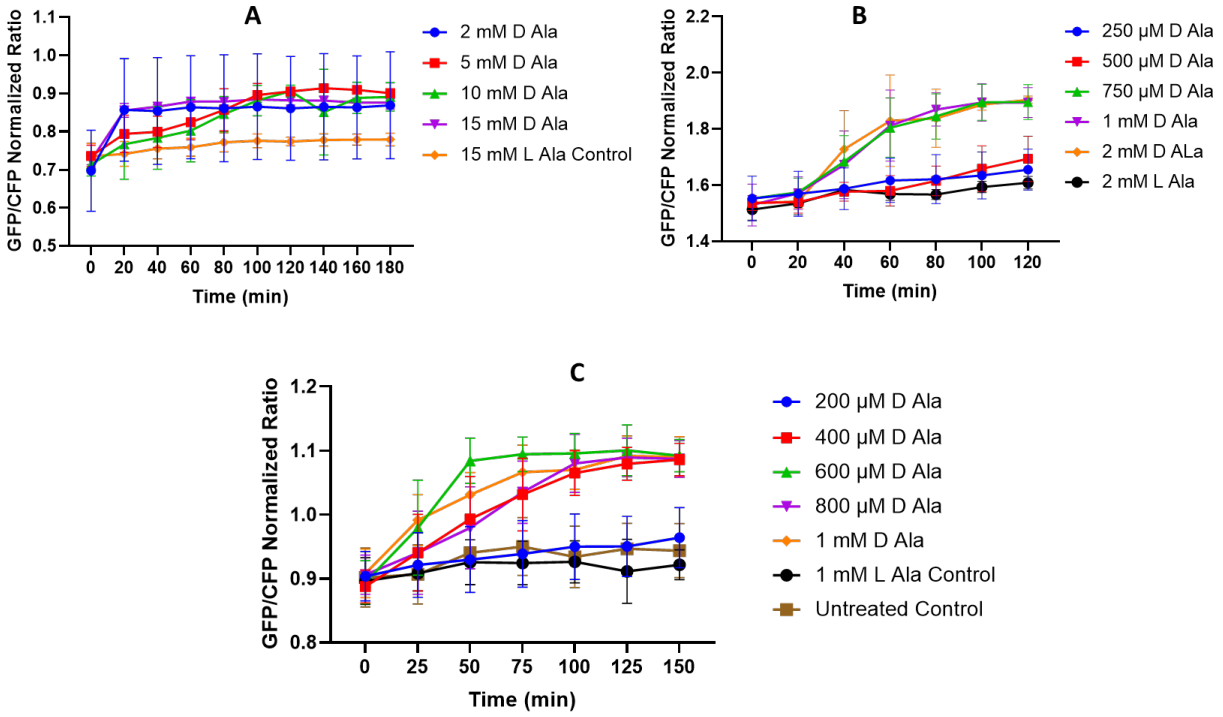

Dose Response Effect Optimization between D-Alanine and DAAO Activity detection by HyPer; (A) Dose-response was not detected, (B) Adjusted lower D-Alanine concentrations showed dose-response effect, (C) Further adjustment of D-Alanine dose showed effect starts at around 400 µM D-Alanine and reached plateau at 600 µM. There was no dose response with L-Alanine control. 'D-Ala: D-Alanine), n=4 (A and B) and n=12 (C). No Statistical Analysis was performed with these data.

4.4.4 Delivery of DAAO to Subcellular Compartments with HyPer7.2-DAAO Plasmids was Confirmed with Fluorescence Microscopy

The 7th generation of HyPer plasmids, HyPer7.2-DAAO with localization sequences directing delivery to subcellular compartments, were transfected into A549 cells. With the GFP channel in fluorescence microscopy, cytoplasmic, nuclear, and mitochondrial delivery and expression of DAAO along with HyPer7.2 were confirmed. There was strong fluorescence all over the cells with dark nuclei where DAAO was delivered to the cytoplasm by HyPer7.2-DAAO-NES (Figure 4.4.4A). The nuclear expression of DAAO by HyPer7.2-DAAO-NLS was confirmed by a strong fluorescence signal of attached HyPer7.2 from the nucleus with other parts of the cell invisible (Figure 4.4.4B). The mitochondrial delivery and expression of DAAO by HyPer7.2-DAAO-Mito was similar to cytoplasmic expression with dark nuclei, but the fluorescence light appeared to be small spots of fluorescence throughout the cytosol instead of solid fluorescence (Figure 4.4.4C).

Figure 4.4.4A

Cytoplasmic Localization of HyPer7.2-DAAO Delivered by HyPer7.2-DAAO-NES

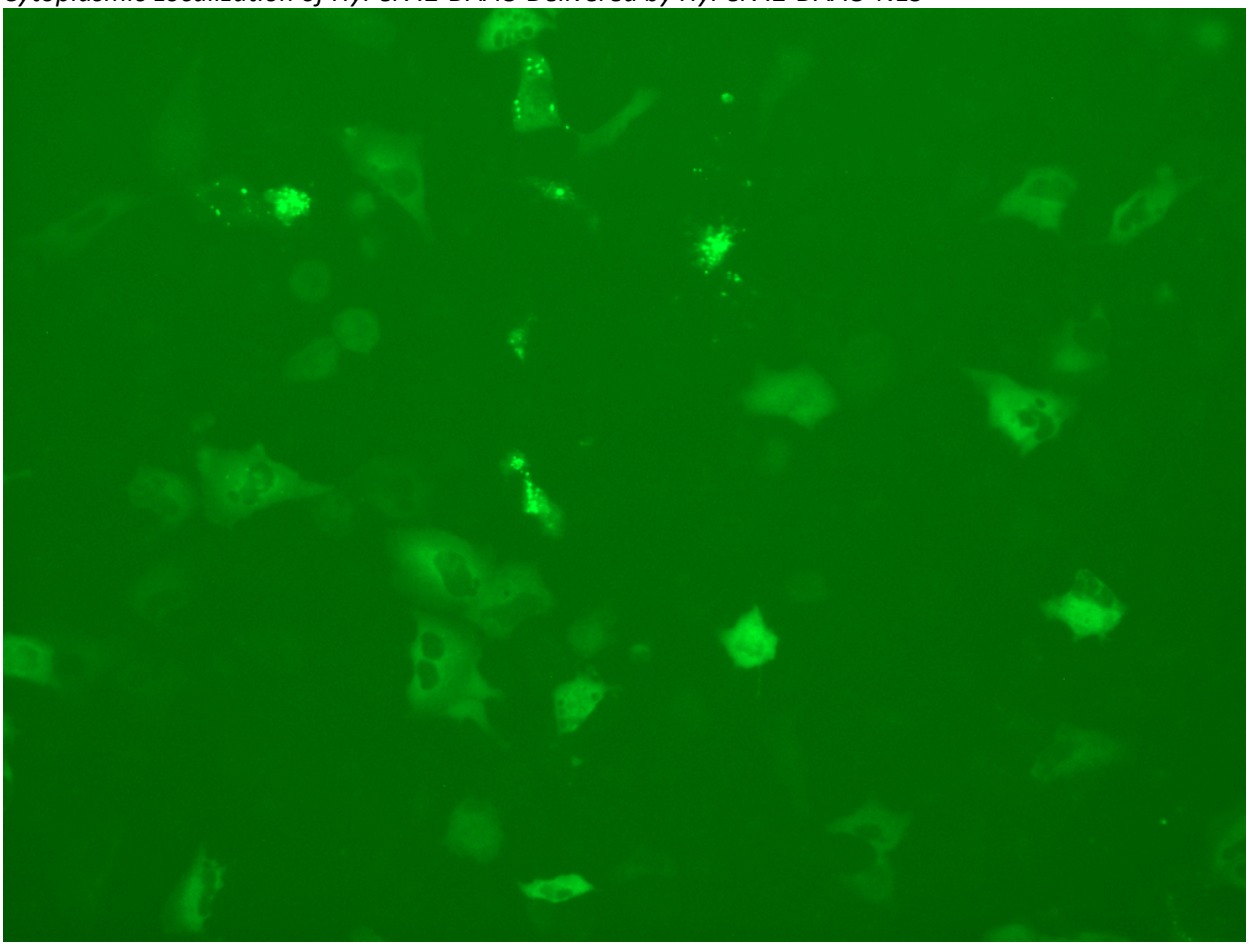

Cytoplasmic localization of HyPer7.2 DAAO delivered by HyPer7.2-DAAO-NES (20X Image at GFP Channel)

Figure 4.4.4B

Nuclear Localization of HyPer7.2-DAAO Delivered by HyPer7.2-DAAO-NLS

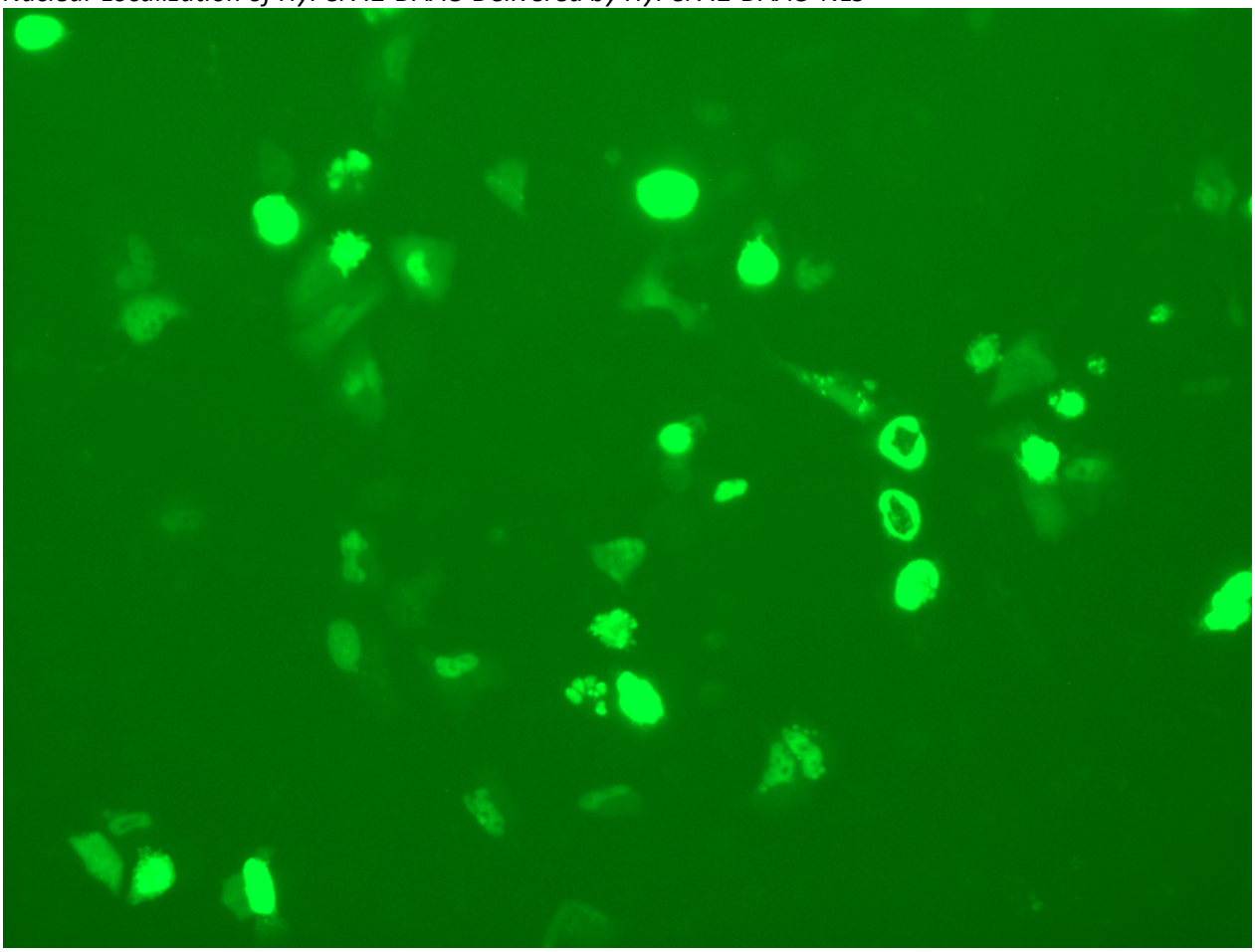

Localization of HyPer7.2-DAAO-NLS at the nucleus of A549 cells (images taken with 20x lens GFP channel)

Figure 4.4.4 C

Mitochondrial Localization of HyPer7.2-DAAO Delivered by HyPer7.2-DAAO-Mito

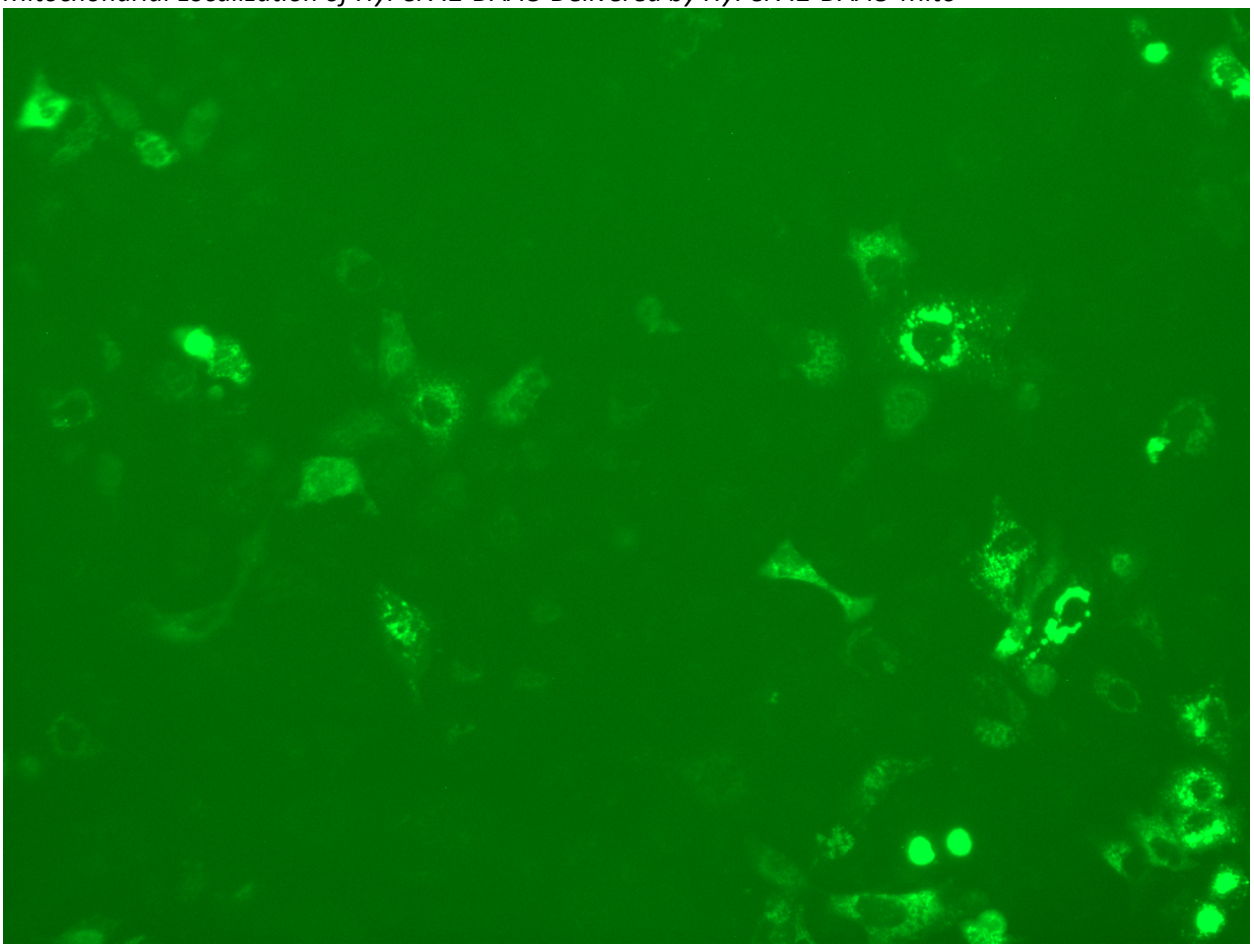

Localization of HyPer7.2-DAAO-Mito at mitochondria of A549 cells (images taken with 20x lens GFP channel)

4.4.5 Chemiluminescence Assays Confirmed DAAO Activity of HyPer7.2-DAAO Plasmids

Experiments to detect DAAO activity with HyPer7.2 fluorescence change were performed in a similar fashion as for 3rd generation HyPer, but the closest available channel (GFP) in the EVOS microscope could not detect any fluorescence change (Data not shown). Therefore, chemiluminescence assays with AquaSpark reagent was utilized which confirmed that the DAAO expressed in different subcellular locations are functional (Figure 4.4.5A and 4.4.5B). However, this assay required Peroxidase inhibitors (2 µM Auranofin and 25 mM 3-Amino-1,2,4-Triazole) to prevent neutralization of DAAO generated H_2O_2.

Figure 4.4.5A

Chemiluminescence Assay Confirmed HyPer7.2-DAAO-NES delivered DAAO Activity

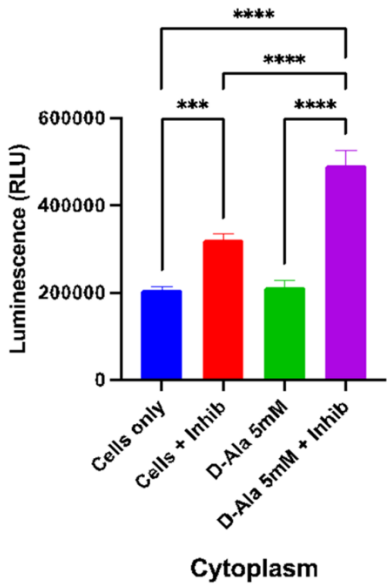

Chemiluminescence Assay Confirmed DAAO activity in HyPer7.2-DAAO-NES transfected A549 cells in the presence of Peroxidase Inhibitors (Inhib). One Way ANOVA, 95% CI, n=3, P: <0.0001(****), 0.0002(***).

Figure 4.4.5B

Chemiluminescence Assay Confirmed HyPer7.2-DAAO-NLS and HyPer7.2-DAAO-Mito delivered DAAO Activity

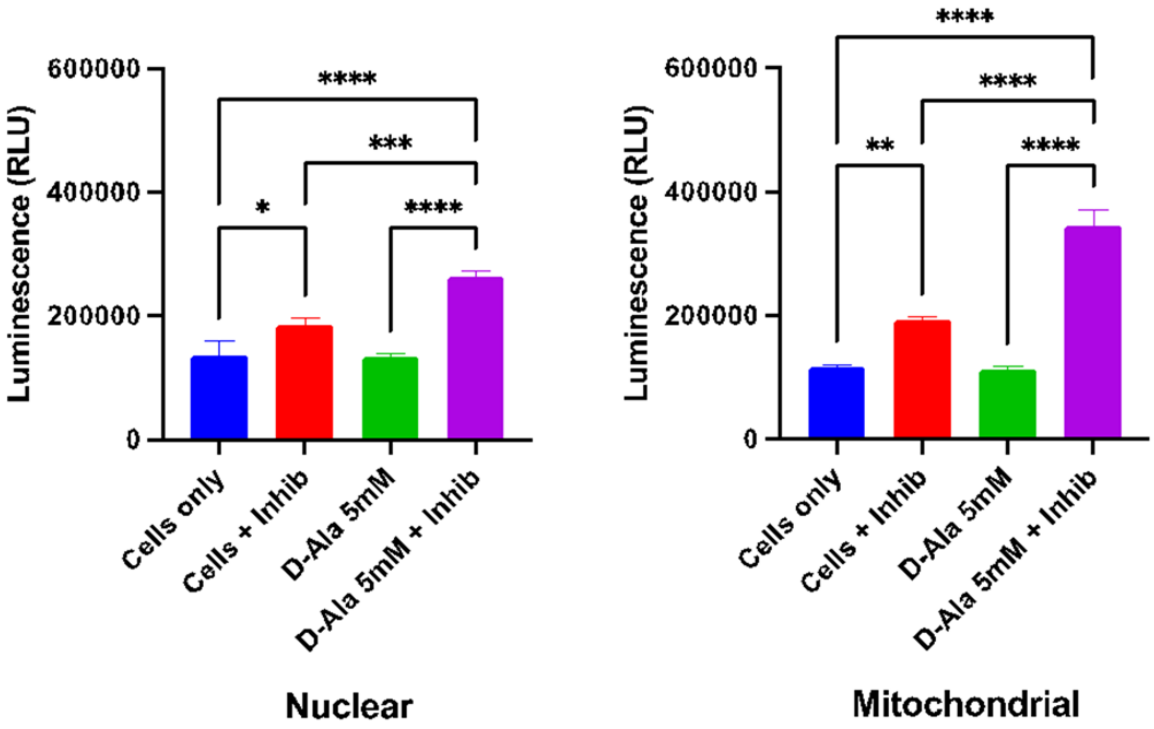

Chemiluminescence Assay Confirmed DAAO activity in HyPer7.2-DAAO-NLS and HyPer7.2-DAAO-Mito transfected A549 cells in the presence of Peroxidase Inhibitors (Inhib), One Way ANOVA, 95% CI, n=3, P: <0.0001(****), 0.0002(***), 0.0021(**), 0.0332(*).

4.4.6 Transfection Efficiency Remained Very Low with Chemical Transfection Method

Transfection Efficiency remained very low with chemo-genetic methods (§3.5). The best transfection efficiency which was achieved with these methods is shown in Figure 4.4.6 below for each plasmid type of 7th generation. Chemical transfection with Polyjet© reagent (§3.5.2) was the most successful…

Figure 4.4.6

Low Transfection Efficiency with Chemical Transfection Methods

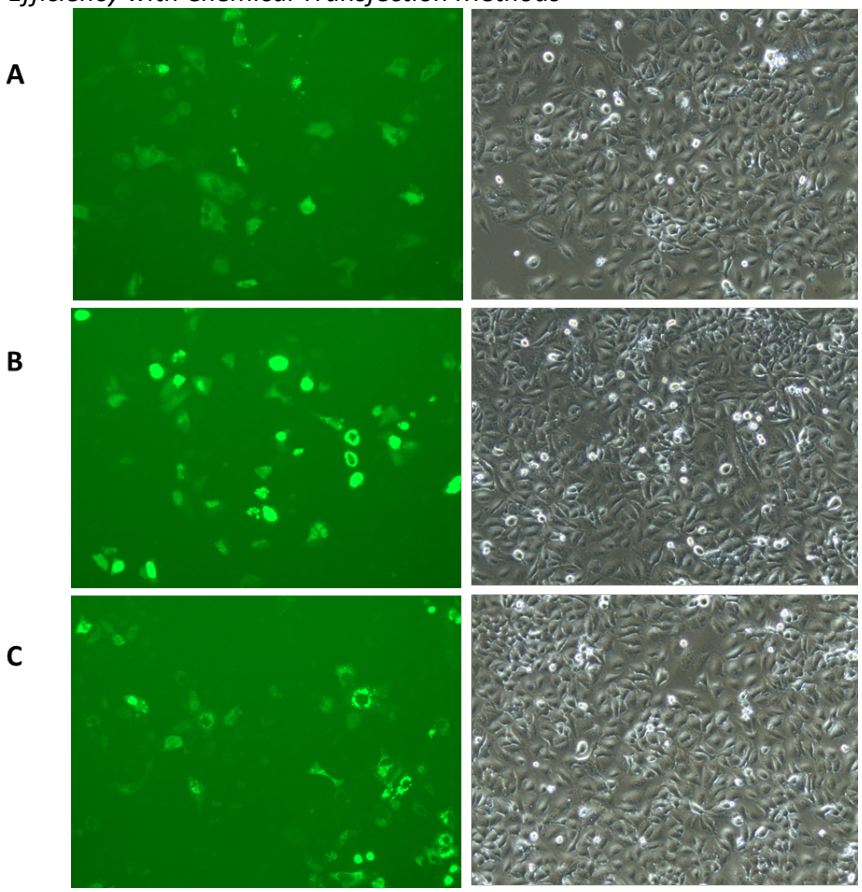

Very Low Transfection Efficiency Observed, (A) Cytoplasmic, (B) Nuclear and (C) Mitochondrial transfection (images taken with 20x lens GFP channel and corresponding Phase contrast). These pictures represent the best transfection efficiency after several optimizations

4.4.7 Electroporation method did not improve transfection efficiency

Electroporation (§3.5.2) was applied several times in an attempt to improve the transfection efficiency but was unsuccessful (Figure 4.4.7). Electroporation resulted in much higher cytotoxicity along with inconsistent transfection efficiency.

Figure 4.4.7

Inconsistent and Low Transfection Efficiency with Electroporation Methods

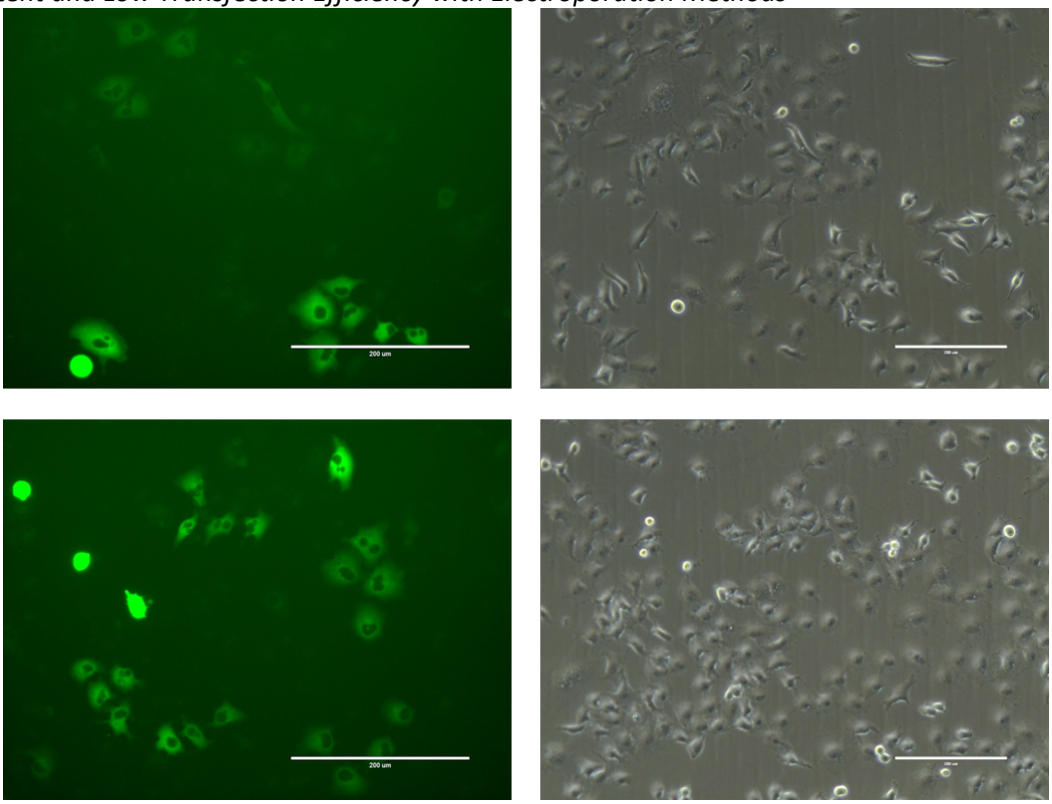

Transfection Efficiency not improved significantly but showed higher toxicity (images taken with 20x lens GFP channel and corresponding Phase contrast). These pictures represent the best transfection efficiency after several optimization with electroporation methods. pAAV-HyPer-DAAO-NES plasmids were used here (Left: GFP image, Right: Corresponding phase contrast image)

4.4.8 Persistence of H_2O_2 by Peroxidase Inhibition

Peroxidase inhibition, particularly catalase inhibition by 3-amino-1,2,4-triazole (3AT) and thioredoxin inhibition by Auranofin resulted in accumulation of H_2O_2 (Figure 4.4.8A and 4.4.5A and 4.4.5B). As 3AT was found to be major inducer of EMT among the two peroxidase inhibitors (Figure 4.7.1.5), the chemiluminescence experiment was performed later with 3AT only to cause persistence of H_2O_2 (Figure 4.4.8A). Also, the cytotoxicity assays for these drugs showed no toxicity for prolonged exposure whether used alone or in combination at low concentrations (Figure 4.4.8). Buthionine sulfoximine (BSO) which inhibits GSH synthesis (and thereby starves glutathione peroxidase activity) (287) was not used in this project.

Figure 4.4.8A

Increased accumulation of H_2O_2 by Catalase inhibition with 3AT

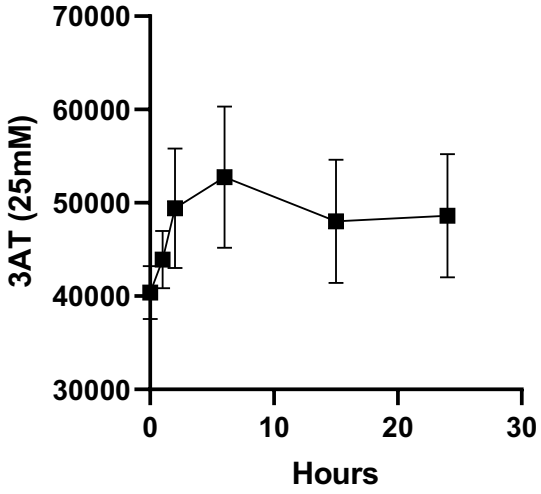

Increased accumulation of intracellular H_2O_2 with 25 mM 3AT. n=8

Figure 4.4.8B

Cytotoxicity Assay of Peroxidase Inhibition

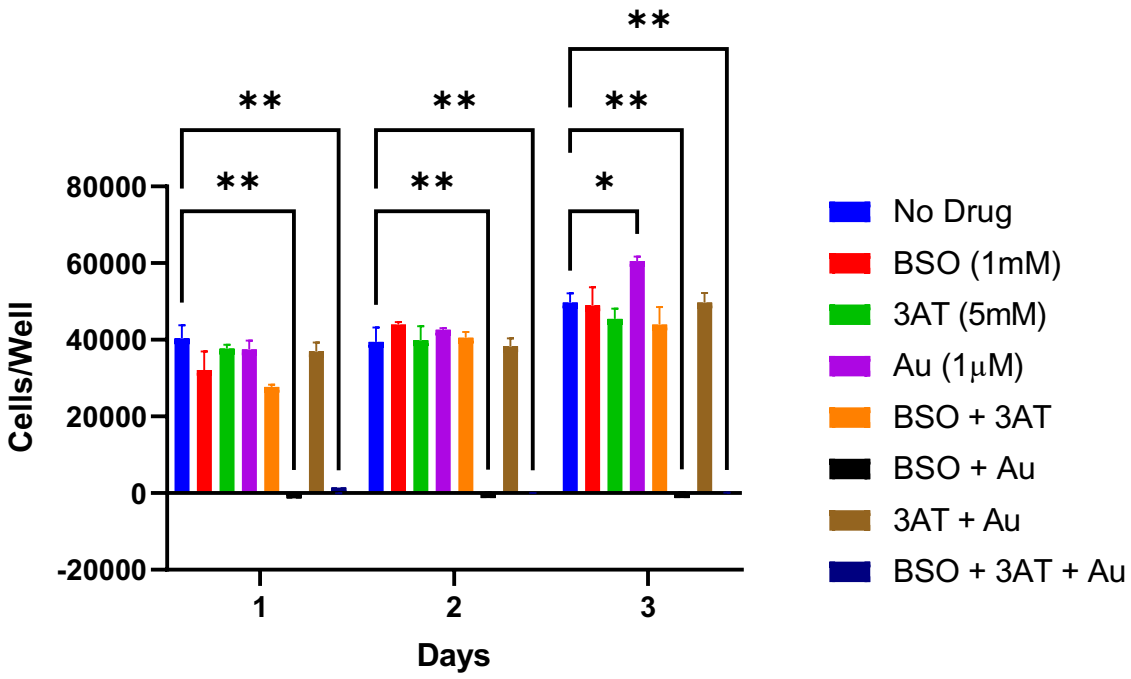

Cytotoxicity assay showed no cytotoxicity by 5 mM 3AT and 1μM Auranofin whether used alone or in combination for 3 days. Note: Buthionine sulfoximine (BSO) which inhibits GSH synthesis (and thereby starves glutathione peroxidase activity) was not used in this project. TWO WAY ANOVA, 95% CI, n=3, P: <0.0001(****), 0.0002(***), 0.0021(**), 0.0332(*).

4.4.9 Quinone Metabolism Generates H_2O_2

Quinone chemicals such as Menadione and 2,3-Dimethoxy-naphthoquinone (DMNQ) were used to generate H_2O_2 and a chemiluminescence reagent (AquaSpark) was used to produce light when reacted with the generated H_2O_2. Different concentrations of quinones were used (1µM, 5 µM, 10 µM and 25 µM) both alone and with a combination of peroxidase inhibitors (25mM 3AT and 10µM auranofin). A dose response effect was observed for both drugs and it appeared to plateau (and possibly decline) after 80-90 minutes or so (Figure 4.4.9.1). When measured at pH 8.5, DMNQ generated a much higher amount of H_2O_2 compared to menadione (Figure 4.4.9.2).

4.5 In-Cell Western (ICW) Assays to Investigate EMT Progression by Intracellular H_2O_2 Generation

To investigate the effect of intracellular H_2O_2 generation on EMT, In-Cell Western (ICW) assays (method in §3.7.3) were performed to generate a larger amount of data in less time. For these experiments, chemo-genetic approaches were used for intracellular H_2O_2 generation. As ICW experiments were in 96-well plates and cell growth quickly filled the wells to full confluence, morphological observation over time was not possible.

Figure 4.4.9.1

Generation of H_2O_2 with Quinone Metabolism

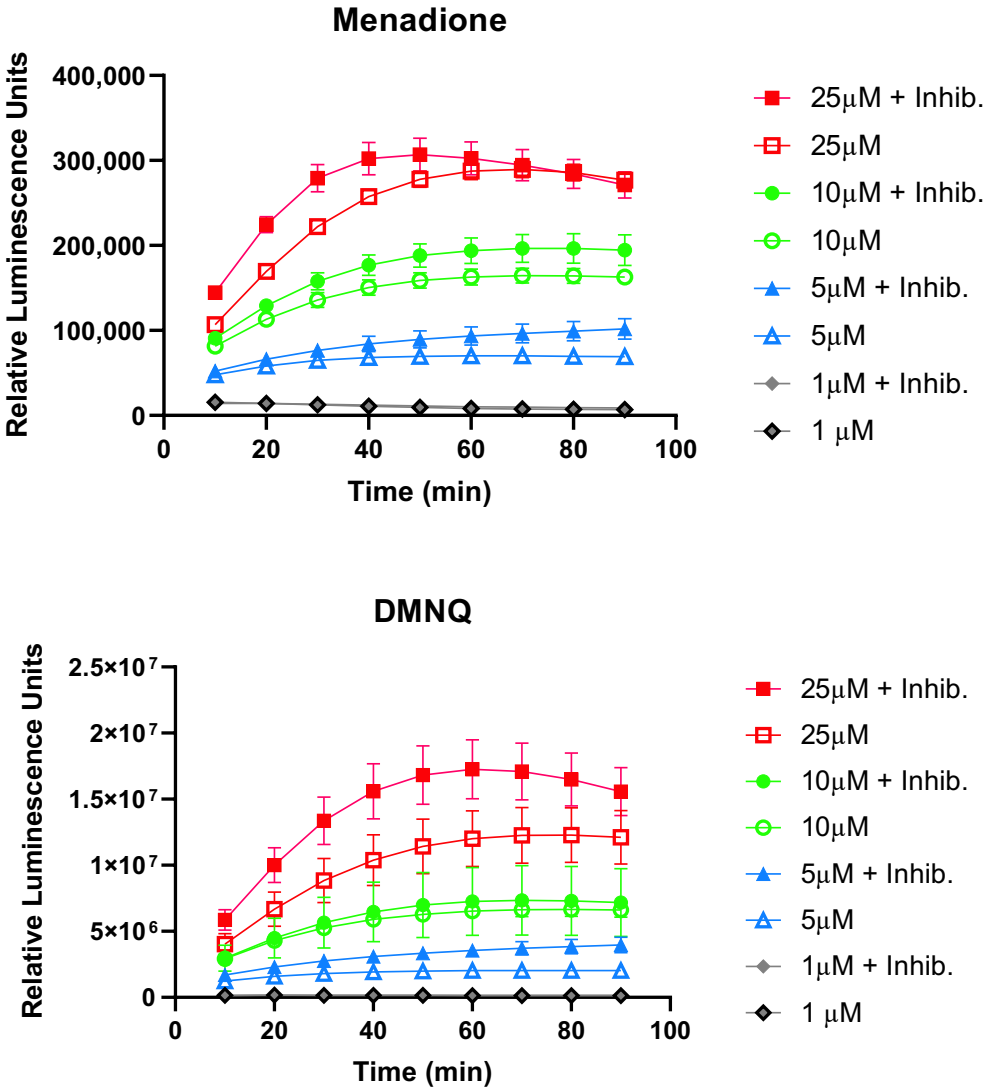

Initial experiment showing generation of H_2O_2 by two quinone drugs; Menadione (Top) and DMNQ (bottom). Generated H_2O_2 was quantified measuring luminescence using AquaSpark Chemiluminescence reagent. Inh: 25mM 3AT and 10μM auranofin. n=4

Figure 4.4.9.2

Comparison between Menadione and DMNQ on Generation of H_2O_2 with Quinone Metabolism

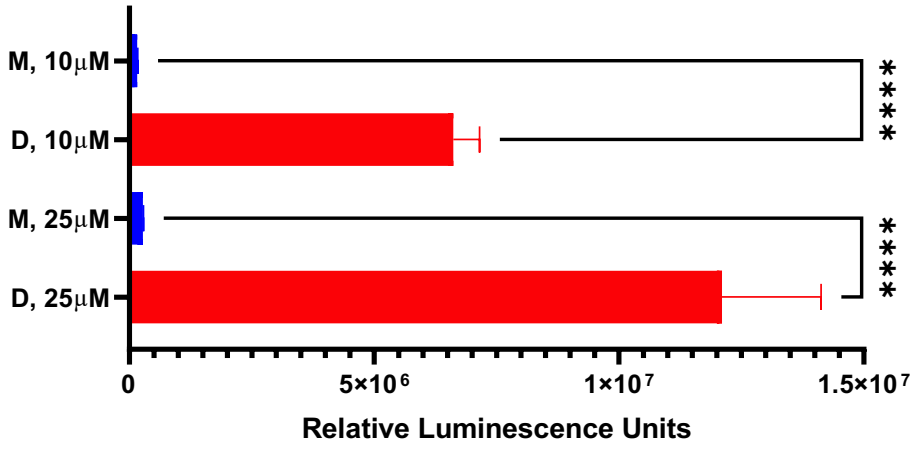

Comparison of H_2O_2 generation between Menadione and DMNQ. DMNQ generated much higher amount of H_2O_2, Compared to menadione. M: Menadione, D: DMNQ. One Way ANOVA, 95% CI, n=4, P: <0.0001(****).

4.5.1 Initial ICW Experiments Showed EMT Progression on Day 07 with Intracellular H_2O_2 Generation for 3 hours with DAAO and D-Alanine

Early ICW experiments to investigate the effect of intracellular H_2O_2 generation on EMT were performed with E-cadherin and fibronectin expression was evaluated. Cells transfected with the pAAV-HyPer-DAAO-NES plasmid were treated with different concentrations of D-Alanine (200 µM, 400 µM, 600 µM, 800 µM and 1 mM) for 3 hours. Cells were then allowed to grow for 7 days and were then fixed and processed for ICW. These experiments showed significant downregulation of E-Cadherin in treated cells and higher expression of mesenchymal fibronectin compared to control cells (Figure 4.5.1). However, no dose-response effect was observed with these conditions.

4.5.2 ICW Experiments Failed to Show Reproducible Data

ICW experiments started to show inconsistent results in further experiments (Figure 4.5.2). In one experiment E-cadherin expression went down significantly (Figure 4.5.2 B), but in another one, it was not significant (4.5.2 A). Fibronectin expression was much lower than the untreated cells and most importantly, TGFβ treated cells also showed unpredictable results. As a result, the in-cell western assay method was abandoned.

Figure 4.5.1

EMT Progression with Cytoplasmic H_2O_2 Generation measured by in-cell western assay

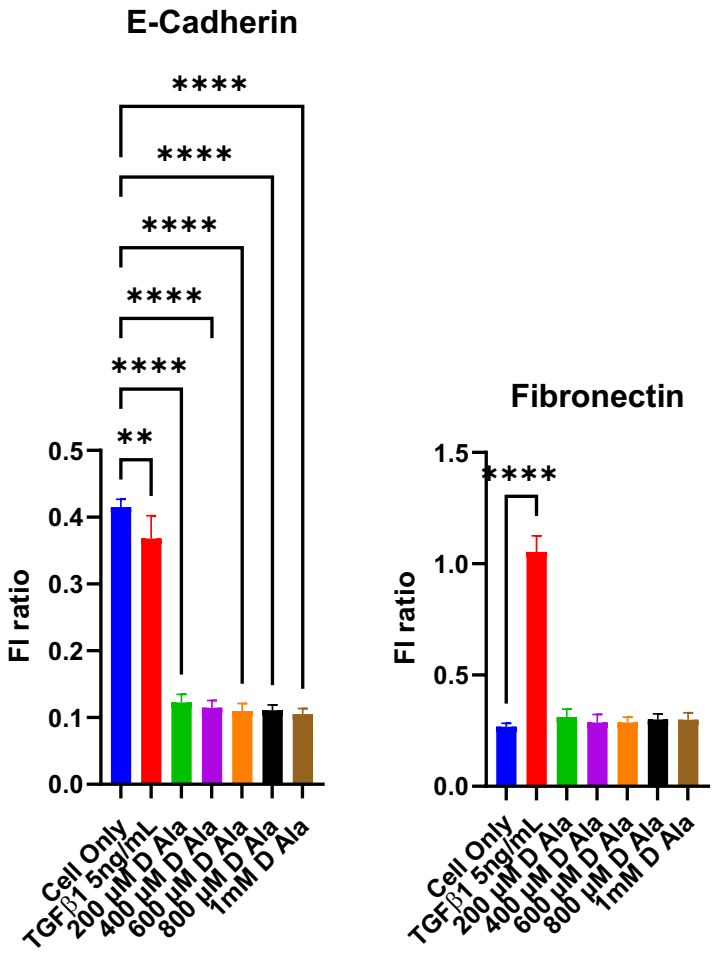

Preliminary ICW experiment showed EMT Progression on day 07, but no significant dose-response effect between the amount of H_2O_2 generation and EMT Marker expressions, Epithelial marker E-Cadherin expression went down significantly, but mesenchymal marker fibronectin expression did not increase significantly compared to untreated 'Cell only' group; (One-Way ANOVA, 95% CI, n=6, P<.0001(****), 0.0021(**).

Figure 4.5.2

Non-reproducible ICW Results for EMT Study

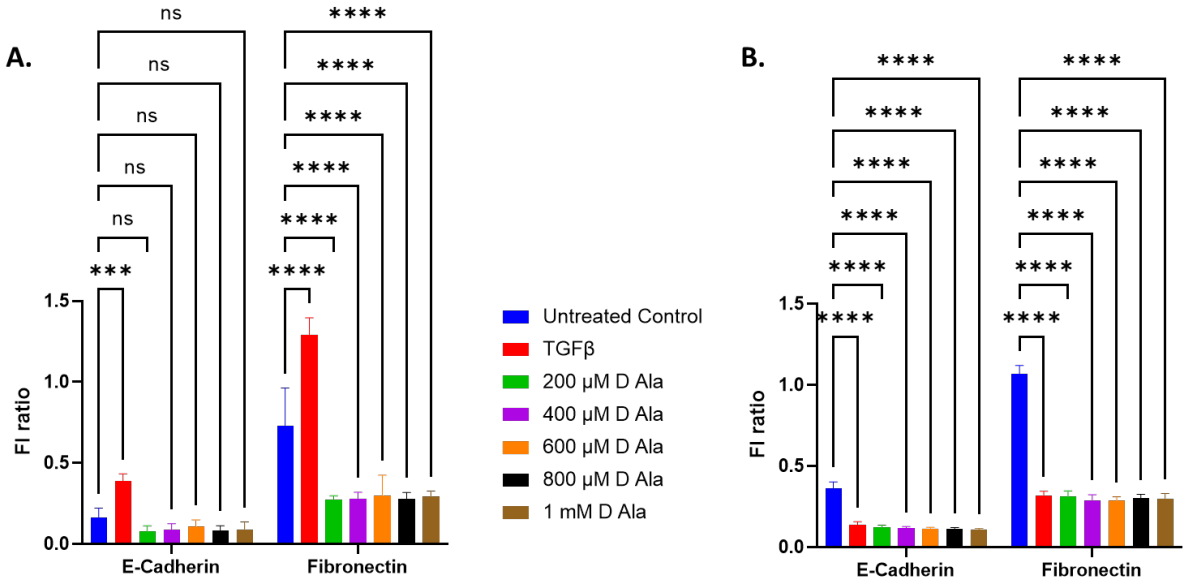

ICW Experiments showed inconsistent results: (A) E-Cadherin expression went up significantly compared to untreated cells instead of going down, D-Alanine treatments decreased E-Cadherin expressions, but were not significant here. Fibronectin Expression was significantly high in TGFβ treatment, it was significantly low (instead of higher) in all D-Alanine treatments. (B) E-Cadherin expressions were decreased significantly in all treatments compared to untreated control as expected, but fibronectin results were unexplainable. Two Way ANOVA, 95% CI, P****<.0001, P***.0002); A: n=8, B: n=6

4.6 Subcellular H_2O_2 Generation induced EMT

After subcellular H_2O_2 generation in the cytoplasmic, nuclear and mitochondrial compartments, cells were allowed to grow after treatment removal. In the initial experiments, the cells were treated for about 24 hours to generate H_2O_2, then morphology was observed periodically until fully confluence was obtained. Scratch wound healing assays were also performed 48 hours prior to cell lysate collection for western blot assays of marker expression.

4.6.1 EMT-related Morphological Changes were observed after cytoplasmic H_2O_2 generation while Nuclear and mitochondrial H_2O_2 Generation Showed Negligible Changes of Morphology

HyPer7.2-DAAO-NES transfected A549 cells treated with D-alanine for 24 hours started to show mesenchymal morphology development from day 04 compared to untreated cells (Figure 4.6.1A). Also, cells treated with D-alanine along with peroxidase inhibitors (*i.e.*, 25 mM 3-amino-1,2,4-triazole (3AT) and 2 μM Auranofin) showed phenotypic changes. Many cells in the treatment groups started to become loosely connected to each other, gaining elongated spindle shapes by the end of day 05.

The same D-alanine treatment to generate nuclear H_2O_2 also developed phenotypic changes, but to a much lesser extent than cells with cytoplasmic peroxide generation (Figure 4.6.1B). However, the presence of peroxidase inhibitors combined with nuclear peroxide generation showed similar phenotypic changes to those treated with cytoplasmic peroxide generators.

The mitochondrial H_2O_2 generation showed negligible phenotypic changes even in the presence of peroxidase inhibitors (Figure 4.6.1C). However, peroxidase inhibitor-only treated groups showed some mesenchymal features regardless of the subcellular location where H_2O_2 was generated.

Figure 4.6.1A

EMT Morphology Changes Started from Day 04 in A549 cells after Cytoplasmic H_2O_2 Generation

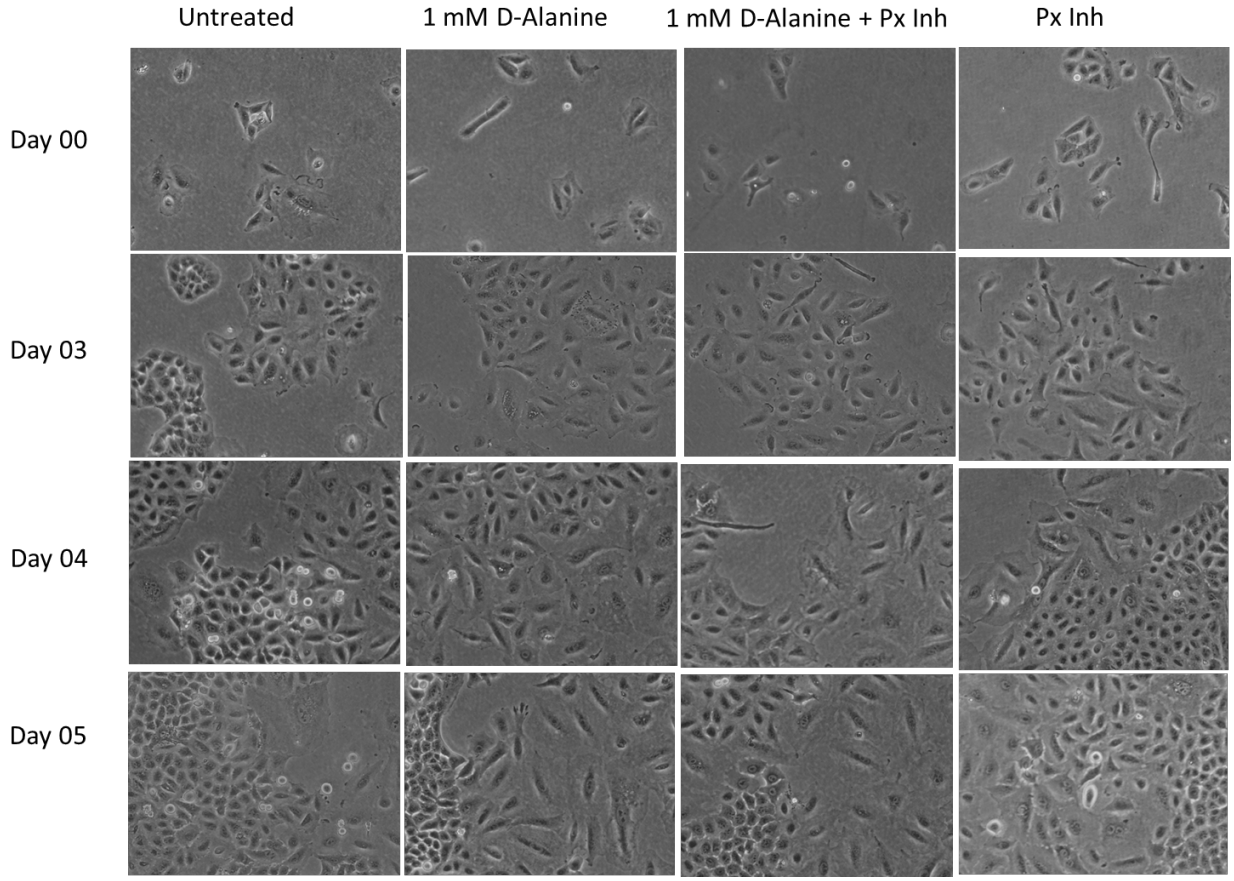

Epithelial to Mesenchymal Morphology Change from Day 04 after Cytoplasmic H_2O_2 Generation by the reaction between DAAO and D-Alanine. Both D-Alanine and D-Alanine in the presence of peroxidase inhibitors (25 mM 3-AT and 2µM Auranofin) caused A549 cells to become spindle like elongated shaped and loosely connected. Px Inh: Peroxidase Inhibitors only group also showed slight morphological change.

Figure 4.6.1B

EMT Morphology Changes in A549 cells after Nuclear H_2O_2 Generation

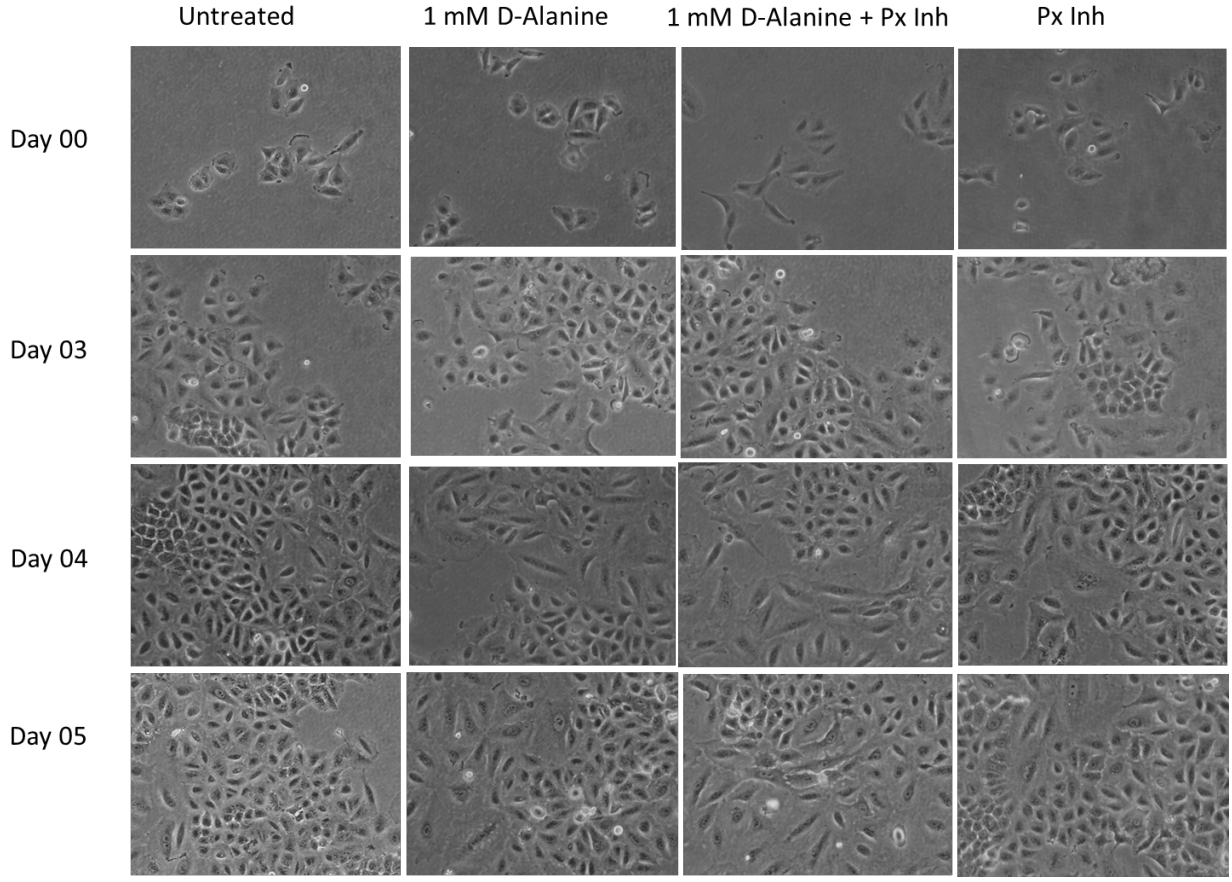

Epithelial to Mesenchymal Morphology Change from Day 04 after Nuclear H_2O_2 Generation by the reaction between DAAO and D-Alanine. Here, D-Alanine in the presence of peroxidase inhibitors (25 mM 3-AT and 2µM Auranofin) caused A549 cells to become spindle like elongated shaped and loosely connected. Px Inh: Peroxidase Inhibitors only group also showed negligible morphological change.

Figure 4.6.1C

Negligible EMT Morphology Changes in A549 cells after Mitochondrial H_2O_2 Generation

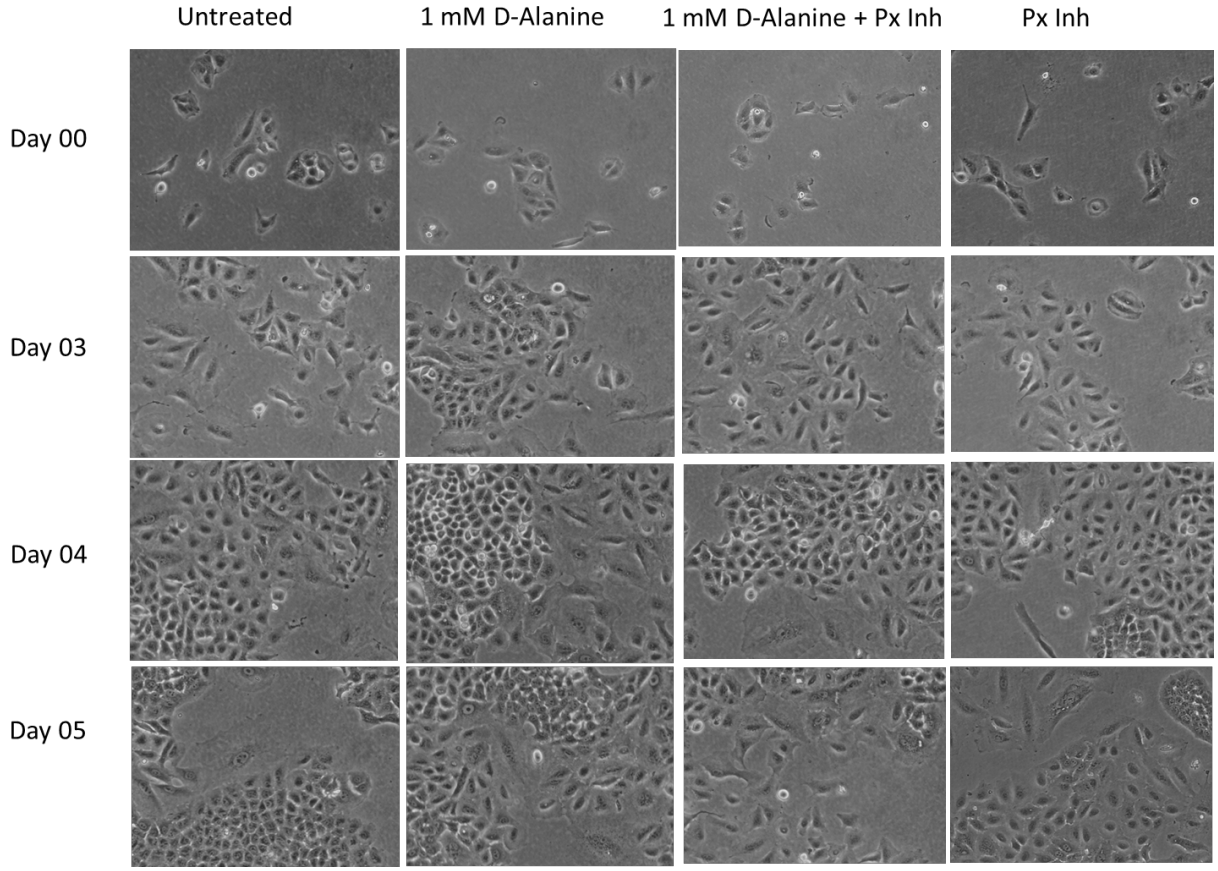

Negligible Epithelial to Mesenchymal Morphology Change after Mitochondrial H_2O_2 Generation by the reaction between DAAO and D-Alanine. Here, D-Alanine in the presence of peroxidase inhibitors (25 mM 3-AT and 2µM Auranofin) caused A549 cells to become spindle like elongated shaped and loosely connected. Px Inh: Peroxidase Inhibitors only group on day 05 showed some phenotypic changes here.

4.6.2.1 EMT induction after Cytoplasmic Peroxide Generation in the Presence of Peroxidase Inhibitors 7 days after Treatment Withdrawal

The Western blots were processed after collecting cell lysates on day 07 after removal of peroxide generating treatments. The results showed EMT progression with decreased expression of the epithelial marker E-cadherin and upregulation of the mesenchymal marker N-cadherin (Figure 4.6.2.1A) after peroxide was generated in the cytoplasm. However, such induction of EMT was significant only with D-alanine treatment along with peroxidase inhibitors (Figure 4.6.2.1B). The positive control TGFβ (5 ng/mL) also induced EMT significantly in these studies. However, no dose response effect was found in these studies between the amount of H_2O_2 produced from D-alanine/DAAO reaction and the intensity of EMT marker expression.

Figure 4.6.2.1A

Preliminary Western Blot Results Showing EMT Progression on Day 07 after Cytoplasmic H_2O_2 Production in A549 Cells

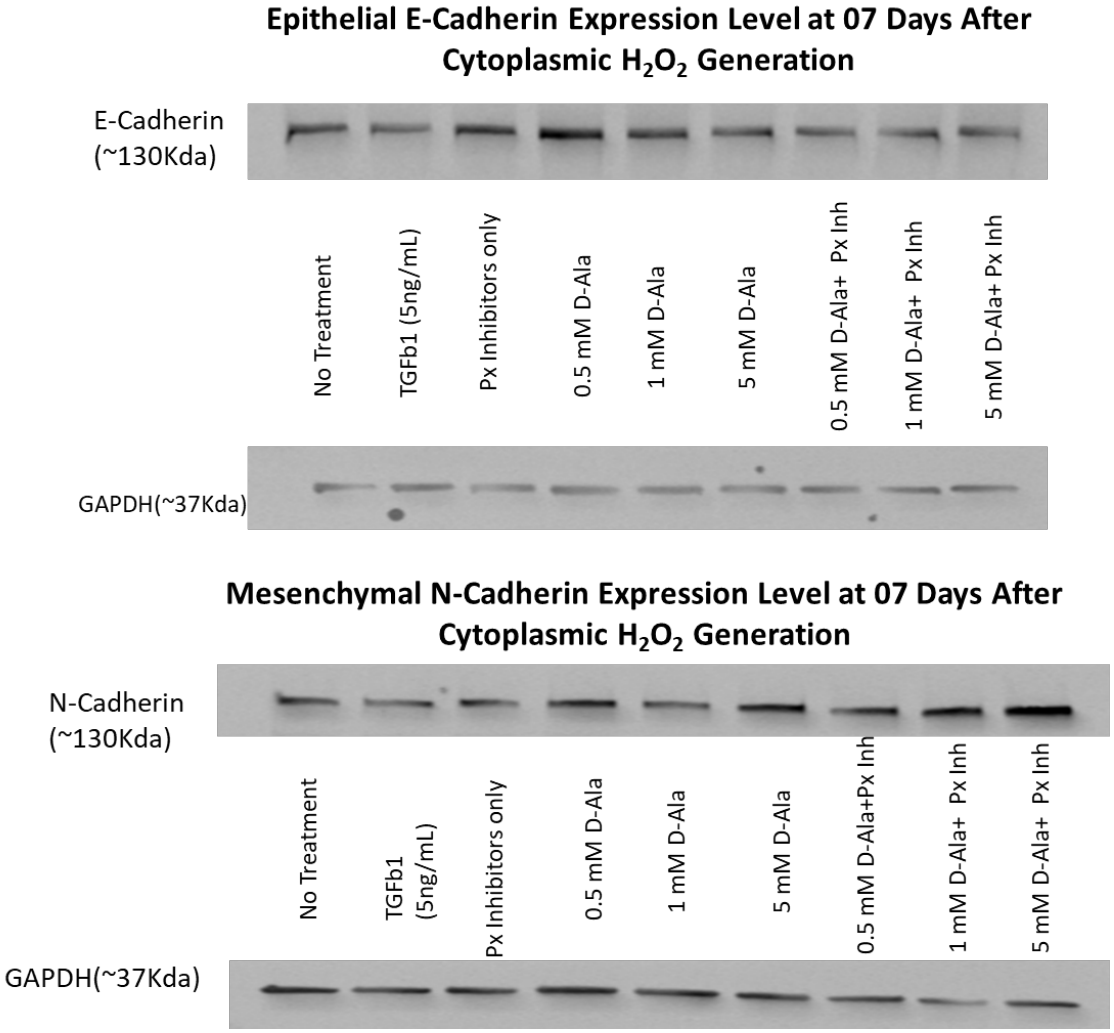

Changes in epithelial (Top) and mesenchymal marker (bottom) progression on day 07-after cytoplasmic H_2O_2 production; Px Inh: Peroxidase inhibitors (2µM Auranofin + 25mM 3-AT)

Figure 4.6.2.1B

Analysis of Western Blot Results Showing Significant EMT Progression on Day 07 after Cytoplasmic H_2O_2 Production in A549 Cells by D-Alanine+ Px Inhibitors

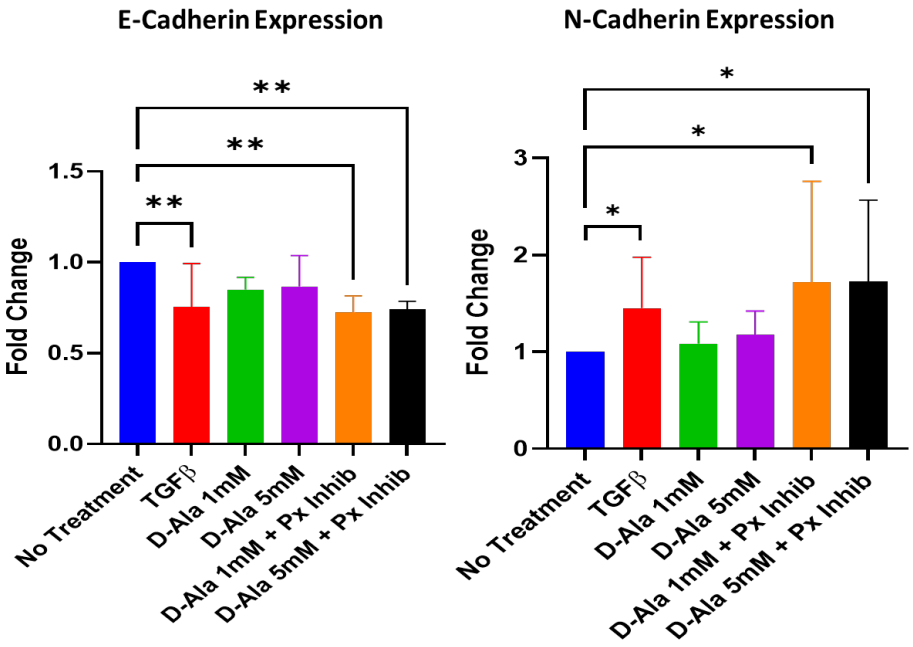

Western Blot Analysis Showing Significant EMT Progression on Day 07 after Cytoplasmic H_2O_2 Production in A549 Cells particularly by D-Alanine+ Px Inhibitors groups. One Way ANOVA, 95% CI, n=6 for E-Cadherin, n=7 for N-cadherin P: <0.0021(**), 0.0332(*).

4.6.2.2 No Significant EMT Progression was observed in A549 Cells after Nuclear and Mitochondrial Peroxide Generation

Western blot results showed no significant EMT progression with inconsistent expression of epithelial E-cadherin and mesenchymal N-cadherin in A549 cells where peroxide was generated in the nucleus (Figure 4.6.2.2A and 4.6.2.2B) and mitochondria (4.6.2.2C and 4.6.2.2D). Here, the presence of peroxidase inhibitors was not effective in promoting EMT marker expression. The positive control TGFβ (5 ng/mL) induced EMT significantly in these studies.

Figure 4.6.2.2A

Preliminary Western blot Results Showed No Significant EMT Progression on Day 07 after Nuclear H_2O_2 Production in A549 Cells

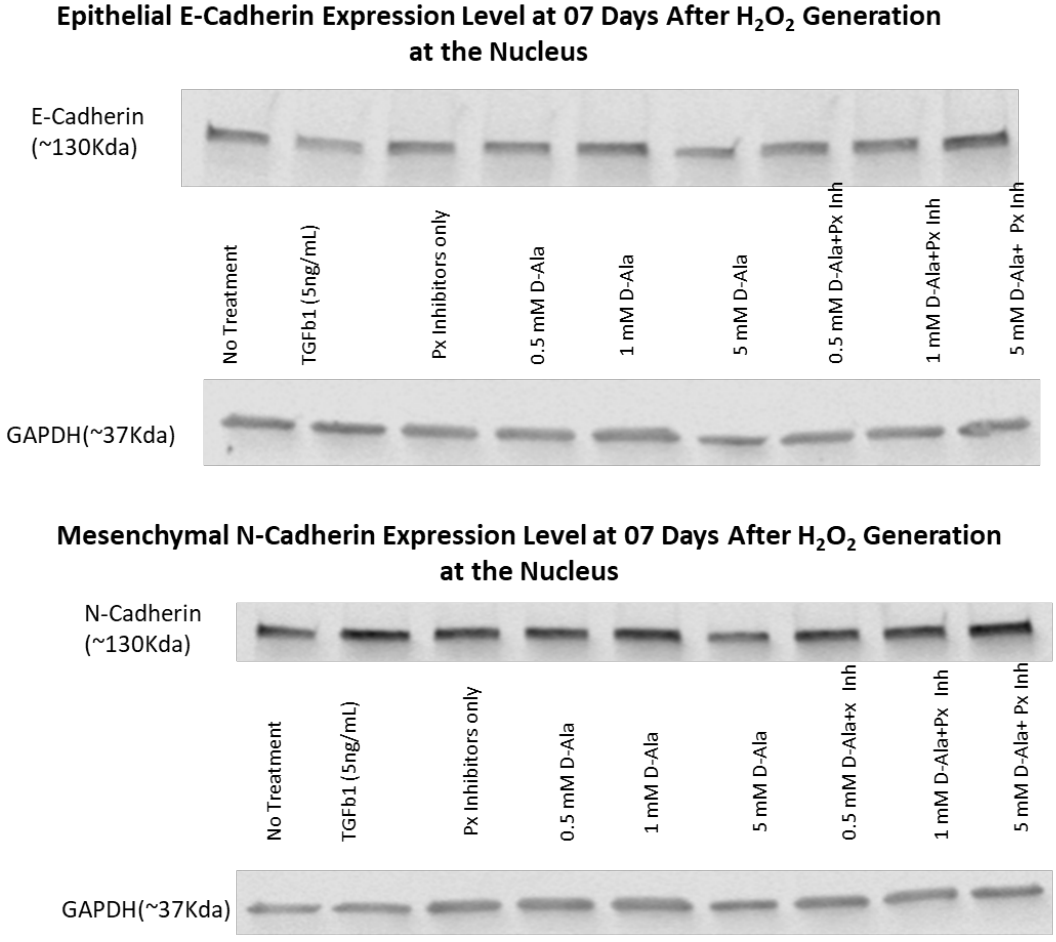

Changes in epithelial (Top) and mesenchymal marker (bottom) progression after 7-days of Nuclear H_2O_2 production; Px Inh: Peroxidase inhibitors (2uM Auranofin + 25mM 3-Aminotrazole)

Figure 4.6.2.2B

Analysis of Western Blot Results Showing Inconsistent EMT Progression on Day 07 after Nuclear H_2O_2 Production in A549 Cells

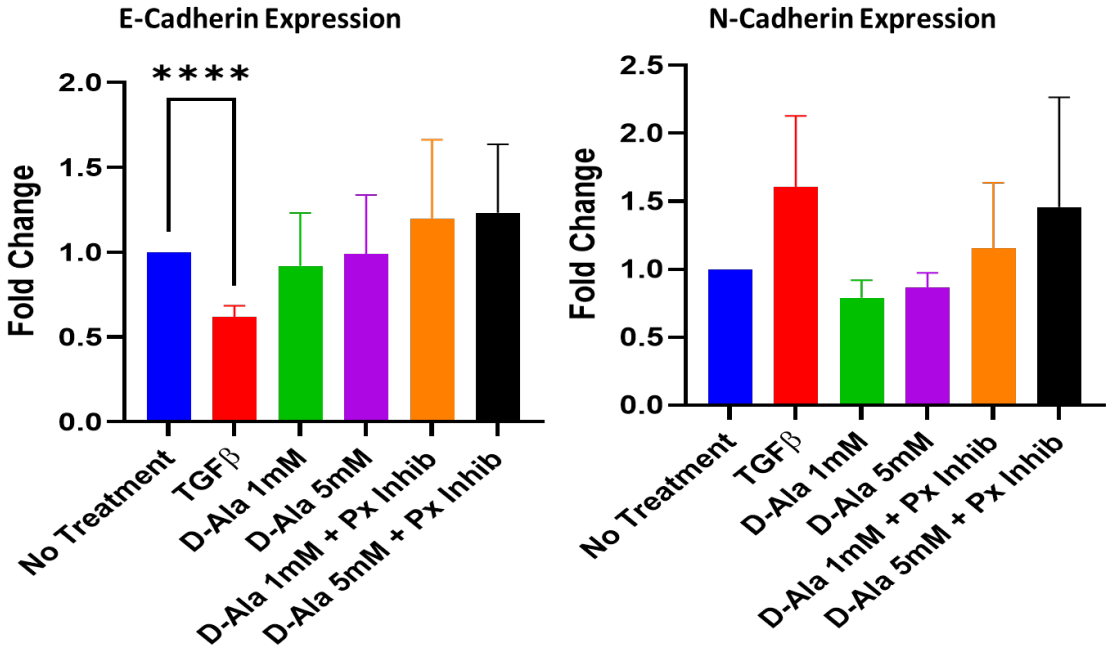

Western Blot Analysis showing inconsistent EMT Progression on Day 07 after Nuclear H_2O_2 Production in A549 Cells. One Way ANOVA, 95% CI, n=4, P: <0.0001(****).

Figure 4.6.2.2C

Preliminary Western blot Results Showed No Significant EMT Progression on Day 07 after Mitochondrial H_2O_2 Production in A549 Cells

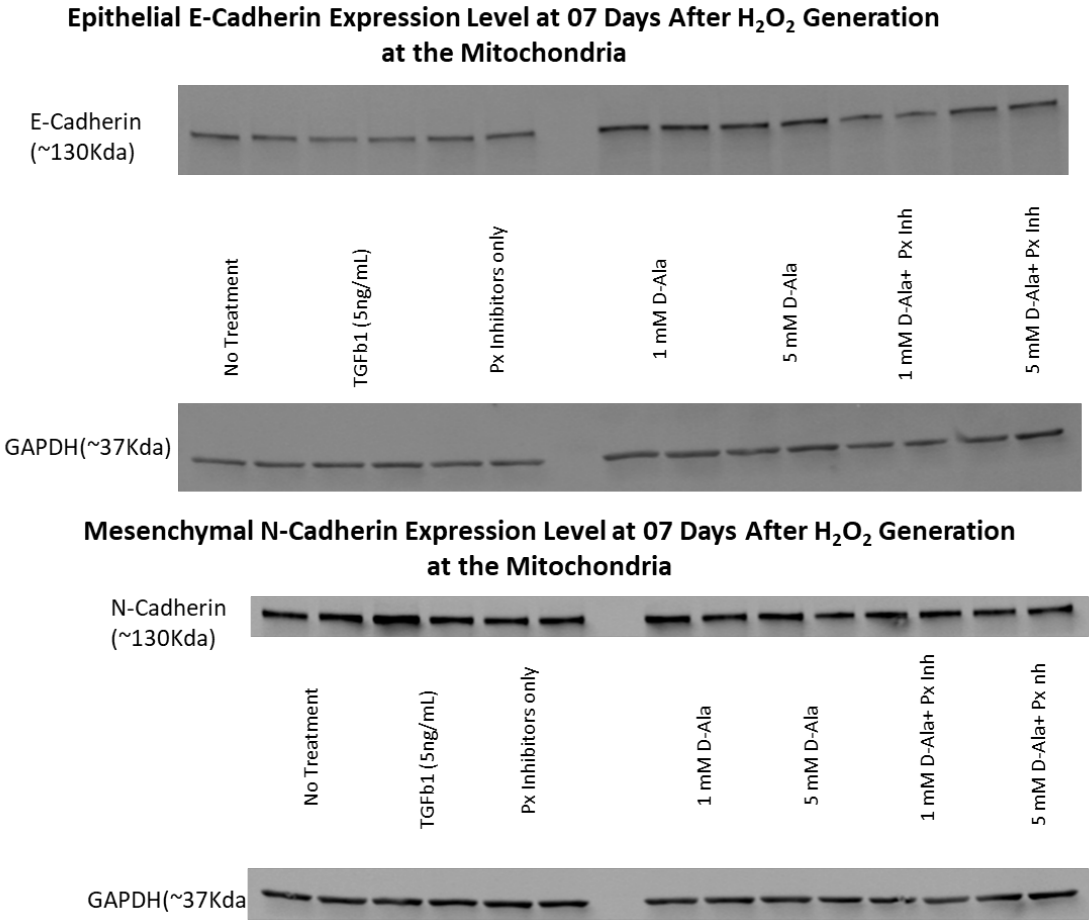

Western Blots Showing Changes in epithelial (Top) and mesenchymal marker (bottom) progression after 7-days of mitochondrial H_2O_2 production; Px Inh: Peroxidase inhibitors (2uM Auranofin + 25mM 3-Aminotrazole) Each sample was loaded in pair.

Figure 4.6.2.2D

Preliminary Western Blot Results Showing Inconsistent or No EMT Progression on Day 07 after Mitochondrial H_2O_2 Production in A549 Cells

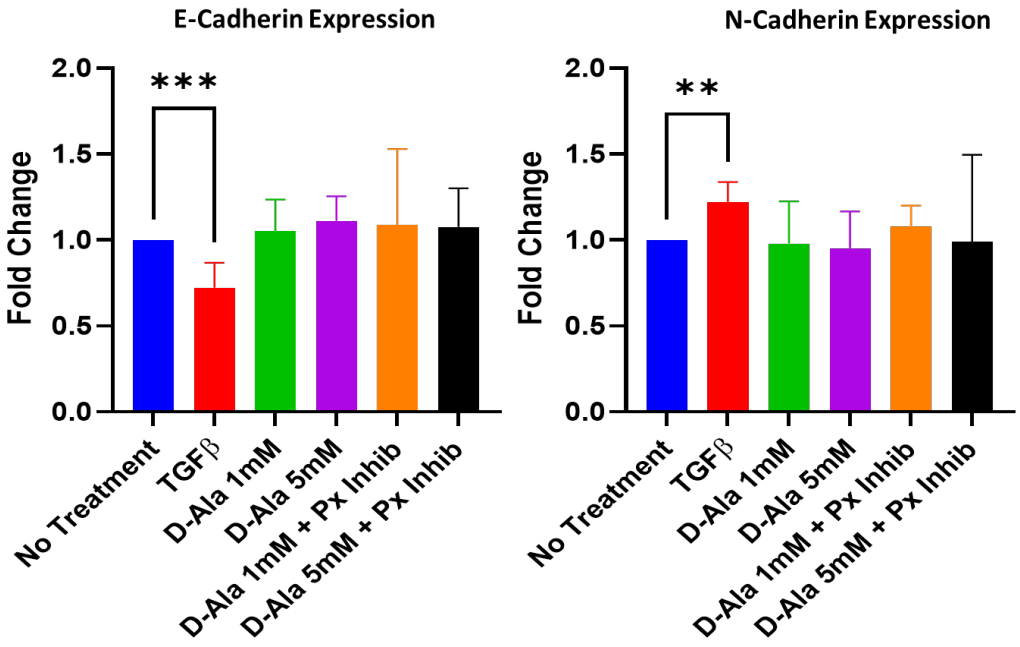

Western Blot Analysis showing inconsistent or no EMT Progression on Day 07 after Mitochondrial H_2O_2 Production in A549 Cells. One Way ANOVA, 95% CI, n=6, P: <0.0002(***), 0.0021(**).

4.7 Induction of EMT by Peroxidase Inhibition

4.7.1 EMT-related Marker Expression Changes Showed Induction of EMT by Peroxidase Inhibition

Treatment of A549 cells with 25 mM 3-amino-1,2,4-triazole (3-AT) and 2 µM Auranofin for 24 hours resulted EMT related marker expression changes in A549 cells by day 07 (Figure 4.7.1). The epithelial marker E-cadherin (E-CAD) expression was significantly downregulated, and mesenchymal marker N-cadherin (N-CAD) was significantly upregulated in all cases. The positive control TGFβ1 (5ng/mL) also showed EMT progression with relevant marker expression changes.

Figure 4.7.1

EMT-related Marker Expression Change Showing EMT by Peroxidase Inhibitors

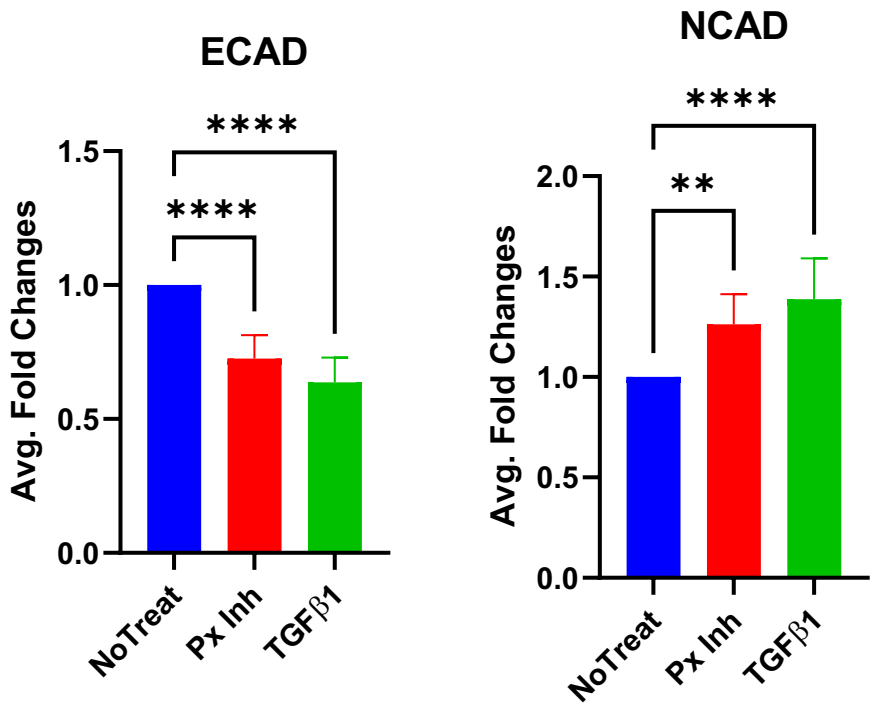

Peroxidase inhibition induced EMT, One Way ANOVA, 95% CI, n=8, P: <0.0001(****), 0.0021(**).

4.7.1.1 EMT induction was mostly attributable to 3-Amino-1,2,4-Triazole

3-Amino-1,2,4-triazole was found to be the major EMT contributor in the peroxidase inhibitor combinations tested (Figure 4.7.1.1). In western blot analysis, Auranofin (Au) was found to have a negligible effect on EMT marker expression and the 3AT effect was very close to the effect of the peroxidase inhibitor combination. Also, it was found that on day 05 after treatment, the EMT marker expression was already altered to a significant extent. This result is interpreted to mean that catalase inhibition is likely adequate to induce EMT. In later studies, the effect of 3AT remained consistent as an EMT inducer.

4.7.2 EMT-like Morphology Changes Are Induced by Peroxidase Inhibitors

Morphological changes were also observed during the time when cells were allowed to grow after peroxidase inhibitor treatments. However, the cells became confluent on day 05 and it was not possible to follow their morphological change observation beyond that. Also, some of the image data were lost (particularly for NLS and Mito groups on day 03) due to technical challenges.

Cells in untreated groups did not show any morphological change relevant to EMT (Figure 4.7.2.1), but cells with peroxidase inhibitor treatments showed some EMT related morphological features on day 03 and day 05 regardless of their transfection status. These treated cells became spindle-like, elongated, and loosely connected with each other (Figure 4.7.2.2).

Figure 4.7.1.1

3AT was Found to be the Major Inducer of EMT in Peroxidase Inhibitor Combinations

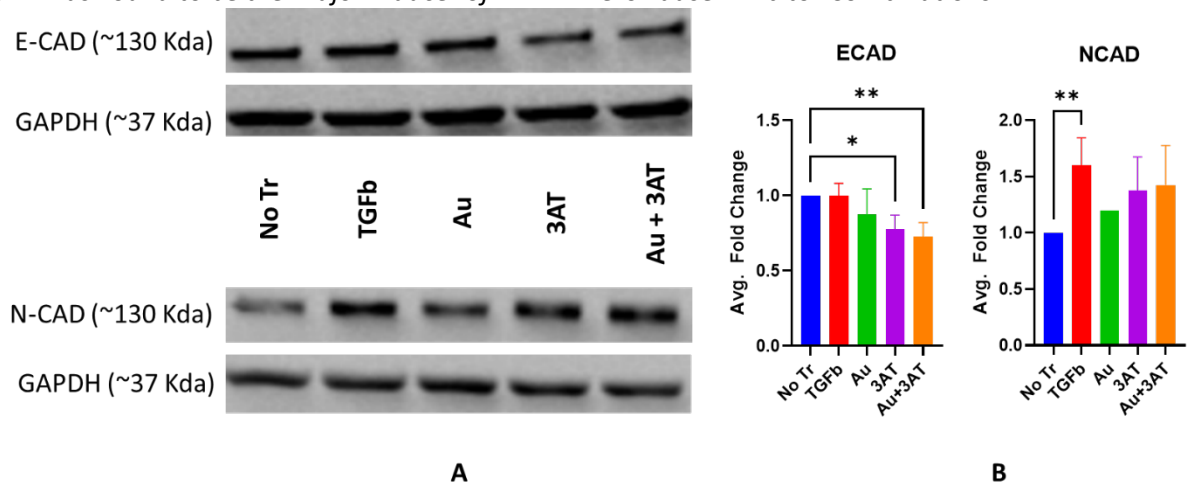

3AT alone was found to be the main player to induce EMT and within 5 days, (A) Western Blot results showing significant downregulation of E-Cadherin (E-CAD) and upregulation of mesenchymal N-Cadherin (N-CAD) in 3AT treated cells. Au: Auranofin, 3AT: 3-Aminotrazole. (B) Statistical analysis, One Way ANOVA, 95% CI, n=4 P: < 0.0021(**), 0.0332(*).

Figure 4.7.2.1

No EMT-related Morphological Changes in Untreated Control Cells

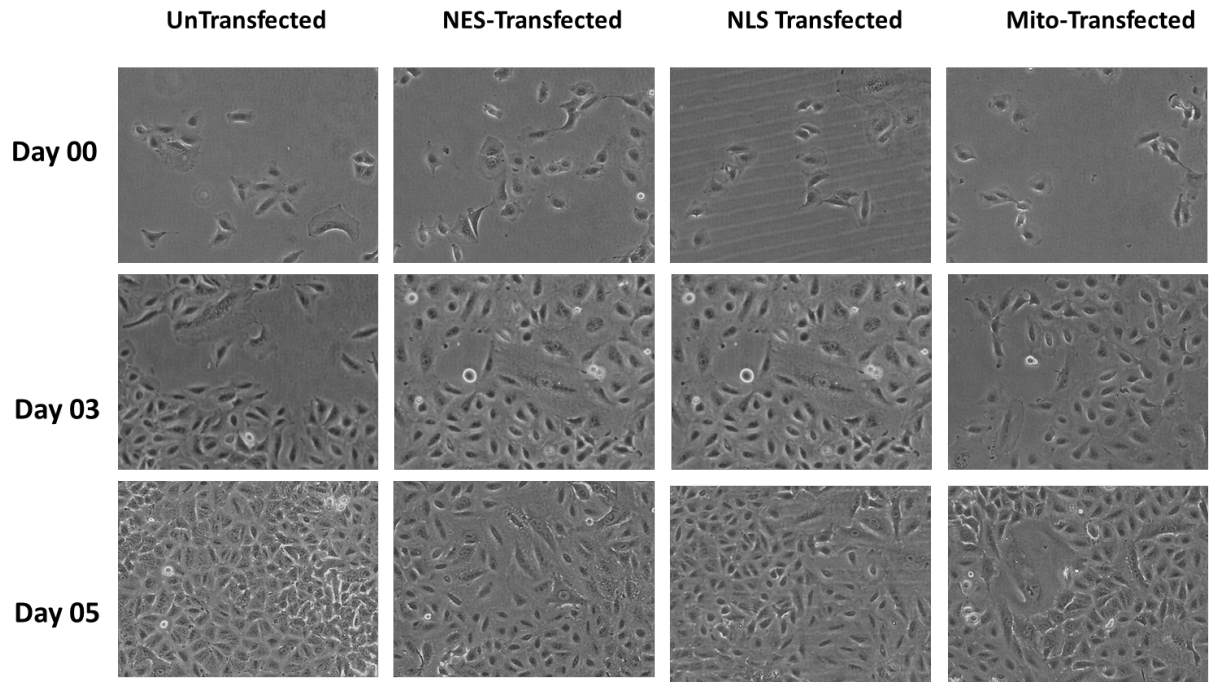

No EMT-related morphological changes were observed until day 05 in cells where there was no treatment of peroxidase inhibitors

Figure 4.7.2.2

EMT-related Morphological Changes Observed in Peroxidase Inhibitor Treated Cells

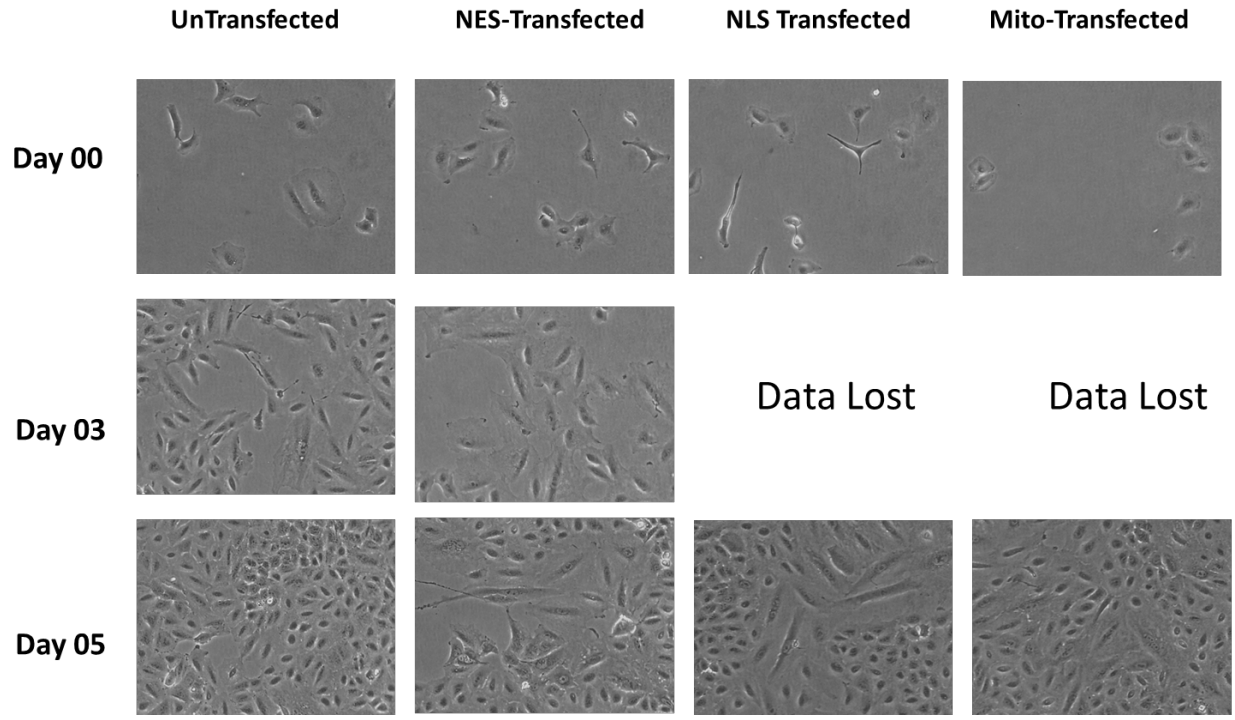

EMT-related morphological changes (elongated, spindle like, loosely connected) were observed until day 05 in cells treated with peroxidase inhibitors (25 mM 3-amino-1,2,4-triazole (3-AT) and 2 µM Auranofin). Data on Day03 for NLS and mito group was lost.

4.7.3 Cells Treated with Peroxidase Inhibitors showed increased motility in wound-healing assays.

As 3-AT was found to induce EMT in previous experiments, scratch wound healing assay was performed with 25 mM 3-AT treatment only, Auranofin was ditched. In these experiments, cells were treated with 25 mM 3-AT for 6 hours after 24 hours of serum starvation. After 6 hours of treatment, the media were replaced with fresh RPMI complete medium and allowed to grow for 5 days with 50% media replacement on every other day. Scratches were made on day 03, images were taken every 12 hours, up to 48 hours. Cells treated with 3-AT showed faster wound healing compared to untreated controls and it was statistically significant at 12, 24 and 36 hours (Figure 4.7.3A and B).

4.8 Intracellular H_2O_2 Generation for 6 hours after 24 Hours of Serum Starvation was Adequate to Induce EMT

Further experiments showed that 6 hours duration of several treatments to generate intracellular H_2O_2 was sufficient to induce EMT after 5 days. The cells were serum starved for 24 hours before adding the treatments.

4.8.1: Peroxide production for 6 hours induced EMT-related Marker Expression Changes

The Western Blot results confirmed both 3AT alone and D-Alanine+3AT can induce EMT via significant upregulation of mesenchymal N-CAD (Figure 4.8.1) by day 05. Here, the treatment duration by 3AT or D-Alanine + 3AT was for 6 hours. The DMNQ treatment was for 1 hour which had no influence on EMT.

Figure 4.7.3A

3-AT Treatment Showed Faster Motility compared to untreated Controls

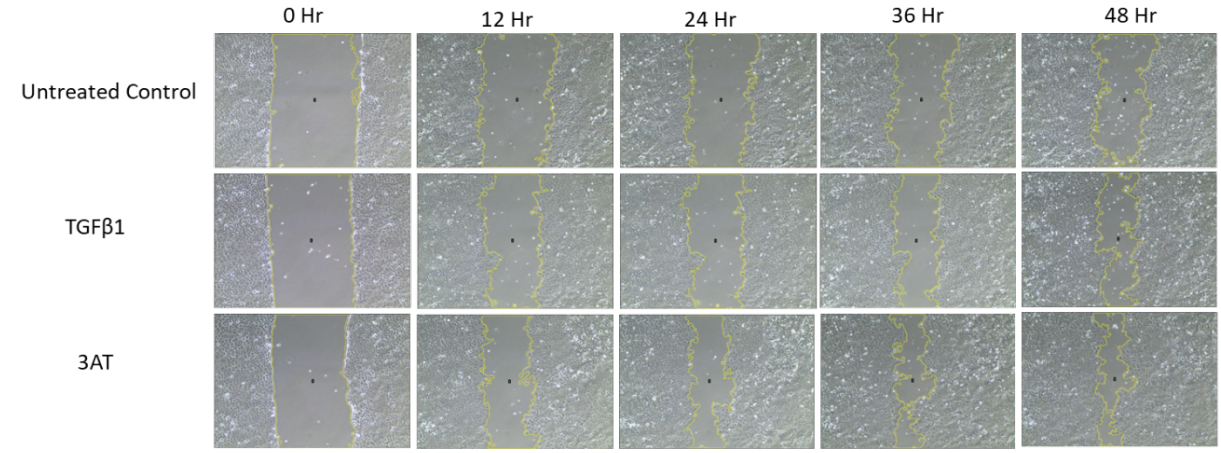

Figure 4.7.3A Motility Assay by 3-AT Showing faster wound healing compared to untreated controls

Figure 4.7.3B

3-AT Treatment Showed Faster Motility compared to untreated Controls, which was statistically significant at 24 hours

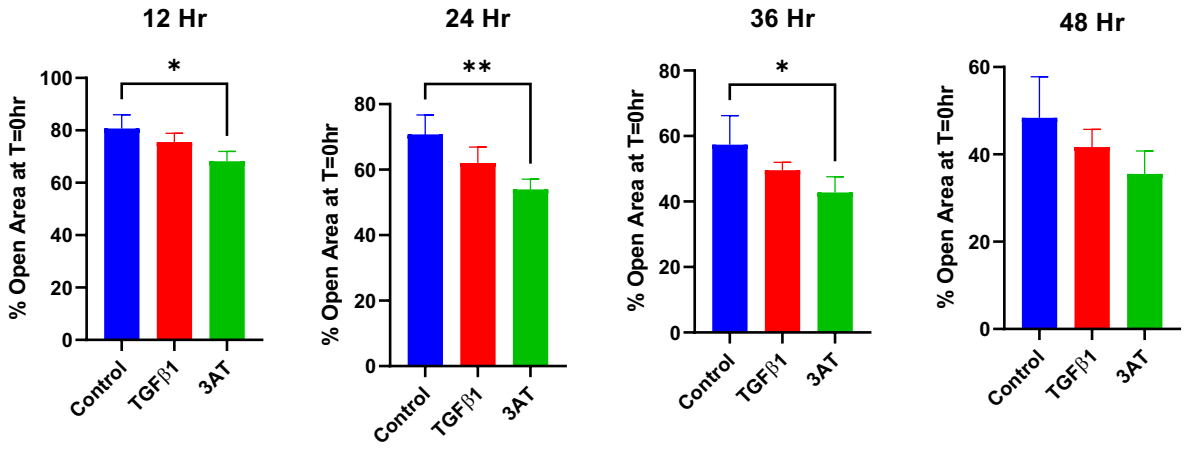

Motility Assay by 3-AT Showing faster wound healing which was statistically significant. One Way ANOVA, 95% CI, n=3, P: <0.0021(**), 0.0332(*).

Figure 4.8.1

Western Blot Results Showing EMT Induction by Intracellular H_2O_2 Generation within 5 Days

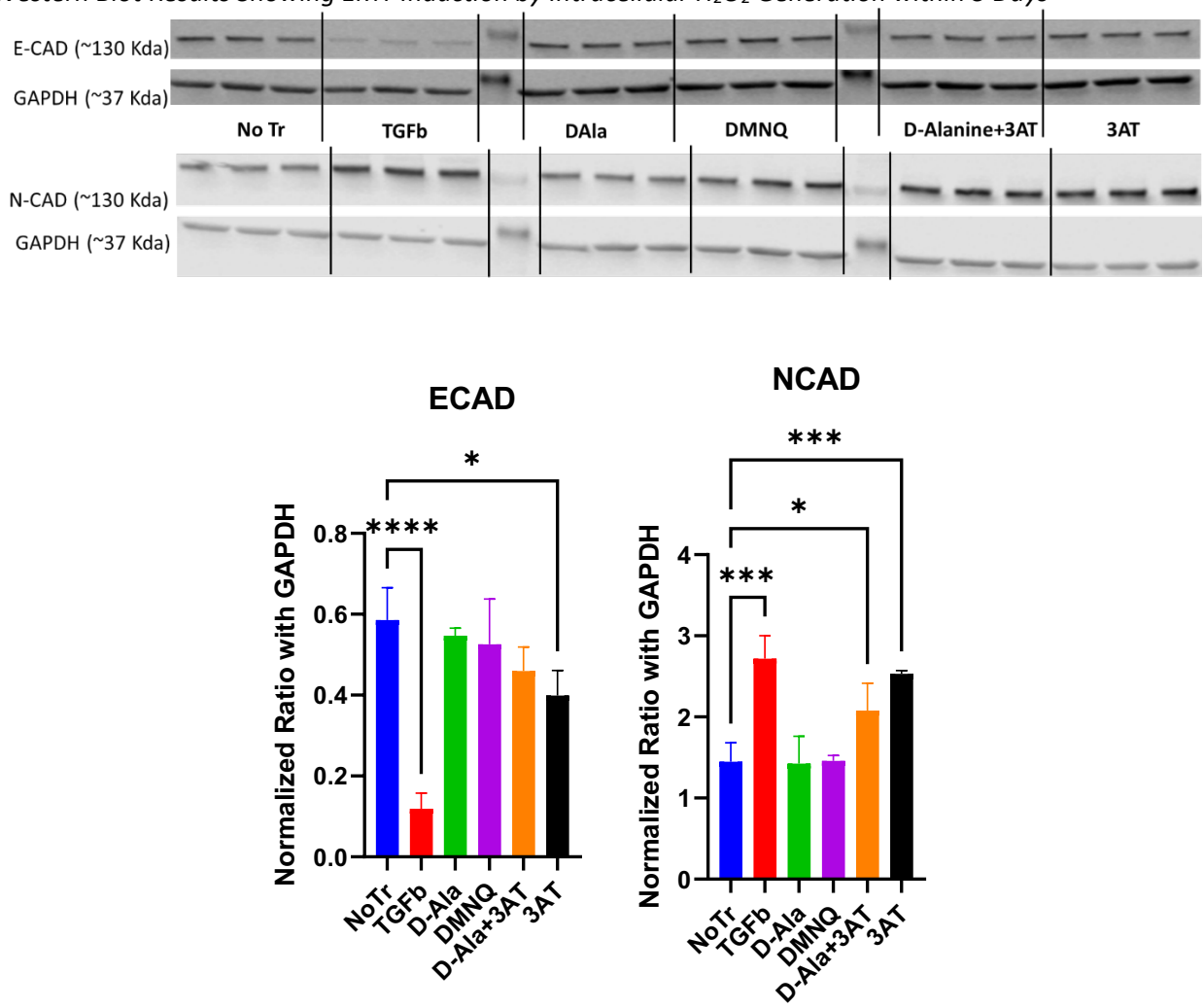

Western Blot Results (3 biological replicates for each treatment) showing EMT Induction by TGFb, D-Alanine+3AT and by 3AT alone. D-Alanine and 3AT treatments were for 6 hours after serum starvation. One Way ANOVA, 95% CI, n=3, P: <0.0001(****), 0.0002(***), 0.0332(*).

4.8.2 Scratch Wound Healing Assay Results Showed Faster Wound Healing Trends

The scratch wound healing assays were also performed by scratching the cells on day 03 after treatment removal. Images were captured at about 24 hours and about 48 hours. All the treatments showed faster wound healing trend compared to untreated controls (Figure 4.8.2A), but the results were not statistically significant (Figurer 4.8.2B).

4.9 Quinone Metabolism Is Associated with EMT Induction

Quinone metabolism to generate hydrogen peroxide and thus to promote EMT was performed for DMNQ (2,3-Dimethoxy-naphthoquinone) metabolism only. Cells were treated with 10 µM DMNQ for 1 hour in complete media immediately after 24 hour of serum starvation. Cells were then allowed to grow for 3 days when scratches were made, morphology was observed, and on day 05 cell lysates were collected for measurement of marker expression.

4.9.1 EMT-related Marker Expression Changes were not induced by DMNQ Treatment

The western blot assay did not show any EMT-related marker expression changes after 1 hour DMNQ treatment (Figure 4.9.1).

Figure 4.8.2A

Scratch Wound Healing Assay Showing 5 days Post-Treatment Growth was sufficient to induce EMT-like motility

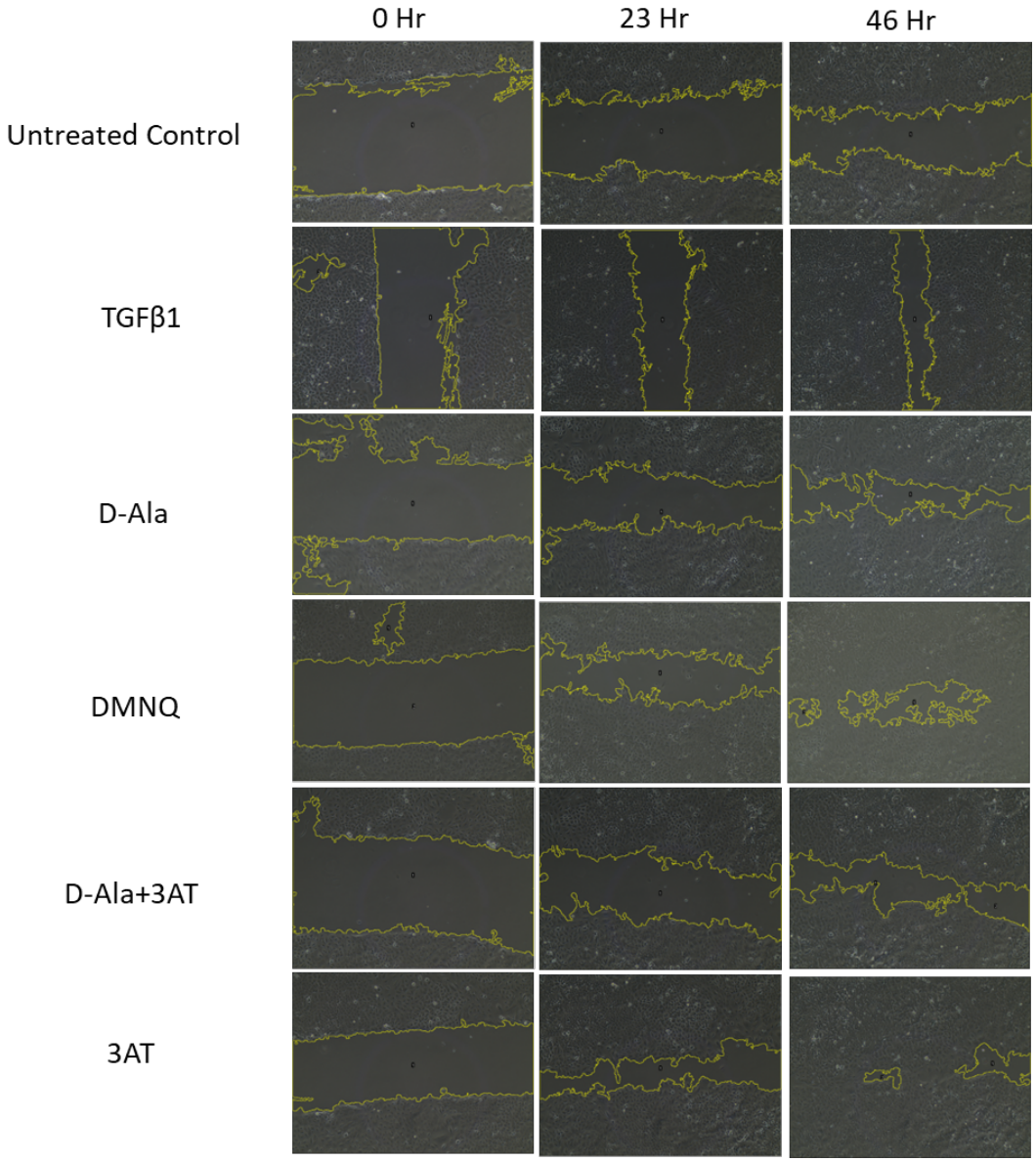

Scratch Wound Healing Assay Showing increased motility in A549 cells where intracellular H_2O_2 was allowed to accumulate and cytoplasmic H_2O_2 was generated

Figure 4.8.2B

Scratch Wound Healing Assay Showing 5 days Post-Treatment Growth trended toward EMT-like motility

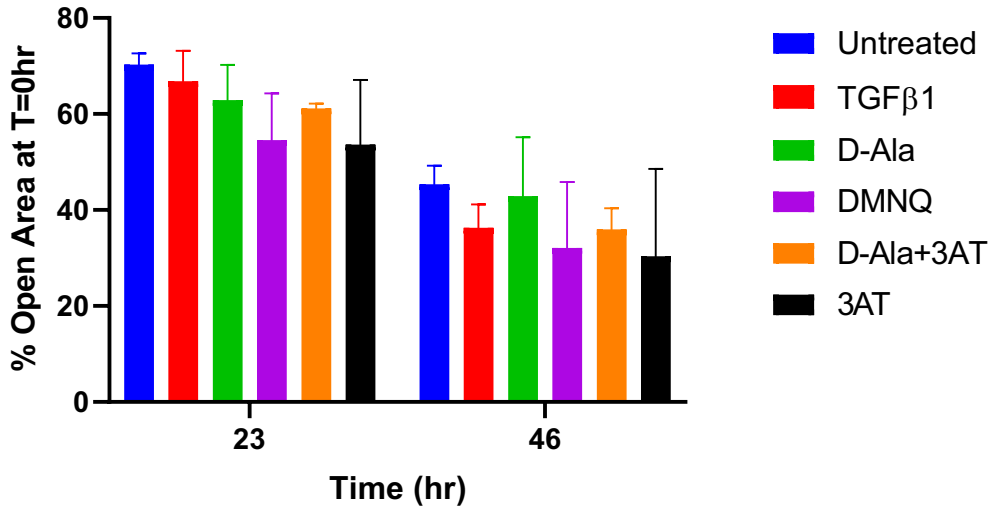

Statistical Analysis showing a trend toward enhanced motility up to 46 hours in A549 cells with different treatments to increase intracellular H_2O_2, but the results were not statistically significant (One Way ANOVA, n=3)

Figure 4.9.1

EMT-related Marker Expression Change Results by DMNQ Treatment

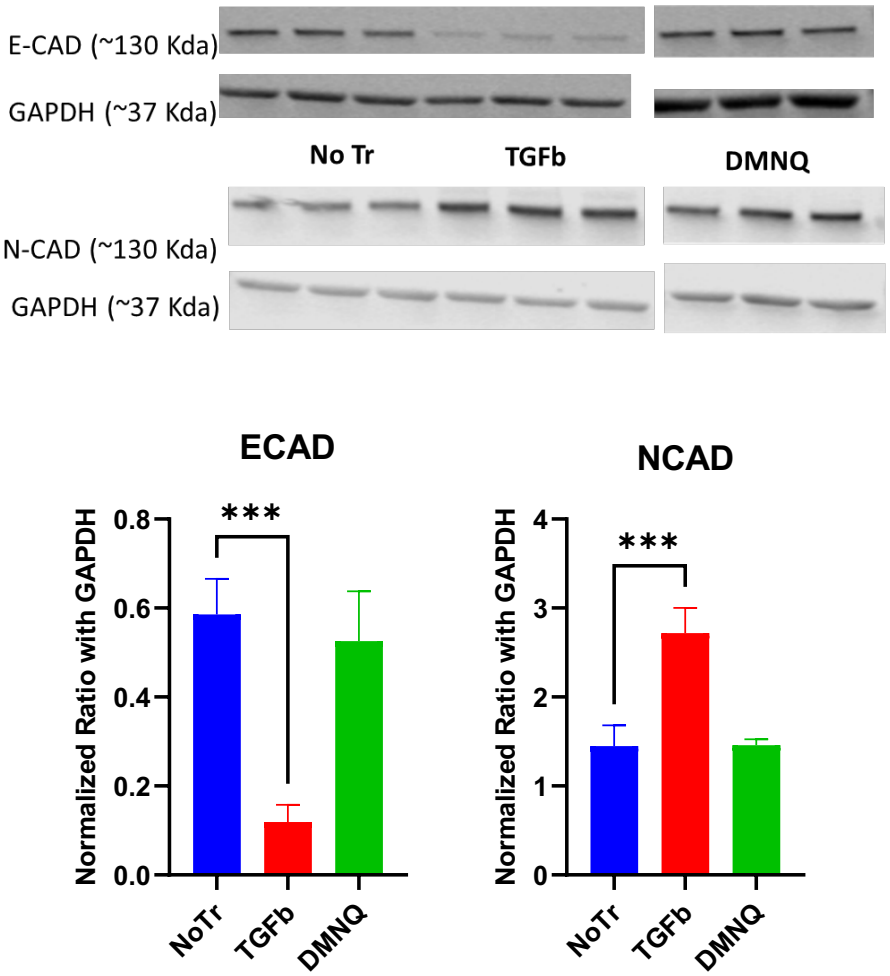

Western Blot Results (3 biological replicates for each treatment) showing no significant changes of EMT related marker expression changes by DMNQ. Samples shown were from the same blot. One Way ANOVA, 95% CI, n=3, P: <0.0002(***).

4.9.2 Scratch Wound Healing Results by DMNQ Treatment

The scratch wound healing assays were performed after treatment with 10 µM DMNQ for 1 hour, immediately following 24 hours of serum starvation. After treatment removal, cells were allowed to grow and on day 03, scratches were made, images captured at about every 12 hours, up to about 48 hours. Although the marker expression results were not positive, DMNQ treated cells here showed much faster motility compared to untreated cells (Figure 4.9.2A), and this change was statistically significant at all time points (Figure 4.9.2B).

Figure 4.9.2A

DMNQ Treatment Showed Faster Motility Compared to untreated Control

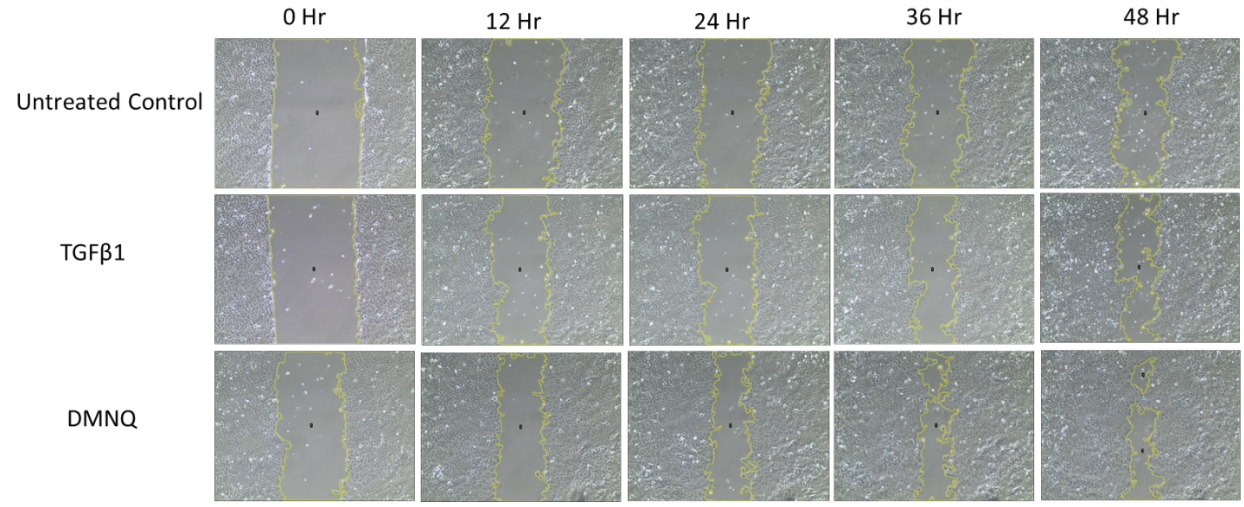

Motility Assay by DMNQ Showing faster wound healing compared to untreated controls

Figure 4.9.2B

DMNQ Treatment Showed Faster Motility Compared to untreated Control and was Statistically Significant at 24 hours

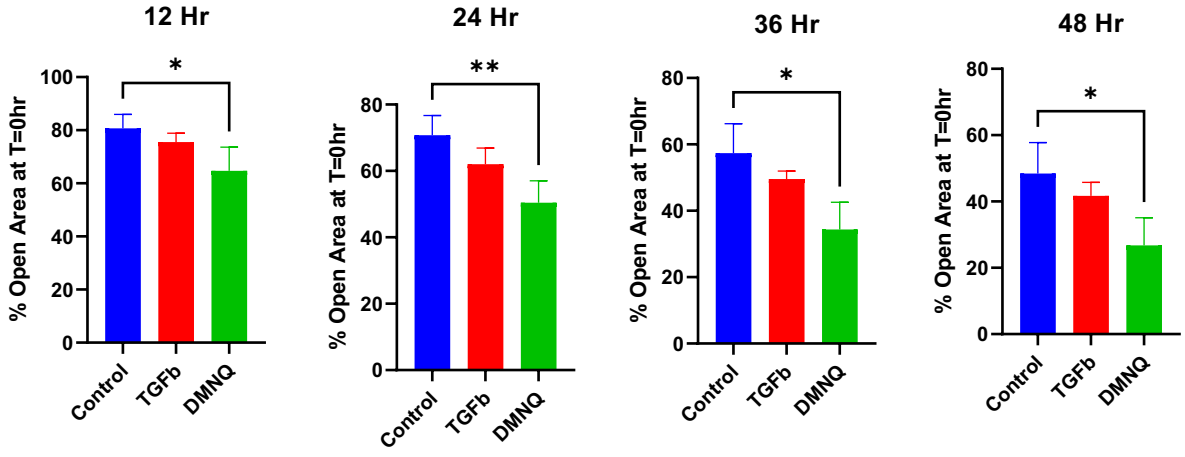

Motility Assay by DMNQ Showing faster wound healing which was statistically significant. TWO WAY ANOVA, 95% CI, n=3, P: <0.0021(**), 0.0332(*).

4.10 Intracellular Target Identification Results

4.10.1 Selection of Candidate Targets and Criteria for Selection

To determine the intracellular target(s) whose oxidation induces EMT by H_2O_2, a thorough literature review was performed, and EMT-regulatory networks were identified. Several criteria were considered for selecting the candidate target(s). The target must have at least one oxidizable cysteine residue (288), must be present mostly in the cytoplasm, has been reported to be involved in EMT or fibrosis, and proper antibodies against these target proteins must be commercially available.

4.10.2: Initial Target List

Based on the above criteria, the followings were selected as initial target list.

Table 4.10.2

Details of the Selected Target Proteins for Protein-A Mode Redoxifluor Experiments

Protein	UniProt Id	Number of oxidizable Cysteine residue
β-catenin	P35222	8
Pan-AKT	P31749	4
SMAD2/3	Q15796, P84022	6, 3
SNAI1/2	O43623*	1

* SNAI2 only

4.10.3 Global Mode Oxidation Measurements

To interrogate the EMT-regulatory targets identified as potentially modifiable by oxidative events (§4.5.1.1), the 'Redoxifluor' method was used (6). A549 cells were treated with one of several intracellular H_2O_2-generating systems. Since oxidative events are likely to be corrected quickly after their generation (by virtue of their radical nature or the presence of reductive protective mechanisms (134, 289), no time was allowed for such recovery after oxidative treatment. Instead, cells were washed at the end of the exposure period and lysed in the presence of the first fluorescent-maleimide (FMAL1) for labeling of native thiol groups on proteins. Lysate samples were processed as noted in §3.x.x, with subsequent tris-carboxyethylphosphine (TCEP) reduction and derivatization with the second fluorescent-maleimide (FMAL2) to label oxidation sites that can be biochemically reduced (including disulfides, sulfenic acids, and persulfides).

Parallel cell samples untreated with oxidants were lysed in the presence of dithiothreitol (DTT), a mild but effective reducing agent for native (uninduced) oxidized thiols (290). After lysate processing and removal of the DTT, samples were derivatized with single FMAL reagents to simulate a fully reduced or fully oxidized thiol proteome. These samples were then processed in parallel with experimental samples to "anchor" the measurement of reduced/total thiol redox.

Measurement of the "global" oxidation level with this procedure by quantifying the fluorescence from both wavelength channels allowed estimation of the overall oxidation of thiol proteome in H_2O_2-generating conditions.

DAAO + D-alanine

Peroxidase inhibition by 3-AT

DMNQ metabolism

In the presence of 5µM DMNQ for about 24 hours, the A549 global thiol proteome showed a significant level of oxidation, with about 30% less reduced thiols in the treated samples (Figure 4.10.3).

4.10.4 Protein-A Mode Oxidation of Initial Targets

Protein-A mode is the principal method for identifying oxidation of individual candidate protein targets. The method is still being optimized for our experimental system. The method has been explained in detail in section 3.9.

4.10.4.1 Targeting Beta Catenin and SMAD2/3

Using samples from 25mM 3-AT treatments for 24 hours, beta-catenin and SMAD2/3 were investigated. None of the candidate target proteins showed more oxidation compared to the untreated control samples (Figure 4.10.4.1). 5µM DMNQ treatment led to more reduction of beta-catenin and 3-AT treatment significantly reduced SMAD2/3.

Figure 4.10.3

Global Mode Redoxifluor Results with DMNQ

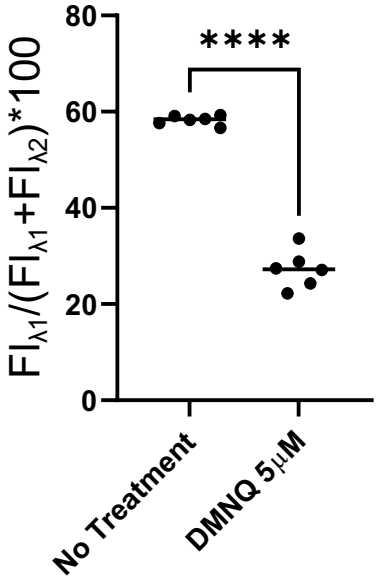

Figure 4.10.3: Global mode Redoxifluor experiments showing higher oxidation in DMNQ treated samples. Unpaired t-test (Two tailed), n=6, P: <0.0001(****), 0.0002(***), 0.0021(**), 0.0332(*).

Figure 4.10.4.1

Protein-A Mode Results for Beta Catenin and SMAD2/3

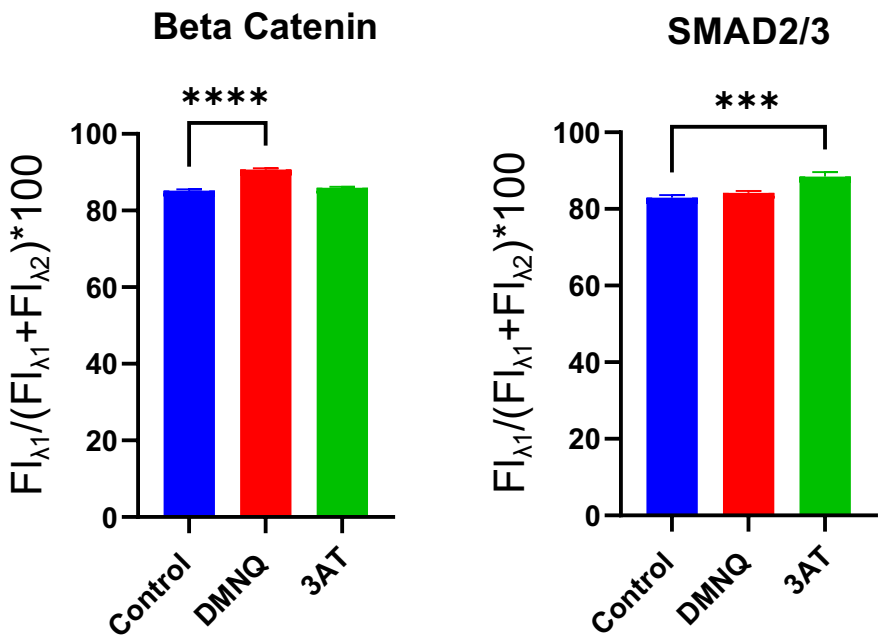

Protein-A mode Redoxifluor Results for beta catenin and SMAD2/3. Beta catenin was found significantly reduced by DMNQ and SMAD2/3 was significantly reduced by 3-AT. One way ANOVA, 95% CI, n=3, P: <0.0001(****), 0.0002(***).

4.10.4.2 Targeting panAKT & SNAI1/2

Using the cell lysates from the samples treated with 24 hours of DMNQ (5µM) and 3-AT (25mM), protein-A mode investigation was conducted to determine if Snail1/2 and/or panAKT were more oxidized compared to untreated controls (Figure 4.10.4.2). Both protein targets were found to be significantly oxidized by the 3-AT treatments, but not by DMNQ. DMNQ led to significant reduction of these proteins instead.

4.11 Investigation of Superoxide Formation by Chemiluminescence Assay

Our intracellular generation of hydrogen peroxide (H_2O_2) is dependent on enzymes which may provide one- or two-electron reduction of oxygen to yield superoxide anion radical ($O_2^{-\bullet}$) as an intermediate prior to dismutation into hydrogen peroxide (H_2O_2) and molecular oxygen (O_2)(291). It was important to determine if superoxide was being generated since it can react in vivo with nitric oxide to produce the toxic byproduct peroxynitrite (-OONO) (292). Here, we used a cell-permeable superoxide dismutase mimic manganese tetrakis-benzoic acid porphyrin (MnTBAP) at different concentrations to try to promote peroxide generation faster and more completely than non-enzymatic dismutation. DMNQ 5µM and 10µM concentrations were used to generate H_2O_2.

Here, we used a cell-permeable superoxide dismutase mimic manganese tetrakis-benzoic acid porphyrin (MnTBAP) at different concentrations to promote peroxide generation faster and more completely than non-enzymatic dismutation. DMNQ 5µM and 10µM concentrations were used to generate superoxide and H_2O_2.

At both 5 and 10µM DMNQ, there was a significantly elevated amount of H_2O_2 detected when up to 10µM Manganese TBA-porphyrin was included in the reaction mixture (Figure 4.11). This may represent dismutase action of the porphyrin, indicating that superoxide is being produced. At higher concentrations of the porphyrin, this elevated peroxide was suppressed, suggesting the possibility of

dismutation of peroxide or inhibition of the DMNQ metabolizing enzyme. Thus, interpretation of results where H_2O_2 was generated with DMNQ metabolism, should be interpreted with caution.

Figure 4.10.4.2

Protein-A Mode Results for SNAI1/2 and panAKT

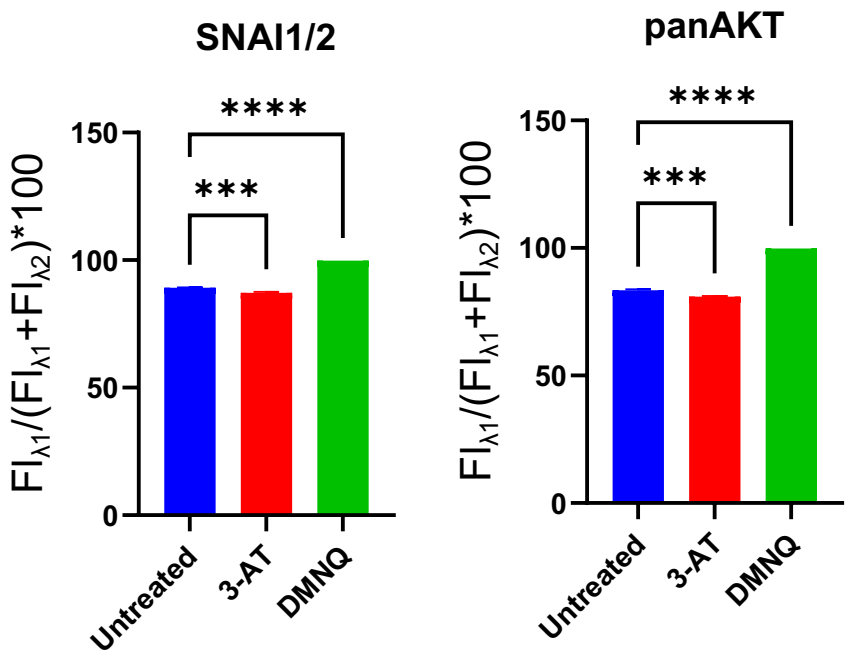

Figure 4.10.4.2: Protein A Mode results of Snail1/2 and panAKT oxidation by 3-AT and/or DMNQ. 3-AT treatment led to significant oxidation of both Snail1/2 and panAKT, whereas DMNQ results were opposite. One Way ANOVA, 95% CI, n=3, P: <0.0001(****), 0.0002(***).

Figure 4.11

Chemiluminescence Assay Showing Probable Superoxide Generation by DMNQ

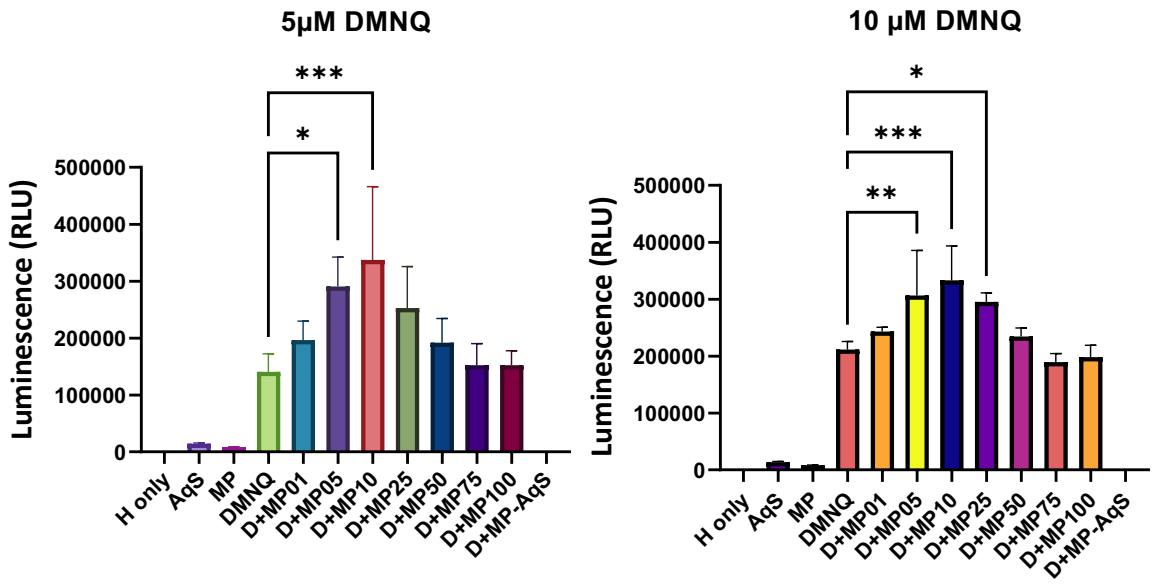

Results Showing there was a significantly elevated amount of H_2O_2 detected when up to 10µM Manganese TBA-porphyrin was included at both 5 and 10µM DMNQ. One Way ANOVA, 95% CI, n=4, P: < 0.0002(***), 0.0021(**), 0.0332(*). Here, MP: MnTBAP, AqS; AquasPark Chemiluminescent reagent.

CHAPTER 5: DISCUSSION

In this project, efficacy of redox state alteration by H_2O_2 to induce EMT was explored. Extracellular H_2O_2 was tested first for its ability to induce markers of EMT along with functional aspects of this process, including morphology change, and EMT-related marker expression changes. Extracellular H_2O_2 showed EMT progression by mesenchymal type morphology development, downregulation of epithelial marker E-Cadherin and upregulation of mesenchymal marker fibronectin. However, it was important to find out the subcellular location of molecular target of H_2O_2, intracellular H_2O_2 at different sub-cellular locations was produced or increased with various methods such as plasmid-based chemo-genetic methods, peroxide persistence by peroxidase enzyme inhibition, and quinone metabolism. The EMT progression was measured by morphology observations, motility rate, and EMT-related marker expression changes. This project found that cytoplasm is the probable subcellular site where the molecular target is present. Also, peroxide persistence particularly by catalase inhibition has been found strong enough to induce EMT. However, it is important to mention that there was no evidence of ferroptosis happening in these experiments. The identification of molecular target is still in process with a fluorescence-based microplate technique 'Redoxifluor©. β-catenin, SNAI1/2, SMAD2/3 and pan-AKT have been selected as initial molecular targets have been selected. In our preliminary study, SNAI1/2 and panAKT have been found significantly oxidized when H_2O_2 persistence was increased by 3-AT.

Initially, it was necessary to determine if EMT is inducible in our A549 cell culture and to ascertain if the presence of H_2O_2 has an effect on EMT progression. To answer the first question, TGFβ1 was chosen as it is a well-known inducer of EMT in many cancer cell lines (293). In our experimental system we optimized the dose and condition to induce EMT by TGFβ1. In our laboratory, both 5 ng/mL and 10 ng/mL doses were used and both doses efficiently induced EMT in various experiments. At first,

TGFβ1 treatments were applied to cells in serum free medium for 48 hours, but later we found 5ng/mL TGFβ1 in complete media for 48 hours immediately after serum starvation induced EMT more intensely as evidenced by EMT related marker expression (Figure 4.1.2). Moreover, 5ng/mL TGFβ1 also showed enhanced motility after scratching the cells, although the rate of wound healing was not statistically significant (Figure 4.1.1). The morphology observation with TGFβ1 treatment was not possible as the cells became confluent prior to or concurrent with mesenchymal change. However, the combination of marker expression and motility result showed that TGFβ1 was a good choice as a positive control for EMT induction. Also, TGFβ1 was used a successful positive control to induce EMT in A549 cells in our lab previously.

Next, the high throughput screening method, in-cell western (ICW) assays were performed to determine how epithelial and mesenchymal markers change their expression for 10 to 12 days. 10 - 12 days were allotted based on a study (261) which reported 12 days are required to see the effect of H_2O_2 on EMT in the A549 cell line. In these experiments, the epithelial markers E-cadherin, ZO-1 and the mesenchymal markers N-cadherin, fibronectin, and α-smooth muscle actin (α-SMA) were investigated. The ICW studies found similar results on day 10 (Figure 4.2.1). E-Cadherin expression went down significantly on both day 10 and day 12 after 400 μM H_2O_2 treatment. The mesenchymal marker α-smooth muscle actin (α-SMA) went up significantly on day 10 with TGFβ and H_2O_2 combined treatment (although not significant by H_2O_2 treatment alone). Although the expression of some other epithelial (ZO-1) and mesenchymal markers (N-cadherin and fibronectin) did not change significantly, this provided clues that 10 days after peroxide treatment could be sufficient to induce EMT in our system.

However, we noticed that cells started to change their morphological features from day 04 or day 05 (Figure 4.3.1). These results are similar to a study (86) reporting that EMT was induced significantly on day 2 and 3 after 200 μM H_2O_2 treatment in breast cancer cells. Another study reported morphological changes starting after 24 hours of oxidative stress by hypoxia (294). So, we explored the

idea that 10 days growth after H_2O_2 treatment may not be necessary and therefore shortening the experiments could be possible. So, a large experiment with several ICW plates for different time points was conducted. Cells were fixed and processed for ICW on day 04, 06, 08, 10, 12 and 14, with investigation of the expression of the epithelial marker E-cadherin and the mesenchymal marker fibronectin (Figure 4.2.2). Although the mesenchymal marker fibronectin results were unacceptable, the epithelial E-Cadherin started to be downregulated from day 4 and it became significant from day 08. Also this ICW experiment may have had a confound: we saw that E-cadherin expressions went up significantly every day, but it should be constant due to normalization.

As we noticed morphological changes in our experimental system started to appear on day 4 or 5, we decided to allow cells to grow at least 6 - 8 days after extracellular H_2O_2 treatment so that they can express EMT marker proteins adequately. Several western blot experiments were also performed for which cell lysates were collected on day 06, 07 and 08 to check at which day EMT marker protein expression was optimal. These immunoassays investigated the expression of the epithelial E-cadherin marker protein and the mesenchymal marker protein fibronectin. The E-cadherin expression went down on day 06, 07 and 08, but this decrease became significant on day 07 (Figure 4.3.2A). On the other hand, mesenchymal marker fibronectin was upregulated on day 06 and 07 and became significant on day 07 (Figure 4.3.2B). Therefore, we decided to allow cells to grow and develop EMT for 7 days in our EMT studies. However, we decided to go intracellular to find out the exact subcellular location where the cysteine redox state is altered. Also, the dose of H_2O_2 (400 µM) was very high (106) in these experiments and may trigger many other stress pathways including ferroptosis.

Next, we explored the option to generate H_2O_2 intracellularly, because extracellular H_2O_2 is subject to the need for uptake mechanisms (peroxiporins) that limit the actual concentration that alters intracellular targets. Also, when present extracellularly, H_2O_2 may be neutralized by extracellular enzymes and may affect the tumor microenvironment. We also aimed to identify the trigger point or

target inside the cell that is responsible for promoting EMT. Several methods were successfully used to generate H_2O_2 intracellularly including in specific subcellular locations.

Our first approach to intracellular peroxide delivery was to generate ROS with plasmid-delivered D-amino acid oxidase. It was a chemo-genetic approach using pAAV-HyPer-DAAO plasmids developed by Thomas Michel lab which was purchased from addgene (265). With this plasmid, we successfully generated intracellular H_2O_2 (Figure 4.4.2.1), and regulated with various D-Alanine concentrations (Figure 4.4.3).

To generate H_2O_2 at different subcellular locations, additional plasmids were gifted to us by Thomas Michel Laboratory. These plasmids had the latest 7th generation HyPer gene attached to the DAAO along with different subcellular localization sequences. While HyPer v.7.2 is claimed to have better sensitivity to H_2O_2 along with pH stability and reversible reaction (295) we were unable to use it as a peroxide sensor due to its spectral requirements.

The functionality of DAAO in the presence of D-Alanine was tested. Cells were transfected with pAAV-HyPer-DAAO-NES plasmids which delivered DAAO to the cytoplasm (NES = Nuclear Exclusion Sequence). The cytoplasmic localization of HyPer-DAAO was visible with the GFP and CFP channel in our EVOS auto microscope. Then addition of D-alanine, but not L-alanine, increased the fluorescence (Figure 4.4.2.1 and Figure 4.4.2.2, respectively). This result coincides with the study conducted by Thomas Michel Laboratory for cardiac muscle cells and was similar to a result reported in zebrafish larvae tissue (296). The main reason for choosing DAAO as a peroxide generator is that most of the amino acids present in the physiological system are L-isoforms and lung cells are not known to have D-amino acids (297). DAAO can only react with D-isoform of an amino acid and therefore, it was controllable by altering D-Amino acid concentration given from outside.

After confirming the functionality of DAAO with the fluorescence change of this 3rd generation HyPer, the relationship between D-alanine concentration and HyPer ratiometric fluorescence was

investigated. After several trials, it was found that in A549 cells, the HyPer activity becomes noticeable at about 400 µM D-alanine concentration and the effect reached plateau with 600 µM D-Alanine (Figure 4.4.3). This finding is similar to Thomas Michel research group, but they found dose response effect started from 1 mM D-Alanine to 10 mM D-Alanine in cardiac myocytes (262).

The next step was to determine if the HyPer7.2 containing plasmids can deliver the HyPer7.2-DAAO to their assigned subcellular locations. The HyPer7.2-DAAO plasmids were successfully expressed based on their respective localization sequences. These plasmids were expressed in A549 cells successfully which was similar to that reported for vascular endothelial cells (266).

We attempted to determine by HyPer ratiometric fluorescence whether DAAO in these subcellular compartments is functional. Due to a lack of proper instrumentation, we were unable to detect HyPer7.2 fluorescence. The excitation maximum peak for HyPer7.2 is 520nm and its excitation curve is very narrow and sharp (264). The emission maxima for GFP is 510 nm (298) therefore was not able to detect subtle changes in fluorescence, in spite of rapid image capture, high D-alanine treatments, and the presence of peroxidase inhibitors (264, 266). We also attempted to determine the exact excitation and emission spectrum of these HyPer7.2 by using the PTI spectrofluorimeter in Dr. Thomas' Laboratory (data not shown), but these attempts were unsuccessful. Finally, a chemiluminescence assay was designed using AquaSpark reagent (280). With these chemiluminescence experiments, we were successful in detecting DAAO activity when delivered by HyPer7.2-DAAO-NES plasmids. For all three subcellularly localized DAAO, the enzyme function was detected significantly higher with D-alanine with peroxidase inhibitors compared to untreated cells or with only peroxidase inhibitor treated cells or only D-alanine treated cells (Figure 4.4.5A and 4.4.5B). Interestingly, cells treated with peroxidase inhibitors only showed significantly higher luminescence compared to cell only untreated groups, indicating that peroxidase enzymes (particularly catalase and thioredoxin reductase)

are active in A549 cells to neutralize the D-alanine generated H_2O_2. This study confirms the reported natural antioxidant capability of cells by many studies (289, 299-302).

After the DAAO functionality was confirmed, the next task was to achieve maximum transfection efficiency with minimal toxicity. Initially the efforts were made with Lipofectamine 3000 transfection reagent. Transfection efficiency was low and this reagent resulted in substantial cytotoxicity (data not shown). Changing to the PolyJet transfection agent did not improve transfection efficiency significantly, but it was very gentle on A549 cells, no toxicity was observed. Several ratios of DNA to Polyjet were tested to obtain the optimum transfection efficiency. The best transfection efficiency was observed with 1:1.5 DNA-to PolyJet ratio (Figure 4.4.6), but it was only about 20-30%.

We also used an electroporation method using a BioRad Gene Pulser II instrument. Transfection efficiency was not improved significantly even after several attempted optimizations (including voltage, cell number, and DNA amount) (Figure 4.4.7). Moreover, there was clear inconsistency of protein expressions among the cells along with extremely high cytotoxicity.

Intracellular H_2O_2 was also generated utilizing the metabolism of the quinone drugs menadione and 2,3-dimethoxy-naphthoquinone (DMNQ). Menadione has been reported to generate superoxide and oxidative stress particularly in mitochondria (303-306). DMNQ generates intracellular H_2O_2 through redox cycling (307). Both drugs generated intracellular H_2O_2 (Figure 4.4.9.1), but DMNQ generated significantly higher amount of H_2O_2 than menadione (4.4.9.2). Moreover, both drugs showed dose response effects (Figure 4.4.9.1) for the production of peroxide during metabolism.

To determine if the dose response effect of intracellular H_2O_2 generation is also reflected in EMT induction, we first performed an ICW experiment on pAAV-HPer-DAAO-NES transfected A549 cells with various concentrations of D-Alanine (from 200 µM to 1 mM). On day 7, the epithelial E-Cadherin expression was significantly downregulated in all D-alanine treated cells regardless of their doses. The mesenchymal marker fibronectin expression also went up for all D-alanine treated cells but were neither

dose responsive nor significant (Figure 4.5.1). However, in our further trials with ICW experiments, the results were highly inconsistent, particularly with the mesenchymal marker fibronectin (Figure 4.5.2). These inconsistent results with fibronectin could be due to an artifact of the ICW procedure. Before the cells were fixed, the media from the wells is removed. As fibronectin is a component of extracellular matrix (308-310), it is highly probable that this fibronectin is lost when the media is removed. We made several procedural attempts to avoid this issue but none of these modifications preserved the fibronectin. When the plates were centrifuged before fixing, the fibronectin was sedimented at the center of the wells and this solved the problem of mesenchymal markers, but the measurement of epithelial markers was compromised. As we were unable to solve this issue in a robust analytical way, the data from these experiments were not shown here and the ICW method was abandoned for further studies.

The EMT studies involved regular morphology observation of cells to detect any phenotypic change, evaluation of EMT marker expression by western blot, and scratch wound healing assays. In case of subcellular H_2O_2 generation, morphological changes were mostly found in cells where H_2O_2 were generated in the cytoplasm (Figure 4.6.1A) and, to a lesser degree in cells with nuclear H_2O_2 production (Figure 4.6.1B). Several studies have reported such morphological changes with extracellularly applied H_2O_2 (86, 294) , but the observation on EMT related morphology changes following specific subcellular H_2O_2 generation appears to be a novel part of this project. Although the EMT related morphology changes were predominant in D-alanine treated and D-alanine with peroxidase inhibitors treated cells, interestingly, a few EMT related morphological changes were detected in cells treated with peroxidase inhibitors only regardless of the transfection status. This outcome, however, coincides with the chemiluminescence results where significant H_2O_2 levels were detected as luminescence compared to untreated cells. It was also another novel observation, as we could no literature reporting the EMT related morphology changes due to peroxidase inhibition.

Western blot studies were performed from cell lysates collected on day 07 after D-alanine treatment different subcellular locations. Both, E-cadherin and N-cadherin are at the surface of the cells (311) and therefore have less chance of being lost during cell lysate collection. Cytoplasmic H_2O_2 generation regardless of the presence of peroxidase inhibitors showed a trend toward EMT progression in these studies (Figure 4.6.2.1A). However, statistical analysis showed such progression significant only in the presence of peroxidase inhibitors (Figure 4.6.2.1B). However, there was no dose-response effect with these treatments. Although nuclear H_2O_2 generation showed EMT related morphological changes in a few cases, this treatment did not show consistency in EMT related marker expression (Figure 4.6.2.2A and Figure 4.6.2.2B). Mitochondrial H_2O_2 generation also showed random expression of EMT related markers which coincides with the morphology observations (Figure 4.6.2.2C and 4.6.2.2D). In all these studies, the positive control TGFβ1 showed EMT progression through significant E-cadherin downregulation and significant N-Cadherin upregulation. The TGFβ1 results showing EMT induction coincides with many studies (312-316). However, the variances were high which may be related to the inconsistent and low transfection efficiency throughout various experiments. So, our finding from these experiments was that the cytoplasm of A549 cells could be the location from where EMT is triggered.

As morphology and EMT-related marker expressions support the conclusion of the cytoplasm as containing an EMT trigger, we performed motility assay after scratching the cells after cytoplasmic generation by HyPer7.2-DAAO-NES. A trend toward higher motility was detected in D-alanine and D-alanine + 3AT treated cells (Figure 4.8.1A), but the results were not statistically significant (Figure 4.8.1B). Higher transfection efficiency might show significant motility with this treatment.

Next, we investigated the effect of peroxidase inhibitors alone on EMT induction. The duration of these experiments was also shortened to 5 days based on morphology change observations on day 04 after treatment removal. 25 mM 3AT and 2 μM Auranofin as peroxidase inhibitors showed EMT progression by downregulating E-cadherin and upregulating N-cadherin, regardless of the transfection

status (Figure 4.7.1.1 to Figure 4.7.1.4). Although, some of these results were not statistically significant, these results did indicate a trend of inducing EMT. Later, we confirmed using 3-AT alone is sufficient to induce EMT and auranofin played a very little role (Figure 4.7.1.5). The effect of 3AT was almost same as the effect of 3AT + Auranofin, but auranofin alone was not close to the combination.

Morphological observation also showed that cells treated with 3AT + Auranofin were more elongated, spindle shaped and loosely connected (Figure 4.7.2.2) compared to untreated controls (Figure 4.7.2.1). The motility assays were also performed after scratching the cells on day 03. The 3-AT treated cells showed faster wound healing compared to untreated cells (Figure 4.7.3A) and was significant at 24 hours after scratching (Figure 4.7.3B).

These results are novel outcomes of this project as no literature has previously reported that catalase inhibition can induce EMT. Catalase is known for decomposing H_2O_2, thereby reducing oxidative stress (125). Therefore, our hypothesis is that EMT induction by the catalase inhibitor 3AT is due to accumulation of H_2O_2. In support of this hypothesis, our chemiluminescence results also showed H_2O_2 accumulation by peroxidase inhibitors (Figure 4.4.5A and 4.4.5B).

We further optimized the experiment conditions, making all cells serum free for 24 hours before adding any treatment. Even the untreated cells were serum starved in parallel with the treatment groups. Fetal Bovine Serum (FBS) may vary batch to batch and therefore may lead to inconsistent results (317). Therefore 24-hour serum starvation has been a common practice to synchronize all cells to the same cell cycle phase. In many treatments, duration was also decreased from 24 hours to only 6 hours for D-alanine and 3AT groups. In addition to using D-alanine to generate cytoplasmic H_2O_2, we also used a quinone, 2,3-dimethoxy-1,4-naphthalenedione (DMNQ) for 1 hour to generate cytoplasmic H_2O_2. Western blot results again showed EMT progression in cells with 3AT alone and D-Ala + 3AT on day 05 (Figure 4.8.1). The motility assays also showed a trend toward faster wound healing in cells

treated with H_2O_2 generators, (Figure 4.8.2A) but this result was not statistically significant (Figure 4.8.2B).

We did not examine EMT by generating intracellular H_2O_2 with menadione, as this quinone structure did not produce significant levels of H_2O_2 in our experimental system. Only a few experiments with DMNQ were performed to examine EMT promotion, but these needed further optimization, particularly with respect to the treatment duration. Western blot results in our low-dose studies did not show any EMT induction by 10µM DMNQ (Figure 4.9.1), but the motility results were positive (Figure 4.9.2A) and was significant at 24 hours after scratching (Figure 4.9.2B). However, these experiments need further optimization.

While these EMT experiments need further optimization, it was also important to begin investigating the molecular targets for peroxide oxidation. As our experiments indicated the cytoplasm to be the primary location from where EMT is triggered by H_2O_2, we selected probable molecular targets present in the cytoplasmic space. Literature reports describing regulatory molecular targets were reviewed for possible redox "switches" or proteins whose function may be significantly enhanced or inhibited by cysteine oxidation with H_2O_2. The subcellular locations of these potential targets were compiled using their UniprotID and a database of available oxidizable cysteine residues (iCysMod) was consulted. Based on our literature review, we selected beta-catenin, SMAD2/3, SNAI1/2 and pan-AKT.

To identify if these potential targets are significantly oxidized by our EMT induction methods, the "Redoxifluor" technique was utilized (6) (§4.10.3). First, we investigated if we could see significant oxidation throughout the cell lysate (global mode) after DMNQ treatment to examine the proof of concept. There was significantly high oxidation in DMNQ treated cells compared to untreated controls (Figure 4.10.3).

Next, using protein-A mode (in which antibodies recognizing the potential target allow isolation of individual fluorescence-derivatized proteins), we first investigated beta-catenin and SMAD2/3

oxidation. These initial experiments found opposite results from what we expected (Figure 4.10.4.1). These targets were reduced more compared to untreated controls when H_2O_2 was generated by DMNQ or increased by 3AT. However, our investigation for SNAI1/2 and pan-AKT found that treatment with 3AT for 6 hours caused significant oxidation of these targets (Figure 4.10.4.2). These findings are also novel as there is no study on 3AT showing redox alteration of SNAI1/2 or pan-AKT. However, we are still optimizing these experiments and generating samples to find clear molecular targets. If these optimizations confirm SNAI1/2 and/or panAKT as cysteine-redox target(s), the downstream targets of these transcription factors will be examined for activation or inhibition. With these more complete target investigations, the influence of the production of H_2O_2 by transfected cells for target alteration will also be examined.

We also examined if our methods of intracellular generation of hydrogen peroxide (H_2O_2) are also generating superoxide since this form of reactive oxygen can also react *in vivo* with nitric oxide to produce the toxic byproduct peroxynitrite (-OONO) (292). Here, we used a cell-permeable superoxide dismutase mimic manganese tetrakis-benzoic acid porphyrin (MnTBAP) at different concentrations to try to promote peroxide generation faster and more completely than relying on native SOD enzymatic or non-enzymatic dismutation. DMNQ (at both 5 and 10µM concentrations), produced a significantly elevated amount of H_2O_2 when up to 10µM Manganese TBA-porphyrin was included (Figure 4.11). This may represent dismutase action of the porphyrin, indicating that superoxide is being produced. At higher concentrations of the porphyrin, this elevated peroxide was suppressed, suggesting the possibility of dismutation of peroxide or inhibition of the DMNQ metabolizing enzyme. However, the superoxide has been known to react mostly with Fe–S clusters in proteins leading to Fenton reaction, but H_2O_2 is known to react mostly with Cys-S sites (106, 318).

Although we have a few novel findings in this project such as the promotion of EMT by the cytoplasmic H_2O_2 generation as well as by catalase inhibition by 3AT, there are significant limitations to

this project. A major deficiency was the low transfection efficiency with chemical or electroporation methods; a viral transfection method may have been able to improve this limitation. Also, due to time constraints, we worked mostly with only one epithelial marker E-Cadherin and one mesenchymal marker N-cadherin. Target identification will require a broader range of potential targets as well as clear delineation of positive and negative outcomes with this fluorescence technique. Targets positively identified by RedoxiFluor will require mass spectrometry proteomic analyses for confirmation of the critical cysteine(s) that are oxidatively modified. A single cell line was used, and no *in-vivo* experiments were performed to determine if oxidative events result in more widespread or quantitatively greater metastatic outcomes. In addition to A549 cell line used in this project, examining the results with at least another type of NSCLC cell line (*e.g.* H1648, Calu-3, H460) (319) was important. But due to time constraints we could not expand the tests into another cell line. Also, *in-vivo* experiments were required to see if the results are similar in physiological system. But we did not have enough funds to afford the in-vivo experiments. We observed generation of superoxide along with H_2O_2 when DMNQ metabolism method was used, but we did not have enough time to investigate whether these superoxides play any role in EMT induction through Fe-S oxidation.

Future studies may include a more complete examination of targets for cysteine-redox changes. Such examination would include functional studies on downstream targets as well as proteomic analysis by mass spectroscopy.

In conclusion we can say that we have found cytoplasmic H_2O_2 generation and H_2O_2 persistence by catalase inhibition to induce EMT in lung A549 cells. SNAI1/2 and pan-AKT may be the molecular target of redox alteration leading to EMT.

REFERENCES

1. Weinberg RK, Robert A. The basics of epithelial-mesenchymal transition. *The Journal of Clinical Investigation*. 2009;119(6):1420-8.
2. Chaffer CL, Weinberg RA. A perspective on cancer cell metastasis. *Science*. 2011;331(6024):1559-64.
3. OncoLink CRf, Treatment RCCTP. All About Non-Small Cell Lung Cancer | OncoLink 2021 [Available from: https://www.oncolink.org/cancers/lung/non-small-cell-lung-cancer-nsclc/all-about-non-small-cell-lung-cancer.
4. Lu W, Kang Y. Epithelial-Mesenchymal Plasticity in Cancer Progression and Metastasis. *Developmental Cell*. 2019;49(3):361-74.
5. Law S, Chatterjee R. Association of ROS with Epithelial-Mesenchymal Transition and Acquisition of Stemness During Carcinogenesis. In: Chakraborti S, Ray BK, Roychowdhury S, editors. *Handbook of Oxidative Stress in Cancer: Mechanistic Aspects*. Singapore: Springer Singapore; 2020. p. 1-13.
6. Tuncay A, Noble A, Guille M, Cobley JN. RedoxiFluor: A microplate technique to quantify target-specific protein thiol redox state in relative percentage and molar terms. *Free Radic Biol Med*. 2022;181:118-29.
7. WHO. Cancer 2022 [Available from: https://www.who.int/news-room/fact-sheets/detail/cancer.
8. WHO. Cancer 2023 [Available from: https://www.who.int/health-topics/cancer#tab=tab_1.
9. Cancer Biology | NIH Intramural Research Program 2023 [Available from: https://www.ncbi.nlm.nih.gov/pubmed/.
10. CDC. What Is Lung Cancer? | CDC 2022 [updated 2022-10-25T10:50:00Z. Available from: https://www.cdc.gov/cancer/lung/basic_info/what-is-lung-cancer.htm.
11. Alberg AJ, Brock MV, Ford JG, Samet JM, Spivack SD. Epidemiology of lung cancer: Diagnosis and management of lung cancer, 3rd ed: American College of Chest Physicians evidence-based clinical practice guidelines. *Chest*. 2013;143(5 Suppl):e1S-e29S.
12. Sun S, Schiller JH, Gazdar AF. Lung cancer in never smokers--a different disease. *Nat Rev Cancer*. 2007;7(10):778-90.
13. Gridelli C, Rossi A, Carbone DP, Guarize J, Karachaliou N, Mok T, Petrella F, Spaggiari L, Rosell R. Non-small-cell lung cancer. *Nature Reviews Disease Primers*. 2015;1(1):15009.
14. team TACSmaec. What Is Lung Cancer? | Types of Lung Cancer: *@cancer.org*; 2023 [Available from: https://www.cancer.org/cancer/lung-cancer/about/what-is.html.
15. Casal-Mouriño A, Ruano-Ravina A, Lorenzo-González M, Rodríguez-Martínez Á, Giraldo-Osorio A, Varela-Lema L, Pereiro-Brea T, Barros-Dios JM, Valdés-Cuadrado L, Pérez-Ríos M. Epidemiology of stage III lung cancer: frequency, diagnostic characteristics, and survival. *Transl Lung Cancer Res*. 2021;10(1):506-18.
16. Siegel RL, Miller KD, Jemal A. Cancer statistics, 2018. *CA Cancer J Clin*. 2018;68(1):7-30.
17. Weibel ER. What makes a good lung? *Swiss Med Wkly*. 2009;139(27-28):375-86.
18. Suster DI, Mino-Kenudson M. Molecular Pathology of Primary Non-small Cell Lung Cancer. *Archives of Medical Research*. 2020;51(8):784-98.
19. Gallicchio L, Devasia TP, Tonorezos E, Mollica MA, Mariotto A. Estimation of the Number of Individuals Living With Metastatic Cancer in the United States. *JNCI: Journal of the National Cancer Institute*. 2022;114(11):1476-83.

20. Fares J, Fares MY, Khachfe HH, Salhab HA, Fares Y. Molecular principles of metastasis: a hallmark of cancer revisited. *Signal Transduction and Targeted Therapy*. 2020;5(1):28.
21. Welch DR, Hurst DR. Defining the Hallmarks of Metastasis. *Cancer Research*. 2019;79(12):3011-27.
22. Maitra A. Molecular envoys pave the way for pancreatic cancer to invade the liver. *Nature*. 2019;567(7747):181-2.
23. Massagué J, Obenauf AC. Metastatic colonization by circulating tumour cells. *Nature*. 2016;529(7586):298-306.
24. Lambert AW, Pattabiraman DR, Weinberg RA. Emerging Biological Principles of Metastasis. *Cell*. 2017;168(4):670-91.
25. Bakhoum SF, Ngo B, Laughney AM, Cavallo JA, Murphy CJ, Ly P, Shah P, Sriram RK, Watkins TBK, Taunk NK, Duran M, Pauli C, Shaw C, Chadalavada K, Rajasekhar VK, Genovese G, Venkatesan S, Birkbak NJ, McGranahan N, Lundquist M, LaPlant Q, Healey JH, Elemento O, Chung CH, Lee NY, Imielenski M, Nanjangud G, Pe'er D, Cleveland DW, Powell SN, Lammerding J, Swanton C, Cantley LC. Chromosomal instability drives metastasis through a cytosolic DNA response. *Nature*. 2018;553(7689):467-72.
26. Cheung KJ, Ewald AJ. A collective route to metastasis: Seeding by tumor cell clusters. *Science*. 2016;352(6282):167-9.
27. Yang J, Antin P, Berx G, Blanpain C, Brabletz T, Bronner M, Campbell K, Cano A, Casanova J, Christofori G, Dedhar S, Derynck R, Ford HL, Fuxe J, García de Herreros A, Goodall GJ, Hadjantonakis A-K, Huang RYJ, Kalcheim C, Kalluri R, Kang Y, Khew-Goodall Y, Levine H, Liu J, Longmore GD, Mani SA, Massagué J, Mayor R, McClay D, Mostov KE, Newgreen DF, Nieto MA, Puisieux A, Runyan R, Savagner P, Stanger B, Stemmler MP, Takahashi Y, Takeichi M, Theveneau E, Thiery JP, Thompson EW, Weinberg RA, Williams ED, Xing J, Zhou BP, Sheng G, On behalf of the EMTIA. Guidelines and definitions for research on epithelial–mesenchymal transition. *Nature Reviews Molecular Cell Biology*. 2020;21(6):341-52.
28. Kalluri R, Weinberg RA. The basics of epithelial-mesenchymal transition. *Journal of Clinical Investigation*. 2009;119(6):1420-8.
29. Strutz F, Zeisberg M, Ziyadeh FN, Yang CQ, Kalluri R, Müller GA, Neilson EG. Role of basic fibroblast growth factor-2 in epithelial-mesenchymal transformation. *Kidney Int*. 2002;61(5):1714-28.
30. Nieto MA, Huang RY, Jackson RA, Thiery JP. EMT: 2016. *Cell*. 2016;166(1):21-45.
31. Ocaña OH, Córcoles R, Fabra A, Moreno-Bueno G, Acloque H, Vega S, Barrallo-Gimeno A, Cano A, Nieto MA. Metastatic colonization requires the repression of the epithelial-mesenchymal transition inducer Prrx1. *Cancer Cell*. 2012;22(6):709-24.
32. Tsai JH, Donaher JL, Murphy DA, Chau S, Yang J. Spatiotemporal regulation of epithelial-mesenchymal transition is essential for squamous cell carcinoma metastasis. *Cancer Cell*. 2012;22(6):725-36.
33. Tsai JH, Yang J. Epithelial-mesenchymal plasticity in carcinoma metastasis. *Genes Dev*. 2013;27(20):2192-206.
34. Brabletz T. To differentiate or not--routes towards metastasis. *Nat Rev Cancer*. 2012;12(6):425-36.
35. Chaffer CL, San Juan BP, Lim E, Weinberg RA. EMT, cell plasticity and metastasis. *Cancer Metastasis Rev*. 2016;35(4):645-54.
36. Lee JM, Dedhar S, Kalluri R, Thompson EW. The epithelial-mesenchymal transition: new insights in signaling, development, and disease. *J Cell Biol*. 2006;172(7):973-81.

37. Zeisberg M, Kalluri R. Cellular mechanisms of tissue fibrosis. 1. Common and organ-specific mechanisms associated with tissue fibrosis. *Am J Physiol Cell Physiol*. 2013;304(3):C216-25.
38. Chaffer CL, Thompson EW, Williams ED. Mesenchymal to epithelial transition in development and disease. *Cells Tissues Organs*. 2007;185(1-3):7-19.
39. Kalluri R, Weinberg RA. The basics of epithelial-mesenchymal transition. *J Clin Invest*. 2009;119(6):1420-8.
40. Lamouille S, Xu J, Derynck R. Molecular mechanisms of epithelial–mesenchymal transition. *Nature Reviews Molecular Cell Biology*. 2014;15(3):178-96.
41. Thiery JP, Acloque H, Huang RY, Nieto MA. Epithelial-mesenchymal transitions in development and disease. *Cell*. 2009;139(5):871-90.
42. Thiery JP, Sleeman JP. Complex networks orchestrate epithelial-mesenchymal transitions. *Nat Rev Mol Cell Biol*. 2006;7(2):131-42.
43. Arnouk H, Yum G, Shah D. Cripto-1 as a Key Factor in Tumor Progression, Epithelial to Mesenchymal Transition and Cancer Stem Cells. *International Journal of Molecular Sciences*. 2021;22(17):9280.
44. Villarejo A, Cortés-Cabrera Á, Molina-Ortíz P, Portillo F, Cano A. Differential Role of Snail1 and Snail2 Zinc Fingers in E-cadherin Repression and Epithelial to Mesenchymal Transition. *Journal of Biological Chemistry*. 2014;289(2):930-41.
45. Nieto MA. The snail superfamily of zinc-finger transcription factors. *Nat Rev Mol Cell Biol*. 2002;3(3):155-66.
46. Tan EJ, Thuault S, Caja L, Carletti T, Heldin C-H, Moustakas A. Regulation of Transcription Factor Twist Expression by the DNA Architectural Protein High Mobility Group A2 during Epithelial-to-Mesenchymal Transition*. *Journal of Biological Chemistry*. 2012;287(10):7134-45.
47. Qin Q, Xu Y, He T, Qin C, Xu J. Normal and disease-related biological functions of Twist1 and underlying molecular mechanisms. *Cell Research*. 2012;22(1):90-106.
48. Zhang P, Sun Y, Ma L. ZEB1: at the crossroads of epithelial-mesenchymal transition, metastasis and therapy resistance. *Cell Cycle*. 2015;14(4):481-7.
49. Wong T-S, Gao W, Chan JY-W. Transcription Regulation of E-Cadherin by Zinc Finger E-Box Binding Homeobox Proteins in Solid Tumors. *BioMed Research International*. 2014;2014:921564.
50. Stemmler MP, Eccles RL, Brabletz S, Brabletz T. Non-redundant functions of EMT transcription factors. *Nature Cell Biology*. 2019;21(1):102-12.
51. Cano A, Pérez-Moreno MA, Rodrigo I, Locascio A, Blanco MJ, del Barrio MG, Portillo F, Nieto MA. The transcription factor Snail controls epithelial–mesenchymal transitions by repressing E-cadherin expression. *Nature Cell Biology*. 2000;2(2):76-83.
52. Xu J, Lamouille S, Derynck R. TGF-β-induced epithelial to mesenchymal transition. *Cell research*. 2009;19(2):156-72.
53. Aybar MJ, Nieto MA, Mayor R. Snail precedes slug in the genetic cascade required for the specification and migration of the Xenopus neural crest. 2003.
54. del Barrio MG, Nieto MA. Overexpression of Snail family members highlights their ability to promote chick neural crest formation. 2002.
55. Martínez-Álvarez C, Blanco MaJ, Pérez R, Rabadán MA, Aparicio M, Resel E, Martínez T, Nieto MA. Snail family members and cell survival in physiological and pathological cleft palates. *Developmental biology*. 2004;265(1):207-18.
56. Nieto MA, Sargent MG, Wilkinson DG, Cooke J. Control of cell behavior during vertebrate development by Slug, a zinc finger gene. *Science*. 1994;264(5160):835-9.

57. Ikenouchi J, Matsuda M, Furuse M, Tsukita S. Regulation of tight junctions during the epithelium-mesenchyme transition: direct repression of the gene expression of claudins/occludin by Snail. *Journal of cell science*. 2003;116(10):1959-67.
58. Whiteman EL, Liu CJ, Fearon ER, Margolis B. The transcription factor snail represses Crumbs3 expression and disrupts apico-basal polarity complexes. *Oncogene*. 2008;27(27):3875-9.
59. Hsu DS-S, Wang H-J, Tai S-K, Chou C-H, Hsieh C-H, Chiu P-H, Chen N-J, Yang M-H. Acetylation of snail modulates the cytokinome of cancer cells to enhance the recruitment of macrophages. *Cancer cell*. 2014;26(4):534-48.
60. Rembold M, Ciglar L, Yáñez-Cuna JO, Zinzen RP, Girardot C, Jain A, Welte MA, Stark A, Leptin M, Furlong EEM. A conserved role for Snail as a potentiator of active transcription. *Genes & Development*. 2014;28(2):167-81.
61. Javaid S, Zhang J, Anderssen E, Black Josh C, Wittner Ben S, Tajima K, Ting David T, Smolen Gromoslaw A, Zubrowski M, Desai R, Maheswaran S, Ramaswamy S, Whetstine Johnathan R, Haber Daniel A. Dynamic Chromatin Modification Sustains Epithelial-Mesenchymal Transition following Inducible Expression of Snail-1. *Cell Reports*. 2013;5(6):1679-89.
62. Peinado H, Olmeda D, Cano A. Snail, Zeb and bHLH factors in tumour progression: an alliance against the epithelial phenotype? *Nature Reviews Cancer*. 2007;7(6):415-28.
63. Casas E, Kim J, Bendesky A, Ohno-Machado L, Wolfe CJ, Yang J. Snail2 is an essential mediator of Twist1-induced epithelial mesenchymal transition and metastasis. *Cancer research*. 2011;71(1):245-54.
64. Yang M-H, Wu M-Z, Chiou S-H, Chen P-M, Chang S-Y, Liu C-J, Teng S-C, Wu K-J. Direct regulation of TWIST by HIF-1α promotes metastasis. *Nature Cell Biology*. 2008;10(3):295-305.
65. Lee TK, Poon RT, Yuen AP, Ling MT, Kwok WK, Wang XH, Wong YC, Guan XY, Man K, Chau KL. Twist overexpression correlates with hepatocellular carcinoma metastasis through induction of epithelial-mesenchymal transition. *Clinical cancer research*. 2006;12(18):5369-76.
66. Yang J, Mani SA, Donaher JL, Ramaswamy S, Itzykson RA, Come C, Savagner P, Gitelman I, Richardson A, Weinberg RA. Twist, a master regulator of morphogenesis, plays an essential role in tumor metastasis. *cell*. 2004;117(7):927-39.
67. Comijn J, Berx G, Vermassen P, Verschueren K, van Grunsven L, Bruyneel E, Mareel M, Huylebroeck D, Van Roy F. The two-handed E box binding zinc finger protein SIP1 downregulates E-cadherin and induces invasion. *Molecular cell*. 2001;7(6):1267-78.
68. Eger A, Aigner K, Sonderegger S, Dampier B, Oehler S, Schreiber M, Berx G, Cano A, Beug H, Foisner R. DeltaEF1 is a transcriptional repressor of E-cadherin and regulates epithelial plasticity in breast cancer cells. *Oncogene*. 2005;24(14):2375-85.
69. Aigner K, Dampier B, Descovich L, Mikula M, Sultan A, Schreiber M, Mikulits W, Brabletz T, Strand D, Obrist P. The transcription factor ZEB1 (δEF1) promotes tumour cell dedifferentiation by repressing master regulators of epithelial polarity. *Oncogene*. 2007;26(49):6979-88.
70. Spaderna S, Schmalhofer O, Wahlbuhl M, Dimmler A, Bauer K, Sultan A, Hlubek F, Jung A, Strand D, Eger A. The transcriptional repressor ZEB1 promotes metastasis and loss of cell polarity in cancer. *Cancer research*. 2008;68(2):537-44.
71. Vandewalle C, Comijn J, De Craene B, Vermassen P, Bruyneel E, Andersen H, Tulchinsky E, Van Roy F, Berx G. SIP1/ZEB2 induces EMT by repressing genes of different epithelial cell–cell junctions. *Nucleic acids research*. 2005;33(20):6566-78.
72. Bindels S, Mestdagt M, Vandewalle C, Jacobs N, Volders L, Noël A, Van Roy F, Berx G, Foidart J-M, Gilles C. Regulation of vimentin by SIP1 in human epithelial breast tumor cells. *Oncogene*. 2006;25(36):4975-85.

73. Postigo AA, Dean DC. Differential expression and function of members of the zfh-1 family of zinc finger/homeodomain repressors. *Proceedings of the National Academy of Sciences*. 2000;97(12):6391-6.
74. Stryjewska A, Dries R, Pieters T, Verstappen G, Conidi A, Coddens K, Francis A, Umans L, van IJcken WF, Berx G. Zeb2 regulates cell fate at the exit from epiblast state in mouse embryonic stem cells. *Stem Cells*. 2017;35(3):611-25.
75. Krebs AM, Mitschke J, Lasierra Losada M, Schmalhofer O, Boerries M, Busch H, Boettcher M, Mougiakakos D, Reichardt W, Bronsert P. The EMT-activator Zeb1 is a key factor for cell plasticity and promotes metastasis in pancreatic cancer. *Nature cell biology*. 2017;19(5):518-29.
76. Caramel J, Papadogeorgakis E, Hill L, Browne GJ, Richard G, Wierinckx A, Saldanha G, Osborne J, Hutchinson P, Tse G. A switch in the expression of embryonic EMT-inducers drives the development of malignant melanoma. *Cancer cell*. 2013;24(4):466-80.
77. Denecker G, Vandamme N, Akay Ö, Koludrovic D, Taminau J, Lemeire K, Gheldof A, De Craene B, Van Gele M, Brochez L. Identification of a ZEB2-MITF-ZEB1 transcriptional network that controls melanogenesis and melanoma progression. *Cell Death & Differentiation*. 2014;21(8):1250-61.
78. Dave N, Guaita-Esteruelas S, Gutarra S, Frias A, Beltran M, Peiro S, de Herreros AG. Functional cooperation between Snail1 and twist in the regulation of ZEB1 expression during epithelial to mesenchymal transition. *Journal of Biological Chemistry*. 2011;286(14):12024-32.
79. Long J, Zuo D, Park M. Pc2-mediated sumoylation of Smad-interacting protein 1 attenuates transcriptional repression of E-cadherin. *Journal of Biological Chemistry*. 2005;280(42):35477-89.
80. Wang Z, Li Y, Sarkar FH. Signaling mechanism (s) of reactive oxygen species in epithelial-mesenchymal transition reminiscent of cancer stem cells in tumor progression. *Current stem cell research & therapy*. 2010;5(1):74-80.
81. Venditti P, Di Meo S. The Role of Reactive Oxygen Species in the Life Cycle of the Mitochondrion. *International journal of molecular sciences*. 2020;21(6):2173.
82. Di Meo S, Reed TT, Venditti P, Victor VM. Role of ROS and RNS sources in physiological and pathological conditions. *Oxidative medicine and cellular longevity*. 2016;2016.
83. Shimojo Y, Akimoto M, Hisanaga T, Tanaka T, Tajima Y, Honma Y, Takenaga K. Attenuation of reactive oxygen species by antioxidants suppresses hypoxia-induced epithelial-mesenchymal transition and metastasis of pancreatic cancer cells. *Clinical & experimental metastasis*. 2013;30:143-54.
84. Nci. Definition of reactive oxygen species - NCI Dictionary of Cancer Terms - NCI 2011 [updated 02/02/2011 - 07:00. Available from: https://www.cancer.gov/publications/dictionaries/cancer-terms/def/reactive-oxygen-species.
85. Radisky DC, Levy DD, Littlepage LE, Liu H, Nelson CM, Fata JE, Leake D, Godden EL, Albertson DG, Angela Nieto M. Rac1b and reactive oxygen species mediate MMP-3-induced EMT and genomic instability. *Nature*. 2005;436(7047):123-7.
86. Lee SY, Ju MK, Jeon HM, Lee YJ, Kim CH, Park HG, Han SI, Kang HS. Reactive oxygen species induce epithelial-mesenchymal transition, glycolytic switch, and mitochondrial repression through the Dlx-2/Snail signaling pathways in MCF-7 cells. *Mol Med Rep*. 2019;20(3):2339-46.
87. Chatterjee R, Chatterjee J. ROS and oncogenesis with special reference to EMT and stemness. *European Journal of Cell Biology*. 2020;99(2):151073.
88. Fukawa T, Kajiya H, Ozeki S, Ikebe T, Okabe K. Reactive oxygen species stimulates epithelial mesenchymal transition in normal human epidermal keratinocytes via TGF-beta secretion. *Experimental cell research*. 2012;318(15):1926-32.
89. Liou G-Y, Storz P. Reactive oxygen species in cancer. *Free Radical Research*. 2010;44(5):479-96.

90. Sies H, Belousov VV, Chandel NS, Davies MJ, Jones DP, Mann GE, Murphy MP, Yamamoto M, Winterbourn C. Defining roles of specific reactive oxygen species (ROS) in cell biology and physiology. *Nat Rev Mol Cell Biol*. 2022;23(7):499-515.
91. Bedard K, Krause K-H. The NOX family of ROS-generating NADPH oxidases: physiology and pathophysiology. *Physiological reviews*. 2007;87(1):245-313.
92. Brand M. Mitochondrial proton and electron leaks essays in biochemistry. *Essays Biochem*. 2010;47:53-67.
93. Fridovich I. Superoxide anion radical (O· 2), superoxide dismutases, and related matters. *Journal of biological chemistry*. 1997;272(30):18515-7.
94. Konno T, Melo EP, Chambers JE, Avezov E. Intracellular Sources of ROS/H(2)O(2) in Health and Neurodegeneration: Spotlight on Endoplasmic Reticulum. *Cells*. 2021;10(2).
95. Sinenko SA, Starkova TY, Kuzmin AA, Tomilin AN. Physiological Signaling Functions of Reactive Oxygen Species in Stem Cells: From Flies to Man. *Frontiers in Cell and Developmental Biology*. 2021;9.
96. Thannickal VJ, Fanburg BL. Reactive oxygen species in cell signaling. *American Journal of Physiology-Lung Cellular and Molecular Physiology*. 2000;279(6):L1005-L28.
97. Reczek CR, Chandel NS. ROS-dependent signal transduction. *Current opinion in cell biology*. 2015;33:8-13.
98. Wang Y, Branicky R, Noë A, Hekimi S. Superoxide dismutases: Dual roles in controlling ROS damage and regulating ROS signaling. *Journal of Cell Biology*. 2018;217(6):1915-28.
99. Paulsen CE, Carroll KS. Orchestrating redox signaling networks through regulatory cysteine switches. *ACS chemical biology*. 2010;5(1):47-62.
100. van der Reest J, Lilla S, Zheng L, Zanivan S, Gottlieb E. Proteome-wide analysis of cysteine oxidation reveals metabolic sensitivity to redox stress. *Nat Commun*. 2018;9(1):1581.
101. Tiana L, Caib Q, Wei H. Alterations of antioxidant enzymes and oxidative damage to macromolecules in different organs of rats during aging. *Free Radical Biology and Medicine*. 1998;24(9):1477-84.
102. Schieber M, Chandel NS. ROS function in redox signaling and oxidative stress. *Current biology*. 2014;24(10):R453-R62.
103. Paiva CN, Bozza MT. Are reactive oxygen species always detrimental to pathogens? *Antioxidants & redox signaling*. 2014;20(6):1000-37.
104. DeNicola GM, Karreth FA, Humpton TJ, Gopinathan A, Wei C, Frese K, Mangal D, Yu KH, Yeo CJ, Calhoun ES. Oncogene-induced Nrf2 transcription promotes ROS detoxification and tumorigenesis. *Nature*. 2011;475(7354):106-9.
105. Li R, Jia Z, Trush MA. Defining ROS in biology and medicine. *Reactive oxygen species (Apex, NC)*. 2016;1(1):9.
106. Sies H, Jones DP. Reactive oxygen species (ROS) as pleiotropic physiological signalling agents. *Nature Reviews Molecular Cell Biology*. 2020;21(7):363-83.
107. Nishikawa M. Reactive oxygen species in tumor metastasis. *Cancer letters*. 2008;266(1):53-9.
108. Clerkin J, Naughton R, Quiney C, Cotter T. Mechanisms of ROS modulated cell survival during carcinogenesis. *Cancer letters*. 2008;266(1):30-6.
109. Trachootham D, Alexandre J, Huang P. Targeting cancer cells by ROS-mediated mechanisms: a radical therapeutic approach? *Nature reviews Drug discovery*. 2009;8(7):579-91.
110. Wang J, Yi J. Cancer cell killing via ROS: to increase or decrease, that is the question. *Cancer biology & therapy*. 2008;7(12):1875-84.
111. Ushio-Fukai M, Nakamura Y. Reactive oxygen species and angiogenesis: NADPH oxidase as target for cancer therapy. *Cancer letters*. 2008;266(1):37-52.

112. Galanis A, Pappa A, Giannakakis A, Lanitis E, Dangaj D, Sandaltzopoulos R. Reactive oxygen species and HIF-1 signalling in cancer. *Cancer letters*. 2008;266(1):12-20.
113. Goetz ME, Luch A. Reactive species: a cell damaging rout assisting to chemical carcinogens. *Cancer letters*. 2008;266(1):73-83.
114. Gilgun-Sherki Y, Melamed E, Offen D. Oxidative stress induced-neurodegenerative diseases: the need for antioxidants that penetrate the blood brain barrier. *Neuropharmacology*. 2001;40(8):959-75.
115. Liu Z, Ren Z, Zhang J, Chuang C-C, Kandaswamy E, Zhou T, Zuo L. Role of ROS and Nutritional Antioxidants in Human Diseases. *Front Physiol*. 2018;9:477-.
116. Doskey CM, Buranasudja V, Wagner BA, Wilkes JG, Du J, Cullen JJ, Buettner GR. Tumor cells have decreased ability to metabolize H2O2: Implications for pharmacological ascorbate in cancer therapy. *Redox Biology*. 2016;10:274-84.
117. Cho C-S, Lee S, Lee GT, Woo HA, Choi E-J, Rhee SG. Irreversible inactivation of glutathione peroxidase 1 and reversible inactivation of peroxiredoxin II by H2O2 in red blood cells. *Antioxidants & redox signaling*. 2010;12(11):1235-46.
118. Graczyk-Jarzynka A, Goral A, Muchowicz A, Zagozdzon R, Winiarska M, Bajor M, Trzeciecka A, Fidyt K, Krupka JA, Cyran J. Inhibition of thioredoxin-dependent H2O2 removal sensitizes malignant B-cells to pharmacological ascorbate. *Redox biology*. 2019;21:101062.
119. Masaki H, Okano Y, Sakurai H. Differential role of catalase and glutathione peroxidase in cultured human fibroblasts under exposure of H 2 O 2 or ultraviolet B light. *Archives of dermatological research*. 1998;290:113-8.
120. Jeeva JS, Sunitha J, Ananthalakshmi R, Rajkumari S, Ramesh M, Krishnan R. Enzymatic antioxidants and its role in oral diseases. *J Pharm Bioallied Sci*. 2015;7(Suppl 2):S331-S3.
121. Rafique S, Hassan S, Mughal S, Hassan S, Shabbir N, Perveiz S, Mushtaq M, Farman M. Biological attributes of lemon: A review. *J Addict Med Ther Sci*. 2020;6(1):030-4.
122. Di Matteo A, Simeone GDR, Cirillo A, Rao MA, Di Vaio C. Morphological characteristics, ascorbic acid and antioxidant activity during fruit ripening of four lemon (Citrus limon (L.) Burm. F.) cultivars. *Scientia Horticulturae*. 2021;276:109741.
123. Byers T, Perry G. Dietary carotenes, vitamin C, and vitamin E as protective antioxidants in human cancers. *Annual review of Nutrition*. 1992;12(1):139-59.
124. Renerre M, Poncet K, Mercier Y, Gatellier P, Métro B. Influence of dietary fat and vitamin E on antioxidant status of muscles of turkey. *Journal of Agricultural and Food Chemistry*. 1999;47(1):237-44.
125. Nandi A, Yan L-J, Jana CK, Das N. Role of Catalase in Oxidative Stress- and Age-Associated Degenerative Diseases. *Oxidative medicine and cellular longevity*. 2019;2019:9613090-.
126. Gebicka L, Didik J. Catalytic scavenging of peroxynitrite by catalase. *Journal of inorganic biochemistry*. 2009;103(10):1375-9.
127. Heinzelmann S, Bauer G. Multiple protective functions of catalase against intercellular apoptosis-inducing ROS signaling of human tumor cells. 2010.
128. Brunelli L, Yermilov V, Beckman JS. Modulation of catalase peroxidatic and catalatic activity by nitric oxide. *Free Radical Biology and Medicine*. 2001;30(7):709-14.
129. Johansson LH, Borg LH. A spectrophotometric method for determination of catalase activity in small tissue samples. *Analytical biochemistry*. 1988;174(1):331-6.
130. Vetrano AM, Heck DE, Mariano TM, Mishin V, Laskin DL, Laskin JD. Characterization of the oxidase activity in mammalian catalase. *Journal of Biological Chemistry*. 2005;280(42):35372-81.
131. Terlecky SR, Koepke JI, Walton PA. Peroxisomes and aging. *Biochimica et Biophysica Acta (BBA)-Molecular Cell Research*. 2006;1763(12):1749-54.

132. Middelkoop E, Wiemer EA, Schoenmaker DT, Strijland A, Tager JM. Topology of catalase assembly in human skin fibroblasts. *Biochimica et Biophysica Acta (BBA)-Molecular Cell Research*. 1993;1220(1):15-20.
133. Radi R, Turrens JF, Chang LY, Bush KM, Crapo JD, Freeman BA. Detection of catalase in rat heart mitochondria. *Journal of Biological Chemistry*. 1991;266(32):22028-34.
134. Bauer G. Tumor cell-protective catalase as a novel target for rational therapeutic approaches based on specific intercellular ROS signaling. *Anticancer research*. 2012;32(7):2599-624.
135. Aly D, Shahin R. Oxidative stress in lichen planus. *Acta Dermatoven APA*. 2010;19(1):3-11.
136. Doskey CM, Buranasudja V, Wagner BA, Wilkes JG, Du J, Cullen JJ, Buettner GR. Tumor cells have decreased ability to metabolize H(2)O(2): Implications for pharmacological ascorbate in cancer therapy. *Redox biology*. 2016;10:274-84.
137. Cullen JJ, Mitros FA, Oberley LW. Expression of antioxidant enzymes in diseases of the human pancreas: another link between chronic pancreatitis and pancreatic cancer. *Pancreas*. 2003;26(1):23-7.
138. Ho JC-m, Zheng S, Comhair SA, Farver C, Erzurum SC. Differential expression of manganese superoxide dismutase and catalase in lung cancer. *Cancer research*. 2001;61(23):8578-85.
139. Kwei KA, Finch JS, Thompson EJ, Bowden GT. Transcriptional repression of catalase in mouse skin tumor progression. *Neoplasia*. 2004;6(5):440-8.
140. Subapriya R, Kumaraguruparan R, Ramachandran C, Nagini S. Oxidant-antioxidant status in patients with oral squamous cell carcinomas at different intraoral sites. *Clinical biochemistry*. 2002;35(6):489-93.
141. Yoo DG, Song YJ, Cho EJ, Lee SK, Park JB, Yu JH, Lim SP, Kim JM, Jeon BH. Alteration of APE1/ref-1 expression in non-small cell lung cancer: the implications of impaired extracellular superoxide dismutase and catalase antioxidant systems. *Lung cancer*. 2008;60(2):277-84.
142. Wu D, Yotnda P. Production and detection of reactive oxygen species (ROS) in cancers. *JoVE (Journal of Visualized Experiments)*. 2011(57):e3357.
143. Wu W-S. The signaling mechanism of ROS in tumor progression. *Cancer and Metastasis Reviews*. 2006;25:695-705.
144. Sen S, Kawahara B, Chaudhuri G. Maintenance of higher H2O2 levels, and its mechanism of action to induce growth in breast cancer cells: important roles of bioactive catalase and PP2A. *Free Radical Biology and Medicine*. 2012;53(8):1541-51.
145. Ueda M, Kinoshita H, Yoshida T, Kamasawa N, Osumi M, Tanaka A. Effect of catalase-specific inhibitor 3-amino-1,2,4-triazole on yeast peroxisomal catalase in vivo. *FEMS Microbiology Letters*. 2003;219(1):93-8.
146. Margoliash E, Novogrodsky A. A study of the inhibition of catalase by 3-amino-1:2:4-triazole. *Biochemical Journal*. 1958;68(3):468-75.
147. Ruiz-Ojeda FJ, Gomez-Llorente C, Aguilera CM, Gil A, Rupérez AI. Impact of 3-Amino-1,2,4-Triazole (3-AT)-Derived Increase in Hydrogen Peroxide Levels on Inflammation and Metabolism in Human Differentiated Adipocytes. *PLOS ONE*. 2016;11(3):e0152550.
148. Tattar TA. 20 - Chemical Injury. In: Tattar TA, editor. *Diseases of Shade Trees (Revised Edition)*. San Diego: Academic Press; 1989. p. 288-305.
149. Smith GF. Designing Drugs to Avoid Toxicity. In: Lawton G, Witty DR, editors. *Progress in Medicinal Chemistry*. 50: Elsevier; 2011. p. 1-47.
150. Lu J, Holmgren A. The thioredoxin antioxidant system. *Free Radic Biol Med*. 2014;66:75-87.
151. Lechner S, Müller-Ladner U, Neumann E, Spöttl T, Schlottmann K, Rüschoff J, Schölmerich J, Kullmann F. Thioredoxin Reductase 1 Expression in Colon Cancer: Discrepancy between In Vitro and In Vivo Findings. *Laboratory Investigation*. 2003;83(9):1321-31.

152. Tanaka T, Hosoi F, Yamaguchi-Iwai Y, Nakamura H, Masutani H, Ueda S, Nishiyama A, Takeda S, Wada H, Spyrou G. Thioredoxin-2 (TRX-2) is an essential gene regulating mitochondria-dependent apoptosis. *The EMBO journal*. 2002;21(7):1695-703.
153. Nakamura H, Masutani H, Yodoi J. Extracellular thioredoxin and thoredoxin-binding protein 2 in control of cancer. *Seminars in cancer biology*. 2007;16:444-51.
154. Marks PA. Thioredoxin in cancer--role of histone deacetylase inhibitors. *Seminars in cancer biology*. 2006;16(6):436-43.
155. Gao Z-Y, Gu N-J, Wu M-Z, Wang S-Y, Xu H-T, Li Q-C, Wu G-P. Human papillomavirus16 E6 but not E7 upregulates GLUT1 expression in lung cancer cells by upregulating thioredoxin expression. *Technology in Cancer Research & Treatment*. 2021;20:153303382110671.
156. Hwang-Bo H, Jeong JW, Han MH, Park C, Hong SH, Kim GY, Moon SK, Cheong J, Kim WJ, Yoo YH, Choi YH. Auranofin, an inhibitor of thioredoxin reductase, induces apoptosis in hepatocellular carcinoma Hep3B cells by generation of reactive oxygen species. *Gen Physiol Biophys*. 2017;36(2):117-28.
157. Abel EL, Angel JM, Riggs PK, Langfield L, Lo H-H, Person MD, Awasthi YC, Wang L-E, Strom SS, Wei Q. Evidence that Gsta4 modifies susceptibility to skin tumor development in mice and humans. *Journal of the National Cancer Institute*. 2010;102(21):1663-75.
158. Henderson CJ, Ritchie KJ, McLaren A, Chakravarty P, Wolf CR. Increased skin papilloma formation in mice lacking glutathione transferase GSTP. *Cancer research*. 2011;71(22):7048-60.
159. Ritchie KJ, Walsh S, Sansom OJ, Henderson CJ, Wolf CR. Markedly enhanced colon tumorigenesis in ApcMin mice lacking glutathione S-transferase Pi. *Proceedings of the National Academy of Sciences*. 2009;106(49):20859-64.
160. Li J, Wang Q, Yang Y, Lei C, Yang F, Liang L, Chen C, Xia J, Wang K, Tang N. GSTZ1 deficiency promotes hepatocellular carcinoma proliferation via activation of the KEAP1/NRF2 pathway. *Journal of Experimental & Clinical Cancer Research*. 2019;38(1):1-17.
161. Barrett CW, Ning W, Chen X, Smith JJ, Washington MK, Hill KE, Coburn LA, Peek RM, Chaturvedi R, Wilson KT. Tumor Suppressor Function of the Plasma Glutathione Peroxidase Gpx3 in Colitis-Associated CarcinomaLoss of Gpx3 Promotes Tumor Initiation in AOM/DSS Tumorigenesis. *Cancer research*. 2013;73(3):1245-55.
162. Zhang Y, Ikeno Y, Qi W, Chaudhuri A, Li Y, Bokov A, Thorpe SR, Baynes JW, Epstein C, Richardson A. Mice deficient in both Mn superoxide dismutase and glutathione peroxidase-1 have increased oxidative damage and a greater incidence of pathology but no reduction in longevity. *Journals of Gerontology Series A: Biomedical Sciences and Medical Sciences*. 2009;64(12):1212-20.
163. Van Remmen H, Ikeno Y, Hamilton M, Pahlavani M, Wolf N, Thorpe SR, Alderson NL, Baynes JW, Epstein CJ, Huang T-T. Life-long reduction in MnSOD activity results in increased DNA damage and higher incidence of cancer but does not accelerate aging. *Physiological genomics*. 2003;16(1):29-37.
164. McLoughlin MR, Orlicky DJ, Prigge JR, Krishna P, Talago EA, Cavigli IR, Eriksson S, Miller CG, Kundert JA, Sayin VI. TrxR1, Gsr, and oxidative stress determine hepatocellular carcinoma malignancy. *Proceedings of the National Academy of Sciences*. 2019;116(23):11408-17.
165. Luo M, Shang L, Brooks MD, Jiagge E, Zhu Y, Buschhaus JM, Conley S, Fath MA, Davis A, Gheordunescu E. Targeting breast cancer stem cell state equilibrium through modulation of redox signaling. *Cell metabolism*. 2018;28(1):69-86. e6.
166. Harris IS, Treloar AE, Inoue S, Sasaki M, Gorrini C, Lee KC, Yung KY, Brenner D, Knobbe-Thomsen CB, Cox MA. Glutathione and thioredoxin antioxidant pathways synergize to drive cancer initiation and progression. *Cancer cell*. 2015;27(2):211-22.

167. Diehn M, Cho RW, Lobo NA, Kalisky T, Dorie MJ, Kulp AN, Qian D, Lam JS, Ailles LE, Wong M. Association of reactive oxygen species levels and radioresistance in cancer stem cells. *nature*. 2009;458(7239):780-3.
168. Harris IS, Endress JE, Coloff JL, Selfors LM, McBrayer SK, Rosenbluth JM, Takahashi N, Dhakal S, Koduri V, Oser MG. Deubiquitinases maintain protein homeostasis and survival of cancer cells upon glutathione depletion. *Cell metabolism*. 2019;29(5):1166-81. e6.
169. Harris IS, DeNicola GM. The Complex Interplay between Antioxidants and ROS in Cancer. *Trends in Cell Biology*. 2020;30(6):440-51.
170. Oshimori N, Oristian D, Fuchs E. TGF-β promotes heterogeneity and drug resistance in squamous cell carcinoma. *Cell*. 2015;160(5):963-76.
171. Peklak-Scott C, Smitherman PK, Townsend AJ, Morrow CS. Role of glutathione S-transferase P1-1 in the cellular detoxification of cisplatin. *Molecular cancer therapeutics*. 2008;7(10):3247-55.
172. Liu CJ, Yang JH, Huang FZ, Nie WP, Liu CP, Mao XH, Yin XM, Shen XB, Peng C, Chen MF. Glutathione-s-transferase A 4 (GSTA4) suppresses tumor growth and metastasis of human hepatocellular carcinoma by targeting AKT pathway. *American Journal of Translational Research*. 2017;9(2):301.
173. Schoenfeld JD, Sibenaller ZA, Mapuskar KA, Wagner BA, Cramer-Morales KL, Furqan M, Sandhu S, Carlisle TL, Smith MC, Hejleh TA. O2·− and H2O2-mediated disruption of Fe metabolism causes the differential susceptibility of NSCLC and GBM cancer cells to pharmacological ascorbate. *Cancer cell*. 2017;31(4):487-500. e8.
174. Yun J, Mullarky E, Lu C, Bosch KN, Kavalier A, Rivera K, Roper J, Chio IIC, Giannopoulou EG, Rago C. Vitamin C selectively kills KRAS and BRAF mutant colorectal cancer cells by targeting GAPDH. *Science*. 2015;350(6266):1391-6.
175. Taylor PR, Albanes D. Selenium, vitamin E, and prostate cancer—ready for prime time? : Oxford University Press; 1998. p. 1184-5.
176. Lippman SM, Klein EA, Goodman PJ, Lucia MS, Thompson IM, Ford LG, Parnes HL, Minasian LM, Gaziano JM, Hartline JA. Effect of selenium and vitamin E on risk of prostate cancer and other cancers: the Selenium and Vitamin E Cancer Prevention Trial (SELECT). *Jama*. 2009;301(1):39-51.
177. Klein EA, Thompson IM, Tangen CM, Crowley JJ, Lucia MS, Goodman PJ, Minasian LM, Ford LG, Parnes HL, Gaziano JM. Vitamin E and the risk of prostate cancer: the Selenium and Vitamin E Cancer Prevention Trial (SELECT). *Jama*. 2011;306(14):1549-56.
178. Lippman SM, Goodman PJ, Klein EA, Parnes HL, Thompson IM, Kristal AR, Santella RM, Probstfield JL, Moinpour CM, Albanes D. Designing the selenium and vitamin E cancer prevention trial (SELECT). *Journal of the National Cancer Institute*. 2005;97(2):94-102.
179. Sayin VI, Ibrahim MX, Larsson E, Nilsson JA, Lindahl P, Bergo MO. Antioxidants accelerate lung cancer progression in mice. *Science translational medicine*. 2014;6(221):221ra15-ra15.
180. Le Gal K, Ibrahim MX, Wiel C, Sayin VI, Akula MK, Karlsson C, Dalin MG, Akyürek LM, Lindahl P, Nilsson J. Antioxidants can increase melanoma metastasis in mice. *Science translational medicine*. 2015;7(308):308re8-re8.
181. Pan J-S, Hong M-Z, Ren J-L. Reactive oxygen species: a double-edged sword in oncogenesis. *World journal of gastroenterology: WJG*. 2009;15(14):1702.
182. Han J, Sun P. The pathways to tumor suppression via route p38. *Trends in biochemical sciences*. 2007;32(8):364-71.
183. Wu C, Miloslavskaya I, Demontis S, Maestro R, Galaktionov K. Regulation of cellular response to oncogenic and oxidative stress by Seladin-1. *Nature*. 2004;432(7017):640-5.
184. Lafarga V, Cuadrado A, Nebreda AR. p18Hamlet mediates different p53-dependent responses to DNA damage inducing agents. *Cell Cycle*. 2007;6(19):2319-22.

185. Cuadrado A, Lafarga V, Cheung PC, Dolado I, Llanos S, Cohen P, Nebreda AR. A new p38 MAP kinase-regulated transcriptional coactivator that stimulates p53-dependent apoptosis. *The EMBO journal*. 2007;26(8):2115-26.
186. Bulavin DV, Higashimoto Y, Popoff IJ, Gaarde WA, Basrur V, Potapova O, Appella E, Fornace Jr AJ. Initiation of a G2/M checkpoint after ultraviolet radiation requires p38 kinase. *Nature*. 2001;411(6833):102-7.
187. Hirose Y, Katayama M, Stokoe D, Haas-Kogan DA, Berger MS, Pieper RO. The p38 mitogen-activated protein kinase pathway links the DNA mismatch repair system to the G2 checkpoint and to resistance to chemotherapeutic DNA-methylating agents. *Molecular and cellular biology*. 2003;23(22):8306-15.
188. Loft S, Poulsen HE. Cancer risk and oxidative DNA damage in man. *Journal of molecular medicine*. 1996;74:297-312.
189. Waris G, Ahsan H. Reactive oxygen species: role in the development of cancer and various chronic conditions. *Journal of carcinogenesis*. 2006;5:14.
190. Lunec J, Holloway KA, Cooke MS, Faux S, Griffiths HR, Evans MD. Urinary 8-oxo-2′-deoxyguanosine: redox regulation of DNA repair in vivo? *Free Radical Biology and Medicine*. 2002;33(7):875-85.
191. Denissenko MF, Venkatachalam S, Ma Y-H, Wani AA. Site-specific induction and repair of benzo [a] pyrene diol epoxide DNA damage in human H-ras protooncogene as revealed by restriction cleavage inhibition. *Mutation Research/DNA Repair*. 1996;363(1):27-42.
192. Du MQ, Carmichael PL, Phillips DH. Induction of activating mutations in the human c-Ha-ras-1 proto-oncogene by oxygen free radicals. *Molecular carcinogenesis*. 1994;11(3):170-5.
193. Brash DE, Rudolph JA, Simon JA, Lin A, McKenna GJ, Baden HP, Halperin AJ, Ponten J. A role for sunlight in skin cancer: UV-induced p53 mutations in squamous cell carcinoma. *Proceedings of the National Academy of Sciences*. 1991;88(22):10124-8.
194. Hollstein M, Sidransky D, Vogelstein B, Harris CC. p53 mutations in human cancers. *Science*. 1991;253(5015):49-53.
195. Harris CC, Hollstein M. Clinical implications of the p53 tumor-suppressor gene. *New England Journal of Medicine*. 1993;329(18):1318-27.
196. Behrend L, Henderson G, Zwacka R. Reactive oxygen species in oncogenic transformation. *Biochemical society transactions*. 2003;31(6):1441-4.
197. McCubrey JA, Steelman LS, Chappell WH, Abrams SL, Wong EW, Chang F, Lehmann B, Terrian DM, Milella M, Tafuri A. Roles of the Raf/MEK/ERK pathway in cell growth, malignant transformation and drug resistance. *Biochimica et Biophysica Acta (BBA)-Molecular Cell Research*. 2007;1773(8):1263-84.
198. Komatsu D, Kato M, Nakayama J, Miyagawa S, Kamata T. NADPH oxidase 1 plays a critical mediating role in oncogenic Ras-induced vascular endothelial growth factor expression. *Oncogene*. 2008;27(34):4724-32.
199. Nishida N, Yano H, Nishida T, Kamura T, Kojiro M. Angiogenesis in cancer. *Vascular health and risk management*. 2006;2(3):213-9.
200. Carmeliet P, Jain RK. Angiogenesis in cancer and other diseases. *nature*. 2000;407(6801):249-57.
201. Tonini T, Rossi F, Claudio PP. Molecular basis of angiogenesis and cancer. *Oncogene*. 2003;22(42):6549-56.
202. Rajabi M, Mousa SA. The Role of Angiogenesis in Cancer Treatment. *Biomedicines*. 2017;5(2):34.
203. Cook JA, Gius D, Wink DA, Krishna MC, Russo A, Mitchell JB, editors. Oxidative stress, redox, and the tumor microenvironment. *Seminars in radiation oncology*; 2004: Elsevier.

204. Durand JK, Baldwin AS. Chapter Three - Targeting IKK and NF-κB for Therapy. In: Donev R, editor. *Advances in Protein Chemistry and Structural Biology*. 107: Academic Press; 2017. p. 77-115.
205. Xia Y, Shen S, Verma IM. NF-κB, an active player in human cancers. *Cancer immunology research*. 2014;2(9):823-30.
206. Li J, Cao F, Yin H-l, Huang Z-j, Lin Z-t, Mao N, Sun B, Wang G. Ferroptosis: past, present and future. *Cell Death & Disease*. 2020;11(2):88.
207. Zhang C, Liu X, Jin S, Chen Y, Guo R. Ferroptosis in cancer therapy: a novel approach to reversing drug resistance. *Molecular Cancer*. 2022;21(1):47.
208. Stockwell BR. Ferroptosis turns 10: Emerging mechanisms, physiological functions, and therapeutic applications. *Cell*. 2022;185(14):2401-21.
209. Dixon SJ, Pratt DA. Ferroptosis: A flexible constellation of related biochemical mechanisms. *Molecular Cell*. 2023;83(7):1030-42.
210. Jiang J, Wang K, Chen Y, Chen H, Nice EC, Huang C. Redox regulation in tumor cell epithelial–mesenchymal transition: molecular basis and therapeutic strategy. *Signal Transduction and Targeted Therapy*. 2017;2(1):17036.
211. Rhyu DY, Yang Y, Ha H, Lee GT, Song JS, Uh S-t, Lee HB. Role of reactive oxygen species in TGF-β1-induced mitogen-activated protein kinase activation and epithelial-mesenchymal transition in renal tubular epithelial cells. *Journal of the american society of nephrology*. 2005;16(3):667-75.
212. Zhang K-H, Tian H-Y, Gao X, Lei W-W, Hu Y, Wang D-M, Pan X-C, Yu M-L, Xu G-J, Zhao F-K. Ferritin heavy chain–mediated iron homeostasis and subsequent increased reactive oxygen species production are essential for epithelial-mesenchymal transition. *Cancer research*. 2009;69(13):5340-8.
213. Yoon Y-S, Lee J-H, Hwang S-C, Choi KS, Yoon G. TGF β1 induces prolonged mitochondrial ROS generation through decreased complex IV activity with senescent arrest in Mv1Lu cells. *Oncogene*. 2005;24(11):1895-903.
214. Chen X, Yan H, Chen Y, Li G, Bin Y, Zhou X. Moderate oxidative stress promotes epithelial-mesenchymal transition in the lens epithelial cells via the TGF-β/Smad and Wnt/β-catenin pathways. *Mol Cell Biochem*. 2021;476(3):1631-42.
215. Li J, Chen Y, Han C, Huang S, Chen S, Luo L, Liu Y. JNK1/β-catenin axis regulates H2O2-induced epithelial-to-mesenchymal transition in human lens epithelial cells. *Biochemical and Biophysical Research Communications*. 2019;511(2):336-42.
216. Ren Y, Wang Y, Hao S, Yang Y, Xiong W, Qiu L, Tao J, Tang A. NFE2L3 promotes malignant behavior and EMT of human hepatocellular carcinoma (HepG2) cells via Wnt/β-catenin pathway. *Journal of Cancer*. 2020;11(23):6939.
217. Karicheva O, Rodriguez-Vargas JM, Wadier N, Martin-Hernandez K, Vauchelles R, Magroun N, Tissier A, Schreiber V, Dantzer F. PARP3 controls TGFβ and ROS driven epithelial-to-mesenchymal transition and stemness by stimulating a TG2-Snail-E-cadherin axis. *Oncotarget*. 2016;7(39):64109.
218. Min C, Eddy SF, Sherr DH, Sonenshein GE. NF-κB and epithelial to mesenchymal transition of cancer. *Journal of cellular biochemistry*. 2008;104(3):733-44.
219. Wu Y, Deng J, Rychahou PG, Qiu S, Evers BM, Zhou BP. Stabilization of snail by NF-κB is required for inflammation-induced cell migration and invasion. *Cancer cell*. 2009;15(5):416-28.
220. Dong R, Wang Q, He X, Chu Y, Lu J, Ma Q. Role of nuclear factor kappa B and reactive oxygen species in the tumor necrosis factor-a-induced epithelial-mesenchymal transition of MCF-7 cells. *Brazilian Journal of Medical and Biological Research*. 2007;40:1071-8.

221. Inumaru J, Nagano O, Takahashi E, Ishimoto T, Nakamura S, Suzuki Y, Niwa Si, Umezawa K, Tanihara H, Saya H. Molecular mechanisms regulating dissociation of cell–cell junction of epithelial cells by oxidative stress. *Genes to Cells*. 2009;14(6):703-16.
222. Cichon MA, Radisky DC. ROS-induced epithelial-mesenchymal transition in mammary epithelial cells is mediated by NF-κB-dependent activation of Snail. *Oncotarget*. 2014;5(9):2827.
223. Li W, Cao L, Han L, Xu Q, Ma Q. Superoxide dismutase promotes the epithelial-mesenchymal transition of pancreatic cancer cells via activation of the H2O2/ERK/NF-κB axis. *International Journal of Oncology*. 2015;46(6):2613-20.
224. Joseph JV, Conroy S, Pavlov K, Sontakke P, Tomar T, Eggens-Meijer E, Balasubramaniyan V, Wagemakers M, den Dunnen WF, Kruyt FA. Hypoxia enhances migration and invasion in glioblastoma by promoting a mesenchymal shift mediated by the HIF1α–ZEB1 axis. *Cancer letters*. 2015;359(1):107-16.
225. Zhang W, Shi X, Peng Y, Wu M, Zhang P, Xie R, Wu Y, Yan Q, Liu S, Wang J. HIF-1α promotes epithelial-mesenchymal transition and metastasis through direct regulation of ZEB1 in colorectal cancer. *PloS one*. 2015;10(6):e0129603.
226. Wang Y, Ma J, Shen H, Wang C, Sun Y, Howell SB, Lin X. Reactive oxygen species promote ovarian cancer progression via the HIF-1α/LOX/E-cadherin pathway. *Oncology reports*. 2014;32(5):2150-8.
227. Xi Y, Wei Y, Sennino B, Ulsamer A, Kwan I, Brumwell AN, Tan K, Aghi MK, McDonald DM, Jablons DM. Identification of pY654-β-catenin as a critical co-factor in hypoxia-inducible factor-1α signaling and tumor responses to hypoxia. *Oncogene*. 2013;32(42):5048-57.
228. Napetschnig J, Wu H. Molecular basis of NF-κB signaling. *Annual review of biophysics*. 2013;42:443-68.
229. Gerald D, Berra E, Frapart YM, Chan DA, Giaccia AJ, Mansuy D, Pouysségur J, Yaniv M, Mechta-Grigoriou F. JunD reduces tumor angiogenesis by protecting cells from oxidative stress. *Cell*. 2004;118(6):781-94.
230. Pan Y, Mansfield KD, Bertozzi CC, Rudenko V, Chan DA, Giaccia AJ, Simon MC. Multiple factors affecting cellular redox status and energy metabolism modulate hypoxia-inducible factor prolyl hydroxylase activity in vivo and in vitro. *Molecular and cellular biology*. 2007;27(3):912-25.
231. Rankin EB, Fuh KC, Castellini L, Viswanathan K, Finger EC, Diep AN, LaGory EL, Kariolis MS, Chan A, Lindgren D. Direct regulation of GAS6/AXL signaling by HIF promotes renal metastasis through SRC and MET. *Proceedings of the National Academy of Sciences*. 2014;111(37):13373-8.
232. Huang J-S, Cho C-Y, Hong C-C, Yan M-D, Hsieh M-C, Lay J-D, Lai G-M, Cheng A-L, Chuang S-E. Oxidative stress enhances Axl-mediated cell migration through an Akt1/Rac1-dependent mechanism. *Free Radical Biology and Medicine*. 2013;65:1246-56.
233. Dibble CC, Cantley LC. Regulation of mTORC1 by PI3K signaling. *Trends in cell biology*. 2015;25(9):545-55.
234. Prasad CP, Rath G, Mathur S, Bhatnagar D, Parshad R, Ralhan R. Expression analysis of E-cadherin, Slug and GSK3β in invasive ductal carcinoma of breast. *BMC cancer*. 2009;9(1):1-10.
235. Nakanishi A, Wada Y, Kitagishi Y, Matsuda S. Link between PI3K/AKT/PTEN pathway and NOX proteinin diseases. *Aging and disease*. 2014;5(3):203.
236. Lee S-R, Yang K-S, Kwon J, Lee C, Jeong W, Rhee SG. Reversible inactivation of the tumor suppressor PTEN by H2O2. *Journal of Biological Chemistry*. 2002;277(23):20336-42.
237. Kwon J, Lee S-R, Yang K-S, Ahn Y, Kim YJ, Stadtman ER, Rhee SG. Reversible oxidation and inactivation of the tumor suppressor PTEN in cells stimulated with peptide growth factors. *Proceedings of the National Academy of Sciences*. 2004;101(47):16419-24.

238. Ngkelo A, Meja K, Yeadon M, Adcock I, Kirkham PA. LPS induced inflammatory responses in human peripheral blood mononuclear cells is mediated through NOX4 and Giα dependent PI-3kinase signalling. *Journal of inflammation*. 2012;9(1):1-7.
239. Mitra SK, Schlaepfer DD. Integrin-regulated FAK–Src signaling in normal and cancer cells. *Current opinion in cell biology*. 2006;18(5):516-23.
240. Tomar A, Schlaepfer DD. Focal adhesion kinase: switching between GAPs and GEFs in the regulation of cell motility. *Current opinion in cell biology*. 2009;21(5):676-83.
241. Lawson C, Lim S-T, Uryu S, Chen XL, Calderwood DA, Schlaepfer DD. FAK promotes recruitment of talin to nascent adhesions to control cell motility. *Journal of Cell Biology*. 2012;196(2):223-32.
242. Sulzmaier FJ, Jean C, Schlaepfer DD. FAK in cancer: mechanistic findings and clinical applications. *Nature reviews cancer*. 2014;14(9):598-610.
243. Wang Y, McNiven MA. Invasive matrix degradation at focal adhesions occurs via protease recruitment by a FAK–p130Cas complex. *Journal of Cell Biology*. 2012;196(3):375-85.
244. Lim S-T, Chen XL, Lim Y, Hanson DA, Vo T-T, Howerton K, Larocque N, Fisher SJ, Schlaepfer DD, Ilic D. Nuclear FAK promotes cell proliferation and survival through FERM-enhanced p53 degradation. *Molecular cell*. 2008;29(1):9-22.
245. Ribeiro-Pereira C, Moraes JA, Souza MdJ, Laurindo FR, Arruda MA, Barja-Fidalgo C. Redox modulation of FAK controls melanoma survival-role of NOX4. *PLoS One*. 2014;9(6):e99481.
246. Giannoni E, Chiarugi P. Redox circuitries driving Src regulation. *Antioxidants & Redox Signaling*. 2014;20(13):2011-25.
247. Canel M, Serrels A, Frame MC, Brunton VG. E-cadherin–integrin crosstalk in cancer invasion and metastasis. *Journal of cell science*. 2013;126(2):393-401.
248. Hong JY, Oh I-H, McCrea PD. Phosphorylation and isoform use in p120-catenin during development and tumorigenesis. *Biochimica et Biophysica Acta (BBA)-Molecular Cell Research*. 2016;1863(1):102-14.
249. Avizienyte E, Fincham VJ, Brunton VG, Frame MC. Src SH3/2 domain-mediated peripheral accumulation of Src and phospho-myosin is linked to deregulation of E-cadherin and the epithelial-mesenchymal transition. *Molecular biology of the cell*. 2004;15(6):2794-803.
250. Zhang H, Forman HJ. TGFβ1 rapidly activates Src through a non-canonical redox mechanism. *Free Radical Biology and Medicine*. 2014;75:S4.
251. Giannoni E, Buricchi F, Raugei G, Ramponi G, Chiarugi P. Intracellular reactive oxygen species activate Src tyrosine kinase during cell adhesion and anchorage-dependent cell growth. *Molecular and cellular biology*. 2005;25(15):6391-403.
252. Lim S-K, Choi YW, Lim IK, Park TJ. BTG2 suppresses cancer cell migration through inhibition of Src-FAK signaling by downregulation of reactive oxygen species generation in mitochondria. *Clinical & experimental metastasis*. 2012;29:901-13.
253. Corcoran A, Cotter TG. FLT3-driven redox-modulation of Ezrin regulates leukaemic cell migration. *Free Radical Research*. 2013;47(1):20-34.
254. Fuhrmann J, Subramanian V, Thompson PR. Targeting the arginine phosphatase YwlE with a catalytic redox-based inhibitor. *ACS Chemical Biology*. 2013;8(9):2024-32.
255. Jang JY, Min JH, Chae YH, Baek JY, Wang SB, Park SJ, Oh GT, Lee S-H, Ho Y-S, Chang T-S. Reactive oxygen species play a critical role in collagen-induced platelet activation via SHP-2 oxidation. *Antioxidants & redox signaling*. 2014;20(16):2528-40.
256. Hiraga R, Kato M, Miyagawa S, Kamata T. Nox4-derived ROS signaling contributes to TGF-β-induced epithelial-mesenchymal transition in pancreatic cancer cells. *Anticancer research*. 2013;33(10):4431-8.

257. Frijhoff J, Dagnell M, Godfrey R, Östman A. Regulation of protein tyrosine phosphatase oxidation in cell adhesion and migration. *Antioxidants & redox signaling*. 2014;20(13):1994-2010.
258. Weibrecht I, Böhmer S-A, Dagnell M, Kappert K, Östman A, Böhmer F-D. Oxidation sensitivity of the catalytic cysteine of the protein-tyrosine phosphatases SHP-1 and SHP-2. *Free Radical Biology and Medicine*. 2007;43(1):100-10.
259. Wang SB, Jang JY, Chae YH, Min JH, Baek JY, Kim M, Park Y, Hwang GS, Ryu J-S, Chang T-S. Kaempferol suppresses collagen-induced platelet activation by inhibiting NADPH oxidase and protecting SHP-2 from oxidative inactivation. *Free Radical Biology and Medicine*. 2015;83:41-53.
260. Taddei ML, Parri M, Mello T, Catalano A, Levine AD, Raugei G, Ramponi G, Chiarugi P. Integrin-mediated cell adhesion and spreading engage different sources of reactive oxygen species. *Antioxidants and Redox Signaling*. 2007;9(4):469-81.
261. Gorowiec MR, Borthwick LA, Parker SM, Kirby JA, Saretzki GC, Fisher AJ. Free radical generation induces epithelial-to-mesenchymal transition in lung epithelium via a TGF-β1-dependent mechanism. *Free radical biology & medicine*. 2012;52(6):1024-32.
262. Steinhorn B, Sorrentino A, Badole S, Bogdanova Y, Belousov V, Michel T. Chemogenetic generation of hydrogen peroxide in the heart induces severe cardiac dysfunction. *Nat Commun*. 2018;9(1):4044-.
263. Belousov VV, Fradkov AF, Lukyanov KA, Staroverov DB, Shakhbazov KS, Terskikh AV, Lukyanov S. Genetically encoded fluorescent indicator for intracellular hydrogen peroxide. *Nat Methods*. 2006;3(4):281-6.
264. Pak VV, Ezeriņa D, Lyublinskaya OG, Pedre B, Tyurin-Kuzmin PA, Mishina NM, Thauvin M, Young D, Wahni K, Martínez Gache SA, Demidovich AD, Ermakova YG, Maslova YD, Shokhina AG, Eroglu E, Bilan DS, Bogeski I, Michel T, Vriz S, Messens J, Belousov VV. Ultrasensitive Genetically Encoded Indicator for Hydrogen Peroxide Identifies Roles for the Oxidant in Cell Migration and Mitochondrial Function. *Cell Metabolism*. 2020;31(3):642-53.e6.
265. Michel T. Addgene: pAAV-HyPer-DAAO-NES 2023 [Available from: https://www.addgene.org/119164/.
266. Saeedi Saravi SS, Eroglu E, Waldeck-Weiermair M, Sorrentino A, Steinhorn B, Belousov V, Michel T. Differential endothelial signaling responses elicited by chemogenetic H(2)O(2) synthesis. *Redox Biol*. 2020;36:101605.
267. Addgene: You have just received your plasmids from Addgene. Now what? 2023 [Available from: https://www.addgene.org/recipient-instructions/myplasmid/.
268. Biolabs NE. Monarch® Plasmid Miniprep Kit [Available from: https://www.neb.com/protocols/2015/11/20/monarch-plasmid-dna-miniprep-kit-protocol-t1010.
269. Addgene: Protocol - Bacterial Transformation 2023 [Available from: https://www.addgene.org/protocols/bacterial-transformation/.
270. Scientific T. PureLink™ HiPure Plasmid Filter Purification Kits - for Midi and Maxi preparation of Plasmid DNA - US 2023 [Available from: https://www.thermofisher.com/us/en/home/references/protocols/nucleic-acid-purification-and-analysis/dna-extraction-protocols/purelink-hipure-plasmid-filter-purification-kits.html.
271. Biolabs NE. BsaBI. 2023.
272. Biolabs NE. PsiI-v2. 2023.
273. Biolabs NE. HpaI. 2023.
274. Biolabs NE. PshAI. 2023.
275. addgene. How do I store my plasmid (long-term)? 2023 [Available from: https://help.addgene.org/hc/en-us/articles/206127275-How-do-I-store-my-plasmid-long-term-.

276. Lipofectamine 3000 Reagent USER GUIDE 2023 [Available from: https://www.thermofisher.com/document-connect/document-connect.html?url=https://assets.thermofisher.com/TFS-Assets%2FLSG%2Fmanuals%2Flipofectamine3000_protocol.pdf.
277. PolyJet In Vitro DNA Transfection Reagent: A General Protocol for Transfecting Mammalian Cell 2023 [
278. Cinquanta L, Fontana DE, Bizzaro N. Chemiluminescent immunoassay technology: what does it change in autoantibody detection? *Auto Immun Highlights*. 2017;8(1):9-.
279. A-8170_P00 | 2390553-21-4 | AquaSpark® 510 Peroxide Probe, 10 mM in DMSO, Ramot at Tel-Aviv University Ltd. Patent family WO 2017/130191 2023 [Available from: https://www.biosynth.com/p/a-8170_P00.
280. Calabria D, Guardigli M, Mirasoli M, Punzo A, Porru E, Zangheri M, Simoni P, Pagnotta E, Ugolini L, Lazzeri L, Caliceti C, Roda A. Selective chemiluminescent TURN-ON quantitative bioassay and imaging of intracellular hydrogen peroxide in human living cells. *Anal Biochem*. 2020;600:113760.
281. Liang C-C, Park AY, Guan J-L. In vitro scratch assay: a convenient and inexpensive method for analysis of cell migration in vitro. *Nature Protocols*. 2007;2(2):329-33.
282. In-Cell Western™ Assay: *LI-COR*; 2023 [Available from: https://www.licor.com/bio/applications/in-cell-western-assay.
283. General Protocol for Western Blotting: *BIO-RAD*; [Available from: https://www.bio-rad.com/webroot/web/pdf/lsr/literature/Bulletin_6376.pdf.
284. Scientific T. Pierce BCA Protein Assay Kit User Guide 2023 [Available from: https://www.thermofisher.com/document-connect/document-connect.html?url=https://assets.thermofisher.com/TFS-Assets%2FLSG%2Fmanuals%2FMAN0011430_Pierce_BCA_Protein_Asy_UG.pdf.
285. Kim BN, Ahn DH, Kang N, Yeo CD, Kim YK, Lee KY, Kim T-J, Lee SH, Park MS, Yim HW, Park JY, Park CK, Kim SJ. TGF-β induced EMT and stemness characteristics are associated with epigenetic regulation in lung cancer. *Scientific Reports*. 2020;10(1):10597.
286. Yeh H-W, Hsu E-C, Lee S-S, Lang Y-D, Lin Y-C, Chang C-Y, Lee S-Y, Gu D-L, Shih J-H, Ho C-M, Chen C-F, Chen C-T, Tu P-H, Cheng C-F, Chen R-H, Yang R-B, Jou Y-S. PSPC1 mediates TGF-β1 autocrine signalling and Smad2/3 target switching to promote EMT, stemness and metastasis. *Nature Cell Biology*. 2018;20(4):479-91.
287. Masaki H, Okano Y, Sakurai H. Differential role of catalase and glutathione peroxidase in cultured human fibroblasts under exposure of H2O2 or ultraviolet B light. *Arch Dermatol Res*. 1998;290(3):113-8.
288. integrative database for protein Cysteine Modifications in eukaryotes [Internet]. 2023.
289. Stanley BA, Sivakumaran V, Shi S, McDonald I, Lloyd D, Watson WH, Aon MA, Paolocci N. Thioredoxin Reductase-2 Is Essential for Keeping Low Levels of H2O2 Emission from Isolated Heart Mitochondria. *Journal of Biological Chemistry*. 2011;286(38):33669-77.
290. Lukesh JC, 3rd, Palte MJ, Raines RT. A potent, versatile disulfide-reducing agent from aspartic acid. *J Am Chem Soc*. 2012;134(9):4057-9.
291. Ayla O, Metin O. Biochemistry of Reactive Oxygen and Nitrogen Species. In: Sivakumar Joghi Thatha G, editor. *Basic Principles and Clinical Significance of Oxidative Stress*. Rijeka: IntechOpen; 2015. p. Ch. 3.
292. Pacher P, Beckman JS, Liaudet L. Nitric oxide and peroxynitrite in health and disease. *Physiol Rev*. 2007;87(1):315-424.

293. Hao Y, Baker D, Ten Dijke P. TGF-β-Mediated Epithelial-Mesenchymal Transition and Cancer Metastasis. *Int J Mol Sci*. 2019;20(11).
294. Shi Y, Wang S, Yang R, Wang Z, Zhang W, Liu H, Huang Y. ROS Promote Hypoxia-Induced Keratinocyte Epithelial-Mesenchymal Transition by Inducing SOX2 Expression and Subsequent Activation of Wnt/β-Catenin. *Oxidative Medicine and Cellular Longevity*. 2022;2022:1-23.
295. Matthaeus C, Taraska JW. Energy and Dynamics of Caveolae Trafficking. *Frontiers in Cell and Developmental Biology*. 2021;8.
296. Bilan DS, Pase L, Joosen L, Gorokhovatsky AY, Ermakova YG, Gadella TW, Grabher C, Schultz C, Lukyanov S, Belousov VV. HyPer-3: a genetically encoded H(2)O(2) probe with improved performance for ratiometric and fluorescence lifetime imaging. *ACS Chem Biol*. 2013;8(3):535-42.
297. Yoshimura T, Esak N. Amino acid racemases: functions and mechanisms. *J Biosci Bioeng*. 2003;96(2):103-9.
298. Scientific T. Green Fluorescent Protein (GFP) - US 2023 [Available from: https://www.thermofisher.com/us/en/home/life-science/cell-analysis/fluorophores/green-fluorescent-protein.html.
299. Riley MV. Physiologic neutralization mechanisms and the response of the corneal endothelium to hydrogen peroxide. *CLAO J*. 1990;16(1 Suppl):S16-21; discussion S-2.
300. Elkins JG, Hassett DJ, Stewart PS, Schweizer HP, McDermott TR. Protective Role of Catalase in Pseudomonas aeruginosa Biofilm Resistance to Hydrogen Peroxide. *Applied and Environmental Microbiology*. 1999;65(10):4594-600.
301. Ransy C, Vaz C, Lombès A, Bouillaud F. Use of H2O2 to Cause Oxidative Stress, the Catalase Issue. *International Journal of Molecular Sciences*. 2020;21(23):9149.
302. Joardar N, Guevara-Flores A, Martínez-González JdJ, Sinha Babu SP. Thiol antioxidant thioredoxin reductase: A prospective biochemical crossroads between anticancer and antiparasitic treatments of the modern era. *International Journal of Biological Macromolecules*. 2020;165:249-67.
303. Wang H, Bouzakoura S, de Mey S, Jiang H, Law K, Dufait I, Corbet C, Verovski V, Gevaert T, Feron O, Van den Berge D, Storme G, De Ridder M. Auranofin radiosensitizes tumor cells through targeting thioredoxin reductase and resulting overproduction of reactive oxygen species. *Oncotarget*. 2017;8(22):35728-42.
304. Fath MA, Ahmad IM, Smith CJ, Spence J, Spitz DR. Enhancement of Carboplatin-Mediated Lung Cancer Cell Killing by Simultaneous Disruption of Glutathione and Thioredoxin Metabolism. *Clinical Cancer Research*. 2011;17(19):6206-17.
305. Kiebala M, Skalska J, Casulo C, Brookes PS, Peterson DR, Hilchey SP, Dai Y, Grant S, Maggirwar SB, Bernstein SH. Dual targeting of the thioredoxin and glutathione antioxidant systems in malignant B cells: A novel synergistic therapeutic approach. *Experimental Hematology*. 2015;43(2):89-99.
306. Habermann KJ, Grünewald L, van Wijk S, Fulda S. Targeting redox homeostasis in rhabdomyosarcoma cells: GSH-depleting agents enhance auranofin-induced cell death. *Cell Death & Disease*. 2017;8(10):e3067-e.
307. Shi M, Gozal E, Choy HA, Forman HJ. Extracellular glutathione and γ-glutamyl transpeptidase prevent H2O2-induced injury by 2,3-dimethoxy-1,4-naphthoquinone. *Free Radical Biology and Medicine*. 1993;15(1):57-67.
308. To WS, Midwood KS. Plasma and cellular fibronectin: distinct and independent functions during tissue repair. *Fibrogenesis & Tissue Repair*. 2011;4(1):21.

309. Parisi L, Toffoli A, Ghezzi B, Mozzoni B, Lumetti S, Macaluso GM. A glance on the role of fibronectin in controlling cell response at biomaterial interface. *Jpn Dent Sci Rev*. 2020;56(1):50-5.
310. Pankov R, Yamada KM. Fibronectin at a glance. *J Cell Sci*. 2002;115(Pt 20):3861-3.
311. Pećina-Slaus N. Tumor suppressor gene E-cadherin and its role in normal and malignant cells. *Cancer cell international*. 2003;3(1):17-.
312. Cufí S, Vazquez-Martin A, Oliveras-Ferraros C, Martin-Castillo B, Joven J, Menendez JA. Metformin against TGFβ-induced epithelial-to-mesenchymal transition (EMT): From cancer stem cells to aging-associated fibrosis. *Cell Cycle*. 2010;9(22):4461-8.
313. Meng X, Ezzati P, Wilkins JA. Requirement of podocalyxin in TGF-beta induced epithelial mesenchymal transition. *PloS one*. 2011;6(4):e18715.
314. Mahdi SH, Cheng H, Li J, Feng R. The effect of TGF-beta-induced epithelial–mesenchymal transition on the expression of intracellular calcium-handling proteins in T47D and MCF-7 human breast cancer cells. *Archives of biochemistry and biophysics*. 2015;583:18-26.
315. Boudreau HE, Casterline BW, Rada B, Korzeniowska A, Leto TL. Nox4 involvement in TGF-beta and SMAD3-driven induction of the epithelial-to-mesenchymal transition and migration of breast epithelial cells. *Free Radical Biology and Medicine*. 2012;53(7):1489-99.
316. Sheahan S, Bellamy CO, Hartland SN, Harrison DJ, Prost S. TGFbeta induces apoptosis and EMT in primary mouse hepatocytes independently of p53, p21 Cip1 or Rbstatus. *BMC cancer*. 2008;8(1):1-11.
317. Rashid M-u, Coombs KM. Serum-reduced media impacts on cell viability and protein expression in human lung epithelial cells. *Journal of Cellular Physiology*. 2019;234(6):7718-24.
318. Castro L, Tórtora V, Mansilla S, Radi R. Aconitases: Non-redox Iron-Sulfur Proteins Sensitive to Reactive Species. *Acc Chem Res*. 2019;52(9):2609-19.
319. Coldren CD, Helfrich BA, Witta SE, Sugita M, Lapadat R, Zeng C, Barón A, Franklin WA, Hirsch FR, Geraci MW, Bunn PA, Jr. Baseline gene expression predicts sensitivity to gefitinib in non-small cell lung cancer cell lines. *Mol Cancer Res*. 2006;4(8):521-8.